Thomas Rüberg

Non-conforming Coupling of Finite and Boundary Element Methods in Time Domain

Monographic Series TU Graz

Computation in Engineering and Science

Monographic Series TU Graz

Computation in Engineering and Science; 3

Thomas Rüberg

_____

**Non-conforming Coupling of Finite and
Boundary Element Methods in Time Domain**

_____

Abstract

The combination of finite and boundary element methods for the numerical solution of coupled problems has a long tradition. It has proved to be the method of choice for several applications among which are the acoustic-structure coupling or the soil-structure interaction. In this work, the concept of combining these two approximation methods is carried forward to dynamic problems by developing a coupling framework in which the local discretization method can be chosen independently. In fact, a Lagrange multiplier domain decomposition approach is preferred which allows for the most flexible combination of discretization methods within the same solution algorithm. Therefore, Dirchlet-to-Neumann maps are realized on the discrete level for the static case or at each time step for the dynamic case. Moreover, the treatment of nonconforming interface meshes, i.e., interface discretizations which do not have coincident nodes or equal interpolation orders, is included easily into this approach. The considered physical models are the acoustic wave equation and the linear elastodynamic system together with their static limits, Laplace equation and elastostatics.

Zusammenfassung

Die gekoppelte Verwendung der Methode der finiten Elemente und der Methode der Randelemente als numerische Näherungsverfahren hat sich als sinnvolle Wahl für viele Problemstellungen erwiesen. Zum Beispiel wird diese Kombination häufig im Bereich der Akustik-Struktur Kopplung oder der Boden-Bauwerk Interaktion eingesetzt. In der vorliegenden Arbeit wird diese Methodik weiterentwickelt, indem ein Kopplungsalgorithmus formuliert wird, der den unabhängigen Einsatz beider Verfahren zur Anwendung auf statische oder dynamische Aufgaben in sowohl zwei als auch drei Raumdimensionen ermöglicht. Dafür werden lokale Dirichlet-Neumann-Abbildungen in der diskreten Formulierung für die jeweilige Methode realisiert. Dieses geschieht bei der Behandlung dynamischer Aufgaben in jedem Zeitschritt. Das hier vorgestellte Verfahren erlaubt es darüber hinaus, dass die Vernetzung der Trennflächen des gekoppelten Problems nicht zusammenpassen müssen. Das bedeutet, dass auf der jeweiligen Seite solch einer Trennfläche nicht nur das Diskretisierungsverfahren sondern auch die Netze und die zugehörigen Ansatzordnungen unabhängig gewählt werden können. Die betrachteten physikalischen Modelle sind die skalare Wellengleichung und die lineare Elastodynamik einschließlich der statischen Grenzfälle der Laplace-Gleichung beziehungsweise der linearen Elastostatik.

CONTENTS

Notation

General Notation

$a, b, \ldots, \alpha, \beta, \ldots$	scalar values
$\mathbf{a}, \mathbf{b}, \ldots, \boldsymbol{\alpha}, \boldsymbol{\beta}, \ldots$	vectors (first-order tensors)
$\mathbf{A}, \mathbf{B}, \ldots$	higher-order tensors
$\mathsf{a}, \mathsf{b}, \ldots, \alpha, \beta$	$m \times 1$-matrices
$\mathsf{A}, \mathsf{B}, \ldots, \Sigma, \ldots$	$m \times n$-matrices
$\mathcal{A}, \mathcal{B}, \ldots$	linear operators
$\mathsf{a}[i]$	component of a, $1 \leq i \leq m$
$\mathbf{A}[i, j]$	component of $\mathbf{A}$, $1 \leq i \leq m$, $1 \leq j \leq n$
$\mathsf{A}[i, j]$	component of A, $1 \leq i \leq m$, $1 \leq j \leq n$
$\mathbf{a} \cdot \mathbf{b}$	scalar product of $\mathbf{a}$ and $\mathbf{b}$
$\mathbf{a} \times \mathbf{b}$	vector product of $\mathbf{a}$ and $\mathbf{b}$
$\mathbf{A} : \mathbf{B}$	double contraction of $\mathbf{A}$ and $\mathbf{B}$
$\operatorname{tr} \mathbf{A}$	trace of $\mathbf{A}$
$\mathsf{A}^\top$	transpose of A
$\det \mathsf{A}$	determinant of A
∇	Nabla operator, $\nabla[i] = \partial/\partial x_i$, $i = 1, \ldots, d$
∇a	gradient of a
Δa	Laplacian of a, $\Delta a = \nabla \cdot \nabla a$
$\nabla \cdot \mathbf{a}$	divergence of $\mathbf{a}$
$\nabla \times \mathbf{a}$	curl of $\mathbf{a}$
$\dot{a}, \ddot{a}$	first and second time derivative of $a(t)$
δA	first variation of the functional A
$\hat{f}(s)$	Laplace transform of $f(t)$, $\hat{f}(s) = \int_0^\infty f(t) \exp(st) \, \mathrm{d}t$
$\overline{\Omega}$	closure of the set Ω
$g * h$	convolution $\int_0^t g(t - \tau) h(\tau) \, \mathrm{d}\tau$

Special symbols

(a, b), $[a, b]$	open and closed intervals between a and b
$\langle u, v \rangle$	L_2-scalar product of u and v
$a(u, v)$	bilinear form
$a_t(u, v)$	parametrized bilinear form
a	vector of acceleration coefficients

A	finite element stiffness matrix
Ã	finite element dynamic stiffness matrix
$B_\varepsilon(\mathbf{x})$	d-dimensional ball with center $\mathbf{x}$ and radius ε
B	boundary element mass matrix
c	fluid wave speed
c_1, c_2	compression and shear wave speeds
$\mathcal{C}$	integral free term
C	discretized integral free term
$C^{(r)}$	connectivity matrix of subdomain $\Omega^{(r)}$
d	Cartesian dimension of the problem
E	Young's modulus
f	generalized force term
$\mathbf{f}$	body force vector
f	finite element force vector
f_D, f_N	force vectors due to prescribed Dirichlet and Neumann data
F, G	FETI matrices for the dual problem
g_D, g_N	prescribed Dirichlet and Neumann data
g_{FE}, g_{BE}	finite and boundary element discretized boundary force term
G	Gram determinant
h	mesh width
$H(t)$	Heaviside function
$\mathbf{I}$	identity tensor
$\mathcal{I}$	identity operator
$\mathbf{J}$	Jacobi matrix of coordinate transformation
$J^{(r)}$	indices of subdomains sharing an interface with $\Omega^{(r)}$
$K_j(z)$	modified Bessel function of second kind and j-th order
$\mathcal{K}$	double layer operator
$\mathcal{K}_t$	time-dependent double layer operator
K	discretized double layer operator
$\tilde{\mathsf{K}} := \mathsf{C} + \mathsf{K}$	abbreviation
$\mathscr{K}$	kinetic energy
ℓ	linear momentum
$\ell(v)$	linear form
$\ell(v)$	parametrized linear form
$\log z$	natural logarithm of z
$\mathcal{L}$	elliptic partial differential operator of second order
M	finite element mass matrix
$\mathbf{n}$	unit outward normal vector
$\mathcal{N}_0 f$	Newton potential
$\mathcal{N}_t f$	time-dependent Newton potential
N	basis of null space
$\mathcal{O}(g)$	asymptotic behavior (Landau notation)
p_0, p_{total}, p	equilibrium pressure, total pressure, and pressure fluctuation

q	(acoustic) flux
$q_\Gamma := \mathcal{T}u$	generalized normal derivative
$q_{\Gamma,h}$	approximation of q_Γ
$\mathcal{R}$	zero energy modes
$\mathcal{S}$	Steklov-Poincaré operator
$S_h(\Omega_h)$	finite element space
$S_h(\Gamma_h)$	boundary element space
S_{FE}, S_{BE}	finite and boundary element discretizations of $\mathcal{S}$
t	time, $t \in [0,\infty)$
$t_n := n\Delta t$	time point on time grid
Tr	boundary trace operator
$\mathcal{T}$	generalized conormal derivative (traction operator)
u	unknown function
$u^{(r)}$	restriction of u to $\Omega^{(r)}$
$u^*(\mathbf{x},\mathbf{y})$	fundamental solution
$u_\Gamma := \mathrm{Tr}\,u$	boundary trace of u
$u(0^+)$	limit $\tau \to 0$ of $u(\tau)$ from above
u_0, u_1	prescribed initial states of u and its first time derivative $\dot{u}$
$u_h, u_{\Gamma,h}$	approximation of u and u_Γ
$\mathbf{u}$	displacement field
u	coefficient vector of approximation of u
u_n	coefficients of approximation of u at $t = t_n$
u_I, u_Γ	coefficients of u belonging to the interior and to the boundary of Ω_h
$\mathscr{U}$	potential energy
v	vector of velocity coefficients
$\mathcal{V}$	single layer operator
$\mathcal{V}_t$	time-dependent single layer operator
V	discretized single layer operator
$\mathbf{x}, \mathbf{y}$	points in global coordinates
x_i	i-th coordinate direction, $1 \leq i \leq d$
$\mathbf{x}(\xi)$	coordinate transformation
$\mathbf{x}_\ell^*$	ℓ-th collocation point
α	rigid body mode amplitudes
β, γ	parameters of the Newmark method
$\Gamma := \partial\Omega$	boundary
Γ_D, Γ_N	boundary parts with prescribed Dirichlet and Neumann data
Γ_h	boundary of Ω_h
$\Gamma^{(r)}$	boundary of subdomain $\Omega^{(r)}$
$\Gamma^{(rp)}$	interface shared by $\Omega^{(r)}$ and $\Omega^{(p)}$
Γ_s	skeleton of domain partitioning
$\delta(\mathbf{x})$	Dirac delta distribution
Δt	size of time step

ε	strain tensor
κ	fluid bulk modulus
λ, μ	Lamé constants
λ	Lagrange multiplier
λ_h, λ	approximation of λ and the coefficient vector
ν	Poisson ration
ξ	reference coordinates
Π	potential
$\rho_0, \rho_{total}, \rho$	equilibrium density, total density, and density fluctuation
σ	stress tensor
τ_e	e-th element of a triangulation
φ, ψ	trial functions
χ	CFL number
ω_n	integration weight of convolution quadrature method
ω	rotation tensor
Ω	domain
Ω_h	computational domain
$\Omega^{(r)}$	r-th subdomain
$\Omega^{(M)}, \Omega^{(S)}$	master and slave subdomains

1 INTRODUCTION

The use of numerical approximation methods for the analysis of engineering problems has gained more and more interest in the recent past. The finite element method is clearly the method which is most widely employed in the field of structural mechanics. Among its alternatives, there is the boundary element method which can be basically considered as a numerical approximation scheme of boundary integral representations.

Finite element methods in their current state of development are applicable to various kinds of physical problems, which can be highly nonlinear or exhibit anisotropic and inhomogeneous material behavior. Moreover, standard finite element discretizations of boundary value problems with symmetric positive operators yield symmetric positive definite system matrices which are sparsely populated. Therefore, many efficient solution procedures for these systems of equations have been designed. But finite element methods are commonly restricted to the treatment of bounded domains and often perform weakly in situations where a good resolution of high stress concentrations is required, unless the scheme is adaptive.

The boundary integral representations of boundary value problems can only be established if a fundamental solution for the underlying partial differential operator is available. Therefore, boundary element methods are in principle restricted to a certain class of problems only. The treatment of, for instance, elastoplastic problems requires an enormous additional effort which usually defeats the advantages of the method. Another drawback of the method are the fully populated system matrices which severely restrict the size of applications in terms of their degrees of freedom. Many promising techniques have been developed for a data sparse representation of the system matrix which reduce the numerical complexity of the method. On the other hand, a boundary element solution exactly fulfills the considered partial differential equation inside the domain. Therefore, this method is useful if a high precision of the solution and its derivatives at specific points is required. Moreover, unbounded domains are represented exactly by the boundary integral representation and the method is thus very powerful when problems in media of infinite extent are considered. Especially in the case of dynamic problems, this feature is of great benefit because spurious wave reflections which pollute the solution in case of classical finite element approaches can be excluded. Finally, a great advantage of the method is the fact that only the surface of the considered domain has to be discretized. Especially in the case of complex three-dimensional geometries the volume discretization needed for a finite element approach can be too demanding such that a boundary element method prevails.

In comparison, one can establish the point of view that these two discretization methods, namely finite element and boundary element methods, are rather mutually exclusive, i.e., each performs well where the other one is inappropriate. The conclusion is to exploit this

fact and combine these two methods in such a way that the respective advantages can be used. But care has to be taken in designing a coupled solution strategy where both methods are employed. Each of these approximation schemes has its specific structural peculiarities which complicate the structure of the software. Especially the different characters of the resulting system matrices and the consequently different solution procedures have to be considered carefully. At last, the application of different discretization methods to subdomains with possibly different physical behavior is restrained if the interface discretizations are required to be spatially conforming. If only coincident nodes of the interface discretizations together with equal orders of approximation are possible, a flexible combination of these different methods is impeded significantly.

In this work, a coupling strategy is developed which employs the approximation schemes of finite and boundary element methods in a very flexible manner. The range of each method is exclusively restricted to each subdomain and the coupling is established by means of Lagrange multipliers. Therefore, the respective characteristics of each method can be handled independently. Moreover, due to the use of Lagrange multiplier fields the treatment of nonconforming interface discretizations is straightforward.

1.1 State of the Art

It follows a brief overview of the current state of research in the fields touched in this work. This list is of course not intended to be exhaustive. In order to improve legibility, the following is arranged in paragraphs according to specific subtopics which possibly causes overlaps in the references.

Finite Element Methods. For the time being, the method of finite elements is being used for the numerical solution of boundary value problems for more about five decades. It dominates in the field of structural mechanics but also in other engineering disciplines and sciences it is the method of choice for numerical approximations. The textbooks of Bathe [6] and Hughes [49] provide good introductions to the method itself and several specializations of it. Strang and Fix [110] were among the first to give a concise mathematical analysis of the method. Whereas this book is basically concerned with the classical finite element method, the concepts of *h*- and *p*-adaptivity are given for instance by Szabó and Babuška [112]. Some physical problems, as for instance incompressible elasticity or Stokes flow (see Brezzi and Fortin [10] or Bathe [6]), are formulated by a coupled set of partial differential equations or in combination with algebraic equations and their discretization leads to mixed finite element methods. The mathematical analysis of these methods can be found in the book of Braess [9] among others.

Finite element methods are not only applicable to elliptic boundary value problems but also to initial boundary value problems, e.g., the acoustic wave equation or the elastodynamic system, which are the two dynamic models considered in this work. The classical approach

to such problems is to use the finite element framework for the spatial discretization of the dynamic problem such that a system of ordinary differential equations is obtained. This can then be tackled by time integration methods like the famous Newmark method [72]. A survey of dealing with initial boundary value problems by means of finite elements and time integration methods is given by Hughes [49] and Hulbert [50]. At last, it has to be emphasized that finite element methods are established for the treatment of nonlinear problems as for instance plasticity or large deformations, see Simo and Hughes [101].

In this work it is not intended to make use of the latest developments in finite element research but employ the method in its classical formulation. Here, the main interest does not lie in the method itself but in its combination with boundary element methods for the solution of coupled problems. However, in view of the numerical treatment of more complicated physical phenomena, the classical finite element method used in the following could be easily replaced by a more enhanced and up-to-date version of it. Especially, the use of fast iterative solvers (e.g., preconditioned conjugate gradient methods) would greatly reduce the numerical complexity of the finite element part of this work. An overview of such algorithms for sparse finite element system matrices is given by Saad [95].

Boundary Element Methods. Another numerical approximation method, almost as old as the finite element method, is the boundary element method which is based on boundary integral representations of the considered boundary value problem. Despite their obvious benefits of reducing the computational domain by one dimension and the harmonic extension to the interior of the domain, boundary element methods have been living a shadowy existence in comparison to the finite element method. This is mainly due to the numerical difficulties with singular integrals and fully populated system matrices. An engineering point of view of the underlying complexity is given by Watson [117]. Nevertheless, the method has survived as a niched method especially useful for several problems such as the treatment of unbounded domains. A good engineering introduction to the method is the book of Gaul et al. [33]. A thorough mathematical analysis, on the other hand, can be found in the books of Steinbach [107] and Sauter and Schwab [96]. Hsiao and Wendland [48] provide an overview of the mathematical state of the art of boundary element analysis. Among other variants, the collocation and the Galerkin method are the most prominent numerical techniques applied to boundary integral equations in order to obtain systems of simultaneous equations. Whereas the former lacks mathematical rigor but still exists as the most direct approach in the engineering community, the latter Galerkin method gains more and more interest also outside the mathematical community because it does not only come up with convergence proofs but also with system matrices which are manageable by iterative solvers in a robust way. In this work, a modified collocation approach is chosen which can be found for instance in the thesis of Steinbach [103], where comparisons between Galerkin and collocation methods are given, too.

Boundary element methods have also been successfully applied to dynamic problems as for instance by Mansur [70] who made use of time-domain fundamental solutions. By

means of the convolution quadrature method of Lubich [67, 68], Laplace domain fundamental solutions are sufficient means for the treatment of time-domain problems. This approach has been used by Schanz and Antes [99, 100] and extended by Schanz [98] to poroelastodynamic wave propagation. A survey of time-domain boundary element methods is given in the publication of Costabel [13]. The convolution quadrature method is the method of choice in this work for the used time-domain boundary element method.

It has to be added that so-called fast boundary element methods have made an enormous advance in the recent past. Among those are the fast multipole method going back to the early works of Greengard and Rokhlin [39] (see also Greengard [38] and the overview of Nishimura [73]) and the panel clustering of Hackbusch and Nowak [43]. Moreover, the adaptive cross approximation of Bebendorf and Rjasanow [7] provides an efficient setup of a data sparse matrix representation leading to fast solution techniques. The algebra of such data sparse matrix representations has been developed by Hackbusch [42].

The fast multipole algorithm has been successfully used by Of [74] for elastostatics and by Fischer and Gaul [31] for acoustics. Finally, the recent book of Rjasanow and Steinbach [94] gives many details on these fast boundary element methods and shows several applications of the adaptive cross approximation.

The boundary element part in this work plays a larger role than the finite element method simply due to its significantly more involved implementation. Nevertheless, it has not been the primal aim to develop a boundary element method according to the latest mathematical standards but to use it in the coupling algorithm. As before, the formulations are here such that the used nonsymmetric collocation approach can be replaced in a future work by a more robust symmetric Galerkin method without altering the coupling framework. The mentioned fast boundary element methods could be incorporated in the same manner. Moreover, preconditioned iterative solution procedures, as presented, for instance, by Steinbach [104], could be introduced for the acceleration of the presented boundary element solver.

Coupled solution strategies. The idea of spatially subdividing the domain under consideration has a long history, see, for instance, the book of Przemieniecki [87] for the concept of substructuring or the book of Toselli and Widlund [114] for a mathematical overview of non-overlapping Schwarz methods. The partitioning could be physically motivated or aimed to increase the efficiency of the solution procedure or both. Especially the here presented combination of finite and boundary element methods is commonly carried out for both reasons. The underlying physics might require the use of boundary element methods (unbounded domains, high stress resolution, etc.) but most likely more efficiency is gained by using a finite element method in regions where the boundary element method is not required. On the other hand, local nonlinearities might demand the use of finite elements. This idea of making the optimal use of both methods goes back to Zienkiewicz et al. [121] and has since then been often applied to coupled problems. The engineering works of von Estorff and Hagen [23] and of Fischer and Gaul [31] are just two of many examples for this

approach. On the other hand, the monograph of Steinbach [106] and the overview article of Stephan [108] contain the mathematical background of the coupling of boundary with finite element methods.

The former of these references also falls into the context of domain decomposition methods which are commonly understood as efficient solution procedures by means of partitioning. At the beginning of the last decade, Farhat and Roux [28, 29] introduced the method of finite element tearing and interconnecting (FETI) which provides a robust and parallel solution algorithm. This method has been modified to fourth order and dynamic problems by Farhat et al. [24]. It has been transferred to boundary element coupling by Langer and Steinbach [61] and by the same authors to the combination of finite and boundary element methods [62]. An overview of the mathematical analysis of FETI can be found in the book of Toselli and Widlund [114]. The extension of the original FETI idea to an all-floating variant is given by Of [74], but in the context of boundary element methods. Similarly, Dostál et al. [20] have developed such an extension for the original FETI method.

FETI methods and their relatives are commonly designed for matching interface discretizations, i.e., spatial discretizations which have matching nodes and approximation orders across the interfaces of the partitioning. A relaxation of this constraint became famous in the context of so-called mortar methods, see, e.g., the monograph of Wohlmuth [119].

In this work, the FETI method is chosen as a framework within which the considered numerical approximation methods can be combined in the most independent fashion. Moreover, without changing the structure of the method, nonmatching interface discretizations are allowed for by changing the approximation of the Lagrange multiplier fields. Such a combination of the mortar methods with the FETI-framework has been proposed for instance by Stefanica [102].

1.2 One-dimensional Example

This section conveys the basic concepts of the used numerical methods and their combined application to the case of a simple rod subjected to an axial force. At first the static and then a dynamic situation is regarded. Finally, the dynamic case for an unbounded rod is considered. The explanations are condensed to some important items and are not intended to be exhaustive.

1.2.1 Static case

In figure 1.1, a simple problem from basic structural analysis is given. A rod is fixed at one end and subjected to an axial force F at its other end. Under the assumptions of small deformations and constant stiffness, the governing equation is

$$-EAu''(x) = 0\,. \tag{1.1}$$

$u = 0$
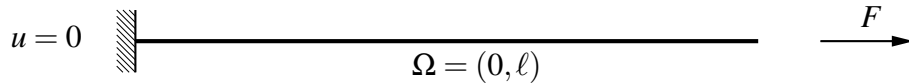
Figure 1.1: Rod loaded with an axial force.

$\Omega = \{x \mid 0 < x < \ell\}$ is the domain of the problem and boundary points $x = 0$ and $x = \ell$. EA is the extensional stiffness and $N(x) = EAu'(x)$ denotes the axial force. The boundary conditions are

$$u(0) = 0 \quad \text{and} \quad N(\ell) = F.$$

The analytical solution for the displacement function $u(x)$ is easily obtained by integration

$$u(x) = \frac{F}{EA}x.$$

Now, two different numerical approaches for the solution to the given problem are considered.

Finite element method.   The simplest approach is the use of finite elements with piecewise linear shape functions. One such element with its nodal displacements and forces is shown in figure 1.2. In the given case, the element matrix relation then becomes

$$\frac{EA}{h} \begin{pmatrix} 1 & -1 \\ -1 & 1 \end{pmatrix} \begin{pmatrix} u_1 \\ u_2 \end{pmatrix} = \begin{pmatrix} F_1 \\ F_2 \end{pmatrix}$$

with the element length h. The chosen linear approximation yields an exact solution to the given problem, as long as the right hand side of equation (1.1) is zero.
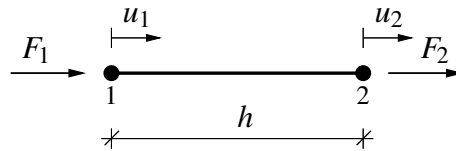
Figure 1.2: Finite element for the rod.

Boundary integral method.   Note that for one-dimensional problems the term *boundary element method* is not really applicable for the obvious reason that the boundary is made up of two points only and there is no need for discretization. Even the term *boundary integral* is inauspicious since due to the same reason the integration reduces to a point evaluation. Nevertheless, it will be kept for the sake of distinction.

The following results are according to the lecture notes of Antes [4] (see also the book of Hartmann [45]). The solution to the differential equation (1.1) with a unit point load at y is the so-called fundamental solution

$$u^*(x, y) = -\frac{1}{2EA}|y - x|.$$

The corresponding axial force solution is then

$$N^*(x,y) = EA\frac{\partial}{\partial y}u^*(x,y) = \frac{1}{2} - H(y-x)$$

with the Heaviside function $H(x)$, $H(x) = 0$ for $x < 0$ and $H(x) = 1$ for $x > 0$. By means of these functions the axial displacement $u(x)$ inside the rod can be expressed by the representation formula

$$u(x) = [u^*(x,y)N(y)]_{y=0}^{\ell} - [N^*(x,y)u(y)]_{y=0}^{\ell} \, .$$

Letting x tend to the limits 0 and ℓ yields a relation using boundary values only

$$\begin{pmatrix} u(0) \\ u(\ell) \end{pmatrix} = \frac{\ell}{2EA}\begin{pmatrix} 0 & -1 \\ 1 & 0 \end{pmatrix}\begin{pmatrix} N(0) \\ N(\ell) \end{pmatrix} + \frac{1}{2}\begin{pmatrix} 1 & 1 \\ 1 & 1 \end{pmatrix}\begin{pmatrix} u(0) \\ u(\ell) \end{pmatrix},$$

where the limits of the Heaviside function $H(x)$ have been taken from the right and the left side of the discontinuity, $\lim_{x\to 0^+} H(x) = 1$ and $\lim_{x\to 0^-} H(x) = 0$, respectively. Rearranging the terms of the above equation gives

$$\frac{\ell}{2EA}\begin{pmatrix} 0 & -1 \\ 1 & 0 \end{pmatrix}\begin{pmatrix} N(0) \\ N(\ell) \end{pmatrix} = \frac{1}{2}\begin{pmatrix} 1 & -1 \\ -1 & 1 \end{pmatrix}\begin{pmatrix} u(0) \\ u(\ell) \end{pmatrix}.$$

Solving this equation for the axial forces $[N(0), N(\ell)]^\top$ and using the relation between internal axial forces and nodal forces at the boundary points

$$F_0 = -N(0) \quad \text{and} \quad F_\ell = N(\ell),$$

the map from boundary displacements to nodal forces is

$$\frac{EA}{\ell}\begin{pmatrix} 1 & -1 \\ -1 & 1 \end{pmatrix}\begin{pmatrix} u_0 \\ u_\ell \end{pmatrix} = \begin{pmatrix} F_0 \\ F_\ell \end{pmatrix}.$$

Note the equivalence between this expression and the finite element matrix equation resulting for one element for the whole rod, i.e., $h = \ell$.

Two-domain formulation. The given problem is now subdivided in two subdomains Ω_1 and Ω_2 each of equal length $H = \ell/2$ as indicated in figure 1.3. The left subdomain Ω_1
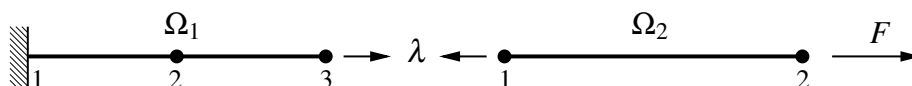

Figure 1.3: Division in 2 subdomains of the statically loaded rod.

is discretized with two finite elements of length $h = H/2 = \ell/4$ and the right subdomain is treated by the above presented boundary integral formulation. Ω_1 has two degrees of

freedom, $u_2^{(1)}$ and $u_3^{(1)}$, where the former belongs to the interior of the subdomain and the latter to its right boundary. Note that $u_1^{(1)}$ is not a degree of freedom but prescribed with zero due to the given boundary conditions. The right subdomain has two degrees of freedom, $u_1^{(2)}$ and $u_2^{(2)}$, both of course on the boundary. In both subdomains, equation (1.1) has to hold. In addition, the solution has to obey the interface conditions

$$u_3^{(1)} = u_1^{(2)} \quad \text{and} \quad N_3^{(1)} + N_1^{(2)} = 0,$$

which are the continuity of the displacement field and the equilibrium at the interface, respectively. These conditions will be incorporated by means of a Lagrange multiplier λ, which - physically speaking - is the interface force. The system of equations for Ω_1 now reads

$$\frac{4EA}{\ell} \begin{pmatrix} 2 & -1 \\ -1 & 1 \end{pmatrix} \begin{pmatrix} u_2^{(1)} \\ u_3^{(1)} \end{pmatrix} = \begin{pmatrix} 0 \\ \lambda \end{pmatrix}$$

and for Ω_2

$$\frac{2EA}{\ell} \begin{pmatrix} 1 & -1 \\ -1 & 1 \end{pmatrix} \begin{pmatrix} u_1^{(2)} \\ u_2^{(2)} \end{pmatrix} = \begin{pmatrix} -\lambda \\ F \end{pmatrix}.$$

These two systems can be assembled in a global system of equations with local degrees of freedom $u_i^{(j)}$ and the Lagrange multiplier λ

$$\begin{pmatrix} 8EA/\ell & -4EA/\ell & & & \\ -4EA/\ell & 4EA/\ell & & & -1 \\ & & 2EA/\ell & -2EA/\ell & 1 \\ & & -2EA/\ell & 2EA/\ell & \\ & -1 & 1 & & \end{pmatrix} \begin{pmatrix} u_2^{(1)} \\ u_3^{(1)} \\ u_1^{(2)} \\ u_2^{(2)} \\ \lambda \end{pmatrix} = \begin{pmatrix} 0 \\ 0 \\ 0 \\ F \\ 0 \end{pmatrix},$$

where the zero entries are not shown. The additional last line of this system ensures the continuity of the displacements at the interface. The direct solution of this system gives as expected the nodal values of the exact solution.

Partitioned solution. When solving the above equation, one will make use of the separate local systems of equations. Solving the first system (the finite element approach) for the interface displacement gives

$$u_3^{(1)} = \frac{\ell}{2EA} \lambda.$$

The second system (the boundary integral approach) cannot be directly solved for the interface displacement. Trying to eliminate $u_2^{(2)}$ from the system yields the relation

$$\lambda = F.$$

Obviously, the right subdomain does not have any displacement boundary conditions and, therefore, the local solution to equation (1.1) is not unique. Any rigid body motion could

be added to the solution without violation of the force boundary condition. Nevertheless, the previous result $\lambda = F$ is the *solvability condition* of the local problem. Moreover, such a subdomain, whose local problem is not uniquely solvable, is commonly called *floating subdomain* [29].

From linear algebra it is known that the solution to the right subsystem can be expressed by

$$\begin{pmatrix} u_1^{(2)} \\ u_2^{(2)} \end{pmatrix} = \frac{\ell}{2EA} \begin{pmatrix} 1 & 0 \\ 0 & 0 \end{pmatrix} \begin{pmatrix} -\lambda \\ F \end{pmatrix} + \begin{pmatrix} 1 \\ 1 \end{pmatrix} \alpha \,.$$

Here, $(1, 1)^\top$ contains the rigid body mode of the system and α is the unknown amplitude of that mode. The matrix on the right hand side is a generalized inverse of the singular system matrix and the vector $(1, 1)^\top$ represents its kernel. Hence, the interface displacement of subdomain Ω_2 becomes

$$u_1^{(2)} = -\frac{\ell}{2EA}\lambda + \alpha \,.$$

Using the expressions for the local interface displacements together with the continuity equation $-u_3^{(1)} + u_1^{(2)} = 0$ and the solvability condition $\lambda = F$, results in a system for the unknown Lagrange parameter and the rigid body mode amplitude

$$\begin{pmatrix} -\ell/EA & 1 \\ 1 & 0 \end{pmatrix} \begin{pmatrix} \lambda \\ \alpha \end{pmatrix} = \begin{pmatrix} 0 \\ F \end{pmatrix} \,.$$

Once this system is solved, the local problems are uniquely defined and every degree of freedom can be determined. In this simple case, one gets

$$\lambda = F \quad \text{and} \quad \alpha = \frac{F\ell}{EA} \,,$$

where λ has the value of the axial force at the interface. By means of these values, the interface displacements become

$$u_3^{(1)} = u_1^{(2)} = \frac{F\ell}{2EA}$$

corresponding to the exact solution. The computation of the remaining degree of freedom, $u_2^{(1)} = F\ell/4EA$, is then straightforward.

1.2.2 Dynamic case — bounded domain

The example shown in figure 1.4 is similar to the static case, but now the load is applied instantaneously after $t = 0$ and held constant. Therefore, $F(t) = F_0 H(t)$ with the Heaviside function $H(t)$ as previously introduced. Assuming again small deformations, a constant Young's modulus E, and a constant mass density ρ, the governing equation is

$$\ddot{u}(x,t) - c^2 u''(x,t) = 0 \,, \tag{1.2}$$

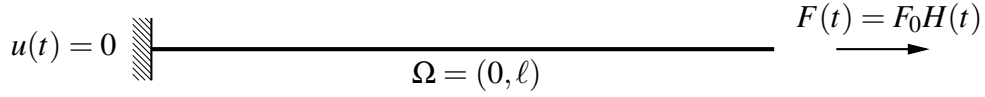$$u(t) = 0 \qquad\qquad \Omega = (0,\ell) \qquad\qquad F(t) = F_0 H(t)$$

Figure 1.4: Rod loaded with a unit step force.

where $c^2 = E/\rho$. c is the wave velocity, the speed at which a disturbance propagates through the rod. Note the notational difference between the temporal derivative $\dot{u}$ and the spatial derivative u'. The solution is now sought in the domain $\Omega = \{x \,|\, 0 < x < \ell\}$ and the time interval $(0,\infty)$. This equation is equipped with boundary conditions

$$u(0,t) = 0 \quad \text{and} \quad N(\ell,t) = F_0 H(t) \quad \forall t \in (0,\infty)$$

(remember $N(x,t) = EAu'(x,t)$) and vanishing initial conditions

$$u(x,0) = 0 \quad \text{and} \quad \dot{u}(x,0) = 0 \quad \forall x \in \Omega.$$

The solution to this initial boundary value problem is given in equation (B.1) of the appendix B.1 and is shown in figure B.1(a). Note that this function resembles a D'Alembert solution, since it is a linear combination of functions describing disturbances propagating in positive and negative x-direction, i.e., $f(ct - x)$ and $f(ct + x)$, respectively. The solution for the axial force $N(x,t)$ is then obtained by taking the derivative.

Finite element method.   The treatment of this dynamic problem with a classical finite element approach leads to the semi-discrete system of equations [49]

$$\frac{\rho A h}{6}\begin{pmatrix} 2 & 1 & & & \\ 1 & 4 & 1 & & \\ & & \ddots & & \\ & & 1 & 4 & 1 \\ & & & 1 & 2 \end{pmatrix}\begin{pmatrix} \ddot{u}_1 \\ \ddot{u}_2 \\ \vdots \\ \ddot{u}_{N-1} \\ \ddot{u}_N \end{pmatrix} + \frac{EA}{h}\begin{pmatrix} 1 & -1 & & & \\ -1 & 2 & -1 & & \\ & & \ddots & & \\ & & -1 & 2 & -1 \\ & & & -1 & 1 \end{pmatrix}\begin{pmatrix} u_1 \\ u_2 \\ \vdots \\ u_{N-1} \\ u_N \end{pmatrix} = \begin{pmatrix} f_1 \\ f_2 \\ \vdots \\ f_{N-1} \\ f_N \end{pmatrix}$$

and all vector coefficients are functions of time. A short notation has the form

$$\mathsf{M}\ddot{\mathsf{u}}(t) + \mathsf{A}\mathsf{u}(t) = \mathsf{f}(t)$$

with the mass matrix M and the stiffness matrix A which is already known from the static problem. Such systems of ordinary differential equations are commonly solved by time-stepping schemes. Here, a standard Newmark method with a displacement-based implementation is used (parameters $\beta = 0.25$ and $\gamma = 0.5$) and yields at every time step i in abbreviated form the system

$$\tilde{\mathsf{A}}\mathsf{u}_i = \tilde{\mathsf{f}}_i.$$

Commonly, the computed unknowns u_i are then used to calculate the velocity and acceleration coefficients for the current time step. All these are, in turn, used to compute the new pseudo force term $\hat{\mathsf{f}}_{i+1}$ and so forth. Hence, the history information and the inertia terms are entirely contained in the current right hand side $\hat{\mathsf{f}}_i$.

Boundary integral method. The fundamental solution of the equation (1.2) for the displacements and the corresponding axial forces are given by (cf. Antes [3])

$$u^*(x,y,t,\tau) = \frac{1}{2\rho Ac} H(c|t-\tau| - |y-x|)$$

$$N^*(x,y,t,\tau) = -\frac{1}{2}\delta(t-\tau - |y-x|/c)\operatorname{sign}(y-x).$$

They represent the responses to a point load at location y and time τ. $\delta(x)$ denotes the Dirac delta distribution and $\operatorname{sign}(x)$ is simply the sign of the argument. By means of these functions, the dynamic representation formula can be established

$$u(x,t) = \int\limits_0^t [u^*(x,y,t-\tau)N(y,\tau) - N^*(x,y,t-\tau)u(y,\tau)]_{y=0}^\ell \, d\tau,$$

which comprises a convolution in time. Using the properties of the Heaviside function $H(t)$ and the Dirac distribution $\delta(x)$, this relation can be used to express the time behavior of the boundary displacements

$$u(0,t) = u(\ell, t - \ell/c) + \frac{1}{\rho Ac}\left[\int\limits_0^{t-\ell/c} N(\ell,\tau)\,d\tau - \int\limits_0^t N(0,\tau)\,d\tau\right]$$

$$u(\ell,t) = u(0, t - \ell/c) + \frac{1}{\rho Ac}\left[\int\limits_0^t N(\ell,\tau)\,d\tau - \int\limits_0^{t-\ell/c} N(0,\tau)\,d\tau\right]. \tag{1.3}$$

It is implicitly assumed that the problem has a quiescent past, i.e., $u(t) = 0$ and $N(t) = 0$ for $t \le 0$. For the given problem, these equations could be solved analytically and would yield the exact solution as shown above. For simplicity, a trapezoidal rule with step size Δt for the numerical solution of the integrals is used instead and gives the system of equations for the i-th time step

$$\frac{2\rho Ac}{\Delta t}\begin{pmatrix}1 & 0 \\ 0 & 1\end{pmatrix}\begin{pmatrix}u_{i,0} \\ u_{i,\ell}\end{pmatrix} = \begin{pmatrix}F_{i,0} \\ F_{i,\ell}\end{pmatrix} + \begin{pmatrix}F_{i-1,0} \\ F_{i-1,\ell}\end{pmatrix} + \frac{2\rho Ac}{\Delta t}\begin{pmatrix}1 & 0 \\ 0 & 1\end{pmatrix}\begin{pmatrix}u_{i-1,0} \\ u_{i-1,\ell}\end{pmatrix}$$
$$+ \frac{2\rho Ac}{\Delta t}\begin{pmatrix}0 & 1 \\ 1 & 0\end{pmatrix}\begin{pmatrix}u_{i-n_c,0} - u_{i-1-n_c,0} \\ u_{i-n_c,\ell} - u_{i-1-n_c,\ell}\end{pmatrix} + \begin{pmatrix}0 & 1 \\ 1 & 0\end{pmatrix}\begin{pmatrix}F_{i-n_c,0} + F_{i-1-n_c,0} \\ F_{i-n_c,\ell} + F_{i-1-n_c,\ell}\end{pmatrix}.$$

The axial force N has been again replaced by the corresponding nodal forces F_0 and F_ℓ. A remark on the used notation has to be made. n_c is the number of time steps until the time point ℓ/c, at which the disturbance has traveled once through the whole rod. Therefore, the notation $()_{i-n_c}$ simply denotes a shift of the index i by the number n_c. According to the assumption of a quiescent past, values with an index less than zero can be neglected. Obviously, the subscripts 0 and ℓ refer to the boundary points $x = 0$ and $x = \ell$. A shorter writing for the above is given by

$$\mathsf{S}\mathsf{u}_i = \mathsf{f}_i + \mathsf{h}_i,$$

i.e., the boundary displacements are mapped on the nodal forces plus some history term. Note that S resembles a Dirichlet-to-Neumann map and will reappear in the later presented coupling algorithms in chapter 4.

Two-domain formulation.   As in the static case, the dynamic problem will be formulated in two subdomains. One will be discretized by finite elements and the other handled by the described boundary integral method. Again a Lagrange multiplier function $\lambda(t)$ is

$$u(t) = 0 \qquad \overset{\Omega_1}{\underset{1 \quad 2 \quad 3 \quad 4 \quad \dots \quad N}{\bullet\!\!-\!\!\bullet\!\!-\!\!\bullet\!\!-\!\!\bullet}} \longrightarrow \lambda \longleftarrow \underset{1}{\bullet}\overset{\Omega_2}{-\!\!-\!\!-\!\!-\!\!-\!\!-}\underset{2}{\bullet} \overset{F(t) = F_0 H(t)}{\longrightarrow}$$
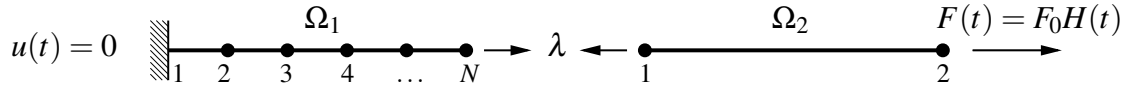
Figure 1.5: Division in 2 subdomains of the dynamically loaded rod.

used to ensure the interface conditions of continuity and equilibrium. Figure 1.5 shows the constellation, where the left side is discretized with $N-1$ finite elements. The global system of equations then becomes for the i-th time step

$$\begin{pmatrix} \tilde{\mathsf{A}} & 0 & \mathsf{B} \\ 0 & \mathsf{S} & \mathsf{C} \\ \mathsf{B}^\top & \mathsf{C}^\top & 0 \end{pmatrix} \begin{pmatrix} \mathsf{u}_i^{(1)} \\ \mathsf{u}_i^{(2)} \\ \lambda_i \end{pmatrix} = \begin{pmatrix} \tilde{\mathsf{f}}_i \\ \mathsf{f}_i + \mathsf{h}_i \\ 0 \end{pmatrix} . \tag{1.4}$$

The matrices $\mathsf{B} = (0, 0, \dots, 0, -1)^\top$ and $\mathsf{C} = (1, 0)^\top$ are used for the interface conditions. The partitioned solution of the local problems is equivalent to the static case with the important difference that one does not have to take care of floating subdomains because the local problems are uniquely solvable due to the initial conditions of the system. Obviously, equation (1.2) has no rigid body modes as trivial solutions.

Example.   The given problem has been solved setting all material and system parameters to one, i.e., $E = A = \rho = \ell = 1$. The units are omitted for the sake of simplicity. Two choices of spatial discretization and time steps have been made. Set 1 refers to 10 finite elements of size $h_1 = 0.1$ and a time step $\Delta t = 0.05$, whereas set 2 refers to 100 finite elements of size $h_2 = 0.01$ and $\Delta t = 0.005$. Obviously, the boundary integral approach does not need any spatial discretization and the time step sizes are chosen of equal size for the finite element and boundary integral methods. Figure 1.6 shows the computed solutions for these two sets. The displacement is displayed for the right end, $x = \ell$, and at the interface, $x = \ell/2$, in the left picture 1.6(a). The axial force is shown for the left end at $x = 0$ and the interface in the right picture 1.6(b). Confer the analytical solutions given in figures B.1(a) and B.1(b) to identify the corresponding displacement and force curves.
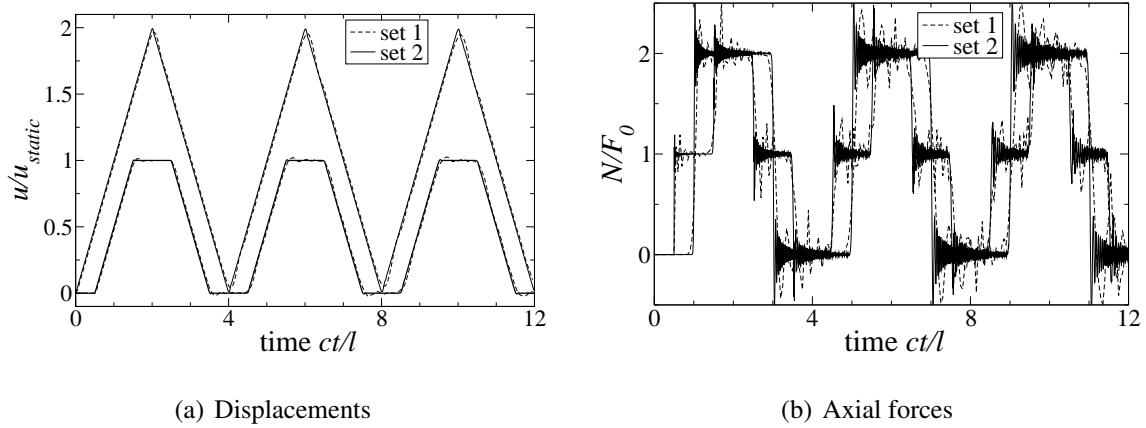
(a) Displacements

(b) Axial forces

Figure 1.6: Computed solution for the displacement at points $x = \ell$ and $x = \ell/2$ and for the axial force at points $x = 0$ and $x = \ell/2$.

1.2.3 Dynamic case — unbounded domain

Here, a dynamic load is applied to an semi-infinite rod as shown in figure 1.7. The considered domain is now $\Omega = \{x \in \mathbb{R} : x < 0\}$ and the load is applied at the position $x = 0$. This problem is also governed by equation (1.2) but the boundary conditions are different.
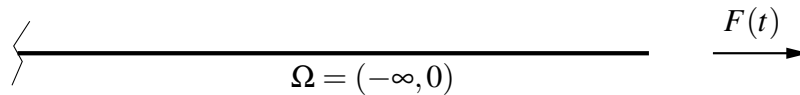

Figure 1.7: Semi-infinite rod loaded with a unit step force.

They now read

$$N(0,t) = F(t) \quad \text{and} \quad \lim_{x \to -\infty} u(x,t) = 0$$

and hold for all times $t \in (0, \infty)$. The latter of these two conditions is physically reasonable because the effect of the applied load should not affect any point at an infinite distance. Moreover, this reasoning also implies that

$$\lim_{x \to -\infty} N(x,t) = 0.$$

The finite element discretization of this problem remains the same as in the previous case of the bounded rod. Clearly, a pure finite element approach cannot be suitable because the discretization has to be truncated at a certain point and this causes unphysical reflections of the wave traveling to infinity. The capability of the presented boundary integral method to treat unbounded domains is shown in the following.

Boundary integral method. Consider again the boundary expressions (1.3) and let the length ℓ get arbitrarily large. Then the displacement at $x = 0$ becomes with vanishing

displacements and axial force for $x \to -\infty$

$$u(0,t) = \frac{1}{\rho A c} \int_0^t N(0,\tau)\,\mathrm{d}\tau.$$

The analytical integration of this expression directly yields the desired solution of the dynamic problem of the unbounded rod. A numerical approach is given by using a trapezoidal rule with step size Δt to approximate this integral and the following scheme is thus obtained

$$\frac{2\rho A c}{\Delta t} u_{i,0} = F_{i,0} + F_{i-1,0} + \frac{2\rho A c}{\Delta t} u_{i-1,0}.$$

This expression gives an approximation for the displacement $u(0, i\Delta t)$ at $x = 0$ at the time point $t = i\Delta t$.

Example. The two-domain formulation of the previous bounded case is repeated for the unbounded rod with the difference that the right subregion $\Omega_2 = (-0.5, 0)$ is discretized by $N - 1$ finite elements and the remaining unbounded subregion $\Omega_1 = (-\infty, -0.5)$ is treated by the boundary integral method, compare figure 1.5. Furthermore, the applied load is now the impulse

$$F(t) = H(t - 0.1\, c/\ell) - H(t - 0.2\, c/\ell).$$

The analytical solution for such a load can be easily obtained by the superposition principle using the analytical solution for the step function given in appendix B.1. The two-domain formulation (1.4) can be directly transferred to this situation and its solution is given below. The sets 1 and 2 are the same as before, i.e., set 1 refers to 10 finite elements and $\Delta t = 0.05$ whereas set 2 represents 100 finite elements with a time step $\Delta t = 0.005$.

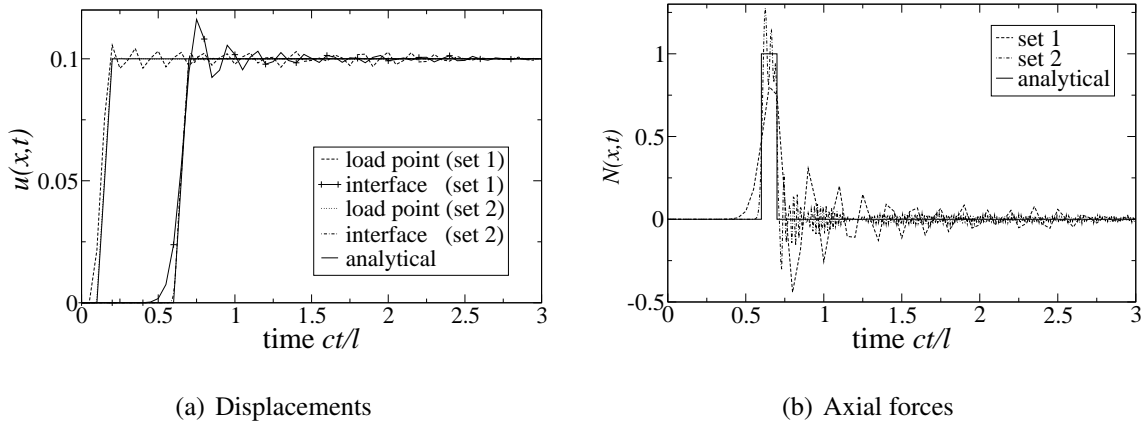(a) Displacements   (b) Axial forces

Figure 1.8: Computed solution for the displacement of the load point at $x = 0$ and of the interface at $x = -0.5$ and for the axial force at the interface.

The numerical solutions are shown in figure 1.8. The displacement results in figure 1.8(a) show a good agreement with the analytical solution for both sets. Especially, the curves

for set 2 are close the exact solution. The outcome for the axial force at the interface, on the other hand, is significantly worse as shown in figure 1.8(b). The spurious oscillations occurring at the jumps at $t = 0.6\ell/c$ and $t = 0.7\ell/c$ do not rapidly decay which is a typically feature of the Newmark method for the chosen parameters $\beta = 0.25$ and $\gamma = 0.5$. The method is unconditionally stable and has second order accuracy but does not have any numerical dissipation [49]. The problem can be alleviated by choosing other parameters and sacrificing one order of accuracy.

1.3 Outline

The remainder of this work is organized as follows. In **chapter 2**, the mathematical models of the acoustic wave equation and the elastodynamic system are introduced together with their static counterparts of the Poisson equation and elastostatics. Moreover, the variational principles and boundary integral representations are given in this chapter, which provide the basis for the numerical approximation methods used in this work. It concludes with some remarks on problems on unbounded domains.

Chapter 3 is then dedicated to approximation methods. At first, finite and boundary element methods are shown as variants of spatial discretizations. Then, the temporal discretizations follow in form of the Newmark method and the convolution quadrature method. The chapter is closed by details on the numerical integration needed for the computation of the matrix coefficients and, finally, the direct solution routines for the systems of algebraic equations resulting from these approximations are presented.

The theoretic part of this work is concluded by **chapter 4** on the coupled solution strategy. It begins with a general section on the notation and some variational principles. After introducing Dirichlet-to-Neumann maps in the continuous and discrete settings, the FETI framework is outlined with emphasis on floating subdomains. The treatment of nonmatching interfaces ends this chapter.

In **chapter 5**, results of some verification tests are presented first for the numerical analysis with either finite or boundary element methods in a single domain. Then these examples are carried over to analyses with various coupled approaches. The results of the static and dynamic analysis of an individual footing on an elastic halfspace are given in the end of this chapter.

Finally, this work is concluded by **chapter 6** with a short summary of the presented methods which is followed by an outlook on future work in this field. Special emphasis is placed on recollecting the several weak points which are pointed out throughout the chapters 2 to 4 in the form of remarks.

2 WAVE EQUATIONS FOR ACOUSTICS AND ELASTODYNAMICS

In this chapter, the basic equations are introduced that will be solved numerically by the later introduced methods. Basically, these are the acoustic wave equation with its static correspondence, the Poisson equation, and the elastodynamic system with the elastostatic system for the static case. The notion of boundary and initial boundary value problems is raised in the following in order to embed the presented equations into complete mathematical statements. Then variational principles and boundary integral representations are brought up being the necessary tools for the later introduced numerical methods.

All considered physical models are based on the assumption that the changes in the state variable (the pressure of the fluid or the displacement field of the solid) are relatively small. Therefore, higher order terms can be neglected and the resulting equations are linear. Hence, it suffices to describe the physical phenomena (e.g., kinematics and balance laws) in the reference configuration only. Moreover, a Cartesian coordinate system will be fully adequate for the spatial description. The position x in the d-dimensional Euclidean point space, $d = 1$, 2, or 3, will be identified by the position vector $\mathbf{x} \in \mathbb{R}^d$, where an arbitrary but fixed reference point has been chosen as the origin (cf. Ogden [75] for a more profound discussion on point and vector spaces). This position vector has the components x_i with the indices $i = 1, \ldots, d$.

2.1 The Acoustic Fluid

The considered fluid is assumed to be homogeneous and compressible. It is at rest in the reference configuration and gravity effects are neglected. Under these assumptions, a fluid is termed *acoustic fluid* [76]. A further classification is made between the *inviscid* and the *dissipative* acoustic fluid. The former does not resist to shear stresses whereas the latter reacts due to viscosity. In the following, the fluid is assumed to be inviscid. The derivation of the acoustic wave equation presented here is similar to the one-dimensional version of Feynman [30]. Alternatively, one can directly start from the continuity equation as shown by Gaul et al. [33].

The motion of the fluid is described by the displacement field $\mathbf{u}(\mathbf{x}, t)$ which is a function of position $\mathbf{x}$ and time t. It has a mass density which can be decomposed into its equilibrium state ρ_0 ($\rho_0 > 0$) and the fluctuation around this state $\rho(\mathbf{x}, t)$, which is relatively small

$$\rho_{total}(\mathbf{x}, t) = \rho_0 + \rho(\mathbf{x}, t) \qquad \text{with} \qquad \max_t |\rho(\mathbf{x}, t)| \ll \rho_0 \quad \forall \mathbf{x}. \tag{2.1}$$

Using a similar decomposition for the hydrostatic pressure

$$p_{total}(\mathbf{x},t) = p_0 + p(\mathbf{x},t) \qquad \text{with} \qquad \max_t |p(\mathbf{x},t)| \ll p_0 \quad \forall \mathbf{x} \tag{2.2}$$

with the equilibrium pressure p_0 and the fluctuation $p(\mathbf{x},t)$, the stress fluctuation in the inviscid fluid is represented by

$$\boldsymbol{\sigma}(\mathbf{x},t) = -p(\mathbf{x},t)\,\mathbf{I}, \tag{2.3}$$

where $\boldsymbol{\sigma}$ denotes the stress tensor and $\mathbf{I}$ the identity or unit tensor.

Now, let dV denote a differential volume of the acoustic fluid at position $\mathbf{x}$ and time t. In reference configuration the same volume is denoted by dV_0. Furthermore, this volume has the mass densities ρ_{total} and ρ_0, respectively. The conservation of mass then dictates under the assumption of no mass production

$$(\rho_0 + \rho(\mathbf{x},t))\,dV(\mathbf{x},t) = \rho_0\,dV_0(\mathbf{x}). \tag{2.4}$$

In a linearized setting, the divergence of the displacement field is relatively small (now with respect to the geometrical extensions) and thus higher order terms can be neglected. Hence, the relative volume change or *dilatation* can be expressed in terms of the divergence of the displacement field

$$\frac{dV(\mathbf{x},t) - dV_0(\mathbf{x})}{dV_0(\mathbf{x})} = \nabla \cdot \mathbf{u}(\mathbf{x},t)$$

and, therefore, the mass balance (2.4) becomes

$$\rho(\mathbf{x},t) = -\rho_{total}(\mathbf{x},t)\nabla \cdot \mathbf{u}(\mathbf{x},t) = -(\rho_0 + \rho(\mathbf{x},t))\nabla \cdot \mathbf{u}(\mathbf{x},t).$$

Finally, the density fluctuation is expressed in terms of the displacement field by

$$\rho(\mathbf{x},t) = -\rho_0 \nabla \cdot \mathbf{u}(\mathbf{x},t). \tag{2.5}$$

Equation (2.5) can be regarded as the *kinematics* of the acoustic fluid. In order to relate the density with pressure fluctuations, a constitutive relation is needed. The fluid is assumed to be elastic. Hence, the total pressure is a function of the total density, $p_{total} = f(\rho_{total})$, and a Taylor expansion yields

$$p_0 + p(\mathbf{x},t) = f(\rho_0 + \rho) = f(\rho_0) + \rho(\mathbf{x},t)f'(\rho_0) + \frac{\rho^2(\mathbf{x},t)}{2}f''(\rho_0) + \cdots.$$

Truncation after the linear term and the necessary condition $p_0 = f(\rho_0)$ yields the constitutive relation

$$p(\mathbf{x},t) = f'(\rho_0)\rho(\mathbf{x},t).$$

In case of a linear constitutive behavior, as assumed here, the proportionality factor of the above constitutive relation is a constant and can be identified with the square of the wave

velocity, $c^2 = f'(\rho_0)$. Alternatively, the pressure fluctuation is directly proportional to the relative density changes or the volume dilatation

$$p(\mathbf{x},t) = \kappa \frac{\rho(\mathbf{x},t)}{\rho_0} = -\kappa \nabla \cdot \mathbf{u}(\mathbf{x},t) \tag{2.6}$$

with the bulk modulus κ ($\kappa > 0$) as proportionality factor. The wave velocity thus becomes

$$c = \sqrt{\frac{\kappa}{\rho_0}}. \tag{2.7}$$

At last, the dynamic equilibrium has to be formulated. Starting from the balance of linear momentum in the reference configuration

$$\int_{V_0} \rho_0 \ddot{\mathbf{u}}(\mathbf{x},t)\,\mathrm{d}\mathbf{x} = \int_{\partial V_0} \mathbf{t}(\mathbf{x},t)\,\mathrm{d}s_{\mathbf{x}} + \int_{V_0} \rho(\mathbf{x})\mathbf{f}(\mathbf{x},t)\,\mathrm{d}\mathbf{x}$$

with the body mass forces $\mathbf{f}$, the surface forces $\mathbf{t}$, and the Cauchy lemma $\mathbf{t} = \sigma \cdot \mathbf{n}$, $\mathbf{n}$ being the outward normal vector to the volume, one obtains by means of the divergence theorem

$$\int_{V_0} (\nabla \cdot \sigma(\mathbf{x},t) + \rho_0 \mathbf{f}(\mathbf{x},t))\,\mathrm{d}\mathbf{x} = \int_{V_0} \rho_0 \ddot{\mathbf{u}}(\mathbf{x},t)\,\mathrm{d}\mathbf{x}.$$

This equation has to hold for every sub-volume $\tilde{V} \subset V_0$ and, therefore, not only in an integral sense but also pointwise for the integrands. With the hydrostatic stress (2.3), the dynamic equilibrium becomes

$$-\nabla p(\mathbf{x},t) + \rho_0 \mathbf{f}(\mathbf{x},t) = \rho_0 \ddot{\mathbf{u}}. \tag{2.8}$$

By inserting the kinematic relation (2.5) into the constitutive relation (2.6) and in turn inserting the result into the equilibrium equation (2.8), a partial differential equation for the displacement field is obtained

$$c^2 \nabla(\nabla \cdot \mathbf{u}(\mathbf{x},t)) + \mathbf{f}(\mathbf{x},t) = \ddot{\mathbf{u}}(\mathbf{x},t).$$

It is usually preferred to express the above relation in terms of the pressure fluctuation. Applying the divergence to the above equation and exchanging temporal with spatial derivatives then yields the *acoustic wave equation* for an inviscid fluid

$$\ddot{p}(\mathbf{x},t) - c^2 \Delta p(\mathbf{x},t) = g(\mathbf{x},t). \tag{2.9}$$

In this equation, the negative divergence of the body force term $\mathbf{f}$ has been abbreviated by g, i.e., $g = -\nabla \cdot \mathbf{f}$. Furthermore, Δ denotes the Laplace operator, $\Delta = \nabla \cdot \nabla = \sum_i \partial^2 / \partial \mathbf{x}_i^2$.

Equation (2.9) is a hyperbolic partial differential equation. In order to embed it into an initial boundary value problem as shown in section 2.3, the acoustic flux is introduced

$$\mathbf{q}(\mathbf{x},t) = \nabla p(\mathbf{x},t) \tag{2.10}$$

$$p \xrightarrow{\text{wave equation}} g$$

$$\text{kinematics} \Big\downarrow \qquad\qquad \Big\uparrow \text{balance law}$$

$$\left\{ \begin{array}{c} \nabla p \\ \dot{p} \end{array} \right\} \xrightarrow[\text{material law}]{} \left\{ \begin{array}{c} \mathbf{q} \\ \rho_0 \dot{p} \end{array} \right\}$$
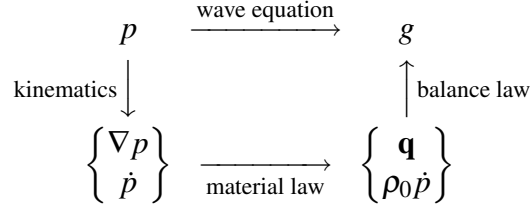
Figure 2.1: Tonti diagram for the acoustic fluid.

as an auxiliary variable. By means of the flux variable, one can set up a Tonti diagram [113] for the acoustic wave equation as depicted in figure 2.1.

In the presented case, the wave equation describes the pressure fluctuation in a homogeneous, compressible, elastic, and inviscid fluid. This model is often used in acoustics for instance. Alternatively, the pressure p can be eliminated from the equation by introducing a displacement potential ψ, $\mathbf{u} = \nabla \psi$, or a velocity potential ϕ, $\dot{\mathbf{u}} = \nabla \phi$. These potentials then obey wave equations with exactly the same operator as in equation (2.9) but with different force terms. Moreover, the same type of equation shows up in many other wave propagation phenomena. For instance, the waves in a string or the longitudinal waves in thin rods (see the book of Graff [37] and also the introductory example in section 1.2) are described by similar equations.

Applying a Laplace transformation to the acoustic wave equation gives

$$s^2 \hat{p}(\mathbf{x}, s) - c^2 \Delta \hat{p}(\mathbf{x}, s) = \hat{g}(\mathbf{x}, s)$$

with the Laplace parameter $s \in \mathbb{C}$ and under the assumption of vanishing initial conditions, i.e., $p(\mathbf{x}, 0) = 0$ and $\dot{p}(\mathbf{x}, 0) = 0$. The circumflex denotes the Laplace transform which is defined as $\hat{p}(s) := \mathscr{L}(p) = \int_0^\infty p(t) \exp(-st) \, dt$. Rearranging the terms in this equation yields

$$\left(\Delta - \frac{s^2}{c^2} \right) \hat{p}(\mathbf{x}, s) = \frac{1}{c^2} \hat{g}(\mathbf{x}, s) \tag{2.11}$$

with the Yukawa operator $(\Delta - s^2/c^2)$. Restricting the range of the Laplace parameter to the imaginary axis, $s = i\omega$ ($i^2 = -1$), yields the *Helmholtz* equation

$$(\Delta + k^2) \tilde{p}(\mathbf{x}, k) = \tilde{g}(\mathbf{x}, k) \tag{2.12}$$

with the wave number $k = \omega/c$. The force term has simply been renamed and the operator $(\Delta + k^2)$ is the well-known Helmholtz operator. Actually, $\tilde{p}(\mathbf{x}, k)$ resembles the Fourier transform of $p(x, t)$, i.e., $\tilde{p}(\mathbf{x}, k) = \int_{-\infty}^{\infty} p(\mathbf{x}, t) \exp(-2\pi i k t) \, dt$.

The dynamic terms are neglected if the fluid tends to incompressibility ($c \to \infty$) or the disturbances are quasi-static, $g(\mathbf{x}, t) = h(\mathbf{x}) \; \forall t$. Then, the pressure function p becomes independent of time and the *Poisson equation* is obtained

$$-\Delta p(\mathbf{x}) = h(\mathbf{x}) \,. \tag{2.13}$$

Equation (2.13) however, appears in the context of many physical phenomena, like heat conduction and electrostatics. It is the prototype of an elliptic partial differential equation. The homogeneous version of the Poisson equation is commonly called *Laplace equation*

$$-\Delta p(\mathbf{x}) = 0.\tag{2.14}$$

The equations presented in this section are valid for one-, two-, and three-dimensional problems. The involved functions are then dependent on the corresponding coordinates, e.g., $p(\mathbf{x},t) = p(x_1,x_2,t)$ for two space dimensions. Accordingly, on has to use the right operator, e.g., $\Delta = \partial^2/\partial x_1^2 + \partial^2/\partial x_2^2$ for the same example.

2.2 Linear Elastodynamics

In the following, the basic components of the linear elastodynamic equations are summarized. Detailed derivations are given in any textbook on the basic theory of elasticity. Special treatment of elastodynamics and wave propagation in solids can be found in the books of Achenbach [1], Graff [37], and Kupradze [56] among others.

A homogeneous elastic solid is considered, which is subjected to dynamic forces. Again, the deviation from the reference configuration is assumed to be small such that the general equations of continuum mechanics [75] are linearized.

The displacement field $\mathbf{u}(\mathbf{x},t)$ depending on position and time is introduced to describe the motion of the solid which is equipped with an equilibrium mass density ρ_0. Measuring the changes of the squares of length of line elements in the undeformed and the deformed state, the linear strain tensor is obtained

$$\varepsilon(\mathbf{x},t) = \frac{1}{2}\left(\nabla\mathbf{u}(\mathbf{x},t) + (\nabla\mathbf{u}(\mathbf{x},t))^\top\right).\tag{2.15}$$

Here, $(\ )^\top$ denotes the transpose and, therefore, ε is the symmetric part of the displacement gradient tensor. Note that the higher-order terms of the exact non-linear strain tensors are neglected according to the assumptions of a small displacement gradient formulation. The effect of the anti-symmetric part of the displacement gradient can be expressed by means of the curl operator [37] introducing the rotation vector

$$\omega(\mathbf{x},t) = \frac{1}{2}\nabla\times\mathbf{u}(\mathbf{x},t).\tag{2.16}$$

Actually, the newly introduced *curl* operator, $\nabla\times(\ )$, can be defined by the relation [75]

$$(\nabla\times\mathbf{u}(\mathbf{x},t))\times\mathbf{a} = \left(\nabla\mathbf{u}(\mathbf{x},t) - (\nabla\mathbf{u}(\mathbf{x},t))^\top\right)\cdot\mathbf{a} \quad \forall\mathbf{a}\in\mathbb{R}^d.$$

It is thus the axial vector of an anti-symmetrical tensor field. Additionally, the velocity is given by the first time derivative of the displacement

$$\dot{\mathbf{u}}(\mathbf{x},t) = \frac{\partial\mathbf{u}(\mathbf{x},t)}{\partial t}.\tag{2.17}$$

The solid is assumed to be linear elastic, homogeneous, and isotropic. The former condition allows for a linear stress-strain relationship

$$\boldsymbol{\sigma}(\mathbf{x},t) = \mathbf{C}(\mathbf{x},t) : \boldsymbol{\varepsilon}(\mathbf{x},t).$$

The colon denotes a double contraction of tensors, e.g., $\mathbf{A} : \mathbf{B} = \sum_{i,j} A_{ij} B_{ij}$ for the two second-order tensors $\mathbf{A}$ and $\mathbf{B}$. Homogeneity lets $\mathbf{C}$ be independent of the position $\mathbf{x}$ and it is additionally assumed that the material behavior does not depend on time either, i.e., $\mathbf{C} = const$. Due to the condition of isotropy, the material law finally takes the form

$$\boldsymbol{\sigma}(\mathbf{x},t) = \lambda \operatorname{tr}(\boldsymbol{\varepsilon}(\mathbf{x},t))\mathbf{I} + 2\mu\boldsymbol{\varepsilon}(\mathbf{x},t). \tag{2.18}$$

The symbol $\operatorname{tr}(\ )$ denotes the trace, i.e., the sum of the diagonal entries or in terms of the contraction $\operatorname{tr}(\mathbf{A}) = \mathbf{A} : \mathbf{I}$. Furthermore, two material parameters λ and μ have been introduced which are called *Lamé parameters*. These can be related to the more common Young's modulus E and Poisson ratio ν by

$$\lambda = \frac{E\nu}{(1+\nu)(1-2\nu)} \qquad \mu = \frac{E}{2(1+\nu)}$$
$$E = \mu\frac{3\lambda + 2\mu}{\lambda + \mu} \qquad \nu = \frac{\lambda}{2(\lambda + \mu)}.$$

As in the case of the acoustic fluid of section 2.1, the stress field $\boldsymbol{\sigma}$ is the deviation from an equilibrium stress $\boldsymbol{\sigma}_0$ which is not considered further. The density of linear momentum ℓ is defined by the relation [75]

$$\ell(\mathbf{x},t) = \rho_0\dot{\mathbf{u}}(\mathbf{x},t). \tag{2.19}$$

In order to complete the set of equations, a balance law is needed. The balance of linear momentum as used for the derivation of the wave equation suffices (cf. the derivation of equation (2.8)) and relates the stresses $\boldsymbol{\sigma}$ and linear momentum density ℓ with the body forces $\mathbf{f}$

$$\nabla \cdot \boldsymbol{\sigma}(\mathbf{x},t) + \mathbf{f}(\mathbf{x},t) = \dot{\ell}(\mathbf{x},t). \tag{2.20}$$

Note that in the derivation of the balance of linear momentum the continuity equation, i.e., balance of mass, is implicitly employed. Furthermore, the rotational momentum is also conserved. In the given setting, the balance of rotational momentum requires symmetry of the stress field $\boldsymbol{\sigma}$ [75]. This symmetry is implicitly included in the constitutive equation (2.18).

The elastodynamic system of equations expressed by the displacement field is finally obtained by inserting the kinematic relation (2.15) and the definition of the velocity (2.17) into the material law (2.18) and the definition of the density of linear momentum (2.19). These results are then inserted into the balance law (2.20). This procedure is graphically represented by the Tonti scheme [113] for elastodynamics in figure 2.2 and the final set of equations is

$$\rho_0\ddot{\mathbf{u}}(\mathbf{x},t) - \mu\nabla\cdot(\nabla\mathbf{u}(\mathbf{x},t)) - (\lambda + \mu)\nabla(\nabla\cdot\mathbf{u}(\mathbf{x},t)) = \mathbf{f}(\mathbf{x},t). \tag{2.21}$$
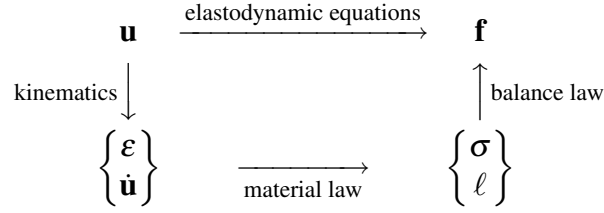
Figure 2.2: Tonti diagram for elastodynamics.

In figure 2.2, equation (2.17) is interpreted as a kinematic relation and (2.19) as a material law. Equations (2.21) are often referred to as *Lamé-Navier equations*. Employing the identity

$$\nabla \cdot (\nabla \mathbf{u}) = \nabla(\nabla \cdot \mathbf{u}) - \nabla \times (\nabla \times \mathbf{u})$$

in equations (2.21), an alternative representation is obtained [37, 56]

$$\rho_0 \ddot{\mathbf{u}}(\mathbf{x},t) - (\lambda + 2\mu)\nabla(\nabla \cdot \mathbf{u}(\mathbf{x},t)) + \mu\nabla \times (\nabla \times \mathbf{u}(\mathbf{x},t)) = \mathbf{f}(\mathbf{x},t)\,.$$

With the abbreviation $\varepsilon = \nabla \cdot \mathbf{u}$ for the volume dilatation and the rotation vector ω from equation (2.16), one gets after dividing by ρ_0

$$\ddot{\mathbf{u}}(\mathbf{x},t) - c_1^2 \nabla \varepsilon(\mathbf{x},t) + c_2^2 \nabla \times \omega(\mathbf{x},t) = \frac{1}{\rho_0}\mathbf{f}(\mathbf{x},t)\,. \tag{2.22}$$

This representation of the elastodynamic system clearly displays the dilation and rotation parts. Moreover, one can identify the two different wave velocities

$$c_1 = \sqrt{\frac{\lambda + 2\mu}{\rho_0}} \quad \text{and} \quad c_2 = \sqrt{\frac{\mu}{\rho_0}}\,, \tag{2.23}$$

which describe the speeds of the compression and the shear wave, respectively. Since it holds that $\lambda \geq 0$ for materials with $\nu \geq 0$, it follows that $c_1 > c_2$, which means that the compression or dilatation wave with speed c_1 is always faster than the shear wave.

Application of the Laplace transform to the system of equations (2.21) results in

$$\rho_0 s^2 \hat{\mathbf{u}}(\mathbf{x},s) - \mu\nabla \cdot (\nabla \hat{\mathbf{u}}(\mathbf{x},s)) - (\lambda + \mu)\nabla(\nabla \cdot \hat{\mathbf{u}}(\mathbf{x},s)) = \hat{\mathbf{f}}(\mathbf{x},s) \tag{2.24}$$

with the Laplace parameter $s \in \mathbb{C}$ and, again, initial conditions have been assumed to be homogeneous, i.e., $\mathbf{u}(\mathbf{x},0) = \mathbf{0}$ and $\dot{\mathbf{u}}(\mathbf{x},0) = \mathbf{0}$.

The elastostatic equations are obtained from (2.21) by the assumption that the displacement field $\mathbf{u}$ and the body forces $\mathbf{f}$ are independent of the time. Hence, one gets

$$-\mu\nabla \cdot (\nabla \mathbf{u}(\mathbf{x})) - (\lambda + \mu)\nabla(\nabla \cdot \mathbf{u}(\mathbf{x})) = \mathbf{f}(\mathbf{x})\,. \tag{2.25}$$

So far, the equations of this section are based on a three-dimensional formulation. The elastodynamic system for one space dimension reduces to equation (1.2) for longitudinal waves in a bar as shown in the introductory section 1.2.2. In two space dimensions, there are the special cases of plane strain and plane stress. In the former, the state of strain is assumed to be independent of the $\mathbf{x}_3$-direction. This is the case if the considered geometry is very large or infinite in this direction and the applied load does not depend on this coordinate either. The above equations remain the same, only the third component u_3 of the displacement field $\mathbf{u}$ vanishes and the partial derivatives $\partial/\partial\mathbf{x}_3$, too. The corresponding stresses are not two-dimensional. It holds that $\sigma_{13} = \sigma_{31} = \sigma_{23} = \sigma_{32} = 0$ but $\sigma_{33} = \lambda\nabla\cdot\mathbf{u}$ in the isotropic case, which is not zero in general. Nevertheless, this stress component does not have to be considered in the set of equations and can be computed afterwards.

The state of plane stress, on the contrary, assumes that the stress tensor is purely two-dimensional. This assumption is usually made in the case of thin plates which are only loaded in the plane of their main extension. Now, $\varepsilon_{33} \neq 0$ holds in general. By means of the substitutions $E \to E(1-\nu)^2$ and $\nu \to \nu(1-\nu)$, a solution obtained by the plane strain formulation can be transformed to the corresponding solution of the state of plane stress.

2.3 Boundary Value Problems

Mathematical models for the considered physical problems described by the equations presented in sections 2.1 and 2.2 are given in the form of boundary value problems. More specific, for the case of static and Laplace domain problems elliptic boundary value problems are formulated and in time-domain hyperbolic *initial* boundary value problems are necessary. Parabolic and other systems are not considered in this work. The distinction between the different types of partial differential equations can be found in the introduction of the book of Braess [9]. For the sake of simplicity, the static cases are dealt with first. The dynamic problems then follow. A good introduction to elliptic boundary value problems is the book of Reddy [90].

2.3.1 Elliptic boundary value problems

The physical models in this work are formulated either in two or in three space dimensions. If not specified, the dimension is denoted by d. Hence, always $d = 2$ in two and $d = 3$ in three space dimensions.

Let the open domain, in which the physical model is formulated, be denoted by Ω. Unless stated otherwise, Ω is supposed to be bounded, i.e., there exists a finite number $R > 0$ such that $\Omega \subset B_R(\mathbf{0})$, where $B_R(\mathbf{y}) = \left\{ \mathbf{x} \in \mathbb{R}^d : |\mathbf{x} - \mathbf{y}| < R \right\}$. In words, Ω can be totally included in a ball around the origin with finite radius R. The boundary of Ω is symbolized by Γ and the unit *outward* normal vector at this boundary by $\mathbf{n}$. In addition, $\overline{\Omega}$ is the closure of Ω, i.e., Ω together with its boundary points. If Ω is bounded, Γ is a *closed* surface.

For the complete description and solvability of a static problem, a proper formulation of boundary conditions is needed. In the cases of the acoustic fluid and the elastic solid, the underlying partial differential equations are formulated in the pressure $p(\mathbf{x})$ and the displacement fields $\mathbf{u}(\mathbf{x})$, respectively. For the moment, the unknown function $u(\mathbf{x})$ shall represent these two. The governing elliptic partial differential equations (the so-called *static* cases in the above) can be abstracted by

$$\mathcal{L}u(\mathbf{x}) = f(\mathbf{x}). \tag{2.26}$$

$\mathcal{L}$ is a linear elliptic partial differential operator, e.g., $\mathcal{L} = -\Delta$ as in the Poisson equation (2.13), and $f(\mathbf{x})$ is a force or source term. It is assumed in the following that $\mathcal{L}$ has constant coefficients throughout the domain Ω and is thus independent of the position $\mathbf{x}$.

Any solution u of the equation (2.26) can be altered by solutions of the homogeneous equation. Therefore, $u_\alpha = u + \alpha u_0$, where $\mathcal{L}u_0 = 0$ and $\alpha \in \mathbb{R}$, is also a solution. Usually, one does not only pose a partial differential equation the solution has to fulfill, but also a certain set of boundary data the solution has to meet. In solid mechanics, the common case is to prescribe displacements or surface forces on the boundary. In acoustics, it would be the sound pressure, the surface flux or impedances that could be prescribed. For the first class of boundary condition (displacements or pressure), the boundary values of the function $u(\mathbf{x})$ itself are given. Therefore, the boundary trace u_Γ is considered

$$u_\Gamma(\mathbf{y}) = \operatorname{Tr} u = \lim_{\Omega \ni \mathbf{x} \to \mathbf{y} \in \Gamma} u(\mathbf{x}). \tag{2.27}$$

The operator Tr for taking the trace was introduced here for later purposes. Although, the distinction between u inside the domain and u_Γ on the boundary seems redundant, it is mathematically relevant, because the regularity requirements on u and u_Γ are different [107].

A condition on u_Γ is commonly called *Dirichlet* boundary condition. If u_Γ is prescribed by a function g_D on the whole boundary Γ, a Dirichlet problem is formulated

$$\begin{aligned} \mathcal{L}u(\mathbf{x}) &= f(\mathbf{x}) & \mathbf{x} \in \Omega \\ u_\Gamma(\mathbf{y}) &= g_D(\mathbf{y}) & \mathbf{y} \in \Gamma. \end{aligned} \tag{2.28}$$

Otherwise, it is also common to prescribe surface forces or fluxes. In such cases, the surface tractions or fluxes in terms of the function u have to be formulated first. In the case of the acoustic fluid, the normal flux on the surface is given by

$$q_n(\mathbf{y}) = \lim_{\Omega \ni \mathbf{x} \to \mathbf{y} \in \Gamma} [\mathbf{q}(\mathbf{x}) \cdot \mathbf{n}(\mathbf{y})]$$

where $\mathbf{q}$ denotes the interior flux. In elasticity, the surface tractions are given in a similar way

$$\mathbf{t}(\mathbf{y}) = \lim_{\Omega \ni \mathbf{x} \to \mathbf{y} \in \Gamma} [\sigma(\mathbf{x}) \cdot \mathbf{n}(\mathbf{y})].$$

An explicit expression of the surface tractions can be found for instance in the book of Kupradze et al. [57]. Note that the functions $\mathbf{q}(\mathbf{x})$ and $\sigma(\mathbf{x})$ can be expressed in terms of the unknown functions p and $\mathbf{u}$, respectively. Therefore, the above equations can be abbreviated by

$$q_\Gamma(\mathbf{y}) = \mathcal{T}u(\mathbf{x}), \tag{2.29}$$

where q_Γ represents either q_n or $\mathbf{t}$ and the operator $\mathcal{T}$ is responsible for the mapping from u to q_Γ. It will be referred to as *traction* operator. It is also called *generalized normal derivative* [65]. Again, the regularity requirements for the function q_Γ are different from the corresponding stress or flux fields in the interior of the domain. Moreover, it has to be noted that the operation (2.29) is not unique, if the boundary point $\mathbf{y}$ is located at a point where the surface Γ is not smooth. If Γ has an edge or a corner at $\mathbf{y}$ the normal vector $\mathbf{n}$ is not uniquely defined. Here, it is assumed that Γ is a piecewise smooth surface and, therefore, one can say that the operation (2.29) is possible *almost everywhere* [94].

A condition on the function q_Γ is called *Neumann* boundary condition. Prescribing q_Γ by a function g_N on the whole boundary yields the Neumann problem

$$\begin{aligned} \mathcal{L}u(\mathbf{x}) &= f(\mathbf{x}) & \mathbf{x} \in \Omega \\ q_\Gamma(\mathbf{y}) &= g_N(\mathbf{y}) & \mathbf{y} \in \Gamma. \end{aligned} \tag{2.30}$$

Note that, depending on the structure of the operator $\mathcal{L}$, the Neumann problem (2.30) may not be uniquely solvable. In elastostatics, for instance, rigid body motions could be added to u such that (2.30) is still fulfilled.

More specifically, let $\mathcal{R}$ denote the space of functions such that

$$\mathcal{L}u_{\mathcal{R}} = 0 \quad \text{and} \quad \mathcal{T}u_{\mathcal{R}} = 0 \quad \forall u_{\mathcal{R}} \in \mathcal{R}. \tag{2.31}$$

Then, any $u_\alpha = u + \alpha u_{\mathcal{R}}$ is also a solution to the Neumann problem (2.30). Additionally, this problem is only well-posed if the *solvability condition*

$$\int\limits_\Omega u_{\mathcal{R}}(\mathbf{x})f(\mathbf{x})\,d\mathbf{x} + \int\limits_\Gamma (\mathrm{Tr}\,u_{\mathcal{R}})(\mathbf{y})g_N(\mathbf{y})\,ds_{\mathbf{y}} = 0 \tag{2.32}$$

is fulfilled for all $u_{\mathcal{R}} \in \mathcal{R}$ [107]. The space $\mathcal{R}$ is of finite dimension and its basis is easily expressed. Here, three different situations have to be considered:

$$\text{Poisson equation:} \quad \mathcal{R} = \mathrm{span}\{1\} \tag{2.33a}$$

$$\text{2D elastostatics:} \quad \mathcal{R} = \mathrm{span}\left\{ \begin{pmatrix} 1 \\ 0 \end{pmatrix}, \begin{pmatrix} 0 \\ 1 \end{pmatrix}, \begin{pmatrix} x_2 \\ -x_1 \end{pmatrix} \right\} \tag{2.33b}$$

$$\text{3D elastostatics:} \quad \mathcal{R} = \mathrm{span}\left\{ \begin{pmatrix} 1 \\ 0 \\ 0 \end{pmatrix}, \begin{pmatrix} 0 \\ 1 \\ 0 \end{pmatrix}, \begin{pmatrix} 0 \\ 0 \\ 1 \end{pmatrix}, \begin{pmatrix} x_2 \\ -x_1 \\ 0 \end{pmatrix}, \begin{pmatrix} x_3 \\ 0 \\ -x_1 \end{pmatrix}, \begin{pmatrix} 0 \\ x_3 \\ -x_2 \end{pmatrix} \right\}. \tag{2.33c}$$

$$g_D = u_\Gamma \xleftarrow[\text{to } \Gamma_D]{\text{project}} u \xrightarrow[\text{system}]{\text{elastostatic}} f$$

$$\text{kinematics} \Big\downarrow \qquad \Big\uparrow \text{equilibrium}$$

$$\varepsilon \xrightarrow[\text{law}]{\text{material}} \sigma \xrightarrow[\text{to } \Gamma_N]{\text{project}} q_\Gamma = g_N$$
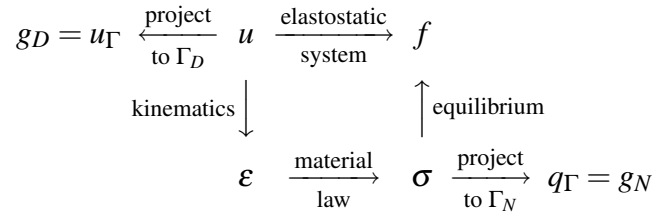
Figure 2.3: Augmented Tonti diagram for the abstract elliptic boundary value problem.

The space of constant functions (2.33a) leads to zero fluxes and, therefore, obviously fulfills (2.31). Any member of the spaces for elastostatics (2.33b) and (2.33c) produces a zero strain, i.e.,

$$\varepsilon(\mathbf{u}_\mathcal{R}) = \mathbf{0} \quad \forall \mathbf{u}_\mathcal{R} \in \mathcal{R},$$

and, therefore, zero tractions. These spaces exactly consist of 2 (3) rigid body translations and 1 (3) infinitesimal rigid body rotations for 2 (3) space dimensions. Note that a finite rotation does not produce a zero strain in this linearized setting. The infinitesimal rotation, on the other hand, is represented by some vector product $\mathbf{x} \times \mathbf{a}$ with $\mathbf{a}$ being a fixed vector from $\mathbb{R}^3$ normal to the plane of rotation. The symmetric gradient of this infinitesimal rotation vanishes.

A third kind of boundary condition appears, when combinations of u_Γ and q_Γ are prescribed. This so-called Robin boundary condition appears for instance in the case of elastically bedded plates or as impedances in acoustics. This type of boundary condition is not further considered in this work.

In many applications, mixed boundary value problems appear where on parts of the boundary a Dirichlet boundary condition and on the remaining parts a Neumann boundary condition are given. Such a mixed boundary value problem is of the form

$$\begin{aligned}
\mathcal{L}u(\mathbf{x}) &= f(\mathbf{x}) & \mathbf{x} \in \Omega \\
u_\Gamma(\mathbf{y}) &= g_D(\mathbf{y}) & \mathbf{y} \in \Gamma_D \\
q_\Gamma(\mathbf{y}) &= g_N(\mathbf{y}) & \mathbf{y} \in \Gamma_N.
\end{aligned} \tag{2.34}$$

Γ_D and Γ_N are subsets of Γ where the Dirichlet and Neumann data are prescribed. Since only Dirichlet and Neumann boundary conditions are considered in this work, $\Gamma = \overline{\Gamma}_D \cup \Gamma_N$ holds, where the bar $\overline{()}$ denotes the closure of a set. Moreover, $\Gamma_D \cap \Gamma_N = \emptyset$, i.e., it cannot occur that on the same part of Γ a Dirichlet *and* a Neumann condition is given. Nevertheless, in vector problems of elasticity it could happen that at the same location a Dirichlet datum is given for a certain direction and Neumann datum for another. In that case, the notation $\Gamma_{D,i}$ and $\Gamma_{N,j}$ will be used to indicate that in the i-th component the Dirichlet datum is prescribed, whereas a Neumann datum is given for the j-th component, respectively. If the boundary surface is not aligned with the global coordinate system the prescribed conditions are then referring to tangential and normal components of the Dirichlet or Neumann

datum, respectively. It could still appear that a mixed boundary value problem is still not uniquely solvable if, for instance, no Dirichlet datum is given for the whole boundary in one direction. Then, the corresponding rigid body mode is not suppressed.

It is convenient not having to switch between the Poisson equation and the elastostatic system all the time. Therefore, ε shall denote the quantity obtained from u by the kinematic relation (either pressure gradient or the strain tensor) and σ represents the quantity to be balanced (internal flux or stress tensor). Then the elliptic boundary value problem can be graphically depicted as shown in figure 2.3.

2.3.2 Hyperbolic initial boundary value problems

Contrary to the elliptic case as discussed in the previous section, initial boundary value problems involve a temporal evolution of the state variable. Therefore, the unknown function does not only depend on the d space dimensions but also on a time dimension. Like before, u shall represent the unknown function in this abstract setting and is now a function of space and time,

$$u = u(\mathbf{x},t), \quad \mathbf{x} \in \overline{\Omega}, \quad t \in [0,\infty).$$

Ω denotes again the spatial domain in which the problem is formulated. Only linearized formulations are considered in this work and, hence, it will not be distinguished between a reference configuration and a current configuration. They are coincident and independent of time. The additional time dimension is as usual described by the interval of non-negative real numbers, $[0,\infty)$. A condensed writing is to use the pairs $(\mathbf{x},t)$ which belong to the $(d+1)$-dimensional region $\overline{\Omega} \times [0,\infty)$.

The problems under consideration are hyperbolic and, therefore, are well posed if boundary conditions are given for the spatial boundary together with initial conditions for the time $t = 0$. Confer Braess [9] and references therein for the definition of a hyperbolic differential equation and the well-posedness of such. In the cases of the elastodynamic system and the acoustic wave equation, the partial differential equation is of the type

$$\left(\rho_0 \frac{\partial^2}{\partial t^2} + \mathcal{L} \right) u(\mathbf{x},t) = f(\mathbf{x},t),$$

where $\mathcal{L}$ denotes a second-order elliptic differential operator like the operators introduced in the previous section. The force term f represents either the acoustic source $\rho_0 g$, see equation (2.9), or the elastodynamic force term $\mathbf{f}$ as in equation (2.21). It is assumed that the operator $\mathcal{L}$ neither depends on $\mathbf{x}$ nor t and, therefore, all its coefficients are constants. Some physical models include the first temporal derivative as well in order to include damping or similar dissipative phenomena. Here, only equations of the above type are used.

On the spatial boundary Γ, conditions for the boundary trace u_Γ and/or the tractions q_Γ are given in the same way as for the elliptic problem. These conditions can be exclusively of

Dirichlet or Neumann type or they can be mixed. Since the boundary conditions only refer to the spatial variable $\mathbf{x}$ they are in general time dependent. For simplicity only the mixed case will be presented

$$\left(\rho_0 \frac{\partial^2}{\partial t^2} + \mathcal{L}\right) u(\mathbf{x},t) = f(\mathbf{x},t) \qquad (\mathbf{x},t) \in \Omega \times (0,\infty)$$

$$u_\Gamma(\mathbf{y},t) = g_D(\mathbf{y},t) \qquad (\mathbf{y},t) \in \Gamma_D \times (0,\infty) \tag{2.35}$$

$$q_\Gamma(\mathbf{y},t) = g_N(\mathbf{y},t) \qquad (\mathbf{y},t) \in \Gamma_N \times (0,\infty).$$

Let either Γ_N or Γ_D be an empty set in order to obtain a Dirichlet or a Neumann problem, respectively. It is assumed here that the partition of Γ into the two disjoint subsets Γ_D and Γ_N does not vary with time.

The problem (2.35) is still lacking the initial conditions. These are given at every point inside Ω at the time $t = 0$ for the unknown function $u(\mathbf{x},t)$ and its first temporal derivative $\dot{u}(\mathbf{x},t)$. The latter is not defined for $t = 0$ and again traces are defined

$$u(\mathbf{x},0^+) := \lim_{\substack{\tau \to 0 \\ \tau > 0}} u(\mathbf{x},\tau) \quad \text{and} \quad \dot{u}(\mathbf{x},0^+) := \lim_{\substack{\tau \to 0 \\ \tau > 0}} \dot{u}(\mathbf{x},\tau).$$

Hence, the mandatory set of initial conditions is

$$\begin{aligned} u(\mathbf{x},0^+) &= u_0(\mathbf{x}) \\ \dot{u}(\mathbf{x},0^+) &= u_1(\mathbf{x}) \end{aligned} \qquad \mathbf{x} \in \Omega \tag{2.36}$$

with given functions $u_0(\mathbf{x})$ and $u_1(\mathbf{x})$. Of course, these functions have to be compatible with the prescribed boundary data and, therefore, the following conditions have to hold

$$(\mathrm{Tr}\, u_0)(\mathbf{y}) = g_D(\mathbf{y},0^+) \quad \text{and} \quad (\mathrm{Tr}\, u_1)(\mathbf{y}) = \dot{g}_D(\mathbf{y},0^+), \quad \mathbf{y} \in \Gamma_D. \tag{2.37}$$

Equations (2.35) and (2.36) together give a well-posed hyperbolic initial boundary value problem. If one has $u(\mathbf{x},t) = 0$ for all $t \le 0$, which implies $u_0(\mathbf{x}) = 0$ and $u_1(\mathbf{x}) = 0$ for all points $\mathbf{x} \in \Omega$, than the function u is said to have a *quiescent past*.

Contrary to the elliptic case, in dynamics a pure Neumann problem is uniquely solvable. Superimposed rigid body modes are not possible since the solution has to meet the initial conditions.

As in the elliptic case, both the acoustic wave equation and the elastodynamic system are abstracted by the introduction of a notation which represents the two models. In addition to the already used variables, u, f, ε, and σ, the dynamic quantities $\dot{u}$ and $\rho_0 \dot{u}$ are used to represent the missing quantities. In figure 2.4, the relations among all the abstract variables are shown.
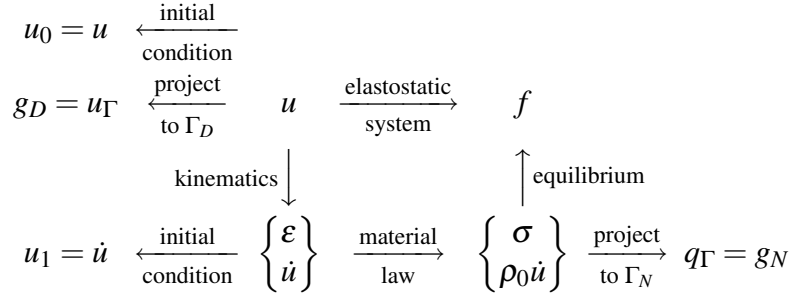
$$u_0 = u \quad \xleftarrow{\text{initial condition}}$$

$$g_D = u_\Gamma \quad \xleftarrow[\text{to } \Gamma_D]{\text{project}} \quad u \quad \xrightarrow[\text{system}]{\text{elastostatic}} \quad f$$

$$\text{kinematics} \Big\downarrow \qquad\qquad \Big\uparrow \text{equilibrium}$$

$$u_1 = \dot{u} \quad \xleftarrow[\text{condition}]{\text{initial}} \quad \begin{Bmatrix} \varepsilon \\ \dot{u} \end{Bmatrix} \quad \xrightarrow[\text{law}]{\text{material}} \quad \begin{Bmatrix} \sigma \\ \rho_0 \dot{u} \end{Bmatrix} \quad \xrightarrow[\text{to } \Gamma_N]{\text{project}} \quad q_\Gamma = g_N$$

Figure 2.4: Augmented Tonti diagram for the abstract hyperbolic initial boundary value problem.

2.4 Variational Principles

Variational principles are indispensable tools for the mathematical analysis of boundary value problems. Also, they are the starting point for many numerical methods, especially, for the finite element method.

In the following, a variational principle for the elastodynamic system is derived. It will then be identified with the well-known Hamilton's principle. The corresponding formulation for the acoustic wave equation is straightforward. Furthermore, the static (or elliptic) cases are easily obtained from the dynamic principles.

The elastodynamic system (2.21) can be written in the residual form

$$\rho_0 \ddot{\mathbf{u}} - \nabla \cdot \sigma(\mathbf{u}) - \mathbf{f} = \mathbf{0}. \tag{2.38}$$

Here, $\sigma(\mathbf{u})$ shall indicate that the stress tensor σ is to be understood as a function of the displacement field $\mathbf{u}$. Moreover, the functional dependencies on the position $\mathbf{x}$ and time t are omitted for the moment for the sake of legibility. Remember that in the context of an initial boundary value problem $\mathbf{u}$ has to obey the set of boundary conditions

$$\mathrm{Tr}\,\mathbf{u} = \mathbf{g}_D \text{ on } \Gamma_D \quad \text{and} \quad \mathcal{T}\mathbf{u} = \mathbf{g}_N \text{ on } \Gamma_N$$

and certain initial conditions (cf. section 2.3 for details).

Now, an arbitrary but admissible vector field $\mathbf{v}(\mathbf{x}, t)$ is taken and equation (2.38) will be multiplied by $\mathbf{v}$ and integrated over the domain Ω

$$\int_\Omega [\rho_0 \ddot{\mathbf{u}} - \nabla \cdot \sigma(\mathbf{u}) - \mathbf{f}] \cdot \mathbf{v}\, d\mathbf{x} = \mathbf{0}.$$

Admissible means in the current context that $\mathbf{v}$ obeys specific regularity requirements in order to ensure the existence of the integrals and that it vanishes on Γ_D, i.e., $\mathrm{Tr}\,\mathbf{v} = \mathbf{0}$

on Γ_D. In engineering literature, $\mathbf{v}$ is often referred to as *virtual displacement*. In this work, the term *test function* is preferred.

Using the identity

$$(\nabla \cdot \boldsymbol{\sigma}) \cdot \mathbf{v} = \nabla \cdot (\boldsymbol{\sigma} \cdot \mathbf{v}) - \boldsymbol{\sigma} : \nabla \mathbf{v}$$

and the divergence theorem

$$\int_\Omega \nabla \cdot \mathbf{v} \, d\mathbf{x} = \int_\Gamma \mathrm{Tr}\, \mathbf{v} \cdot \mathbf{n} \, ds,$$

one obtains the relation

$$\int_\Omega \boldsymbol{\sigma}(\mathbf{u}) : \nabla \mathbf{v} \, d\mathbf{x} + \int_\Omega \rho_0 \ddot{\mathbf{u}} \cdot \mathbf{v} \, d\mathbf{x} - \int_\Omega \mathbf{f} \cdot \mathbf{v} \, d\mathbf{x} - \int_\Gamma (\mathcal{T}\mathbf{u}) \cdot \mathrm{Tr}\, \mathbf{v} \, ds = 0.$$

The gradient of $\mathbf{v}$ can be decomposed into its symmetric and its antisymmetric parts. The contraction of a symmetric tensor with an antisymmetric tensor yields zero and, therefore, only the symmetric part of this decomposition remains in this relation. Then the *principle of virtual work* is obtained

$$\int_\Omega \rho_0 \ddot{\mathbf{u}} \cdot \mathbf{v} \, d\mathbf{x} + \int_\Omega \boldsymbol{\sigma}(\mathbf{u}) : \boldsymbol{\varepsilon}(\mathbf{v}) \, d\mathbf{x} = \int_\Omega \mathbf{f} \cdot \mathbf{v} \, d\mathbf{x} + \int_{\Gamma_N} \mathbf{g}_N \cdot \mathrm{Tr}\, \mathbf{v} \, ds. \qquad (2.39)$$

Similar to the kinematic equation (2.15), $\boldsymbol{\varepsilon}(\mathbf{v})$ denotes the symmetric part of $\nabla \mathbf{v}$. Since the test function $\mathbf{v}$ is assumed to vanish on Γ_D, only the surface integral over Γ_N remains and the Neumann boundary condition has already been employed. Note that both sides of the above relation are still functions of time.

Obviously, the function $\mathbf{u}$, which is a solution to the initial boundary value problem, fulfills relation (2.39). But, in order to be a solution of the underlying partial differential equation, this function $\mathbf{u}$ has to be twice differentiable in space and in time. The variational principle (2.39) only requires the first spatial derivative to be square integrable. The important point is that, if the function $\mathbf{u}$ fulfills this variational principle for any arbitrary but admissible test function $\mathbf{v}$, and if $\mathbf{u}$ is twice differentiable, then it is also a solution of the original initial boundary value problem. Due to the less severe regularity requirements, the solution to this variational principle is commonly called *weak* solution, whereas the solution to the original initial boundary value problem is termed *classical* or *strong* solution. Additionally, the force terms $\mathbf{f}$ and $\mathbf{g}_N$ have to obey weaker conditions than in the classical formulation. Point forces, for instance, are valid in the variational principle. Therefore, the set of weak solutions is wider than the set of classical solutions. Actually, the latter form a subset of the former. On the other hand, the Dirichlet boundary condition is strongly fulfilled by the solution $\mathbf{u}$, i.e., the solution is sought among those functions, which already fulfill the condition $\mathrm{Tr}\, \mathbf{u} = \mathbf{g}_D$ on Γ_D. Strang and Fix [110] provide a good introduction to this matter for the elliptic case.

The initial conditions, which the solution function has to obey, are commonly posed in a weak form, too [49]. This means that they have to be fulfilled in an integral sense for all admissible test functions $\mathbf{v}$

$$\int_\Omega \mathbf{u} \cdot \mathbf{v} \, d\mathbf{x} = \int_\Omega \mathbf{u}_0 \cdot \mathbf{v} \, d\mathbf{x} \quad \text{and} \quad \int_\Omega \dot{\mathbf{u}} \cdot \mathbf{v} \, d\mathbf{x} = \int_\Omega \mathbf{u}_1 \cdot \mathbf{v} \, d\mathbf{x} \quad \text{at } t = 0. \tag{2.40}$$

Now, two time instants t_0 and t_1 are taken and relation (2.39) is integrated over the time between these instants. Additionally, the employed test functions $\mathbf{v}$ are assumed to be once differentiable in time and to vanish at these time points, i.e., $\mathbf{v}(t_0) = \mathbf{v}(t_1) = \mathbf{0}$. Then the first term of equation (2.39) becomes

$$\int_{t_0}^{t_1} \int_\Omega \rho_0 \ddot{\mathbf{u}} \cdot \mathbf{v} \, d\mathbf{x} \, dt = \int_\Omega \rho_0 \dot{\mathbf{u}} \cdot \mathbf{v} \, d\mathbf{x} \Big|_{t_0}^{t_1} - \int_{t_0}^{t_1} \int_\Omega \rho_0 \dot{\mathbf{u}} \cdot \dot{\mathbf{v}} \, d\mathbf{x} \, dt = - \int_{t_0}^{t_1} \int_\Omega \rho_0 \dot{\mathbf{u}} \cdot \dot{\mathbf{v}} \, d\mathbf{x} \, dt.$$

With this result, the temporal integration yields

$$\int_{t_0}^{t_1} \int_\Omega \rho_0 \dot{\mathbf{u}} \cdot \dot{\mathbf{v}} \, d\mathbf{x} \, dt - \int_{t_0}^{t_1} \int_\Omega \sigma(\mathbf{u}) : \varepsilon(\mathbf{v}) \, d\mathbf{x} \, dt +$$

$$\int_{t_0}^{t_1} \int_\Omega \mathbf{f} \cdot \mathbf{v} \, d\mathbf{x} \, dt + \int_{t_0}^{t_1} \int_{\Gamma_N} \mathbf{g}_N \cdot (\mathrm{Tr}\, \mathbf{v}) \, ds \, dt = 0.$$

Introducing the kinetic and strain energies

$$\mathscr{K}(\mathbf{u}) = \frac{1}{2} \int_\Omega \rho_0 \dot{\mathbf{u}} \cdot \dot{\mathbf{u}} \, d\mathbf{x} \quad \text{and} \quad \mathscr{U}(\mathbf{u}) = \frac{1}{2} \int_\Omega \sigma(\mathbf{u}) : \varepsilon(\mathbf{u}) \, d\mathbf{x}, \tag{2.41}$$

respectively, and identifying the right hand side of equation (2.39) with the external virtual work $\delta\mathscr{W}$, Hamilton's principle is recovered [1]

$$\int_{t_0}^{t_1} \delta(\mathscr{K} - \mathscr{U}) \, dt + \int_{t_0}^{t_1} \delta\mathscr{W} \, dt = 0. \tag{2.42}$$

Here, δ denotes the first variation. The difference term is often referred to as the *Lagrangian*, $\mathscr{L} = \mathscr{K} - \mathscr{U}$. In the given context, this principle states that the integral from t_0 to t_1 over the sum of the Lagrangian and the potential of the applied forces is stationary and does not depend on the actual path of integration. Confer the textbooks of Goldstein [35] and Love [66] for more details on Hamilton's principle.

Moreover, if the used test function $\mathbf{v}$ is taken to be the velocity, i.e., $\mathbf{v} = \dot{\mathbf{u}}$, the principle of virtual work (2.39) becomes [75]

$$\int_\Omega \rho_0 \ddot{\mathbf{u}} \cdot \dot{\mathbf{u}} \, d\mathbf{x} + \int_\Omega \sigma(\mathbf{u}) : \dot{\varepsilon}(\mathbf{u}) \, d\mathbf{x} = \int_\Omega \mathbf{f} \cdot \dot{\mathbf{u}} \, d\mathbf{x} + \int_\Gamma (\mathscr{T}\mathbf{u}) \cdot \mathrm{Tr}\, \dot{\mathbf{u}} \, ds.$$

Here, the surface integral has to be extended over the whole boundary Γ because there is no boundary condition on $\dot{\mathbf{u}}$ as there was before for the test function $\mathbf{v}$. Recalling the definitions of the kinetic and strain energies (2.41), this relation becomes

$$\frac{\partial}{\partial t}\mathcal{K}(\mathbf{u}) + \frac{\partial}{\partial t}\mathcal{U}(\mathbf{u}) = \int_\Omega \mathbf{f} \cdot \dot{\mathbf{u}}\, d\mathbf{x} + \int_\Gamma (\mathcal{T}\mathbf{u}) \cdot \mathrm{Tr}\dot{\mathbf{u}}\, ds.$$

The integration from 0 to t over this expression yields the total energy stored in the system [118]

$$\mathcal{K}(\mathbf{u}) + \mathcal{U}(\mathbf{u}) = \int_0^t \int_\Omega \mathbf{f} \cdot \dot{\mathbf{u}}\, d\mathbf{x}\, d\tau + \int_0^t \int_\Gamma (\mathcal{T}\mathbf{u}) \cdot \mathrm{Tr}\dot{\mathbf{u}}\, ds\, d\tau, \tag{2.43}$$

where, for the sake of simplicity, $\mathbf{u}$ is assumed to have a quiescent past, i.e., $\mathbf{u} = \mathbf{0}$ for all $t \leq 0$.

In the static case, these principles can be simplified. Hamilton's principle collapses to the statement

$$\delta\mathcal{U} = \delta\mathcal{W},$$

i.e., the variation of internal strain energy equals the virtual work done by the applied forces. Commonly, a potential is formulated whose minimization gives the above relation. For the given boundary value problem, the potential is of the form

$$\Pi(\mathbf{u}) = \frac{1}{2}\int_\Omega \sigma(\mathbf{u}) : \varepsilon(\mathbf{u})\, d\mathbf{x} - \int_\Omega \mathbf{f} \cdot \mathbf{u}\, d\mathbf{x} - \int_{\Gamma_N} \mathbf{g}_N \cdot (\mathrm{Tr}\,\mathbf{u})\, ds. \tag{2.44}$$

Note that this is only one possible form of such a potential. Many other versions exist in literature (cf. for instance [91]). Moreover, suitable function space have to be established in order to ensure that the minimum can be really attained. Here, function spaces are not considered any further and the book of Strang and Fix [110] is given as a good reference for an introduction to this matter.

Minimization of the potential (2.44) yields

$$\int_\Omega \sigma(\mathbf{u}) : \varepsilon(\mathbf{v})\, d\mathbf{x} = \int_\Omega \mathbf{f} \cdot \mathbf{v}\, d\mathbf{x} + \int_{\Gamma_N} \mathbf{g}_N \cdot (\mathrm{Tr}\,\mathbf{v})\, ds \tag{2.45}$$

for all admissible $\mathbf{v}$, which is exactly (2.39) without the inertia term. This equation is obtained by taking the first variation with respect to the unknown function $\mathbf{u}$ of the potential and setting it to zero, i.e., $\delta_{\mathbf{u}}\Pi = 0$. The second variation then gives

$$\int_\Omega \sigma(\mathbf{v}) : \varepsilon(\mathbf{v})\, d\mathbf{x} > 0 \quad \forall \mathbf{v} \neq \mathbf{0}.$$

The fact that the above result is always positive ensures that the function $\mathbf{u}$ really minimizes the potential.

For the acoustic wave equation

$$\rho_0 \ddot{p} - \kappa \Delta p = \rho_0 g$$

similar principles can be stated. The principle of virtual work for the dynamic equation states

$$\int_\Omega \rho_0 \ddot{p}\, v\, \mathrm{d}\mathbf{x} + \int_\Omega \kappa \nabla p \cdot \nabla v\, \mathrm{d}\mathbf{x} = \int_\Omega \rho_0 g\, v\, \mathrm{d}\mathbf{x} + \int_{\Gamma_N} g_N \operatorname{Tr} v\, \mathrm{d}s \qquad (2.46)$$

and the first term is simply omitted for the static case of Poisson's equation. Again, a test function v has been introduced, which vanishes on the Dirichlet boundary, i.e., $\operatorname{Tr} v = 0$ on Γ_D. And the Dirichlet boundary condition is assumed to be fulfilled by u a priori.

For subsequent purposes, again a shorthand notation is used, which combines both cases of elastodynamics and acoustics. By means of the generic variables already used in section 2.3, the following abbreviation represents equations (2.39) and (2.46)

$$\langle \rho_0 \ddot{u}, v \rangle + a_t(u, v) = \langle f, v \rangle + \langle g_N, \operatorname{Tr} v \rangle_{\Gamma_N}. \qquad (2.47)$$

Here, $\langle \cdot, \cdot \rangle$ is the L_2-scalar product on Ω, $\langle \cdot, \cdot \rangle_{\Gamma_N}$ the L_2-scalar product on Γ_N, and $a_t(\cdot, \cdot)$ a symmetric bilinear form corresponding to the underlying physical model

$$a_t(\mathbf{u}, \mathbf{v}) = \int_\Omega \sigma(\mathbf{u}) : \varepsilon(\mathbf{v})\, \mathrm{d}\mathbf{x} \quad \text{or} \quad a_t(p, v) = \int_\Omega \kappa \nabla p \cdot \nabla v\, \mathrm{d}\mathbf{x} \qquad (2.48)$$

for elastodynamics or acoustics, respectively. In fact, the $a_t(\cdot, \cdot)$ yields a function of time and is thus not a bilinear form in the classical sense. The subscript t is used to indicate this fact.

Using this notation, the introduced energies become

$$\mathscr{K}(u) = \frac{1}{2} \langle \rho_0 \dot{u}, \dot{u} \rangle \quad \text{and} \quad \mathscr{U}(u) = \frac{1}{2} a_t(u, u) \qquad (2.49)$$

for the kinetic and the strain energy, respectively. Additionally, the work of the applied forces can be written as the linear form

$$\ell_t(u) := \mathscr{W}(u) = \langle f, u \rangle + \langle g_N, \operatorname{Tr} u \rangle_{\Gamma_N}. \qquad (2.50)$$

The notation $\ell_t(u)$ is preferred in the rest of this work because it is more common.

Finally, the generic dynamic variational principle states:

Find u with $\operatorname{Tr} u = g_D$ *on* $\Gamma_D \times (0, \infty)$ *such that*

$$
\begin{aligned}
\langle \rho_0 \ddot{u}, v \rangle + a_t(u, v) &= \ell_t(v) & &\text{in} \quad \Omega \times (0, \infty) \\
\langle u, v \rangle &= \langle u_0, v \rangle & &\text{on} \quad \Omega \times 0 \\
\langle \dot{u}, v \rangle &= \langle u_1, v \rangle & &\text{on} \quad \Omega \times 0
\end{aligned}
\qquad (2.51)
$$

for all v with $\operatorname{Tr} v = 0$ *on* $\Gamma_D \times (0, \infty)$.

In statics, this principle reduces to the statement:

Find u with $\mathrm{Tr}\,u = g_D$ *on* Γ_D *such that*

$$a(u,v) = \ell(v) \quad \text{in} \quad \Omega \tag{2.52}$$

for all v with $\mathrm{Tr}\,v = 0$ *on* Γ_D.

The bilinear form $a(\cdot,\cdot)$ used in the latter variational principle does not carry the subscript t because it yields a real number and, therefore, is a bilinear form in the classical sense.

The exact function spaces, u and v are taken from, can be found in textbooks on the matter, e.g., [90, 107] for the static case and [49] for the dynamic case. In the static case, one easily observes that $a(u,u_\mathcal{R}) = 0$ if $u_\mathcal{R}$ belongs to the corresponding space of rigid body modes (2.33). Hence, if a pure Neumann problem is considered, i.e., $\Gamma_D = \emptyset$ and $\Gamma_N = \Gamma$, one gets

$$\ell(u_\mathcal{R}) = 0\,,$$

which is exactly the solvability condition (2.32). Therefore, the Neumann problem is not uniquely solvable.

2.5 Boundary Integral Equations

In this section, boundary integral equations are derived relating the boundary values (traces and tractions) with each other and the given forces. These equations are the key ingredients for the later introduced boundary element method. Additionally, they have been playing a fundamental role in the analysis of partial differential equations.

2.5.1 Representation formulae

Before introducing the final boundary integral equations, the so-called representation formulae are presented. By means of these, the solution function u can be given at any point $\mathbf{x}$ inside the domain Ω (and at any time $t > 0$ in the dynamic case) if the boundary data of the function, i.e., its trace $u_\Gamma := \mathrm{Tr}\,u$, and the tractions $q_\Gamma := \mathcal{T}u$ are known (for all times $0 < \tau < t$).

Elliptic boundary value problems Recall the mixed elliptic boundary value problem in the abstract notation

$$\begin{aligned}
\mathcal{L}u(\mathbf{x}) &= f(\mathbf{x}) & \mathbf{x} &\in \Omega \\
u_\Gamma(\mathbf{y}) &= g_D(\mathbf{y}) & \mathbf{y} &\in \Gamma_D \\
q_\Gamma(\mathbf{y}) &= g_N(\mathbf{y}) & \mathbf{y} &\in \Gamma_N\,.
\end{aligned} \tag{2.53}$$

Here, u is the unknown function, u_Γ its boundary trace, and q_Γ the corresponding traction. The functions f, g_D and g_N are given inside the domain Ω, on the Dirichlet boundary

part Γ_D, and on the Neumann boundary part Γ_N, respectively. Employing a suitable test function $v(\mathbf{x})$, a generalized version of Green's second identity can be established by means of integration by parts

$$\int\limits_{\Omega} (\mathcal{L}u)v\,d\mathbf{x} + \int\limits_{\Gamma} q_{\Gamma}(\mathrm{Tr}\,v)\,ds = \int\limits_{\Omega} (\mathcal{L}v)u\,d\mathbf{x} + \int\limits_{\Gamma} u_{\Gamma}(\mathcal{T}v)\,ds. \tag{2.54}$$

Here, it has already been assumed that the partial differential operator $\mathcal{L}$ is self-adjoint, which holds for the considered problems. Replacing $\mathcal{L}u$ by f and $\mathcal{L}v$ by f^* (i.e., assuming that v is the solution to some other boundary value problem with force term f^*), one obtains Betti's theorem of reciprocity [66].

Now, a function $u^*(\mathbf{x}, \mathbf{y})$ is introduced such that [107]

$$\int\limits_{\Omega} (\mathcal{L}_{\mathbf{y}}u^*(\mathbf{x}, \mathbf{y}))\,u(\mathbf{y})\,d\mathbf{y} = u(\mathbf{x}) \quad \mathbf{x} \in \Omega \tag{2.55}$$

holds. The subscript $\mathbf{y}$ at the differential operator $\mathcal{L}$ denotes that the differentiation is applied with respect to the spatial variable $\mathbf{y}$ and not $\mathbf{x}$. This function u^* turns out to be a fundamental solution. Defining $v(\mathbf{y}) = u^*(\mathbf{x}, \mathbf{y})$ and inserting this relation into Green's second identity (2.54), where the integration variable $\mathbf{x}$ has been replaced by $\mathbf{y}$, yields the *representation formula*

$$u(\mathbf{x}) = \int\limits_{\Gamma} u^*(\mathbf{x}, \mathbf{y})q_{\Gamma}(\mathbf{y})\,ds_{\mathbf{y}} - \int\limits_{\Gamma} \mathcal{T}_{\mathbf{y}}u^*(\mathbf{x}, \mathbf{y})u_{\Gamma}(\mathbf{y})\,ds_{\mathbf{y}} + \int\limits_{\Omega} u^*(\mathbf{x}, \mathbf{y})f(\mathbf{y})\,d\mathbf{y} \quad \mathbf{x} \in \Omega. \tag{2.56}$$

Here, $\mathcal{T}_{\mathbf{y}}$ indicates that the traction operator is applied with respect to the $\mathbf{y}$-variable. Furthermore, $ds_{\mathbf{y}}$ emphasizes that the surface integration is performed with respect to $\mathbf{y}$ as well. Hence, knowing a function $u^*(\mathbf{x}, \mathbf{y})$ with the above property (2.55), the unknown function $u(\mathbf{x})$ is given for any point $\mathbf{x}$ inside the domain Ω if its boundary data u_{Γ} and q_{Γ} are known. This set of boundary data $[u_{\Gamma}, q_{\Gamma}]$ is called *Cauchy* data [107]. In elastostatics, the representation formula (2.56) is commonly known as *Somigliana's identity* [33].

Consider the property (2.55) of the function $u^*(\mathbf{x}, \mathbf{y})$ and recall the screening property of the Dirac delta distribution [109]

$$\int\limits_{\Omega} \delta(\mathbf{y} - \mathbf{x})f(\mathbf{y})\,d\mathbf{y} = f(\mathbf{x}) \quad \mathbf{x} \in \Omega.$$

Then, it becomes clear that

$$\mathcal{L}_{\mathbf{y}}u^*(\mathbf{x}, \mathbf{y}) = \delta(\mathbf{y} - \mathbf{x}) \tag{2.57}$$

holds in a distributional sense and such a function $u^*(\mathbf{x}, \mathbf{y})$ is called *fundamental solution* of the operator $\mathcal{L}_{\mathbf{y}}$ [107]. Physically, it represents the answer at point $\mathbf{y}$ due to a unit point source at point $\mathbf{x}$. A list of the fundamental solutions used in this work is given in appendix A.

The functions $u^*(\mathbf{x}, \mathbf{y})$ used here do not directly depend on $\mathbf{x}$ or $\mathbf{y}$ but on only the difference $\mathbf{x} - \mathbf{y}$. Therefore, the operations

$$\int\limits_\Omega u^*(\mathbf{x}, \mathbf{y}) q_\Gamma(\mathbf{y}) \, d\mathbf{y} \quad \text{and} \quad \int\limits_\Omega \mathcal{T}_{\mathbf{y}} u^*(\mathbf{x}, \mathbf{y}) u_\Gamma(\mathbf{y}) \, d\mathbf{y}$$

turn out to be spatial convolutions, especially since the range of integration can be extended to $\mathbb{R}^d$ by assuming that $u(\mathbf{x}) = 0$ outside $\overline{\Omega}$.

The fundamental solutions used in this work have the following mapping properties

Poisson equation:	$u^* \colon \mathbb{R}^d \times \mathbb{R}^d \to \mathbb{R}$
Elaststatics:	$u^* \colon \mathbb{R}^d \times \mathbb{R}^d \to \mathbb{R}^d$.

Therefore, in the case of elastostatics u^* can be represented as a $d \times d$-tensor with components $\mathbf{U}^*[i, j]$, $i, j = 1, \ldots, d$.

Hyperbolic initial boundary value problems In the dynamic case, the unknown function $u(\mathbf{x}, t)$ has to fulfill the initial boundary value problem

$$
\begin{aligned}
\left(\rho_0 \frac{\partial^2}{\partial t^2} + \mathcal{L} \right) u(\mathbf{x}, t) &= f(\mathbf{x}, t) & (\mathbf{x}, t) &\in \Omega \times (0, \infty) \\
u_\Gamma(\mathbf{y}, t) &= g_D(\mathbf{y}, t) & (\mathbf{y}, t) &\in \Gamma_D \times (0, \infty) \\
q_\Gamma(\mathbf{y}, t) &= g_N(\mathbf{y}, t) & (\mathbf{y}, t) &\in \Gamma_N \times (0, \infty) \\
u(\mathbf{x}, 0^+) &= u_0(\mathbf{x}) & \mathbf{x} &\in \Omega \\
\dot{u}(\mathbf{x}, 0^+) &= u_1(\mathbf{x}) & \mathbf{x} &\in \Omega
\end{aligned}
\tag{2.58}
$$

formulated on the $(d+1)$-dimensional domain $\overline{\Omega} \times [0, \infty)$. Similar to Green's second identity (2.54) or Betti's theorem of reciprocity, for time dependent problems exists the *dynamic reciprocal identity* [118]

$$
\int\limits_\Omega \left[\left(\rho_0 \frac{\partial^2}{\partial t^2} + \mathcal{L} \right) u \right] * v \, d\mathbf{x} + \int\limits_\Omega \rho_0 \left(u_0 \, \dot{v}(t) + u_1 \, v(t) \right) d\mathbf{x} + \int\limits_\Gamma q_\Gamma * (\mathrm{Tr} \, v) \, ds =
$$
$$
\int\limits_\Omega \left[\left(\rho_0 \frac{\partial^2}{\partial t^2} + \mathcal{L} \right) v \right] * u \, d\mathbf{x} + \int\limits_\Omega \rho_0 \left(v_0 \, \dot{u}(t) + v_1 \, u(t) \right) d\mathbf{x} + \int\limits_\Gamma (\mathcal{T} v) * u_\Gamma \, ds. \tag{2.59}
$$

Here, v fulfills another initial boundary value problem with initial conditions v_0 and v_1, respectively. The operation $*$ denotes the Riemann convolution

$$(g * h)(\mathbf{x}, t) = \int\limits_0^t g(\mathbf{x}, t - \tau) h(\mathbf{x}, \tau) \, d\tau \tag{2.60}$$

whose properties are defined for instance in [118]. Moreover, $u(t)$ means that the function $u(\mathbf{x},t)$ is evaluated at the time point t.

Analogously to the previous section, a function $u^*(\mathbf{x},\mathbf{y},t,\tau)$ is introduced which has the property

$$\int\limits_0^t \int\limits_\Omega \left[\left(\rho_0 \frac{\partial^2}{\partial \tau^2} + \mathcal{L}_\mathbf{y} \right) u^*(\mathbf{x},\mathbf{y},t,\tau) \right] u(\mathbf{y},\tau)\, d\mathbf{y}\, d\tau = u(\mathbf{x},t), \quad (\mathbf{x},t) \in \Omega \times (0,\infty) \quad (2.61)$$

and the above test function $v(\mathbf{x},t)$ is defined by

$$v(\mathbf{y},\tau) = u^*(\mathbf{x},\mathbf{y},t,\tau).$$

The function $u^*(\mathbf{x},\mathbf{y},t,\tau)$ depends only on the time difference $t-\tau$ and not explicitly on the absolute times t or τ. Because of this, property (2.61) is also a convolution with respect to time of u with the hyperbolic differential operator applied to u^* as it is defined in equation (2.60).

Inserting this definition together with property (2.61) into the dynamic reciprocal identity (2.59) and replacing the differential equation by its right hand side, yields the *dynamic representation formula*

$$
\begin{aligned}
u(\mathbf{x},t) = &\int\limits_0^t \int\limits_\Gamma u^*(\mathbf{x},\mathbf{y},t,\tau) q_\Gamma(\mathbf{y},\tau)\, ds_\mathbf{y}\, d\tau - \int\limits_0^t \int\limits_\Gamma \mathcal{T}_\mathbf{y} u^*(\mathbf{x},\mathbf{y},t,\tau) u_\Gamma(\mathbf{y},\tau)\, ds_\mathbf{y}\, d\tau \\
&+ \int\limits_0^t \int\limits_\Omega u^*(\mathbf{x},\mathbf{y},t,\tau) f(\mathbf{y},\tau)\, ds_\mathbf{y}\, d\tau \\
&+ \int\limits_\Omega \rho_0 [u^*(\mathbf{x},\mathbf{y},t,0) u_1(\mathbf{y}) + \dot{u}^*(\mathbf{x},\mathbf{y},t,0) u_0(\mathbf{y})]\, d\mathbf{y}.
\end{aligned}
\quad (2.62)
$$

for $\mathbf{x} \in \Omega$ and $t \in (0,\infty)$. As before, this special function $u^*(\mathbf{x},\mathbf{y},t,\tau)$ fulfills the differential equation for a point source at position $\mathbf{x}$ and time t, i.e.,

$$\left(\rho_0 \frac{\partial^2}{\partial \tau^2} + \mathcal{L}_\mathbf{y} \right) u^*(\mathbf{x},\mathbf{y},t,\tau) = \delta(\mathbf{y}-\mathbf{x})\delta(\tau-t). \quad (2.63)$$

This distributional solution to the partial differential equation is again a fundamental solution. The representation formula (2.62) indicates that if the data set $[u_\Gamma, q_\Gamma]$ is known for all times τ with $0 < \tau < t$, then the unknown function u can be computed for the time t at any point $\mathbf{x}$ inside Ω.

2.5.2 Boundary integral operators

The representation formulae previously introduced allow to express the unknown function u at any point in Ω (and at any time $t > 0$), once the Cauchy data (with their full

history) are given. Obviously, these formulae do not directly yield a solution procedure, since on the boundary part Γ_D the datum $\mathrm{Tr}\,u$ is given but $\mathcal{T}u$ is unknown and vice versa on Γ_N. Therefore, boundary integral equations are needed in order to directly relate boundary data with each other. As before, at first the static and then the dynamic case will be regarded.

Elliptic boundary value problems   The following is mainly adapted from the text books of Steinbach [107] and Rjasanow and Steinbach [94]. The idea is now to apply the trace (2.27) of the static representation formula (2.56) on the boundary. Then, one gets

$$\mathrm{Tr}_{\mathbf{x}}\,u(\mathbf{x}) = \mathrm{Tr}_{\mathbf{x}} \int_{\Gamma} u^*(\mathbf{x},\mathbf{y}) q_\Gamma(\mathbf{y})\,\mathrm{d}s_{\mathbf{y}}$$

$$- \mathrm{Tr}_{\mathbf{x}} \int_{\Gamma} \mathcal{T}_{\mathbf{y}} u^*(\mathbf{x},\mathbf{y}) u_\Gamma(\mathbf{y})\,\mathrm{d}s_{\mathbf{y}} + \mathrm{Tr}_{\mathbf{x}} \int_{\Omega} u^*(\mathbf{x},\mathbf{y}) f(\mathbf{y})\,\mathrm{d}s_{\mathbf{y}}, \quad (2.64)$$

where the subscripts $()_{\mathbf{x}}$ and $()_{\mathbf{y}}$ are used in order to emphasize the variable which the respective operators Tr and $\mathcal{T}$ act upon. Furthermore, for the sake of legibility the shorthands $u_\Gamma = \mathrm{Tr}\,u$ and $q_\Gamma = \mathcal{T}u$ are used. In this application of the trace operator the problem occurs that the function u^* and its derivatives become singular as $\mathbf{x}$ approaches $\mathbf{y}$. All considered fundamental solutions u^* in this work and the traction kernels $\mathcal{T}_{\mathbf{y}} u^*$ of the elastic problems exhibit this behavior Due to this degenerate behavior of the integral kernels, one has to be careful with the commutation of integration and trace operator in equation (2.64). Next, each term is considered separately.

For the last term on the right hand side of equation (2.64), integration and trace easily commute and the *Newton* potential can be defined by

$$(\mathcal{N}_0 f)(\mathbf{x}) = \int_{\Omega} (\mathrm{Tr}_{\mathbf{x}} u^*(\mathbf{x},\mathbf{y})) f(\mathbf{y})\,\mathrm{d}\mathbf{y} = \int_{\Omega} u^*(\mathbf{x},\mathbf{y}) f(\mathbf{y})\,\mathrm{d}\mathbf{y} \quad \mathbf{x} \in \Gamma. \quad (2.65)$$

Also, for the first term integration and trace operator are interchangeable and the *single layer operator* is defined by

$$(\mathcal{V} q_\Gamma)(\mathbf{x}) = \int_{\Gamma} (\mathrm{Tr}_{\mathbf{x}} u^*)(\mathbf{x},\mathbf{y}) q_\Gamma(\mathbf{y})\,\mathrm{d}s_{\mathbf{y}} = \int_{\Gamma} u^*(\mathbf{x},\mathbf{y}) q_\Gamma(\mathbf{y})\,\mathrm{d}s_{\mathbf{y}} \quad \mathbf{x} \in \Gamma. \quad (2.66)$$

The operators defined in equations (2.65) and (2.66) contain so-called *weakly singular* integrals [107], i.e., the result of the integration exists although the integrand tends to infinity for $\mathbf{x} \to \mathbf{y}$.

Problematic is the commutation of integration and trace in the second term on the right hand side of equation (2.64). One gets

$$\mathrm{Tr}_{\mathbf{x}} \int_{\Gamma} \mathcal{T}_{\mathbf{y}} u^*(x,y) u_\Gamma(\mathbf{y})\,\mathrm{d}s_{\mathbf{y}} = -\tilde{\mathcal{C}}(\mathbf{x}) u_\Gamma(\mathbf{x}) + (\mathcal{K} u_\Gamma)(\mathbf{x}).$$

The operator $\mathcal{K}$ denotes the *double layer operator*, defined by

$$(\mathcal{K}u_\Gamma)(\mathbf{x}) = \lim_{\varepsilon \to 0} \int_{\Gamma \backslash B_\varepsilon(\mathbf{x})} \mathcal{T}_\mathbf{y} u^*(\mathbf{x},\mathbf{y}) u_\Gamma(\mathbf{y}) \, ds_\mathbf{y} \quad \mathbf{x} \in \Gamma, \tag{2.67}$$

where $B_\varepsilon(\mathbf{x})$ is a d-dimensional ball around $\mathbf{x}$ with radius ε. Here, the integral is only finite, if the limit is taken such that $B_\varepsilon(\mathbf{x})$ shrinks uniformly to zero. Such an integration is called *Cauchy principal value* [41]. In the case of the scalar problems for the Laplace and the acoustic wave equation, the integral kernel in the double layer operator (2.67) becomes zero for $\mathbf{x} \to \mathbf{y}$ and, therefore, the integral exists even in an improper sense as a weakly singular integral. But in elasticity, one has to carry out the integration with properly taking the limit in the sense of principal value integration. Alternatively, there exists a regularized representation for the double layer potential in elasticity, which is obtained by integration by parts and only consists of weakly singular terms. See, for instance, the book of Kupradze et al. [57] for details on this alternative representation.

Since the range of integration has been split in $\Gamma = \lim_{\varepsilon \to 0}[\Gamma \backslash B_\varepsilon(\mathbf{x}) + \partial B_\varepsilon(\mathbf{x}) \cap \Omega]$, the remaining term is

$$\tilde{\mathcal{C}}(\mathbf{x}) = \lim_{\varepsilon \to 0} \int_{\partial B_\varepsilon(\mathbf{x}) \cap \Omega} \mathcal{T}_y u^*(\mathbf{x},\mathbf{y}) \, ds_\mathbf{y},$$

where $\partial B_\varepsilon(\mathbf{x})$ denotes the surface of the ball $B_\varepsilon(\mathbf{x})$. In view of the final integral equation, it is more convenient to define the following operator

$$\mathcal{C}(\mathbf{x}) = \mathcal{I} + \tilde{\mathcal{C}}(\mathbf{x}) = \mathcal{I} + \lim_{\varepsilon \to 0} \int_{\partial B_\varepsilon(\mathbf{x}) \cap \Omega} \mathcal{T}_y u^*(\mathbf{x},\mathbf{y}) \, ds_\mathbf{y}, \tag{2.68}$$

which is often termed *integral free term* or just *free term*. Here, $\mathcal{I}$ denotes the unity operator, i.e., $\mathcal{I}u_\Gamma = u_\Gamma$. The free term depends on the solid angle of the surface Γ at the point $\mathbf{x}$ and in elasticity it also depends on Poisson's ratio ν. Explicit expressions for $\mathcal{C}(\mathbf{x})$ can be found in [33] and [71]. Fortunately, these rather cumbersome geometric expressions reduce to the simple identity

$$\mathcal{C}(\mathbf{x}) = \frac{1}{2}\mathcal{I} \tag{2.69}$$

if Γ is smooth in the neighborhood of the point $\mathbf{x}$. Due to the assumptions made in this work, one can state that expression (2.69) is valid almost everywhere.

Insertion of the definitions (2.65), (2.66), and (2.67) into equation (2.64) yields the boundary integral equation in operator form

$$(\mathcal{C}u_\Gamma)(\mathbf{x}) + (\mathcal{K}u_\Gamma)(\mathbf{x}) = (\mathcal{V}q_\Gamma)(\mathbf{x}) + (\mathcal{N}_0 f)(\mathbf{x}) \quad \mathbf{x} \in \Gamma. \tag{2.70}$$

Independent of the problem (Dirichlet, Neumann, or mixed boundary value problem), the only unknown values in equation (2.70) are boundary data. More specifically, in a Dirichlet problem one has

$$\mathcal{V}q_\Gamma = (\mathcal{C} + \mathcal{K})g_D - \mathcal{N}_0 f, \tag{2.71}$$

where the argument $\mathbf{x}$ has been omitted. Here, g_D is the given Dirichlet datum as in the problem statement (2.28) and the problem can be solved for the unknown datum q_Γ. The problem formulation (2.71) is the so-called *direct* approach, since the unknown q_Γ is directly obtained as the solution. See [107] or [94] for the description of the indirect approach, where an unphysical density function is used as an intermediate result. An integral equation with the structure of (2.71) is called *Fredholm integral equation of the first kind* [41].

Conversely, the Neumann problem yields the formulation

$$(\mathcal{C} + \mathcal{K})u_\Gamma = \mathcal{V}g_N + \mathcal{N}_0 f, \tag{2.72}$$

where g_N is the given Neumann datum as in problem (2.30) and u_Γ is the only unknown. This equation can be solved by a Neumann series [107]. Again, problem (2.72) is not uniquely solvable but any altered solution $u_\alpha = u_\Gamma + \alpha u_\mathcal{R}$, where $u_\mathcal{R} \in \mathrm{Tr}\,\mathcal{R}$, i.e., belongs to the trace of the rigid body motion spaces (2.33), also solves the problem. Equation (2.72) has the form of a *Fredholm integral equation of the second kind* [41].

For the mixed boundary value problem, the formulation is not so straightforward. At first, define by $\tilde{g}_D$ a continuous extension of the given Dirichlet datum such that

$$\tilde{g}_D(\mathbf{x}) = g_D(\mathbf{x}), \quad \mathbf{x} \in \Gamma_D.$$

With this extended function $\tilde{g}_D$ a new unknown function $\tilde{u}_\Gamma$ is defined by

$$\tilde{u}_\Gamma = u_\Gamma - \tilde{g}_D.$$

Obviously, one gets $\tilde{u}_\Gamma(\mathbf{x}) = 0$ if $\mathbf{x} \in \Gamma_D$ since the function u_Γ is assumed to fulfill the Dirichlet boundary condition a priori. Inserting now $u_\Gamma = \tilde{u}_\Gamma + \tilde{g}_D$ into the boundary integral equation (2.70) yields

$$\begin{aligned} \mathcal{V}q_\Gamma + \mathcal{N}_0 f &= (\mathcal{C} + \mathcal{K})u_\Gamma \\ &= (\mathcal{C} + \mathcal{K})\tilde{u}_\Gamma + (\mathcal{C} + \mathcal{K})\tilde{g}_D. \end{aligned}$$

Rearranging this intermediate result and posing the given Neumann boundary condition as a side condition, the mixed boundary value problem can be formulated as

$$\begin{aligned} \mathcal{V}q_\Gamma - (\mathcal{C} + \mathcal{K})\tilde{u}_\Gamma &= (\mathcal{C} + \mathcal{K})\tilde{g}_D - \mathcal{N}_0 f & \mathbf{x} \in \Gamma \\ q_\Gamma &= g_N & \mathbf{x} \in \Gamma_N. \end{aligned} \tag{2.73}$$

The solution of this system for the unknowns q_Γ and $\tilde{u}_\Gamma$ and the revocation of the above extension gives the full set of Cauchy data $[q_\Gamma, u_\Gamma]$.

Alternatively, a *Dirichlet-to-Neumann* map can be established by solving the boundary integral equation (2.70) for the Neumann datum q_Γ

$$q_\Gamma = \mathcal{V}^{-1}(\mathcal{C} + \mathcal{K})u_\Gamma - \mathcal{V}^{-1}\mathcal{N}_0 f$$

and the *Steklov-Poincaré* operator $\mathcal{S}$ is introduced by

$$\underbrace{\mathcal{V}^{-1}(\mathcal{C}+\mathcal{K})}_{\mathcal{S}}u_\Gamma = q_\Gamma + \mathcal{V}^{-1}\mathcal{N}_o f. \tag{2.74}$$

The existence and uniqueness of the inverse of the single layer operator $\mathcal{V}$ is guaranteed for the given problems in three dimensions and with some restrictions in two dimensions as discussed by Steinbach [107]. By means of this new operator, the mixed boundary value problem (2.73) becomes

$$\mathcal{S}\tilde{u}_\Gamma = g_N - \mathcal{S}\tilde{g}_D + \mathcal{V}^{-1}\mathcal{N}_0 f \quad \mathbf{x} \in \Gamma_N. \tag{2.75}$$

Remark 2.1. By application of the traction operator $\mathcal{T}_\mathbf{x}$ (2.29) to the representation formula (2.56), one obtains the hypersingular boundary integral equation

$$(\tilde{C}q_\Gamma(\mathbf{x})) - (\mathcal{K}'q_\Gamma)(\mathbf{x}) = (\mathcal{D}u_\Gamma)(\mathbf{x}) + (\mathcal{N}_1 f)(\mathbf{x}) \quad \mathbf{x} \in \Gamma. \tag{2.76}$$

Here, the adjoint double layer operator $\mathcal{K}'$, the hypersingular operator $\mathcal{D}$ and another Newton potential $\mathcal{N}_1$ have been introduced (cf. [107] for the exact definitions). The important feature is now, that the combination of the two boundary integral equations (2.70) and (2.76) allows for a symmetric formulation of the mixed boundary value problem and, moreover, if a Galerkin projection scheme is used the system matrices will then be symmetric too. A symmetric formulation of the Steklov-Poincaré operator (2.74) is then possible

$$\mathcal{S} = \mathcal{D} + (\mathcal{C} + \mathcal{K}')\mathcal{V}^{-1}(\mathcal{C}+\mathcal{K}) \tag{2.77}$$

by using both integral equations (2.70) and (2.76). $\Diamond$

Hyperbolic initial boundary value problems   In the dynamic case, the same procedure as before is applied, i.e., the application of the trace $\mathrm{Tr}_\mathbf{x}$ (2.27) to the dynamic representation formula (2.62) gives the boundary integral equation in operator form

$$\mathcal{C}(\mathbf{x})u_\Gamma(\mathbf{x},t) + (\mathcal{K}_t * u_\Gamma)(\mathbf{x},t) = (\mathcal{V}_t * q_\Gamma)(\mathbf{x},t) + (\mathcal{N}_t * f)(\mathbf{x},t) \quad \mathbf{x} \in \Gamma. \tag{2.78}$$

In this equation, $*$ denotes again the temporal convolution as defined in equation (2.60). Equation (2.78) is a *Volterra integral equation* [41]. The employed operators are the single layer operator

$$(\mathcal{V}_t * q_\Gamma)(\mathbf{x},t) = \int\limits_0^t \int\limits_\Gamma u^*(\mathbf{x},\mathbf{y},t,\tau)q_\Gamma(\mathbf{y},\tau)\,\mathrm{d}s_\mathbf{y}\,\mathrm{d}\tau, \tag{2.79}$$

the double layer operator

$$(\mathcal{K}_t * u_\Gamma)(\mathbf{x},t) = \lim_{\varepsilon \to 0}\int\limits_o^t \int\limits_{\Gamma\backslash B_\varepsilon(\mathbf{x})} \mathcal{T}_\mathbf{y}u^*(\mathbf{x},\mathbf{y},t,\tau)u_\Gamma(\mathbf{y},\tau)\,\mathrm{d}\mathbf{y}\,\mathrm{d}\tau, \tag{2.80}$$

and the Newton potential

$$(\mathcal{N}_t * f)(\mathbf{x},t) = \int\limits_0^t \int\limits_\Omega u^*(\mathbf{x},\mathbf{y},t,\tau) f(\mathbf{y},\tau)\,\mathrm{d}\mathbf{y}\,\mathrm{d}\tau$$

$$+ \int\limits_\Omega \rho_0 \left[u^*(\mathbf{x},\mathbf{y},t,0)u_1(\mathbf{y}) + \frac{\partial}{\partial t} u^*(\mathbf{x},\mathbf{y},t,0)u_1(\mathbf{y}) \right] \mathrm{d}\mathbf{y}. \quad (2.81)$$

The integral free term $\mathcal{C}(\mathbf{x})$ turns out to be the same as defined in equation (2.68) in the static case [98].

Whereas the treatment of elliptic boundary value problems has been analyzed rather exhaustively, mathematical literature on the like for time-dependent problems is moderate. Moreover, the Steklov-Poincaré operator $\mathcal{S}$ as defined for the static case by equation (2.74) cannot be formulated directly. A good overview is given in a survey article by Costabel [13].

2.6 Unbounded Domains

Until now, it has been assumed that the domain Ω under consideration is bounded and, therefore, has a closed surface Γ. In certain physical applications, this assumption is not valid and the domain Ω is unbounded. One example is the sound emission of a body, where this body occupies a bounded region Ω_{int} and the analysis takes place in its complement $\Omega_{ext} = \mathbb{R}^d \setminus \overline{\Omega}_{int}$. Another example is the wave propagation in an elastic halfspace, for instance $\Omega = \{\mathbf{x} \in \mathbb{R}^d : x_d > 0\}$ with $\Gamma = \{\mathbf{x} \in \mathbb{R}^d : x_d = 0\}$, where the domain and its boundary are both unbounded.

Static case Here, the solution $u(\mathbf{x})$ and its first derivatives have to exhibit a certain decay behavior as $|\mathbf{x}| \to \infty$ in order to ensure the unique solvability of the boundary value problem. At first, the case of a bounded and closed surface $\Gamma = \partial\Omega$ is considered.

Kupradze et al. [57] derive these conditions by means of Green's formula similar to the minimization of the potential (2.45). Taking an auxiliary domain Ω_R which is defined by $\Omega_R = \Omega \cap B_R(\mathbf{x}_0)$, where $B_R(\mathbf{x}_0) = \{\mathbf{x} \in \mathbb{R}^d, R > 0 : |\mathbf{x} - \mathbf{x}_0| < R\}$ is chosen such that it fully contains the boundary Γ. Now,

$$a_R(u,u) = \int\limits_{\Omega_R} f u\,\mathrm{d}\mathbf{x} + \int\limits_{\Gamma_N} g_N u_\Gamma\,\mathrm{d}s + \int\limits_{\partial B_R(\mathbf{x}_0)} q_\Gamma(\mathrm{Tr}\,u)\,\mathrm{d}s \quad (2.82)$$

denotes the strain energy (up to some factor) of the function u for a boundary value problem formulated on Ω_R with given force term f and Neumann boundary conditions g_N on $\Gamma_N \subseteq \Gamma$. The strain energy of the solution on the unbounded domain is then given by

the limit $\lim_{R \to \infty} a_R(u, u)$. This expression shall be finite for obvious physical reasons. This requirement implies the necessary condition that the force function f has a bounded support, i.e., the set $\mathrm{supp}(f) = \{\mathbf{x} \in \Omega : f(\mathbf{x}) \neq 0\}$ is bounded. A diverging behavior of the first integral in (2.82) for the limit $R \to \infty$ is thus prevented. It remains to require (see also [14])

$$\lim_{R \to \infty} \int_{\partial B_R(\mathbf{x}_0)} q_\Gamma \cdot u_\Gamma \, \mathrm{d}s = 0.$$

Therefore, the following conditions are posed [57]

$$\lim_{|\mathbf{x}| \to \infty} |\mathbf{x}| u(\mathbf{x}) = C \in \mathbb{R} \quad \text{and} \quad \lim_{|\mathbf{x}| \to \infty} |\mathbf{x}| |\nabla u| = 0. \tag{2.83}$$

These conditions are obtained for three space dimensions. In two space dimensions, it is sufficient to replace the factor $|\mathbf{x}|$ by its square root

$$\lim_{|\mathbf{x}| \to \infty} \sqrt{|\mathbf{x}|} \, u(\mathbf{x}) = C \in \mathbb{R} \quad \text{and} \quad \lim_{|\mathbf{x}| \to \infty} \sqrt{|\mathbf{x}|} \, |\nabla u| = 0. \tag{2.84}$$

Hence, under conditions (2.83) for three space dimensions (or conditions (2.84) for two space dimensions) the static boundary value problem formulated on the unbounded domain Ω is uniquely solvable.

The question arises, whether the representation formula (2.56) is valid for unbounded domains. Therefore, it will be first formulated on the auxiliary domain $\Omega_R = \Omega \cap B_R(\mathbf{x}_0)$

$$u(\mathbf{x}) = \int_\Gamma u^*(\mathbf{x}, \mathbf{y}) q_\Gamma(\mathbf{y}) \, \mathrm{d}s_\mathbf{y} - \int_\Gamma \mathcal{T}_\mathbf{y} u^*(\mathbf{x}, \mathbf{y}) u_\Gamma(\mathbf{y}) \, \mathrm{d}s_\mathbf{y}$$

$$+ \int_{\partial B_R(\mathbf{x}_0)} u^*(\mathbf{x}, \mathbf{y}) q_\Gamma(\mathbf{y}) \, \mathrm{d}s_\mathbf{y} - \int_{\partial B_R(\mathbf{x}_0)} \mathcal{T}_\mathbf{y} u^*(\mathbf{x}, \mathbf{y}) u_\Gamma(\mathbf{y}) \, \mathrm{d}s_\mathbf{y}.$$

Ideally, the additional integrals over the surface of $B_R(\mathbf{x}_0)$ would vanish if the limit $R \to \infty$ is taken [14]. The fundamental solutions used in this work have the following asymptotic behavior with some finite constant $C \in \mathbb{R}$:

$$d = 3: \qquad \lim_{|\mathbf{x} - \mathbf{y}| \to \infty} |\mathbf{x} - \mathbf{y}| u^*(\mathbf{x}, \mathbf{y}) = C \qquad \lim_{|\mathbf{x} - \mathbf{y}| \to \infty} |\mathbf{x} - \mathbf{y}|^2 \mathcal{T}_\mathbf{y} u^*(\mathbf{x}, \mathbf{y}) = C$$

$$d = 2: \qquad \lim_{|\mathbf{x} - \mathbf{y}| \to \infty} \frac{u^*(\mathbf{x}, \mathbf{y})}{\log |\mathbf{x} - \mathbf{y}|} = C \qquad \lim_{|\mathbf{x} - \mathbf{y}| \to \infty} |\mathbf{x} - \mathbf{y}| \mathcal{T}_\mathbf{y} u^*(\mathbf{x}, \mathbf{y}) = C.$$

By means of the conditions (2.83), it is easy to show that in three dimensions the additional integrals vanish and the representation formula (2.56) is exactly the same for the unbounded domains. In two dimensions, unfortunately, the logarithmic behavior of $u^*(\mathbf{x}, \mathbf{y})$ destroys the pattern and the corresponding integral does not vanish under the given conditions. Therefore, further restrictions on q_Γ are necessary for the validity of the representation formula for unbounded domains in two dimensions, which will not be outlined further.

See the analysis of the ellipticity of the single layer operator in the book of Steinbach [107] for more details.

Note that here, contrary to many textbooks on the matter, the normal vector **n** is pointing out of the domain Ω even if it is an exterior domain that is under consideration.

It is important to mention that the Neumann problem, i.e., problem (2.30), formulated on an unbounded domain together with the conditions (2.83) (or (2.84)) is uniquely solvable. Any function u_0 for which $\mathcal{L}u_0 = 0$ and $\mathcal{T}u_0 = 0$ hold is identically zero if it additionally fulfills conditions (2.83) (or (2.84)) and, therefore, does not alter the solution u of the problem.

These observations are based on the assumption that although Ω is unbounded, its boundary Γ is a closed and bounded surface. In some circumstances, it will be of interest to consider the halfspace $\Omega = \left\{ \mathbf{x} \in \mathbb{R}^d : x_d > 0 \right\}$ or similar geometries, where the boundary is unbounded too. Knops and Payne [54] summarize uniqueness theorems for this case in elastostatics, where the conditions in the limit $R \to \infty$ are less severe and certain unphysical values of Poisson's ratio v have to be excluded. Here, this argument is not followed any longer and the above conditions (2.83) or (2.84) for three or two space dimensions, respectively, are assumed to hold and to be sufficient for the considered problems.

Dynamic case   Wheeler and Sternberg [118] have thoroughly analyzed uniqueness theorems, reciprocal and integral identities for unbounded domains, where the case of an unbounded boundary Γ is included in the considerations. Recall the energy identity (2.43),

$$\mathcal{K}(u) + \mathcal{U}(u) = \int_0^t \int_\Omega f \cdot \dot{u}\, d\mathbf{x}\, d\tau + \int_0^t \int_\Gamma q_\Gamma \cdot (\operatorname{Tr}\dot{u})\, ds\, d\tau, \tag{2.85}$$

where $u = 0$ for all $t \leq 0$ has been additionally assumed. Recall, that f represents either the acoustic source $\rho_0 g$ or the dynamic force term **f**, see equations (2.9) or (2.21), respectively. Expression (2.85) describes the total energy in the system at time $t > 0$. If the right hand side of equation (2.85) is finite, then the left hand side has to be finite as well. Therefore, the conditions on the unique solvability are that these two integrals are bounded. This is ensured by postulating that the force term f and the product $q_\Gamma \cdot (\operatorname{Tr}\dot{u})$ have a bounded support, i.e.,

$$\begin{aligned} f(\mathbf{x},t) &= 0 & (\mathbf{x},t) &\in (\Omega \setminus \Upsilon_t) \times [0,t] \\ q_\Gamma(\mathbf{y},t) \cdot (\operatorname{Tr}\dot{u})(\mathbf{y},t) &= 0 & (\mathbf{x},t) &\in (\Gamma \setminus \Upsilon_t) \times [0,t]. \end{aligned} \tag{2.86}$$

Here, Υ_t is a bounded set in $\mathbb{R}^d$ whose shape and position might depend on the time t. Outside this bounded set the above products vanish and, therefore, the integrals on the right hand side of equation (2.85) are of finite value. Note that the first condition in (2.86) has been implicitly assumed in the consideration of equation (2.82). It only depends on the given data. Conversely, the second condition has to be fulfilled by the unknown itself.

For exterior problems only, one could take the same approach as in the static case by introducing an auxiliary outer boundary which then tends to infinity. This approach then again yields specific requirements on stresses and velocities for $|\mathbf{x}| \to \infty$ (see [118] and references therein).

Under the assumptions (2.86), the dynamic reciprocal identity (2.59) retains its validity

$$\int\limits_{\Omega} \left[\left(\rho_0 \frac{\partial^2}{\partial t^2} + \mathcal{L} \right) u \right] * v \, d\mathbf{x} + \int\limits_{\Gamma} q_{\Gamma} * (\mathrm{Tr}\, v) \, ds =$$

$$\int\limits_{\Omega} \left[\left(\rho_0 \frac{\partial^2}{\partial t^2} + \mathcal{L} \right) v \right] * u \, d\mathbf{x} + \int\limits_{\Gamma} (\mathcal{T} v) * u_{\Gamma} \, ds, \quad (2.87)$$

again with a quiescent past. By means of this identity, the representation formula is easily established by replacing the test function v by the fundamental solution u^*. Finally, the representation formula (2.62) is recovered [1]

$$u(\mathbf{x}, t) = \int\limits_0^t \int\limits_{\Gamma} u^*(\mathbf{x}, \mathbf{y}, t, \tau) q_{\Gamma}(\mathbf{y}, \tau) \, ds_{\mathbf{y}} \, d\tau - \int\limits_0^t \int\limits_{\Gamma} \mathcal{T}_{\mathbf{y}} u^*(\mathbf{x}, \mathbf{y}, t, \tau) u_{\Gamma}(\mathbf{y}, \tau) \, ds_{\mathbf{y}} \, d\tau$$

$$+ \int\limits_0^t \int\limits_{\Omega} u^*(\mathbf{x}, \mathbf{y}, t, \tau) f(\mathbf{y}, \tau) \, ds_{\mathbf{y}} \, d\tau. \quad (2.88)$$

This formula is well applicable to the dynamic analysis of unbounded media even with unbounded boundaries as, for instance, the halfspace. As shown in chapter 5 the halfspace is still approximated in a good way if the unbounded surface Γ is replaced in the numerical analysis by some bounded surface patch.

3 NUMERICAL APPROXIMATIONS

This chapter is dedicated to the numerical approximation methods used in this work to obtain approximate solutions for the considered mathematical models. These models and related representations have been introduced in chapter 2. At first, in section 3.1 some basic concepts of spatial discretization methods are reviewed before the discretization of variational principles by finite elements and of the boundary integral equations by boundary elements are presented in sections 3.1.2 and 3.1.3, respectively. For both methods, the static case is regarded first leading to an algebraic system of equations before considering the dynamic situation which yield semi-discrete equations. The resulting systems of time-continuous equations will then be handled by the methods presented in section 3.2. Specific details on the computation of the final matrix entries are outlined in section 3.3 with emphasis on the singular integrals occurring in the boundary element discretization. Finally, the direct solution techniques employed for obtaining the unknown data are presented in section 3.4.

3.1 Spatial Discretization

In this section, the spatial discretization for static and dynamic problems is considered. To begin with, some basic concepts are shown for static problems, which coin the essence of the afterwards presented discretization methods, finite elements in subsection 3.1.2 and boundary elements in subsection 3.1.3.

3.1.1 Basic concepts

In order to illustrate the respective characteristics of the used numerical methods, some fundamental items are presented first. These are the Ritz method and weighted residuals.

Ritz method   Consider the *Dirichlet problem*

$$-\Delta u(\mathbf{x}) = 0 \quad \text{in } \Omega, \qquad (\text{Tr}\, u)(\mathbf{y}) = g_D(\mathbf{y}) \quad \text{on } \Gamma = \partial\Omega. \tag{3.1}$$

It is well known that a function v, which minimizes the Dirichlet integral [115]

$$J(v) = \frac{1}{2} \int_\Omega \nabla v \cdot \nabla v \, d\mathbf{x} \tag{3.2}$$

and fulfills $v_\Gamma = g_D$ on Γ, is the solution to problem (3.1).

The idea of Ritz [92] was to minimize J in a finite dimensional subspace of the original solution space. Therefore, the approximation

$$v_n(\mathbf{x}) = g(\mathbf{x}) + \sum_{i=1}^{n} a_i \varphi_i(\mathbf{x}) \tag{3.3}$$

is used, where $g(\mathbf{y}) = g_D(\mathbf{y})$ and $\varphi_i(\mathbf{y}) = 0$, $i = 1, \ldots, n$, on Γ. This approximation obviously fulfills the Dirichlet boundary condition of the original problem. Moreover, the functions φ_i are chosen such that

$$\sum_{i=1}^{n} a_i \varphi_i(\mathbf{x}) = 0 \quad \Leftrightarrow \quad a_i = 0, i = 1, \ldots, n,$$

i.e., the φ_i are linear independent. Inserting this approximation (3.3) into the Dirichlet integral (3.2) yields a function of the unknown coefficients a_i

$$J_n(a_1, \ldots, a_n) = \frac{1}{2} \int_\Omega \nabla v_n \cdot \nabla v_n \, d\mathbf{x}. \tag{3.4}$$

A linear system of n equations for the n unknown coefficients is finally obtained by requiring

$$\frac{\partial J_n}{\partial a_1} = 0, \quad \ldots, \quad \frac{\partial J_n}{\partial a_n} = 0. \tag{3.5}$$

This yields the system of equations

$$\mathsf{A}\mathsf{u} = \mathsf{g} \tag{3.6}$$

with the matrix entries

$$\mathsf{A}[i, j] = \int_\Omega \nabla \varphi_i \cdot \nabla \varphi_j \, d\mathbf{x}$$

$$\mathsf{u}[i] = a_i \qquad\qquad i, j = 1, \ldots n. \tag{3.7}$$

$$\mathsf{g}[i] = -\int_\Omega \nabla g \cdot \nabla \varphi_i \, d\mathbf{x}$$

Once the coefficients a_i are computed from equations (3.5), the function v_n as expressed in equation (3.3) gives an approximation to the solution u of problem (3.1) which is optimal when J is used as a measure. Moreover, it easily shown that [115]

$$J_m(a_1, \ldots, a_m) \geq J_n(a_1, \ldots, a_n) \geq J(u),$$

where $m < n$, i.e., the minimal value of J is approached from above.

The described procedure is commonly referred to as *Ritz method*. This method is easily extended to other problems by using the appropriate energy integrals J. For instance, applying this procedure to the elastic potential (2.44) gives an approximation for the displacement field $\mathbf{u}$ which is a solution to the mixed boundary value problem of elastostatics.

It has to be noted that the choice of the trial functions φ_i which constitute the approximation (3.3) is fundamental for the convergence behavior of the method. For instance, taking the monomials x^i for a one-dimensional problem gives a very ill-conditioned system of equations which is not solvable in practice. The most efficient choice would be functions such that the final system matrix A is diagonal, but these are very difficult to obtain. The most established choice of trial functions are finite elements, as they are introduced below. See the introduction of the book of Strang and Fix [110] for an in-depth discussion on this matter. Moreover, in the same reference a discussion of the corresponding function spaces is given in order to ensure the unique solvability of the above described minimization problem.

Weighted residuals The method of weighted residuals, also referred to as *Galerkin* method, starts from the residual of the differential equation $\mathcal{L}u = f$, defined as

$$\mathcal{R}(v) = \mathcal{L}v - f, \tag{3.8}$$

which is obviously zero in the case of v being the solution of the differential equation. The first step is now to use again an approximation as for the Ritz method (3.3)

$$v_n(\mathbf{x}) = g(\mathbf{x}) + \sum_{i=1}^{n} a_i \varphi_i(\mathbf{x}),$$

which fulfills the given Dirichlet boundary condition. Now, the residual $\mathcal{R}(v_n)$ does not vanish (unless v_n is already the solution of the problem). The idea of the method of weighted residuals [33] is to require that

$$\int_{\Omega} \mathcal{R}(v_n) \cdot w_j \, d\mathbf{x} = 0 \quad \forall w_j \tag{3.9}$$

with a certain set of weight functions w_j, $j = 1, \ldots, n$. Note that expression (3.8) requires that the function v has to be twice differentiable. Therefore, the residual $\mathcal{R}(v_n)$ of the Ritz approximation is only a valid expression if this approximation is twice differentiable, too. Nevertheless, the integral of the weighted residual (3.9) exists for suitably chosen weight functions w_j even if the approximation has a lower regularity. See the books of Braess [9] or Strang and Fix [110] for more details on the regularity requirements of trial and weight functions.

The classical Galerkin method, or Bubnov-Galerkin method, is to take as weight functions the same φ_i as for the approximation. The identity (3.9) yields after integration by parts a system of equations for the unknown coefficients a_i of the approximate solution.

This approach gives for the problems considered in this work exactly the same system of equations as for the Ritz method. Alternatively to the two approaches, one can first derive the corresponding variational principle (cf. for instance equation (2.52)) by variation of the potential (2.44) or by the procedure described in section 2.4. Then employing the

approximation (3.3) and taking the functions φ_i as weight functions gives again exactly the same system of equations.

Other than weighting the residual by the trial functions, one can require that this residual of the approximation vanishes at a certain set of points $\mathbf{x}_j^*$, $j = 1, \ldots, n$, which yields the *collocation* method. There, it is stated that

$$\mathcal{R}(v_n)(\mathbf{x}_j^*) = 0 \quad \forall \mathbf{x}_j^*. \tag{3.10}$$

Of course, the choice of the location of these collocation points $\mathbf{x}_j^* \in \Omega$ is critical to this method. By means of the Dirac delta distribution $\delta(\mathbf{x})$ and its screening property [109], the collocation method can be written as

$$\int_\Omega \mathcal{R}(v_n) \cdot \delta(\mathbf{x} - \mathbf{x}_j^*) \, \mathrm{d}\mathbf{x} = 0 \quad \forall \mathbf{x}_j^*.$$

Note that the classical Galerkin method with weight functions taken as the approximation functions φ_i finally yields a symmetric system of equations (at least in the here considered cases, where $\mathcal{L}$ is self-adjoint). On the contrary, the collocation method gives a system matrix, which in general is nonsymmetric.

3.1.2 Finite elements

The method of finite elements as an approximation method for the solution of boundary value problems is well established. It is by far the most popular method in numerical analysis of structural mechanics. The literature on finite elements is vast from both the engineering and mathematical community.

The term *finite elements* refers to a special choice of trial and test functions when solving a boundary value problem by means of a variational principle. This special type of functions has the property that each member is non-zero only inside a small subset of the domain Ω but obeys the same regularity requirements as for the unknown function u and the test functions v. The latter criterion can be relaxed in the context of non-conforming finite element methods, which are not considered further in this work.

The books of Bathe [6], Braess [9], Hughes [49], Jung and Langer [52], Steinbach [107], Strang and Fix [110], Szabó and Babuška [112], and Zienkiewicz and Taylor [120] are just a few examples of the numerous text books on the matter.

Static problems   The first step in construction of a finite element discretization consists in a geometric triangulation of the domain Ω. Therefore, $\overline{\Omega}$ is approximated by

$$\overline{\Omega}_h = \bigcup_{e=1}^{N_e} \overline{\tau}_e, \tag{3.11}$$

which is the union of N_e geometric elements τ_e. These elements are usually of a very simple structure. In three space dimensions tetrahedra and hexahedra are a common choice, whereas in two dimensions triangles and quadrilaterals prevail. Furthermore, every such element τ_e can be expressed as the representation of a coordinate transformation from the reference element $\hat{\tau}$ to the coordinate space in which Ω_h is defined

$$\mathbf{x} \in \tau_e: \quad \mathbf{x}(\xi) = \sum_i \varphi_i^g(\xi) \mathbf{x}_i^e. \tag{3.12}$$

Here, $\mathbf{x}(\xi)$ maps points $\xi = [\xi_1, \ldots, \xi_d]^\top$ from the d-dimensional parameter space to the coordinates in $\mathbb{R}^d$. $\mathbf{x}_i^e$ are the vertices of the element τ_e and the functions φ_i^g are Lagrangian polynomials. With every triangulation the parameter h is associated which is a measure of the mesh width. The elements τ_e are assumed to be of a certain shape regularity (cf. Braess [9]) such that the coordinate transformation (3.12) is well-defined.

Once this triangulation is established, finite element functions are easily constructed. Although many other choices are possible, here the trial function φ_i corresponds to the vertex $\mathbf{x}_i$ and vanishes outside the elements which are connected to this vertex. Its restriction to an element $\varphi_i|_{\tau_e}$ can be expressed by a Lagrangian polynomial when mapped onto the reference element $\hat{\tau}$. For simplicity, the same symbol φ_i is used for $\varphi_i(\mathbf{x})$ in the computational domain Ω_h and for $\varphi_i(\xi)$, the trial function on the reference element. With these trial functions, the unknown function is approximated by (similar to Ritz' idea [92] in equation (3.3))

$$u_h(\mathbf{x}) = \sum_{i=1}^{N} u_i \varphi_i(\mathbf{x}). \tag{3.13}$$

One has to be keep in mind for elastic problems that u then represents the displacement field $\mathbf{u} = [u_1, \ldots, u_d]$ of d components. Then the above approximation has to be done for every component thus leading to $N \times d$ coefficients. Since the φ_i are Lagrangian polynomials, the so-called Kronecker delta property holds, i.e.,

$$\varphi_i(\mathbf{x}_j) = \begin{cases} 1 & \text{if} \quad i = j \\ 0 & \text{else} \end{cases} \tag{3.14}$$

and, therefore, the coefficients u_i of the approximation (3.13) are the function values of the approximate u_h at the vertices $\mathbf{x}_i$.

Here, only *isoparametric* finite elements are employed which means that $\varphi_i^g = \varphi_i$. Hence, in the geometry representation (3.12) the same basis functions are used as for the finite element trial functions in equation (3.13). Moreover, it has to be emphasized that the shape functions are *continuous* and the gradients involved in the bilinear form $a(\cdot, \cdot)$ are thus valid operations.

For convenience, the space of finite element functions is defined by

$$S_h(\Omega_h) = \text{span}\{\varphi_i\}_{i=1}^{N}. \tag{3.15}$$

Furthermore, $S_{h,0}$ is the subspace of S_h whose members vanish on the Dirichlet boundary

$$S_{h,0}(\Omega_h) = \left\{ \varphi \in S_h : \varphi(\mathbf{y}) = 0 \quad \text{on } \Gamma_{D,h} \right\}.$$

Note that $\Gamma_{D,h}$ simply denotes the Dirichlet part of the boundary of Ω_h. At last, $S_{h,D}$ is the subspace of S_h whose members assume the prescribed Dirichlet boundary conditions

$$S_{h,D}(\Omega_h) = \left\{ \varphi \in S_h : \varphi(\mathbf{y}) = g_{D,h}(\mathbf{y}) \quad \text{on } \Gamma_{D,h} \right\}.$$

In this expression, $g_{D,h}$ denotes the approximation of the prescribed Dirichlet datum obtained either by interpolation or by an L_2-projection, see Steinbach [107] for details in these approximations. With these subspaces, the classical finite element method is easily stated by the discrete variational principle:

Find $u_h \in S_{h,D}$ such that

$$a(u_h, v) = \ell(v) \quad \text{in} \quad \Omega_h \tag{3.16}$$

for all $v \in S_{h,0}$.

This principle yields for homogeneous Dirichlet data, i.e., $g_D = 0$, the system of linear equations

$$\mathsf{A}\mathsf{u} = \mathsf{f} \tag{3.17}$$

where the matrices have the following coefficients and dimensions

$$\begin{aligned} \mathsf{A}[i,j] &= a(\varphi_j, \varphi_i) \\ \mathsf{u}[j] &= u_j \qquad\qquad i,j = 1,\ldots,N_0. \\ \mathsf{f}[j] &= \ell(\varphi_j) \end{aligned} \tag{3.18}$$

N_0 is the dimension of the finite element space $S_{h,0}$, i.e., $N_0 = \dim(S_{h,0})$. This matrix A is usually called *stiffness matrix*, a name obviously originating from structural mechanics. Note that

$$a(\varphi_j, \varphi_i) = 0 \quad \text{if} \quad \text{supp}(\varphi_j) \cap \text{supp}(\varphi_i) = \emptyset$$

and, therefore, the number of non-zero entries of the matrix A is relatively small with respect to the total number of entries. The system matrix is referred to as a *sparse* matrix for this reason.

The treatment of problems with prescribed inhomogeneous Dirichlet data is a little more complicated. A function u_D is now introduced with the properties [9]

$$u_D(\mathbf{x}_i) = g_D(\mathbf{x}_i) \quad \forall \mathbf{x}_i \in \Gamma_{D,h} \quad \text{and} \quad u_D(\mathbf{x}_j) = 0 \quad \forall \mathbf{x}_j \in \Omega_h,\, \mathbf{x}_j \notin \Gamma_{D,h}.$$

This function is easily constructed, once the finite element space is available. Then, one can decompose the approximate for the unknown u like

$$u_h = \tilde{u}_h + u_D$$

and obtain the modified variational principle:

Find $\tilde{u}_h \in S_{h,0}$ such that

$$a(\tilde{u}_h, v) = \ell(v) - a(u_D, v) \quad \text{in} \quad \Omega_h \tag{3.19}$$

for all $v \in S_{h,0}$.

This leads to the same system of equations as in equation (3.17)

$$\mathsf{A}\mathsf{u} = \mathsf{f}_D \tag{3.20}$$

but with a different right hand side

$$\mathsf{f}_D[j] = \ell(\varphi_j) - a(u_D, \varphi_j) \quad j = 1, \ldots, N_0. \tag{3.21}$$

Since $\tilde{u}_h$ coincides with u_h at every node which does not belong to the Dirichlet boundary $\Gamma_{D,h}$, the solution of the system (3.20) directly gives the unknown coefficients of the approximate u_h.

Remark 3.1. In elasticity, it may occur that the boundary conditions at a specific part of the boundary are not entirely of Dirichlet or Neumann type but are mixed in the components. Moreover, these components need not coincide with the directions of the global coordinate system. Consider for instance roller bearings where the plane of unrestrained movement is tangential to the boundary but not along any global coordinate direction. In this case, the above approach is not directly applicable but additional equations prescribing the relations among each other, e.g., normal and tangential displacement components have to be employed. This can be done either by modification of the final system matrices [6] or by employing Lagrange multipliers for these equations as side conditions [5]. Although apparent in many engineering applications, such situations are not considered further in this work. Here, the occurrence of mixed boundary conditions at the same point is included only if the corresponding directions coincide with the global system of coordinates. ◇

Dynamic problems In dynamic problems it is common to begin with the same procedure as introduced above by using the approximation

$$u_h(\mathbf{x}, t) = \sum_{i=1}^{N} u_i(t) \varphi_i(\mathbf{x}), \tag{3.22}$$

which is a separation of variables. The trial functions φ_i are constructed in exactly the same manner as for the static case. Also, the finite element spaces are the same as above and the test function v is independent of time and taken from the space $S_{h,0}$, as before.

Contrarily, now the dynamic variational principle (2.51) has to be used for obtaining the system of ordinary differential equations [49]

$$\mathsf{M}\ddot{\mathsf{u}}(t) + \mathsf{A}\mathsf{u}(t) = \mathsf{f}(t). \tag{3.23}$$

Here, the matrix M is called *mass matrix* for obvious reasons. This equation is often referred to as a *semi-discrete* equation, since only the spatial discretization has been carried

out and a system of ordinary differential equations in time remains. The coefficients of the matrices in the system (3.23) are

$$
\begin{aligned}
\mathsf{M}[i,j] &= \langle \rho_0 \varphi_j, \varphi_j \rangle \\
\ddot{\mathsf{u}}(t)[j] &= \ddot{u}_j(t) \\
\mathsf{A}[i,j] &= a(\varphi_j, \varphi_i) \qquad i,j = 1,\dots,N, \\
\mathsf{u}(t)[j] &= u_j(t) \\
\mathsf{f}(t)[j] &= \ell_t(\varphi_j)
\end{aligned}
\tag{3.24}
$$

where it has to emphasized that the external work ℓ_t is now a function of time.

Transferring the treatment of Dirichlet boundary conditions to the dynamic case is straightforward and will not be repeated here. The initial conditions are incorporated by means of the systems

$$
\bar{\mathsf{M}}\mathsf{u}(0^+) = \mathsf{f}_0^0 \quad \text{and} \quad \bar{\mathsf{M}}\dot{\mathsf{u}}(0^+) = \mathsf{f}_1^0,
\tag{3.25}
$$

which have the following coefficients

$$
\begin{aligned}
\bar{\mathsf{M}}[i,j] &= \langle \varphi_j, \varphi_i \rangle \\
\mathsf{f}_0^0[j] &= \langle u_0, \varphi_j \rangle \qquad i,j = 1,\dots,N. \\
\mathsf{f}_1^0[j] &= \langle u_1, \varphi_j \rangle
\end{aligned}
\tag{3.26}
$$

The system of ordinary differential equations can then be solved by a time stepping method as shown in section 3.2.1.

3.1.3 Boundary elements

The numerical solution of boundary value problems using the boundary integral representation (2.70) (or equation (2.78) for dynamics) leads to so-called boundary element methods.

Among the first publications on this matter where the papers of Jaswon and Symm [51,111] for the Laplace equation and of Rizzo [93] for elastostatics. The textbooks of Gaul et al. [33], Hartmann [45], and Steinbach [107] provide good introductions and overviews of the method.

For simplicity, the Newton potentials are not considered any further in this work, i.e.,

$$
(\mathcal{N}_0 f)(\mathbf{x}) = 0 \quad \text{and} \quad (\mathcal{N}_t * f)(\mathbf{x}, t) = 0
\tag{3.27}
$$

for the static and dynamic situation, respectively. These assumptions correspond to a vanishing body force f in statics and in dynamics to vanishing initial conditions, or a quiescent past, and a vanishing body force for all times.

Now, the remaining terms in the boundary integral equations (2.70) and (2.78) are exclusively expressed by means of boundary variables. Therefore, the numerical treatment of these representations only requires the consideration of the surface Γ of the computational domain.

Static problems Beginning again with the static case, the first step is, as in the case of a finite element discretization, to set up an appropriate triangulation of the geometry

$$\overline{\Gamma}_h = \bigcup_{e=1}^{N_e} \overline{\tau}_e. \tag{3.28}$$

In the numerical analysis, the surface Γ is thus represented by Γ_h which is the union of shape regular surface elements τ_e. In a three-dimensional computation these surface elements are usually triangles or quadrilaterals and in two dimensions the one-dimensional surface is approximated by line elements. Again, such geometrical entities can be represented by a coordinate transformation from a reference element $\hat{\tau}$ to the coordinate space similar to equation (3.12). Contrary to the finite element case, here the reference space is $(d-1)$-dimensional.

The next step is to use a suitable approximation for the boundary variables u_Γ and q_Γ. Basically, this is done in the same fashion as in the case of the Ritz approximation (3.3). Therefore, the first boundary variable u_Γ (the boundary pressure or displacement) is approximated by $u_{\Gamma,h}$ and the second boundary variable q_Γ (the surface flux or traction) by $q_{\Gamma,h}$, which are defined by

$$u_{\Gamma,h}(\mathbf{y}) = \sum_i^N u_i \varphi_i(\mathbf{y}) \quad \text{and} \quad q_{\Gamma,h}(\mathbf{y}) = \sum_j^M q_j \psi_j(\mathbf{y}). \tag{3.29}$$

The choice of the same notation for the coefficients u_i as in the finite element approximation (3.13) is taken for simplicity and its particular meaning is determined by the context.

The approximation for u_Γ is the same as for the geometry representation, i.e., $\varphi_i^g = \varphi_i$. Therefore, this approximation is continuous and corresponds to the mapping properties of the double layer operator $\mathcal{K}$ [12]. On the other hand, q_Γ is by its definition (2.29) discontinuous at corner and edge points of the surface Γ. In addition, Γ_h is more likely to have corners and edges than Γ. Consider, e.g., the geometry discretization of a sphere by flat triangles. It is thus reasonable to consider these discontinuities in the approximation of q_Γ. A common approach in engineering is to introduce these discontinuities where necessary by means of so-called *double nodes* or partially discontinuous elements (see also References [33, 79, 84] for more details on these concepts). Both approaches require these locations to be marked during preprocessing and often yield auxiliary equations which spoil the structure of the final system of equations. Here, it is preferred to use a globally discontinuous space for the approximation of q_Γ by taking either constant or piecewise linear discontinuous functions. The implications of the choice of trial functions on the final system of equations are discussed later.

These approximation functions give rise to the boundary element spaces of continuous trial functions

$$S_h(\Gamma_h) = \text{span}\{\varphi_i\}_{i=1}^N \tag{3.30}$$

and of discontinuous trial functions

$$S_h^-(\Gamma_h) = \text{span}\left\{\psi_j\right\}_{j=1}^M. \tag{3.31}$$

Finally, one can define the space of approximation functions which vanish on the Dirichlet part of the boundary

$$S_{h,0}(\Gamma_h) = \left\{\varphi \in S_h(\Gamma_h) : \varphi(\mathbf{y}) = 0 \quad \text{on } \Gamma_{D,h}\right\}, \tag{3.32}$$

whose dimension is denoted by N_0.

By means of the approximation (3.29), the boundary integral equation (2.70) yields the residual

$$\mathcal{R}(u_{\Gamma,h}, q_{\Gamma,h}) = \sum_j^M \mathcal{V}\psi_j q_j - \sum_i^N (\mathcal{C}\varphi_i + \mathcal{K}\varphi_i) u_i, \tag{3.33}$$

which is in general not zero. Now, the concept of weighted residuals as discussed in sub-section 3.1.1 can be applied to equation (3.33) in order to obtain an algebraic system of equations. Multiplication of equation (3.33) by any member of $S_h^-(\Gamma_h)$ and integrating over the surface Γ_h yields a method commonly referred to as the Galerkin boundary element method. This method becomes really effective when using both integral equations as pointed out in remark 2.1 and, thereby, yielding a block skew-symmetric system of equations [107]. Here, only the first integral equation is used and, therefore, a collocation method is preferred. In this method, the residual (3.33) is assumed to vanish at a certain set of points located on the surface Γ_h which are called collocation points and denoted by $\left\{\mathbf{x}_\ell^*\right\}_{\ell=1}^L$. Hence, the system of L equations is obtained

$$\mathsf{V}\mathsf{q} - (\mathsf{C} + \mathsf{K})\mathsf{u} = 0, \tag{3.34}$$

with the matrices

$$\begin{aligned}
\mathsf{C}[\ell,i] &= (\mathcal{C}\varphi_i)(\mathbf{x}_\ell^*) \\
\mathsf{K}[\ell,i] &= (\mathcal{K}\varphi_i)(\mathbf{x}_\ell^*) & i &= 1,\dots,N \\
\mathsf{V}[\ell,j] &= (\mathcal{V}\psi_j)(\mathbf{x}_\ell^*) & j &= 1,\dots,M \\
\mathsf{u}[i] &= u_i & \ell &= 1,\dots,L. \\
\mathsf{q}[j] &= q_j
\end{aligned} \tag{3.35}$$

Note that C is a sparse and K and V are in general fully populated matrices. The specific way, how these matrix entries are finally computed is postponed at this point. See section 3.3 for details on the integrations involved in the computation of the matrix coefficients.

In order to be solvable, the system (3.34) has to be equipped with the given boundary conditions on u_Γ and q_Γ. The classical approach is to move unknown data to the left and known data to the right hand side of equation (3.34). Although apparently the most direct way, this method destroys the structure of the system of equations. The present idea is to exploit the fact that $\mathcal{V}$ is an elliptic operator (in two dimensions only under certain

restrictions) [107] and, therefore, a proper discretization scheme gives a positive definite matrix V. At first the number of collocation points K is chosen such that V becomes a square matrix, i.e., $L = M$. Secondly, given Dirichlet data are treated in the same way as in the case of a finite element discretization. Therefore, the steps outlined in the derivation of equation (2.73) are followed on a discrete level by introducing an extension of the given Dirichlet data defined by

$$u_{\Gamma,D}(\mathbf{x}_i) = g_D(\mathbf{x}_i) \quad \forall \mathbf{x}_i \in \Gamma_{D,h} \quad \text{and} \quad u_{\Gamma,D}(\mathbf{x}_j) = 0 \quad \forall \mathbf{x}_j \in \Gamma_{N,h}, \tag{3.36}$$

which assumes the given Dirichlet data at vertices belonging to the Dirichlet part $\Gamma_{D,h}$ of the approximate boundary and vanishes at the remaining boundary vertices. Decomposition of the unknown $u_{\Gamma,h}$

$$u_{\Gamma,h} = \tilde{u}_{\Gamma,h} + u_{\Gamma,D}$$

then yields the system of equations

$$Vq - \tilde{K}\tilde{u} = \tilde{K}u_D.$$

The abbreviation $\tilde{K} = C + K$ has been introduced for the sake of brevity. Since at every degree of freedom u_i it either holds that $\tilde{u}_i = 0$ or $u_{D,i} = 0$ and, in addition, when $u_{D,i} = 0$ the newly defined approximate $\tilde{u}_{\Gamma,h}$ equals the original approximate $u_{h,\Gamma}$ it suffices to write

$$Vq - \tilde{K}_N u_N = \tilde{K}_D u_D =: f_D, \tag{3.37}$$

where the subscripts D and N refer to those columns of the matrix K and coefficients of the column matrix u which correspond to a given Dirichlet datum or to an unknown boundary displacement degree of freedom, respectively. Note that in case of a pure Dirichlet problem, system (3.37) reduces to

$$Vq = \tilde{K}_D u_D \tag{3.38}$$

which is solvable for the unknown Neumann data q.

In order to solve a mixed boundary value problem, the application of Neumann boundary conditions is still lacking. Therefore the requirement that

$$q_\Gamma = g_N \quad \mathbf{x} \in \Gamma_N,$$

i.e., the second equation of system (2.73), will be added in a weighted form by stating that

$$\langle q_{\Gamma,h}, \varphi_i \rangle = \langle g_N, \varphi_i \rangle \qquad \forall \varphi_i \in S_{h,0}(\Gamma_h), \quad \forall \mathbf{x}_i \in \Gamma_{N,h}. \tag{3.39}$$

The given Neumann datum g_N is extended to the whole boundary by introducing $\tilde{g}_N$, for which holds

$$\tilde{g}_N = g_N \quad \mathbf{x} \in \Gamma_N \quad \text{and} \quad \tilde{g}_N = 0 \quad \mathbf{x} \in \Gamma_D.$$

Defining by g_N the collection of nodal values of this extension, equation (3.39) translates to

$$Bq = Bg_N =: f_N. \tag{3.40}$$

(a) Line element   (b) Triangle element
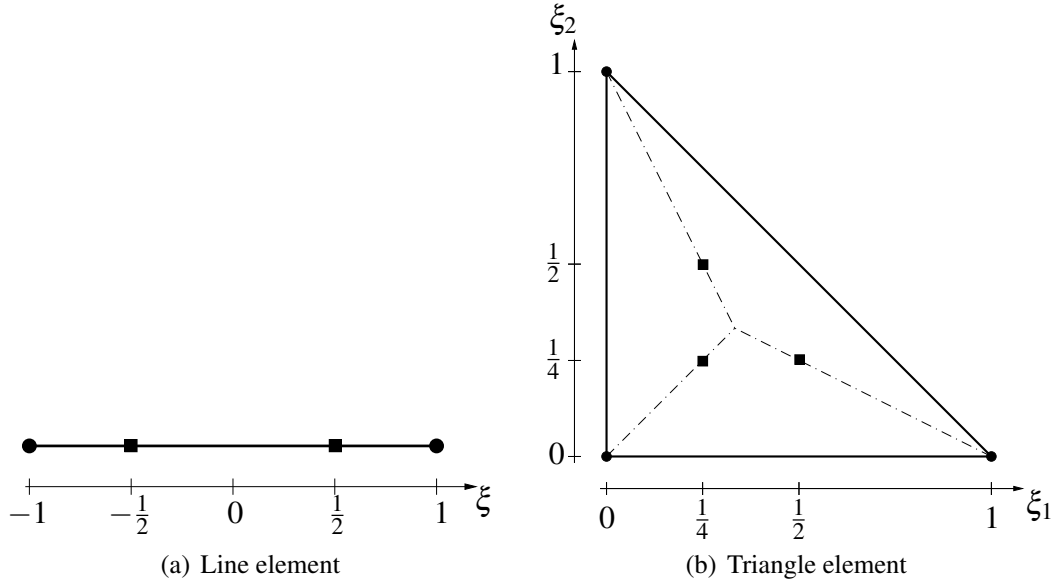
Figure 3.1: Placement of collocation points for line (a) and triangle elements (b).

The matrix B simply consists of the scalar product of pairs of trial functions of the approximation (3.29) and its coefficients are thus

$$B[i,j] = \langle \varphi_i, \psi_j \rangle \qquad i = 1, \dots, N_0, \quad j = 1, \dots, M. \tag{3.41}$$

The matrix B is obviously sparse. Such a matrix is usually referred to as a mass matrix. Although, physically speaking, it does not represent any mass of the system, it is mathematically equivalent to the mass matrix M as used in the finite element discretization of the dynamical system (3.23) and defined in equation (3.24).

The combination of the systems of equations (3.37) and (3.40) yields the system

$$\begin{pmatrix} V & -\tilde{K}_N \\ B & \end{pmatrix} \begin{pmatrix} q \\ u_N \end{pmatrix} = \begin{pmatrix} f_D \\ f_N \end{pmatrix}. \tag{3.42}$$

These are $(M + N_0)$ equations for the M Neumann coefficients q_j and the N_0 unknown Dirichlet coefficients u_i. Solving the first block row for q and inserting this result into the second block row or, in other words, computing the Schur complement, gives the discrete Dirichlet-to-Neumann map

$$\underbrace{BV^{-1}\tilde{K}_N}_{S} u_N = \underbrace{f_N - BV^{-1}f_D}_{g}. \tag{3.43}$$

This mapping is paramount for the later introduced coupling method and S is a boundary element discretization of the Steklov-Poincaré operator $\mathcal{S}$ as introduced in equation (2.74). Although $\mathcal{S}$ is a self-adjoint operator, the presented discretization does not yield a symmetric matrix S. Nevertheless, symmetric discrete representations of $\mathcal{S}$ are feasible, see Steinbach [105, 106].

Remark 3.2. So far, it has only been stated that one has to take as many collocation points as degrees of freedom in the approximation for the second variable q_Γ. The specific choice of the location of these points is a difficulty of the method. The mathematical analysis of collocation methods is poorly developed and, therefore, it remains a matter of empiricism to place these points of evaluation effectively. Since the geometrical coincidence of two or more such collocation points would result in a rank decay of the system matrices, it seems to be a good choice to use positions such that neighboring points are as far away as possible for every point. In case of a piecewise constant approximation of q_Γ, the midpoints of the elements are obviously a good choice for the location of the collocation points. In case of piecewise linear discontinuous functions ψ_j, the collocation points must not be too close to the midpoints in order not to coincide and not be too close to the vertices of the elements in order not to be identical with the collocation points of the neighbor elements. In other words, if these points are too close to each other the condition number of the system matrix will blow up. On the other hand, if they get too close to the neighbor elements, in addition, the integration error will be larger as it can be seen from the discussion below in remark 3.4.

The collocation points for line elements in two dimensions are put at the reference coordinates $\xi = \pm\frac{1}{2}$ in the interval $\xi \in (-1,1)$ as shown in figure 3.1(a). A quadrilateral would then be equipped with the tensor product of these locations. Numerical tests for three-dimensional analysis with triangle elements have shown a *strong* sensitivity on the location of the collocation point. It finally turned out that the best results are obtained by choosing on the reference triangle, $\{\xi_1, \xi_2 : 0 < \xi_1 < 1, 0 < \xi_2 < 1 - \xi_1\}$, the three collocation points located at reference coordinates $(\frac{1}{4}, \frac{1}{4})$, $(\frac{1}{2}, \frac{1}{4})$ and $(\frac{1}{4}, \frac{1}{2})$, see figure 3.1(b). The choice of collocation points inside the element, i.e., neither on a vertex or an edge, yields the identity

$$\mathsf{C}[k,i] = \frac{1}{2}\varphi_i(\mathbf{x}_k^*) \tag{3.44}$$

which is the discrete representation of equation (2.69). ◇

Remark 3.3. The block system of the boundary element discretization (3.42) has the form of a saddle point problem with $\mathsf{B}\mathsf{q} = \mathsf{f}_N$ as a side condition. For the unique solvability of the system it is necessary that B fulfills the discrete Babuška-Brezzi condition [9, 44]. Equivalently, $\mathsf{B}\mathsf{q}_z = 0$ has to imply $\mathsf{q}_z = 0$ [44]. Unfortunately, this condition is violated if the trial functions ψ_j for q_h are piecewise constant and the trial functions φ_i for u_h are piecewise linear. Using this combination of trial functions, the solvability of the system cannot be guaranteed. See [103] for an example. Therefore, it is advocated to use a piecewise linear discontinuous basis for the approximation of q. ◇

Dynamic problems   The articles of Cruse and Rizzo [16, 17] are among the first publications on the treatment of time-domain problems with boundary element methods. Their approach is based on the inverse Laplace transform of the solution of the elastodynamic problem in Laplace domain. A method formulated directly in time-domain is given in the thesis of Mansur [70] treating the acoustic wave equation and elastodynamics in two

space dimensions. A concise overview of boundary integral equation methods for time-dependent methods is given by Costabel [13].

The spatial discretization of the dynamic integral equation (2.78) by boundary elements is carried out similar to the static case but the approximation coefficients remain functions of time as in the finite element case, see equation (3.22). The approximations

$$u_{\Gamma,h}(\mathbf{y},t) = \sum_i^N u_i(t)\varphi_i(\mathbf{y}) \quad \text{and} \quad q_{\Gamma,h}(\mathbf{y},t) = \sum_j^M q_j(t)\psi_j(\mathbf{y}) \tag{3.45}$$

are employed for u_Γ and q_Γ, respectively. Inserting this approximation into the integral equation (2.78) and collocation at the set of points $\{\mathbf{x}_\ell^*\}_{\ell=1}^L$, gives the semi-discrete equation

$$\mathsf{V}(t) * \mathsf{q}(t) = \mathsf{Cu}(t) + \mathsf{K}(t) * \mathsf{u}(t)$$

Defining an auxiliary matrix operator $\tilde{\mathsf{C}}$ by

$$\tilde{\mathsf{C}}(t) * \mathsf{u}(t) = \int_0^t \mathsf{Cu}(\tau)\delta(t-\tau)\,\mathrm{d}\tau = \mathsf{Cu}(t), \tag{3.46}$$

the above used abbreviation, $\tilde{\mathsf{K}}(t) = \tilde{\mathsf{C}}(t) + \mathsf{K}(t)$, can be established and the integral equation thus reads

$$\mathsf{V}(t) * \mathsf{q}(t) = \tilde{\mathsf{K}}(t) * \mathsf{u}(t). \tag{3.47}$$

Note that in these equations convolutions of matrices with vectors appear. These have to be understood in the sense of an ordinary matrix-vector product, where each component multiplication itself is a convolution in time as defined for instance by Wheeler and Sternberg [118].

Due to the assumption that the partition of the boundary Γ in its Dirichlet and Neumann parts Γ_D and Γ_N, respectively, does not vary with time, the application of given Dirichlet boundary conditions is done in the same manner as in the static case, such that

$$\mathsf{V}(t) * \mathsf{q}(t) - \tilde{\mathsf{K}}_N(t) * \mathsf{u}_N(t) = \tilde{\mathsf{K}}_D(t) * \mathsf{u}_D(t) =: \mathsf{f}_D(t). \tag{3.48}$$

Again the subscripts N and D respectively refer to degrees of freedom on the Neumann and Dirichlet parts of the boundary. Moreover, u_D are the time-dependent coefficients of $u_{\Gamma,D}(\cdot,t)$, which is the extension of the given Dirichlet data $g_D(\cdot,t)$ similar to the static case as in equation (3.36). Also, the prescribed Neumann data are handled in the same way as before by requiring that

$$\langle q_{\Gamma,h}(\cdot,t),\varphi_i\rangle = \langle g_N(\cdot,t),\varphi_i\rangle \qquad \forall \varphi_i \in S_{h,0}(\Gamma_h), \quad \forall t \in (0,\infty),$$

which results in the system of equations

$$\mathsf{Bq}(t) = \mathsf{Bg}_N(t) =: \mathsf{f}_N(t). \tag{3.49}$$

Here, the matrix B is exactly the same mass matrix as defined in equation (3.41). The combination of equations (3.48) and (3.49) finally yields the system

$$\begin{pmatrix} V(t) & -\tilde{K}(t) \\ \tilde{B}(t) & \end{pmatrix} * \begin{pmatrix} q(t) \\ u_N(t) \end{pmatrix} = \begin{pmatrix} f_D(t) \\ f_N(t) \end{pmatrix}. \tag{3.50}$$

Note that $\tilde{B}(t)$ is defined, similarly to $\tilde{C}(t)$, by the identity $\tilde{B}(t) * q(t) = Bq(t)$. The time-dependent entries of the matrices appearing in equation (3.50) are as follows

$$V(t)[\ell, j] = \int_\Gamma u^*(\mathbf{x}_\ell^*, \mathbf{y}, t, \tau) \psi_j(\mathbf{y}) \, ds_\mathbf{y}$$

$$\tilde{K}(t)[\ell, i] = \mathcal{C}\delta(t)\varphi_i(\mathbf{x}_\ell^*) + \lim_{\varepsilon \to 0} \int_{\Gamma_h \setminus B_\varepsilon(\mathbf{x}_\ell^*)} \mathcal{T}_\mathbf{y} u^*(\mathbf{x}_\ell^*, \mathbf{y}, t, \tau) \varphi_i(\mathbf{y}) \, ds_\mathbf{y} \tag{3.51}$$

$$\tilde{B}(t)[i, j] = \langle \varphi_i, \psi_j \rangle \delta(t)$$

$$q(t)[j] = q_j(t)$$

$$u_N(t)[i] = u_i(t)$$

with the same range of indices i, j, and ℓ as in equations (3.35) and (3.41). Again, the details for the integrations occurring in the computation of these coefficients is not shown here but outlined in section 3.3.

In order to solve for the approximation of dynamic Cauchy data $[u(t), q(t)]$, the system of equations (3.50) has to be discretized along the time axis as pointed out below in section 3.2.2.

3.2 Temporal Discretization

Whereas the spatial discretization by finite or boundary elements for static problems directly results in an algebraic system of linear equations, the presented dynamic problems yields either a system of ordinary differential equations (3.23) or a system of convolution equations (3.50).

3.2.1 Time stepping methods

In the following, the solution to the system of ordinary differential equations (3.23) is considered. In order to simplify the notation, at first only the test equation

$$m\ddot{u}(t) + ku(t) = f(t) \quad t \in (0, \infty) \tag{3.52}$$

is considered, where m and k are positive real constants and u and f are scalar valued functions of time only. As before, $\ddot{u}$ represents the second time derivative, $\ddot{u}(t) = \partial^2/\partial t^2 u(t)$. Additionally, initial conditions have to be fulfilled

$$u(0^+) = u_0 \quad \text{and} \quad \dot{u}(0^+) = u_1. \tag{3.53}$$

In general, the analytical solution of equation (3.52) is not available and for this reason a numerical approximation scheme is required. Moreover, once such a method is established it can be easily extended to systems of ordinary differential equations as it is the underlying problem of this section.

Equation (3.52) is an ordinary differential equation of second order with constant coefficients and because f does not depend on u the equation is also autonomous. The problem statement of equation (3.52) together with the initial conditions (3.53) compose an *initial value problem* of second order.

Since ordinary differential equations of second order appear so frequently in many areas of application, methods have been developed especially tailored to them. Although many such methods exist (cf. for instance [49]), here only the well-known *Newmark* method [72] is used. At first, the time interval of interest, denoted by $(0, T)$ is subdivided into N sub-intervals of equal size Δt, thereby establishing the time grid

$$t_0 := 0, t_1 := \Delta t, \ldots, t_n := n\Delta t, \ldots, t_N := N\Delta t = T. \tag{3.54}$$

Note that the step size Δt is taken constant for simplicity only, whereas the method itself does not require this. The approximations of the unknown u and its first two time derivatives are introduced

$$u_n \approx u(t_n), \quad v_n \approx \dot{u}(t_n), \quad \text{and} \quad a_n \approx \ddot{u}(t_n). \tag{3.55}$$

Consider the Taylor expansions of the unknown $u(t_n)$ and its first time derivative $\dot{u}(t_n)$ at a time point t_n with $n > 0$

$$u(t_n) = u(t_{n-1}) + \Delta t\, \dot{u}(t_{n-1}) + \frac{\Delta t^2}{2}\ddot{u}(t_{n-1}) + \frac{\Delta t^3}{6}\dddot{u}(t_{n-1}) + \cdots$$

$$\dot{u}(t_n) = \dot{u}(t_{n-1}) + \Delta t\, \ddot{u}(t_{n-1}) + \frac{\Delta t^2}{2}\dddot{u}(t_{n-1}) + \cdots.$$

Now the occurring functions are replaced by their approximations (3.55) and two parameters β and γ control the contribution of the third order term $\dot{a}_{n-1} \approx \dddot{u}(t_{n-1})$

$$u_n = u_{n-1} + \Delta t\, v_{n-1} + \frac{\Delta t^2}{2}a_{n-1} + \beta \Delta t^3 \dot{a}_{n-1}$$

$$v_n = v_{n-1} + \Delta t\, a_{n-1} + \gamma \Delta t^2 \dot{a}_{n-1}$$

The approximation of the third order term by the forward difference

$$\dddot{u}(t_{n-1}) \approx \frac{a_n - a_{n-1}}{\Delta t}$$

finally leads to the family of Newmark methods

$$u_n = u_{n-1} + \Delta t\, v_{n-1} + \left(\frac{1}{2} - \beta\right)\Delta t^2 a_{n-1} + \beta \Delta t^2 a_n$$

$$v_n = v_{n-1} + (1 - \gamma)\Delta t\, a_{n-1} + \gamma \Delta t\, a_n \tag{3.56}$$

$$ma_n = ku_n + f_n,$$

where the differential equation evaluated at the time point t_n has been used and $f_n = f(t_n)$ is simply an abbreviation. Note that the scheme is in general implicit since in every of the three equations unknown values appear on both sides. Nevertheless, the original differential equation is linear and this allows the equations to be reordered such that only one unknown appears on the left hand side at every time step. One possibility would be to insert the first into the third equation which yields a scheme in which at first the approximation of the second derivative a_n is computed and afterwards the remaining unknowns v_n and u_n [49]. In the later explained coupling method it is necessary to have a direct expression for the primary unknown u_n and, for this reason, it is here preferred to express the above in terms of u_n. This yields the algorithm for $0 < n \le N$

$$\left(k + \frac{1}{\beta \Delta t^2} m \right) u_n = f_n + \frac{1}{\beta \Delta t^2} m u_{n-1} + \frac{1}{\beta \Delta t} m v_{n-1} - \left(1 - \frac{1}{2\beta} \right) m a_{n-1} \tag{3.57a}$$

$$v_n = \frac{\gamma}{\beta \Delta t} (u_n - u_{n-1}) + \left(1 - \frac{\gamma}{\beta} \right) v_{n-1} + \Delta t \left(1 - \frac{\gamma}{2\beta} \right) a_{n-1} \tag{3.57b}$$

$$a_n = \frac{1}{\beta \Delta t^2} (u_n - u_{n-1}) - \frac{1}{\beta \Delta t} v_{n-1} + \left(1 - \frac{1}{2\beta} \right) a_{n-1} . \tag{3.57c}$$

For $n = 1$ it is necessary to have previously computed the initial second time derivative, which is easily done by using the differential equation itself with the given initial conditions

$$m a_0 = f_0 - k u_0 . \tag{3.58}$$

It remains to choose the parameters β and γ which determine accuracy and stability of the method. Mathematical analysis has shown that a second order accuracy is only obtained in the case of $\gamma = \frac{1}{2}$ [49]. Moreover, unconditional stability is gained by the inequality $2\beta \ge \gamma \ge \frac{1}{2}$ [49, 89]. Nevertheless, if numerical dissipation is desired as for instance in coupled algorithms, the choice $\gamma > \frac{1}{2}$ might be adequate despite the loss of one order of accuracy. The following choice is fixed throughout this work unless stated otherwise

$$\beta = \frac{1}{4} \quad \text{and} \quad \gamma = \frac{1}{2} . \tag{3.59}$$

In order to apply the Newmark scheme to a system of ordinary differential equations, the coefficients m and k, in the above, basically have to be understood as matrices and the unknowns u_n, v_n, and a_n are then vectors with as many coefficients as spatial degrees of freedom. In view of the system (3.23), equation (3.57a) becomes then the algebraic system of equations

$$\underbrace{\left(\mathsf{A} + \frac{1}{\beta \Delta t^2} \mathsf{M} \right)}_{\tilde{\mathsf{A}}} \mathsf{u}_n = \underbrace{\mathsf{f}_n + \mathsf{M} \left(\frac{1}{\beta \Delta t^2} \mathsf{u}_{n-1} + \frac{1}{\beta \Delta t} \mathsf{v}_{n-1} - \left(1 - \frac{1}{2\beta} \right) \mathsf{a}_{n-1} \right)}_{\tilde{\mathsf{f}}_n} . \tag{3.60}$$

The structure of this system of equations is very similar to the static case (3.17). In fact the left hand side matrix is commonly termed effective or dynamic stiffness matrix, whereas

there appear effective or dynamic forces on the right hand side. Since Δt is constant, the effective stiffness matrix $\tilde{A}$ does not change throughout the computation. Therefore, it is usually preferred to assemble this matrix and precompute a factorization of it, which can be efficiently reused in every time step, where only the right hand side changes. This solution procedure will be described in section 3.4.

3.2.2 Convolution quadrature method

In order to obtain a purely algebraic set of equations, the system (3.50) has to be discretized in time. Therefore, the time grid (3.54) is used again, which is made up of N equally sized steps Δt from $t_0 = 0$ to the final time of computation $t_N = N\Delta t = T$.

The classical approach in time-domain boundary element methods is to employ shape functions for the time dimension and perform the temporal integration analytically. The sequential solution of the unknown data $[u(t_n), q(t_n)]$ for all n, $0 < n \leq N$ is thus possible. Such a method for two-dimensional scalar wave equation and elastodynamics has been introduced by Mansur [70]. A three-dimensional realization can be found in the thesis of Schanz [97].

Here, another approach is considered, based on a quadrature rule tailored for convolution integrals and which uses quadrature weights from Laplace transformed functions. For instance, the application of the single layer operator is of the form (2.79)

$$(\mathcal{V}_t * q_\Gamma)(\mathbf{x},t) = \int\limits_0^t \int\limits_\Gamma u^*(\mathbf{x},\mathbf{y},t,\tau) q_\Gamma(\mathbf{y},\tau)\,\mathrm{d}s_{\mathbf{y}}\,\mathrm{d}\tau, \tag{3.61}$$

and the spatially discretized form is then as given in equation (3.50)

$$(\mathsf{V} * \mathsf{q})(t) = \int\limits_0^t \mathsf{V}(t-\tau)\mathsf{q}(\tau)\,\mathrm{d}\tau$$

with the matrix coefficients as defined by equation (3.51). For simplicity, the convolution of two scalar functions f and g is regarded

$$h(t) := f * g = \int\limits_0^t f(t-\tau)g(t)\,\mathrm{d}\tau, \quad t > 0. \tag{3.62}$$

The here presented method is commonly called *convolution quadrature method* or operational quadrature method and was introduced by Lubich [67,68]. Since a good introduction to this method is given by Schanz [98], it is preferred to summarize only the key ingredients of the method.

In this convolution (3.62), the function f will be replaced by its inverse Laplace transform [11]

$$f(t-\tau) = \frac{1}{2\pi i} \int_C \hat{f}(s) \exp(s(t-\tau)) \, ds,$$

where C denotes a line parallel to the imaginary axis such that $\hat{f}(s)$ is analytical within the half plane to the right of C. The convolution thus becomes after reversing the order of integration

$$h(t) = \frac{1}{2\pi i} \int_C \hat{f}(s) \int_0^t g(\tau) \exp(s(t-\tau)) \, d\tau \, ds. \tag{3.63}$$

The inner integral $I(t,s) = \int_0^t g(\tau) exp(s(t-\tau)) \, d\tau$ is the analytical solution of the following first order initial value problem

$$\frac{dI}{dt} = sI + g, \quad I(0,s) = 0.$$

The application of a k-step method [60] in order to approximate $I(t_n, s)$ by I_n at the time point $t_n = n\Delta t$ on the grid (3.54) leads to the expression

$$\sum_{j=0}^{k} \alpha_j I_{n+j-k} = \Delta t \sum_{j=0}^{k} \beta_j \left[s I_{n+j-k} + g(t_{n+j-k}) \right]$$

with $\{\alpha_j, \beta_j\}_{j=0}^{k}$ being the coefficients determining the multistep method. Moreover, it is assumed that $I(t,s) = 0$ and $g(t) = 0$ if $t \leq 0$. Both sides of this equation are now multiplied by any z^n, $z \in \mathbb{C}$, and summed up for $n = 0$ to $n = \infty$. Resorting the terms gives

$$\left(\sum_{j=0}^{k} \alpha_{k-j} z^j \right) \left(\sum_{n=0}^{\infty} z^n I_n \right) = \Delta t \left(\sum_{j=0}^{k} \beta_{k-j} z^j \right) \left(s \sum_{n=0}^{\infty} z^n I_n + \sum_{n=0}^{\infty} z^n g(n\Delta t) \right),$$

where now the infinite sum over $z^n I_n$ is factored out

$$\sum_{n=0}^{\infty} z^n I_n = \frac{1}{\frac{\gamma(z)}{\Delta t} - s} \sum_{n=0}^{\infty} z^n g(n\Delta t). \tag{3.64}$$

In this expression, $\gamma(z)$ denotes the characteristic polynomial [60] of the underlying multistep method

$$\gamma(z) = \frac{\sum_{j=0}^{k} \alpha_j z^k}{\sum_{j=0}^{k} \beta_j z^k}. \tag{3.65}$$

Replacing the inner integral of equation (3.63) by its approximation I_n, multiplying by z^n and summing over all $n = 0, \ldots, \infty$ results in the expression

$$\sum_{n=0}^{\infty} z^n \tilde{h}(n\Delta t) = \frac{1}{2\pi i} \int_C \hat{f}(s) \frac{1}{\frac{\gamma(z)}{\Delta t} - s} \, ds \sum_{n=0}^{\infty} z^n g(n\Delta t).$$

Note that $\tilde{h}$ denotes the approximation of the original convolution h as defined in equation (3.62). Under certain assumptions on $\hat{f}(s)$ [98] the Cauchy integral formula [11] can be used to solve the integral on the right hand side

$$\sum_{n=0}^{\infty} z^n \tilde{h}(n\Delta t) = \hat{f}\left(\frac{\gamma(z)}{\Delta t}\right) \sum_{n=0}^{\infty} z^n g(n\Delta t). \tag{3.66}$$

The final step is now to express the Laplace transform $\hat{f}$ by a power series

$$\hat{f}\left(\frac{\gamma(z)}{\Delta t}\right) = \sum_{n=0}^{\infty} z^n \omega_n(\Delta t, \hat{f}, \gamma)$$

and insert this result into expression (3.66), where the weights ω_n are given below. Comparing the coefficients gives the quadrature formula

$$\tilde{h}(n\Delta t) = \sum_{j=0}^{n} \omega_{n-j}(\Delta t, \hat{f}, \gamma) g(j\Delta t), \quad n = 0, \dots, \infty. \tag{3.67}$$

It remains to express the quadrature weights ω_n

$$\omega_n(\Delta t, \hat{f}, \gamma) = \frac{R^{-n}}{2\pi} \int_0^{2\pi} \hat{f}\left(\frac{\gamma(R\exp(\mathrm{i}\phi))}{\Delta t}\right) \exp(-\mathrm{i}k\phi)\, \mathrm{d}\phi. \tag{3.68}$$

For details, how to compute this expression efficiently confer Schanz [98]. References for error bounds also can be found there. The resulting expressions can actually be computed by means of a discrete fast Fourier transform [11]. The radius R of the integration path is chosen as $R = \varepsilon^{1/2N}$ with ε being a positive number bounding the error in numerical evaluation of $\hat{f}(s)$ [68] and N the total number of time steps in the computation. Figure (3.2) shows how the argument of $\hat{f}$ varies in the evaluation of the quadrature weights (3.68) for fixed step size $\Delta t = 0.01$ and various step numbers N in the left picture 3.2(a) and in the right picture 3.2(b) the converse is displayed where $N = 1000$ is fixed and the step size Δt varies. For both cases the error bound has been chosen to $\varepsilon = 2 \cdot 0^{-16}$ giving a radius $R = \sqrt{2} \cdot 10^{8/N}$.

By means of formula (3.67), the original convolution $h = f * g$ is approximated by an expression, which samples the original function g at discrete points $j\Delta t$ and uses quadrature weights based on the characteristic polynomial γ of a k-step method and the Laplace transform $\hat{f}$ of the function f. The multistep method to be chosen has to fulfill certain requirements [67], among which is the $A(\alpha)$-stability (cf. [60] for its definition) for some α, such that the region of analyticity of $\hat{f}(s)$ can be enclosed in the region of absolute stability of the multistep method (up to some shift along the real axis). Moreover, the characteristic polynomial of the method has to be an analytic function. Here, the backward differential formula BDF2 is chosen. It is A-stable, meets the other requirements and has second-order consistency [60]. The characteristic polynomial of the BDF2 is

$$\gamma(z) = \frac{3}{2} - 2z + \frac{1}{2}z^2. \tag{3.69}$$

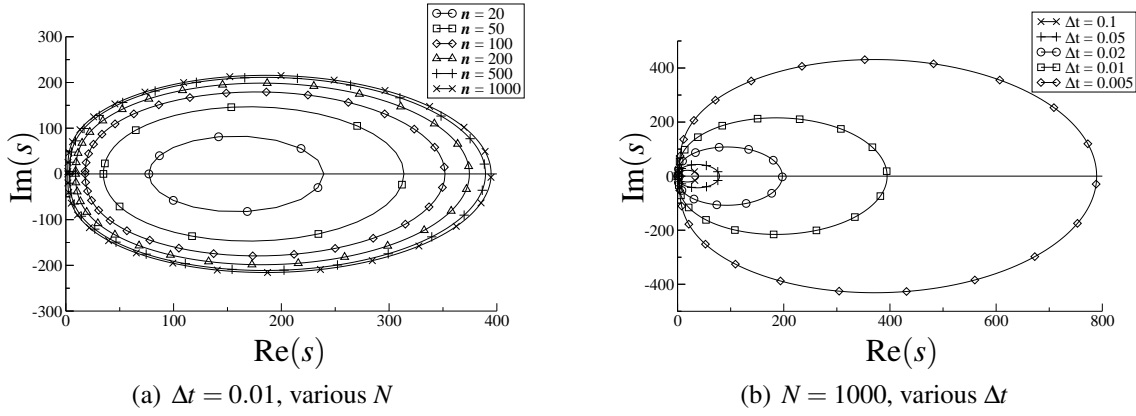(a) $\Delta t = 0.01$, various N　　　　　　　(b) $N = 1000$, various Δt

Figure 3.2: Argument paths for $\hat{f}$ in the computation of the quadrature weights (3.68) for various N for $\Delta t = 0.01$ (a) and various Δt for $N = 1000$ (b). The error bound was chosen as $\varepsilon = 2 \cdot 10^{-16}$.

In view of the application of the single layer operator (3.61), the following formula is obtained

$$
\begin{aligned}
(\mathcal{V}_t * q_\Gamma)(\mathbf{x}, t_n) &= \int_0^{t_n} \int_\Gamma u^*(\mathbf{x}, \mathbf{y}, t, \tau) q_\Gamma(\mathbf{y}, \tau) \, ds_\mathbf{y} \, d\tau \\
&= \int_\Gamma u^*(\mathbf{x}, \mathbf{y}, \cdot, \cdot) * q_\Gamma(\mathbf{y}, \cdot) \, ds_\mathbf{y} \\
&\approx \int_\Gamma \left(\sum_{j=0}^{n} \omega_{n-j}(\Delta t, \hat{u}^*, \gamma) q_\Gamma(\mathbf{y}, j\Delta t) \right) ds_\mathbf{y}.
\end{aligned}
\tag{3.70}
$$

The Laplace transform of the fundamental solution u^* is expressed by $\hat{u}^*$. Similarly, the spatially discretized convolution occurring in the system (3.50) becomes by means of the convolution quadrature

$$
(\mathsf{V} * \mathsf{q})(t_n) = \sum_{j=0}^{n} \omega_{n-j}(\Delta t, \hat{\mathsf{V}}, \gamma) \mathsf{q}(j\Delta t).
\tag{3.71}
$$

The application of the double layer matrix K is of course carried out in the same manner. Needless, to say that the matrix operators $\tilde{\mathsf{C}}$ (3.46) and $\tilde{\mathsf{B}}$ have been only introduced to facilitate the writing of system (3.50) and need not undergo the above procedure. The underlying matrices C and B, respectively, are independent of time. Using the following notation for $n = 0, \ldots, N$

$$
\begin{aligned}
\mathsf{V}_n &:= \omega_n(\Delta T, \hat{\mathsf{V}}, \gamma) & \mathsf{q}_n &:= \mathsf{q}(n\Delta T) \\
\mathsf{K}_n &:= \omega_n(\Delta T, \hat{\mathsf{K}}, \gamma) & \mathsf{u}_n &:= \mathsf{u}(n\Delta T) \\
\tilde{\mathsf{K}}_0 &:= \mathsf{C} + \mathsf{K}_0
\end{aligned}
\tag{3.72}
$$

System (3.50) becomes the sequence of systems of equations

$$
\begin{pmatrix} \mathsf{V}_0 & -\tilde{\mathsf{K}}_0 \\ \mathsf{B} & \end{pmatrix} \begin{pmatrix} \mathsf{q}_n \\ \mathsf{u}_n \end{pmatrix} = \begin{pmatrix} \mathsf{f}_D(n\Delta t) \\ \mathsf{f}_N(n\Delta t) \end{pmatrix} - \sum_{j=1}^{n} \begin{pmatrix} \mathsf{V}_j & -\mathsf{K}_j \\ & \end{pmatrix} \begin{pmatrix} \mathsf{q}_{n-j} \\ \mathsf{u}_{n-j} \end{pmatrix}. \tag{3.73}
$$

Obviously, the left hand side matrix of this equation does not change throughout the computation, whereas at each step a new right hand side has to be computed. A simple approach to solve this system is shown in section 3.4.

It remains to ask, why this rather cumbersome approach is taken instead of going the classical way [70]. The computation of the quadrature weights is fairly expensive and requires complex arithmetic. Nevertheless, this approach has shown to be less sensitive with respect to the size of the time step [99]. Another important advantage of this method is the simple fact that only Laplace transformed fundamental solutions are required. For this reason, it suffices to derive and finally implement the fundamental solution of the Laplace transformed differential equation. Laplace domain fundamental solutions commonly have a simpler structure than the time domain equivalents and are more robustly evaluated. Although not applicable to the models considered in this work, a striking argument is that for many mathematical models only a Laplace domain fundamental solution is available, as it is the case in visco- and poroelasticity. See the publication of Schanz and Antes [100] for the extension of this approach to viscoelastic solids and the monograph of Schanz [98] for the analysis of wave propagation in visco- and poroelstatic media.

3.3 Computation of Matrix Coefficients

In sections 3.1 and 3.2, it is shown how to attain an algebraic system of equations by means of spatial and temporal discretizations, respectively. In the following section 3.4, solution methods for these equations are presented. But before going there, it is necessary to take a closer look at the way, the matrix coefficients are computed. This section could be missed out if every integral occurring in the computation of the matrix entries was easily solvable in an analytical way. Since this is not the case, numerical integration schemes have to be employed.

Geometrically speaking, two types of integrals appear in the presented numerical approximations. The coefficients of the finite element mass and stiffness matrices M and A require the evaluation of the bilinear forms $a(\varphi_i, \varphi_j)$ and $\langle \rho \varphi_i, \varphi_j \rangle$, respectively. These bilinear forms contain integrations over the volume Ω. On the other hand, the applied surface tractions or fluxes enter the equations by means of a surface integral. Furthermore, all spatial integrals appearing in the context of the presented boundary element methods are formulated on the body's surface Γ. Therefore, one can distinguish between volume and surface integrals [55], both in two and three dimensions.

Considering the integral kernels, three different types of integrations are involved. At first, the classical regular integrals occur in the form of volume and surface integrals in the finite

element method. Due to the fact that

$$\lim_{\mathbf{y} \to \mathbf{x}^*} u^*(\mathbf{x}^*, \mathbf{y}) = \infty,$$

special care has to be taken when computing the coefficients of the boundary element matrices. If the collocation point $\mathbf{x}^*$ and the variable of integration $\mathbf{y}$ are relatively far from each other, the surface integrals are regular and can be treated in the usual way. But if these points get closer, the singularity of the kernel has to be considered. The integrals arising in the discretization of the single layer operator $\mathcal{V}$ are *improper* integrals, which means that, although the integrand diverges, the integral is well defined. Such integrals will be referred to as *weakly* singular integrals. The coefficients of the discretized double layer operator $\mathcal{K}$ require further attention. The integrals involved therein are only defined when the integration is carried in the sense of a principal value. More details will follow in the respective subsections.

3.3.1 Regular integrals

The regular volume integrals occurring in the finite element context are commonly approximated by a quadrature rule performed on the reference element. For simplicity, consider the bilinear form of the Laplace equation

$$a(u,v) = \int_{\Omega_h} \kappa \nabla u \cdot \nabla v \, d\mathbf{x}.$$

The matrix entries of the finite element stiffness matrix thus become

$$\mathsf{A}[i,j] = a(\varphi_j, \varphi_i) = \sum_{\ell \in L} \int_{\tau_\ell} \kappa \nabla \varphi_j \cdot \nabla \varphi_i \, d\mathbf{x}, \quad \varphi_i, \varphi_j \in S_{h,0}(\Omega).$$

The region of integration reduces to the intersection of the respective supports of the trial functions φ_i and φ_j since outside this region the integrand vanishes. This is only a patch composed of a certain number of elements such that $\mathrm{supp}(\varphi_i) \cap \mathrm{supp}(\varphi_j) = \bigcup_{\ell \in L} \tau_\ell$, where the set L represents the indices of elements τ_ℓ which contribute to the considered degree of freedom. Each of these elements τ_ℓ is an instance of the coordinate transformation from the reference element $\hat{\tau}$ to the global coordinates as given by (3.12). Remember that the geometry is approximated with the same functions as the unknown u, i.e., $\varphi_i^g = \varphi_i \in S_h(\Omega)$. Therefore, the matrix coefficient is the sum of integrals expressed in local coordinates

$$\mathsf{A}[i,j] = \sum_{\ell \in L} \int_{\hat{\tau}} \kappa \nabla_{\mathbf{x}} \varphi_j(\xi) \cdot \nabla_{\mathbf{x}} \varphi_i(\xi) \det \mathsf{J}_\ell(\xi) \, d\xi.$$

The subscript $\mathbf{x}$ at the gradients $\nabla()$ emphasize the fact that differentiation is with respect to the global coordinates. $\det \mathbf{J}_\ell$ denotes the determinant of the Jacobi matrix $\mathbf{J}_\ell$ of the

coordinate transformation from the reference element to the element τ_ℓ with the coefficients [55]

$$\mathbf{J}_\ell[i,j] = \frac{\partial x_j}{\partial \xi_i}, \quad i,j = 1,\ldots,d, \quad \mathbf{x} \in \tau_\ell. \tag{3.74}$$

It remains to express the partial derivatives with respect to the global coordinates $\mathbf{x}$ by local coordinates ξ. Therefore, the chain rule is applied and results in [6]

$$\frac{\partial}{\partial \mathbf{x}} = \mathbf{J}_\ell^{-1}(\xi) \frac{\partial}{\partial \xi}, \quad \mathbf{x} \in \tau_\ell.$$

Finally, the coefficient of the stiffness matrix becomes

$$\mathsf{A}[i,j] = \sum_{\ell \in L} \int_{\hat{\tau}} \underbrace{\kappa \left(\mathbf{J}^{-1}(\xi) \nabla_\xi \varphi_j(\xi) \right) \cdot \left(\mathbf{J}^{-1}(\xi) \nabla_\xi \varphi_i(\xi) \right) \det \mathbf{J}_\ell(\xi)}_{f_\ell(\xi)} \, d\xi \,. \tag{3.75}$$

Expression (3.75) is now ready for the application of a quadrature rule because all contributions are expressed in terms of reference coordinates. The finite elements used in this work are quadrilaterals in two and hexahedra in three space dimensions. Both can be represented by

$$\hat{\tau} = (-1,1)^d, \quad d = 2,3. \tag{3.76}$$

Therefore, it seems natural to apply a tensor-product integration rule based on a one-dimensional Gauß quadrature. Using a one-dimensional N_g-point rule, i.e., N_g^d points in the tensor-product rule, the matrix coefficient (3.75) can be approximated by

$$\mathsf{A}[i,j] \approx \sum_{\ell \in L} \sum_{g=1}^{N_g^d} f_\ell(\xi_g) w_g \,, \tag{3.77}$$

where ξ_g and w_g denote the coordinates and the weight of the g-th Gauß point, respectively. The treatment of the integrals occurring in the bilinear forms of the stiffness matrix in elasticity and of the mass matrices for the dynamics problems is totally equivalent.

The discretization with boundary elements requires regular and singular integrals over the surface Γ_h. Whereas the latter are treated in the following two subsections, at the moment only regular surface integrals are considered. As an example, regard the matrix entries of the single layer matrix

$$\mathsf{V}[i,j] = (\mathcal{V} \psi_j)(\mathbf{x}_i^*) = \int_{\Gamma_h} u^*(\mathbf{x}_i^*, \mathbf{y}) \psi_j(\mathbf{y}) \, ds_y \,.$$

Using the triangulation (3.28), the matrix coefficients become

$$\mathsf{V}[i,j] = \int_{\tau_j} u^*(\mathbf{x}_i^*, \mathbf{y}) \psi_j(\mathbf{y}) \, ds_\mathbf{y} \,,$$

because the support of the trial function ψ_j extends only over one element τ_j. Contrary to the volume integration, where the coordinate transformation is the mapping $\mathbf{x}\colon \mathbb{R}^d \to \mathbb{R}^d$, the computational surface Γ_h is a $(d-1)$-dimensional manifold embedded in the d-dimensional space. Therefore, one has the mapping

$$\mathbb{R}^{d-1} \ni \xi \to \mathbf{x}(\xi) \in \mathbb{R}^d. \tag{3.78}$$

The Jacobi matrix of this transformation is defined as in equation (3.74) with the difference that the index i ranges only from 1 to $(d-1)$ due to the above described property. By means of the *Gram determinant* [55]

$$G_j(\xi) := \det(\mathbf{J}_j(\xi)\mathbf{J}_j^\top(\xi)), \quad \mathbf{x} \in \tau_j, \tag{3.79}$$

the surface integrals can be transformed to an integration over the reference element

$$\mathsf{V}[i,j] = \int\limits_{\hat{\tau}} u^*(\mathbf{x}_i^*, \mathbf{y}(\xi)) \psi_j(\xi) \sqrt{G_j(\xi)} \, \mathrm{d}\xi. \tag{3.80}$$

Equation (3.80) is now ready for a quadrature rule. It has to be emphasized that $\mathbf{x}_i^* \notin \tau_j$, otherwise the collocation point would lie in the region of integration and thus the kernel diverges. Nevertheless, $\mathbf{x}_i^*$ could lie in one of the elements adjacent to τ_j. Then the so-called *quasi-singular* situation occurs, where the integral is theoretically regular but still difficult to handle by normal quadrature.

Remark 3.4. The best treatment of the regular surface integrals occurring in the computation of matrix coefficients of the boundary element method is clearly the employment of adaptive quadrature rules if analytical integration is ruled out. Several of these exist in literature, e.g., the CUBTRI algorithm [64] for triangles or the idea of Lachat and Watson [58] for quadrilateral elements. A survey of these methods can be found in the book of Krommer and Ueberhuber [55]. ◇

For simplicity, in this work only standard quadrature rules are used with a certain high number of points such that the integration error is kept low. The used reference elements are the one- and two-dimensional simplices, which are the interval $(-1,1)$ and the triangle $\left\{ (\xi_1, \xi_2) \in \mathbb{R}^2 \colon 0 < \xi_2 < 1 - \xi_1, 0 < \xi_1 < 1 \right\}$ (see figure 3.1 for pictures of these elements). For the first case a standard Gauß quadrature is used and for the latter the triangle quadrature rules due to Dunavant [22]. Let again N_g be the number of Gauß points in either case, the approximation of the coefficients of the single layer matrix is

$$\mathsf{V}[i,j] \approx \sum_{g=1}^{N_g} u^*(\mathbf{x}_i^*, \mathbf{y}(\xi_g)) \psi_j(\xi_g) \sqrt{G_j(\xi_g)} w_g. \tag{3.81}$$

Again, ξ_g and w_g are the coordinates and the weight of the g-th integration point. The computation the matrix entries of the double layer matrix K are carried out in the same way, with the difference that, like in the case of finite elements, the shape functions have a support extending over a patch of elements whose contributions are then summed up. The mass matrix B poses no difficulty and can be computed with a low-order rule.

3.3.2 Preliminaries to singular integration

Now the case is considered, where the collocation point is located on the element of integration, i.e., $\mathbf{x}_i^* \in \tau_j$. Obviously, the collocation point $\mathbf{x}_i^*$ and the integration variable $\mathbf{y}$ can get arbitrarily close and, therefore, the integrand diverges. Let ξ^* denote the reference coordinates corresponding to the collocation point. Hence, it holds $\mathbf{x}_i^* = \mathbf{x}(\xi^*)$. For the sake of convenience, the subscripts referring to the number of the collocation point and the reference element is omitted in the following unless necessary. Furthermore, the Landau notation is used

$$f(x) = \mathcal{O}(g(x)) \quad \Leftrightarrow \quad |f(x)| \le C|g(x)|, \quad x \to 0. \tag{3.82}$$

It is henceforth implicitly assumed that this notation is understood for the limit $x \to 0$. By means of the above, the Euclidean distance between $\mathbf{x}^*$ and $\mathbf{y}$ can be expressed through a Taylor expansion in reference coordinates

$$|\mathbf{y} - \mathbf{x}^*| = |\mathbf{x}(\xi) - \mathbf{x}(\xi^*)| = |\mathbf{J}^\top(\xi^*)(\xi - \xi^*)| + \mathcal{O}(|\xi - \xi^*|^2). \tag{3.83}$$

Here, $\mathbf{x}(\xi)$ refers to the coordinate transformation (3.12) such that the expression $\mathbf{y} = \mathbf{x}(\xi)$ is meaningful.

Looking at the time domain kernel functions u^* and $\mathcal{T}_\mathbf{y} u^*$ that occur in the single and double layer matrices, respectively, it can be stated that

$$u_{\text{dyn}}^*(\mathbf{x}, \mathbf{y}, t, \tau) = u_{\text{stat}}^*(\mathbf{x}, \mathbf{y}) + \mathcal{O}(|\mathbf{y} - \mathbf{x}|^0), \tag{3.84}$$

where the subscripts have been added to the functions to point out their different nature. This relation is easily established by replacing the appearing exponential and Bessel functions by the corresponding Taylor series. Note that the awkward term $|\mathbf{y} - \mathbf{x}|^0$ in the asymptotic behavior cannot be simply replaced by a constant. It represents all monomials of the term $|\mathbf{y} - \mathbf{x}|$ of order at least zeroth order. The essence of expression (3.84) is that it suffices to consider the singular behavior of the fundamental solution of the corresponding static problem because the asymptotic behavior for $\mathbf{y} \to \mathbf{x}$ is the same for static and dynamic fundamental solutions.

Remark 3.5. Most of the methods described below work with the decomposition

$$u^*(\mathbf{x}, \mathbf{y}) = u_{\text{sing}}^*(\mathbf{x}, \mathbf{y}) + \left(u^*(\mathbf{x}, \mathbf{y}) - u_{\text{sing}}^*(\mathbf{x}, \mathbf{y})\right),$$

where the singular part of the fundamental solution is extracted in order to be treated by special techniques and the difference term handled like a regular integral. Although the most popular approach in the engineering community, especially when analytical integrations are not feasible, the difference term in this decomposition poses a problem. The term itself is regular in the sense that it does not diverge when $\mathbf{y}$ tends to $\mathbf{x}$, but its derivatives are not regular and show a diverging behavior [55]. The dilemma is that the higher the applied quadrature rule the higher the order of the derivatives which control the error. Therefore, one cannot simply tackle the problem by increasing the order of the quadrature rule. An

adaptive quadrature rule as already suggested in remark 3.4 could mitigate the trouble. Finally, this difference can be numerically unstable because it involves the subtraction of large numbers and thus is a classical problem of cancellation [46]. Therefore, quadrature rules applicable to the fundamental solution as a whole would be the best choice. Unfortunately, in this work only the treatment of weakly singular integrals in three dimensions contains such an approach, whereas for the other cases the decomposition method has to suffice. ◇

3.3.3 Improper surface integrals

Consider again the matrix coefficients of the single layer matrix in the reference coordinates (3.80)

$$\mathsf{V}[i,j] = \int_{\hat{\tau}} u^*(\mathbf{x}_i^*, \mathbf{y}(\xi)) \psi_j(\xi) \sqrt{G_j(\xi)} \, d\xi$$

with $\mathbf{x}_i \in \tau_j$.

The fundamental solutions considered here (cf. the appendix A), show the asymptotic behaviors

$$\mathbf{x} \to \mathbf{y}: \quad u^*(\mathbf{x}, \mathbf{y}) \sim \begin{cases} \log \dfrac{1}{|\mathbf{y} - \mathbf{x}|} & d = 2 \\ \dfrac{1}{|\mathbf{y} - \mathbf{x}|} & d = 3. \end{cases} \tag{3.85}$$

In the following, first the two-dimensional and then the three-dimensional case is examined.

Weakly singular surface line integrals In this case, the subtraction of singularity technique [55] is applied by expressing the two-dimensional fundamental solutions as the sum of their singularity and a difference term

$$u^*(\mathbf{x}^*, \mathbf{y}(\xi)) = C \log \frac{1}{|\xi - \xi^*|} + \left(u^*(\mathbf{x}^*, \mathbf{y}(\xi)) - C \log \frac{1}{|\xi - \xi^*|} \right). \tag{3.86}$$

Note that the constant C used in this expression can be a scalar or a 2×2-matrix in case of elastic problems. Moreover, the reference coordinates ξ boil down to the scalar ξ for a one-dimensional reference element. Included in this expression is the fact that

$$\log \frac{1}{|\mathbf{x}(\xi) - \mathbf{x}(\xi^*)|} \approx \log \frac{1}{\sqrt{G(\xi^*)}|\xi - \xi^*|} = \log \frac{1}{\sqrt{G(\xi^*)}} + \log \frac{1}{|\xi - \xi^*|},$$

where the first approximation follows in two spatial dimensions from the Taylor expansion (3.83) and becomes an identity in the case of a linear geometry approximation. In the following only the logarithmic part, i.e., the first term in equation (3.86), is treated,

whereas the difference term is regular and therefore is computed like a regular surface integral (cf. remark 3.4).

Since special quadrature rules are available for logarithmic singularities, the singular part in (3.86) only has to be transformed into the right form. At first, the singular integral, henceforth termed $I_{w,2}$, is split in two parts

$$I_{w,2} := C \int_{-1}^{1} \log \frac{1}{|\xi - \xi^*|} \sqrt{G(\xi)} \psi(\xi) \, d\xi \tag{3.87}$$

$$= C \int_{-1}^{\xi^*} \log \frac{1}{|\xi - \xi^*|} \psi(\xi) \sqrt{G(\xi)} \, d\xi + C \int_{\xi^*}^{1} \log \frac{1}{|\xi - \xi^*|} \psi(\xi) \sqrt{G(\xi)} \, d\xi \, .$$

Now, auxiliary coordinates are introduced such that the point of singularity ξ^* is mapped to the origin in each of the two integrals,

$$\eta^1 = \xi^* - \xi \quad \text{and} \quad \eta^2 = \xi - \xi^* \, .$$

Then, the singular integral becomes

$$I_{w,2} = C \int_{0}^{1+\xi^*} \log \frac{1}{\eta^1} \psi(\eta^1) \sqrt{G(\eta^1)} \, d\eta^1 + C \int_{0}^{1-\xi^*} \log \frac{1}{\eta^2} \psi(\eta^2) \sqrt{G(\eta^2)} \, d\eta^2 \, ,$$

which now has to be stretched or squeezed, respectively, to the unit interval. Therefore, a new set of coordinates with the properties

$$\zeta^1 = \frac{\eta^1}{1 + \xi^*} \quad \text{and} \quad \zeta^2 = \frac{\eta^2}{1 - \xi^*}$$

is introduced such that one obtains

$$I_{w,2} = C \int_{0}^{1} \log \frac{1}{(1+\xi^*)\zeta^1} \psi(\zeta^1) \sqrt{G(\zeta^1)} (1 + \xi^*) \, d\zeta^1$$

$$+ C \int_{0}^{1} \log \frac{1}{(1-\xi^*)\zeta^2} \psi(\zeta^2) \sqrt{G(\zeta^2)} (1 - \xi^*) \, d\zeta^2 \, .$$

Note that $\psi(\zeta^i) = \psi(\xi(\eta^i(\zeta^i)))$ and similarly for $\sqrt{G(\zeta^i)}$. Unfortunately, this is not yet the right form for using the logarithmic quadrature rule, since the arguments of the logarithm still contain a perturbing factor. Therefore, one has to split up these terms and

get

$$I_{w,2} = C\int\limits_0^1 \log\frac{1}{\zeta^1}\psi(\zeta^1)\sqrt{G(\zeta^1)}(1+\xi^*)\,\mathrm{d}\zeta^1 + C\int\limits_0^1 \log\frac{1}{1+\xi^*}\psi(\zeta^1)\sqrt{G(\zeta^1)}(1+\xi^*)\,\mathrm{d}\zeta^1$$

$$+ C\int\limits_0^1 \log\frac{1}{\zeta^2}\psi(\zeta^2)\sqrt{G(\zeta^2)}(1-\xi^*)\,\mathrm{d}\zeta^2 + C\int\limits_0^1 \log\frac{1}{1-\xi^*}\psi(\zeta^2)\sqrt{G(\zeta^2)}(1-\xi^*)\,\mathrm{d}\zeta^2\,.$$

These are four integrals, two of which of the form $\int_0^1 \log(1/x)f(x)\,\mathrm{d}x$, which can be treated by a logarithmic quadrature rule, and two of which are regular. The latter two have to be transformed back to the interval $(-1,1)$ in order to apply a classical Gauß quadrature, which is a trivial task.

The logarithmic quadrature rule [86] employed in this context is designed such that

$$\int\limits_0^1 \log\frac{1}{x}f(x)\,\mathrm{d}x \approx \sum_{g+1}^{N_g} f(x_g)w_g$$

is carried out exactly, if $f(x)$ is a polynomial of degree at most $2N_g - 1$.

Weakly singular surface area integrals Again the matrix coefficients of the single layer matrix (3.80) are under consideration. Now the integration is carried out on the reference triangle and the integral kernel contains the three-dimensional fundamental solution

$$I_{w,3} := \int\limits_0^1 \int\limits_0^{1-\xi_1} u^*(\mathbf{x}(\xi^*),\mathbf{x}(\xi))\psi(\xi)\sqrt{G(\xi)}\,\mathrm{d}\xi_2\,\mathrm{d}\xi_1\,.$$

The first step is to subdivide the triangle such that the point of singularity $\xi^* = (\xi_1^*, \xi_2^*)$ is located on the vertices of the sub-triangles as displayed in figure 3.3. Two types of subdivision are analyzed, one with three and another with six sub-triangles. Each of these sub-triangles is now mapped onto the reference triangle $\{(\eta_1,\eta_2)\colon 0 < \eta_2 < \eta_1, 0 < \eta_1 < 1\}$, see figure 3.4(a). Therefore, the coordinate transformation

$$\begin{pmatrix} \xi_1 \\ \xi_2 \end{pmatrix} = \begin{pmatrix} \xi_1^* \\ \xi_2^* \end{pmatrix} + \begin{pmatrix} \xi_1^{i,1} - \xi_1^* \\ \xi_2^{i,1} - \xi_2^* \end{pmatrix}\eta_1^i + \begin{pmatrix} \xi_1^{i,2} - \xi_1^{i,1} \\ \xi_2^{i,2} - \xi_2^{i,1} \end{pmatrix}\eta_2^i \tag{3.88}$$

is used, where the coordinates $\xi_j^{i,k}$, i.e., the $(k+1)$-th vertex of the i-th sub-triangle, are taken from table 3.1. The Jacobian determinant of this coordinate transformations is

$$\det\mathbf{J}_i = (\xi_1^{i,1} - \xi_1^*)(\xi_2^{i,2} - \xi_2^{i,1}) - (\xi_2^{i,1} - \xi_2^*)(\xi_1^{i,2} - \xi_1^{i,1}) \tag{3.89}$$
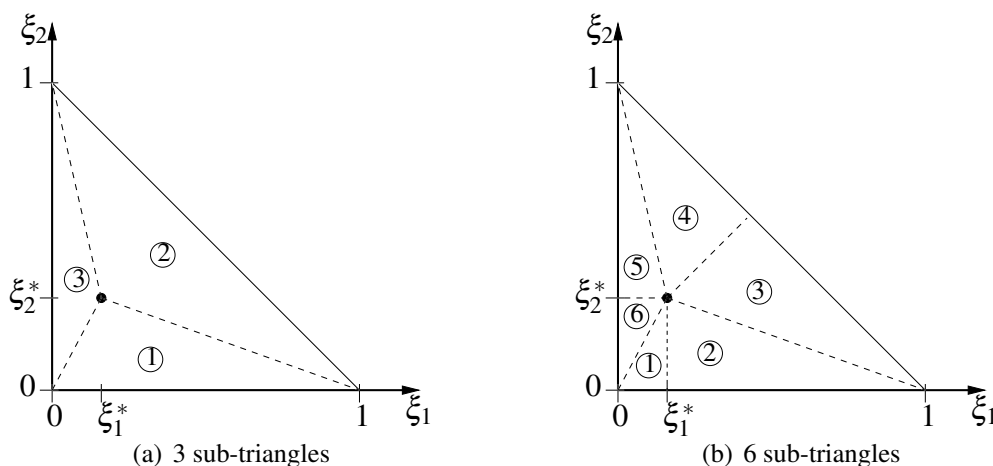
Figure 3.3: Triangle subdivision into 3 (a) and 6 sub-elements (b).

and thus a constant. Then, the considered integral becomes the sum of the contributions of all sub-triangles

$$I_{w,3} = \sum_{i=1}^{\{3|6\}} \int_0^1 \int_0^{\eta_1^i} u^*(\mathbf{x}(\mathbf{0}), \mathbf{x}(\eta^i)) \, \psi(\eta^i) \sqrt{G(\eta^i)} \, \det \mathbf{J}_i \, \mathrm{d}\eta_2^i \, \mathrm{d}\eta_1^i,$$

where the shorthand $\eta^i = (\eta_1^i, \eta_2^i)$ has been used. The idea is now, to use a coordinate transformation which alleviates the singularity. One option are polar coordinates whose functional determinant reduces the order of the singularity by one [33] but the transformed region has a rather complicated shape which requires another coordinate transformation onto the reference square. Here, so-called Duffy coordinates are preferred [21], which map the triangle onto a square by stretching the vertex with the singularity to one side of the square. A similar idea has been actually proposed by Lachat and Watson [58] (see

i	$\xi_1^{i,1}$	$\xi_2^{i,1}$	$\xi_1^{i,2}$	$\xi_2^{i,2}$
1	0	0	1	0
2	1	0	0	1
3	0	1	0	0

(a) 3 sub-triangles

i	$\xi_1^{i,1}$	$\xi_2^{i,1}$	$\xi_1^{i,2}$	$\xi_2^{i,2}$
1	0	0	ξ_1^*	0
2	ξ_1^*	0	1	0
3	1	0	$\frac{1+\xi_1^*-\xi_2^*}{2}$	$\frac{1-\xi_1^*+\xi_2^*}{2}$
4	$\frac{1+\xi_1^*-\xi_2^*}{2}$	$\frac{1-\xi_1^*+\xi_2^*}{2}$	0	1
5	0	1	0	ξ_2^*
6	0	ξ_2^*	0	0

(b) 6 sub-triangles

Table 3.1: Vertices of the sub-triangles for the coordinate transformation (3.88). Subdivision with 3 (a) and 6 triangles (b).
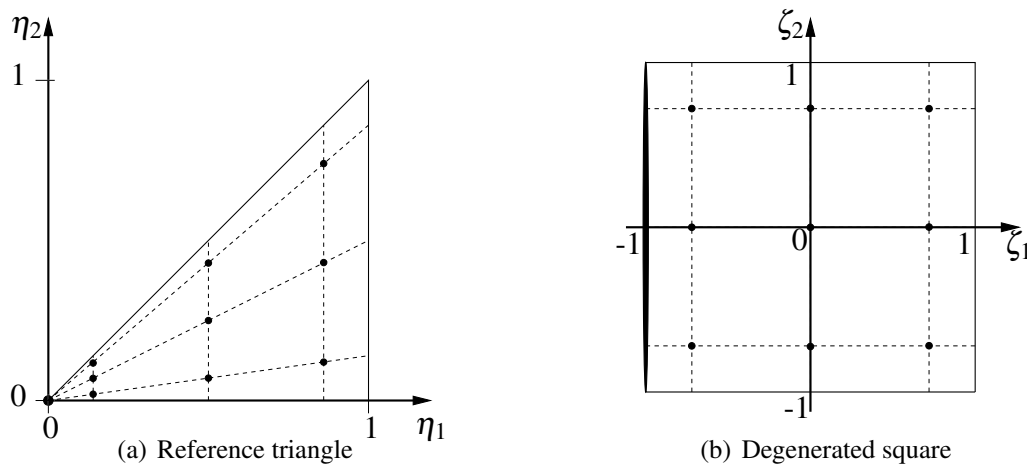
Figure 3.4: Reference triangle (a) and degenerated square (b) with Gauß points.

also [33]) earlier than Duffy. A new set of coordinates $\zeta = (\zeta_1, \zeta_2)$ is used with the properties

$$\eta_1^i = \frac{1}{2}(\zeta_1 + 1) \quad \text{and} \quad \eta_2^i = \frac{1}{4}(\zeta_1 + 1)(\zeta_2 + 2). \tag{3.90}$$

This transformation relates the coordinates ζ of the square $(-1,1)^2$ (see figure 3.4(b)) with the reference triangle depicted in figure 3.4(a). The determinant of the Jacobian matrix is then

$$H(\zeta) := \det \frac{\partial \eta}{\partial \zeta} = \frac{1}{8}(\zeta_1 + 1) \tag{3.91}$$

such that the integral finally becomes

$$I_{w,3} = \sum_{i=0}^{\{3|6\}} \int_{-1}^{1} \int_{-1}^{1} u^*(\mathbf{x}(-1, \zeta_2), \mathbf{x}(\zeta)) \psi(\zeta) \sqrt{G(\zeta)} \det \mathbf{J}_i H(\zeta) \, d\zeta. \tag{3.92}$$

This expression is now ready for a tensor-product Gauß quadrature rule, as for instance the 3×3-rule shown in figure 3.4. Note that

$$H(\zeta_1, \zeta_2) = \mathcal{O}(\zeta_1) \quad \text{and} \quad H(-1, \zeta_2) = 0$$

and these properties alleviate the singularity of the fundamental solution u^*. Moreover, this approach does not require to split the kernel function in singular and regular parts. It can be applied to the static and dynamic fundamental solutions in a black-box fashion. It remains to choose the sub-division of the original reference triangle as shown in figure 3.3. Therefore, the outcome of the described quadrature procedure is compared with the analytical solution given in the appendix of the book of Rjasanow and Steinbach [94], where a constant shape function ψ has been assumed. In this comparison, two different locations of the collocation points have been chosen, $\xi_1^* = (1/4, 1/4)$ and $\xi_2^* = (1/4, 1/2)$, respectively. These locations correspond to piecewise linear triangles, see remark 3.2. The results of this analysis are given in table 3.2 for the two different subdivisions together with

the exact solution. The order in the tables refers to the order of the tensor-product Gauß quadrature rule. It can be seen that the subdivision in 6 sub-triangles is more effective than using only 3 sub-triangles. For instance, the result for $6 \times (14 \times 14) = 1176$ Gauß points, i.e., 6 sub-triangles with a tensor-product rule with 14 points, is better the error of using 3 sub-triangles with a 20 point rule each, i.e., 1200 points in total, whereas both computations have a similarly amount of function evaluations. It is thus preferred to use the subdivision with 6 triangles as in figure 3.3(b).

3.3.4 Cauchy principal value surface integrals

The Cauchy principal value is defined as [55]

$$\fint_{\Gamma} f(\mathbf{x}) \, d\mathbf{x} := \lim_{\varepsilon \to 0} \int_{\Gamma \backslash B_{\varepsilon}(\mathbf{x}_0)} f(\mathbf{x}) \, d\mathbf{x}, \tag{3.93}$$

where $\mathbf{x}_0$ is the location of the singularity of the integrand f and $B_{\varepsilon}(\mathbf{x}_0)$ denotes a ball of radius ε with center $\mathbf{x}_0$. If f is a regular function, the principal value coincides with classical integration. In order to exist, the functions f has to obey certain criteria which are given, for instance, in the book of Sauter and Schwab [96].

Whereas the singularities occurring in the evaluation of the single layer matrix V are all integrable in the sense of improper integrals (weak singularities), the double layer matrix K contains so-called strong singularities. Here, the asymptotic behavior is

$$\mathbf{x} \to \mathbf{y}: \quad \mathcal{T}_{\mathbf{y}} u^*(\mathbf{x}, \mathbf{y}) \sim \begin{cases} \dfrac{1}{|\mathbf{y} - \mathbf{x}|} & d = 2 \\[2mm] \dfrac{1}{|\mathbf{y} - \mathbf{x}|^2} & d = 3. \end{cases} \tag{3.94}$$

A closer look at the kernel functions $\mathcal{T}_{\mathbf{y}} u^*(\mathbf{x}, \mathbf{y})$ reveals that in case of the scalar problems of Laplace and scalar wave equations, the problematic term $|\mathbf{y} - \mathbf{x}|^{1-d}$ is multiplied by the term

$$\frac{\partial |\mathbf{y} - \mathbf{x}|}{\partial \mathbf{n}(\mathbf{y})} = \frac{(\mathbf{y} - \mathbf{x}) \cdot \mathbf{n}(\mathbf{y})}{|\mathbf{y} - \mathbf{x}|}, \tag{3.95}$$

where $\mathbf{n}(\mathbf{y})$ denotes the unit outward normal vector at $\mathbf{y} \in \Gamma$. Obviously, the scalar product of the difference $(\mathbf{y} - \mathbf{x})$ and the normal vector $\mathbf{n}(\mathbf{y})$ vanishes if $\mathbf{y}$ lies on the tangent plane at $\mathbf{x}$. Therefore, this term cancels the singularity and in the case of the scalar fundamental solutions, the double layer operator does not contain any strong singularities. Due to this observation, in the following only the kernel function $\mathcal{T}_{\mathbf{y}} \mathbf{U}^*(\mathbf{x}, \mathbf{y})$ of elastic problems is regarded, which has $d \times d$ components. This function can be expressed as

$$(\mathcal{T}_{\mathbf{y}} \mathbf{U}^*)(\mathbf{x}, \mathbf{y}) = -\frac{1}{2^d \pi (1 - \nu) |\mathbf{y} - \mathbf{x}|^d} \times$$
$$\left[\left((1 - 2\nu) \mathbf{I} + d \frac{(\mathbf{y} - \mathbf{x})(\mathbf{y} - \mathbf{x})^{\top}}{|\mathbf{y} - \mathbf{x}|^2} \right) (\mathbf{y} - \mathbf{x}) \cdot \mathbf{n}(\mathbf{y}) + (1 - 2\nu) \Sigma(\mathbf{x}, \mathbf{y}) \right] \tag{3.96}$$

order	ξ_1^*	ξ_2^*
2	0.185816458342436	0.169263531227941
4	0.188303880801567	0.184070343292020
6	0.188476966386167	0.183569752851678
8	0.188639144444796	0.182465213766623
10	0.188654512298107	0.182179913028121
12	0.188655194402365	0.182189837148910
14	0.188655418573529	0.182225011283474
16	0.188655458424223	0.182237334611801
18	0.18865461710007	0.182238029755407
20	0.18865462157438	0.182236873150163
exact	0.188655462260302	0.182236342753599

(a) 3 sub-triangles

order	ξ_1^*	ξ_2^*
2	0.190686675090202	0.183666318618617
4	0.188617874392945	0.182265263922609
6	0.188656313328276	0.182231113760237
8	0.188655440675359	0.182236707825696
10	0.188655462838450	0.182236328926781
12	0.188655462244554	0.182236342516193
14	0.18865462260730	0.18223634843543
16	0.18865462260287	0.182236342745183
18	0.188655462260303	0.182236342754061
20	0.188655462260302	0.182236342753590
exact	0.188655462260302	0.182236342753599

(b) 6 sub-triangles

Table 3.2: Values of the integral (3.92) for the two considered triangle subdivisions and different quadrature rules.

with the $d \times d$ identity $\mathbf{I}$ and the skew-symmetric tensor Σ with components

$$\Sigma(\mathbf{x}, \mathbf{y})[i, j] = (y_j - x_j)n_i(\mathbf{y}) - (y_i - x_i)n_j(\mathbf{y}) \quad i, j = 1, \dots, d. \tag{3.97}$$

x_i, y_i, and n_i are the i-th components of the vectors $\mathbf{x}$, $\mathbf{y}$, and $\mathbf{n}$, respectively. The considered kernel function is thus composed of a part multiplied by the term (3.95), which will not be considered any further, and a part which really has to be integrated in the sense of a principal value as in equation (3.93). The matrix entries of the double layer matrix are

$$\mathsf{K}[i, j] = \lim_{\varepsilon \to 0} \int_{\Gamma_h \backslash B_\varepsilon(\mathbf{x}_i^*)} \mathcal{T}_y \mathbf{U}^*(\mathbf{x}_i^*, \mathbf{y}) \varphi_j(\mathbf{y}) \, ds_\mathbf{y} = \fint_{\Gamma_h} \mathcal{T}_y \mathbf{U}^*(\mathbf{x}_i^*, \mathbf{y}) \varphi_j(\mathbf{y}) \, ds_\mathbf{y}$$

which become the sum over the elements belonging to the support of the j-th trial function

$$\mathsf{K}[i, j] = \fint_{\Sigma_{\ell \in L} \tau_\ell} \mathcal{T}_y \mathbf{U}^*(\mathbf{x}_i^*, \mathbf{y}) \varphi_j(\mathbf{y}) \, ds_\mathbf{y}.$$

The index set L contains the elements τ_ℓ belonging to the region of integration. The collocation point lies inside one element and thus the integration over the other elements is regular. Denoting by $\tau_{\ell'}$ the element in which the collocation point $\mathbf{x}_i^*$ is located and by L' the index set L without the index ℓ', the above becomes

$$\mathsf{K}[i, j] = \sum_{\ell \in L'} \int_{\tau_\ell} \mathcal{T}_y \mathbf{U}^*(\mathbf{x}_i^*, \mathbf{y}) \varphi_j(\mathbf{y}) \, ds_\mathbf{y} + \fint_{\tau_{\ell'}} \mathcal{T}_y \mathbf{U}^*(\mathbf{x}_i^*, \mathbf{y}) \varphi_j(\mathbf{y}) \, ds_\mathbf{y}.$$

In the following, only the part of the latter integral is treated, which contains the Cauchy principal value

$$\mathsf{I}_{s,d} := \underbrace{-\frac{1 - 2\nu}{2^d \pi (1 - \nu)}}_{C_d} \fint_{\tau_{\ell'}} \frac{1}{|\mathbf{y} - \mathbf{x}^*|^d} \Sigma(\mathbf{x}^*, \mathbf{y}) \varphi(\mathbf{y}) \, ds_\mathbf{y}. \tag{3.98}$$

Remark 3.6. The double layer potential operator of elastostatics can also be represented by the single layer operator of elastostatics and the double layer operator of the Laplace equation [57]. This representation only contains weakly singular integrals and is therefore preferable to the classical expression. The drawback though is that it is derived by means of integration by parts and therefore additional terms on $\partial\Gamma$, i.e., the boundary of the surface Γ, appear, which contain singularities too. In case of a closed surface, no boundary of the surface exists, $\partial\Gamma = \emptyset$, and these additional terms do not show up. But, since in this work the application to open domains is an important item, the classical representation is used. $\diamond$

As in the case of the improper surface integrals, at first the Cauchy principal value integration on a line and then on a two-dimensional surface is looked at.

Strongly singular line integrals   For the time being, it is assumed that the geometry representation is linear. Then, one can establish

$$\frac{\mathbf{y} - \mathbf{x}^*}{|\mathbf{y} - \mathbf{x}^*|} = \frac{\mathbf{J}^\top (\xi - \xi^*)}{|\mathbf{J}^\top (\xi - \xi^*)|} = \mathrm{sign}(\xi - \xi^*)\mathbf{t},$$

where $\mathbf{t} = (t_1, t_2)^\top$ is the unit tangent vector of the element. Moreover, the Jacobi matrix is simply a vector with length of the Gram determinant, $|\mathbf{J}| = \sqrt{G}$, and obviously $\mathbf{t} \cdot \mathbf{n} = 0$ such that $n_1 = t_2$ and $n_2 = -t_1$. With these relations, the principal value integral becomes

$$\mathsf{I}_{s,2} = C_2 \fint_{-1}^{1} \frac{\Sigma(\xi^*, \xi)}{\sqrt{G}|\xi - \xi^*|}\varphi(\xi)\sqrt{G}\,d\xi = C_2 \mathsf{S} \fint_{-1}^{1} \frac{\mathrm{sign}(\xi - \xi^*)}{|\xi - \xi^*|}\varphi(\xi)\,d\xi = C_2 \mathsf{S} \fint_{-1}^{1} \frac{\varphi(\xi)}{\xi - \xi^*}\,d\xi$$

with the matrix $\mathsf{S} = \left(\begin{smallmatrix} 0 & 1 \\ -1 & 0 \end{smallmatrix}\right)$. In case of a non-linear geometry approximation, this derivation is only valid in the vicinity of the singularity ξ^*. In such cases, the above result for $\mathsf{I}_{s,2}$ is subtracted from the integrand in order to obtain a regular difference term. It turns out that the singular part is of the form $\fint_{-1}^{1} f(\xi)/(\xi - \xi^*)\,d\xi$, $\xi \in (-1, 1)$ to which a modified quadrature rule is applied. Such rules especially tailored for Cauchy principal value integration and their analysis can be found in the thesis of Diethelm [19]. Other techniques are explained in the book of Krommer and Ueberhuber [55].

Strongly singular surface area integrals   The treatment of the Cauchy principal value on a two-dimensional surface is done analogously to the approach of Guiggiani and Gigante [40]. The only difference is here that the collocation point is always inside the element and, instead of the rather cumbersome polar coordinate transformation, Duffy coordinates [21] are preferred. Only the basic steps will be repeated here. The derivation starts again with the Taylor expansion (3.83). Then the differences in the reference coordinates are expressed through Duffy coordinates on the i-th sub-triangle ($i = 1, \ldots, 6$ due to the arguments at the end of subsection 3.3.3, see also figure 3.3(b))

$$\xi - \xi^* \overset{(3.88)}{=} (\xi^{i,1} - \xi^*)\eta_1^i + (\xi^{i,2} - \xi^{i,1})\eta_2^i \overset{(3.90)}{=} \underbrace{\left[(\xi^{i,1} - \xi^*) + (\xi^{i,2} - \xi^{i,1})\frac{\zeta_2 + 1}{2}\right]}_{\tilde{\xi}^i(\zeta_2)}\frac{\zeta_1 + 1}{2}.$$

Insertion of this expression into the difference of the global coordinates yields the approximation

$$\mathbf{y} - \mathbf{x}^* \approx \underbrace{\mathbf{J}^\top \tilde{\xi}^i}_{\mathbf{a}^i(\zeta_2)}\frac{\zeta_1 + 1}{2} \tag{3.99}$$

and therefore for the distance function

$$|\mathbf{y} - \mathbf{x}^*| \approx \frac{\zeta_1 + 1}{2}a^i(\zeta_2) \tag{3.100}$$

with $a^i(\zeta_2)$ being the length of the vector $\mathbf{a}^i(\zeta_2)$, defined by equation (3.99). The integral (3.98) thus becomes

$$\mathsf{I}_{s,3} = C_3 \fint_{\tau_{\ell'}} \frac{\Sigma(\mathbf{x}^*, \mathbf{y})}{|\mathbf{y} - \mathbf{x}^*|} \varphi(\mathbf{y}) \, \mathrm{d}s_y$$

$$= C_3 \lim_{\varepsilon \to 0} \sum_{i=1}^{6} \int_{-1}^{1} \int_{-1+\gamma_\varepsilon}^{1} \underbrace{\frac{\Sigma(\mathbf{x}(-1,\zeta_2), \mathbf{x}(\zeta))}{|\mathbf{x}(\zeta) - \mathbf{x}(-1,\zeta_2)|^3} \varphi(\zeta) \sqrt{G(\zeta)} \det \mathbf{J}_i H(\zeta) \, \mathrm{d}\zeta}_{\mathbf{F}_i(\zeta)},$$

where γ_ε is the transformed result of the original ball $B_\varepsilon(\mathbf{x}^*)$ and will be reconsidered later. The kernel function $\mathbf{F}_i$ is now approximated in the following way by using expressions (3.99) and (3.100)

$$\mathbf{F}_i(\zeta)[k,j] \approx \frac{n_k a_j^i(\zeta_2) - n_j a_k^i(\zeta_2)}{(a^i)^3(\zeta_2)} \frac{\frac{\zeta_1+1}{2}}{\left(\frac{\zeta_1+1}{2}\right)^3} \varphi(\zeta) \sqrt{G(\zeta)} \det \mathbf{J}_i \frac{\zeta_1+1}{8}$$

$$= \frac{1}{2(\zeta_1+1)} \frac{n_k a_j^i(\zeta_2) - n_j a_k^i(\zeta_2)}{(a^i)^3(\zeta_2)} \varphi(\zeta) \sqrt{G(\zeta)} \det \mathbf{J}_i$$

$$= \frac{1}{2(\zeta_1+1)} \mathbf{E}_i(\zeta)[k,j].$$

The intermediate result is for the considered integral now

$$\mathsf{I}_{s,3} \approx C_3 \lim_{\varepsilon \to 0} \sum_{i=1}^{6} \int_{-1}^{1} \int_{-1+\gamma_\varepsilon}^{1} \frac{1}{2(\zeta_1+1)} \mathbf{E}_i(\zeta) \, \mathrm{d}\zeta \qquad (3.101)$$

Now, the singularity is subtracted by means of the identity

$$\mathbf{E}_i(\zeta) = \mathbf{E}_i(\zeta_1, \zeta_2) = \mathbf{E}_i(-1, \zeta_2) + (\mathbf{E}_i(\zeta_1, \zeta_2) - \mathbf{E}_i(-1, \zeta_2)).$$

Inserting this decomposition into the integrals (3.101) yields two integrals per sub-triangle, whereas the first contains the singularity and the second is a regular integration over the difference term. The regular contribution is treated by a tensor-product Gauß quadrature and will not be considered any further. The remaining singular integral contributed by the i-th sub-triangle is of the following form and its inner integration can be carried out analytically

$$\tilde{\mathsf{I}}_{s,3}^i := C_3 \lim_{\varepsilon \to 0} \int_{-1}^{1} \int_{-1+\gamma_\varepsilon}^{1} \frac{\mathbf{E}_i(-1, \zeta_2)}{2(\zeta_1+1)} \, \mathrm{d}\zeta_1 \, \mathrm{d}\zeta_2 = \frac{C_3}{2} \lim_{\varepsilon \to 0} \int_{-1}^{1} \mathbf{E}_i(-1, \zeta_2) \log(\zeta_1+1)|_{-1+\gamma_\varepsilon}^{1} \, \mathrm{d}\zeta_2.$$

Due to the coordinate transformations from the global coordinates $\mathbf{x}$ to the local Duffy coordinates ζ, the lower integration bound, i.e., the surface of the ball $B_\varepsilon(\mathbf{x}^*)$ becomes

$$|\mathbf{y} - \mathbf{x}^*| > \varepsilon \quad \longrightarrow \quad \frac{\zeta_1+1}{2} a^i(\zeta_2) > \varepsilon \quad \Leftrightarrow \quad \zeta_1 > \frac{2\varepsilon}{a^i(\zeta_2)} - 1 = \gamma_\varepsilon - 1.$$

By means of this, the remaining singular integral can be finally expressed by summing again over the contributions $\tilde{l}^i_{s,3}$

$$
\begin{aligned}
\mathsf{l}_{s,3} \approx \sum_{i=1}^{6} \tilde{\mathsf{l}}^i_{s,3} &= \sum_{i=1}^{6} \lim_{\varepsilon \to 0} \frac{C_3}{2} \int_{-1}^{1} \mathbf{E}_i(-1, \zeta_2) \log \frac{a^i(\zeta_2)}{\varepsilon} \, \mathrm{d}\zeta_2 \\
&= \sum_{i=1}^{6} \frac{C_3}{2} \int_{-1}^{1} \mathbf{E}_i(-1, \zeta_2) \log a^i(\zeta_2) \, \mathrm{d}\zeta_2 \, .
\end{aligned}
\tag{3.102}
$$

The validity of the last equality has been shown by Guiggiani and Gigante [40] and the result is regular because, by its definition, $a^i(\zeta_2)$ cannot become zero. For this reason, a standard one-dimensional quadrature rule will solve this last integral. It has to be added that in case of a linear geometry representation, the approximations (3.99) and (3.100) become exact and thus expression (3.101), too. In this situation, the only errors committed are due to the employed quadrature rules.

3.4 Direct Solution Methods

In sections 3.1 and 3.2, the considered discretization methods are introduced. In case of a finite element discretization, system (3.17) is obtained for a static analysis and the sequence of systems of equations (3.60) for a dynamic analysis. The boundary element discretizations, on the other hand, yield systems (3.42) and (3.73), respectively. Section 3.3 was then dedicated to details in the computation of the coefficients of the system matrices. These coefficients are computed with limited accuracy only, especially the boundary element matrices are rather error-prone. Consequently, one would have to introduce a notational indication for the distinction between the system matrices and their approximations. In order to avoid a mess of notation, the use of approximately computed matrix coefficients is henceforth implied by expressions A, V, etc. The same holds for the right hand sides which can also be affected by integration errors. At first, the occurring finite element systems are considered before the block systems of the boundary element discretizations follow.

Finite element discretization In case of the considered finite element discretizations it is guaranteed that the system matrix A is symmetric positive definite [9] and it shall be assumed that its approximation does not loose this property. Moreover, the same holds for the mass matrix M [49] such that the linear combination of both with positive coefficients results again in a symmetric positive definite matrix, as it is the case in the system occurring due to the Newmark method (3.60). In addition to this property, these matrices are sparse, i.e., the number of non-zero entries grows only linear with the number of unknowns.

In view of these features and of the fact that the system (3.60) has the same left hand side matrix for all time steps, a Cholesky decomposition [36] is advocated. Therefore,

this decomposition can be precomputed and, in case of a dynamic analysis, reused for every new time step to obtain the current set of unknowns. The sparsity of the system matrix is exploited by using special storage formats as explained for instance in the book of Saad [95]. The system matrix A (or $\tilde{A}$ in the dynamic case) is thus decomposed and then the system $Au = f$ ($\tilde{A}u_n = \tilde{f}_n$) solved in two steps

$$A = LL^\top, \quad y = L^{-1}f \quad \text{and} \quad u = L^{-\top}y. \tag{3.103}$$

In the dynamic case, the last two steps, which are carried out at once and are efficient due to the triangular structure of the factor L, are then repeated at every time step.

Boundary element discretization   Similar to the finite element discretization, the time-domain analysis requires the solution of a sequence of systems of equations where only the right hand side changes. So, by the same reasoning, a direct solver by means of a factorization is preferred to iterative solution procedures. Moreover, the considered block system (3.42) is not symmetric and the blocks V and $\tilde{K}$ are fully populated which complicates the design of an efficient preconditioning procedure, as required for a robust iterative solution algorithm. Here, a block LU-decomposition [36] of the system matrix is employed. At first, the system matrix is decomposed

$$\begin{pmatrix} V & -\tilde{K} \\ B & \end{pmatrix} = \begin{pmatrix} L_V & \\ L_B & I \end{pmatrix} \begin{pmatrix} I & \\ & S \end{pmatrix} \begin{pmatrix} U_V & -U_K \\ & I \end{pmatrix} = \begin{pmatrix} L_V & \\ L_B & L_S \end{pmatrix} \begin{pmatrix} U_V & -U_K \\ & U_S \end{pmatrix} \tag{3.104}$$

with the following factors

$$L_V U_V = V, \quad L_V U_K = \tilde{K}, \quad L_B U_V = B \quad \text{and} \quad S = L_B U_K. \tag{3.105}$$

The first operation is a classical LU-decomposition and the next two are forward and backward substitutions in order to obtain the factors U_K and L_B. Finally, the last matrix-matrix product yields S, which in fact is the same Schur complement as shown in equation (3.43). Another LU-decomposition of this block, $L_S U_S = S$, then gives the factors for the final block decomposition (3.104). As seen below, it will be useful to perform two more substitutions, obtaining auxiliary matrices G and H,

$$G L_V = L_B \quad \text{and} \quad U_V H = U_K. \tag{3.106}$$

All of these operations can be carried out *in place*, which means that no additional storage is required, except for the storage of S or its factors L_S and U_S.

After precomputing all these factors, the system can be solved by the steps

$$g = f_N - H f_D, \quad Su = g, \quad Vy = f_D \quad \text{and} \quad q = y + Gu. \tag{3.107}$$

The necessity of the auxiliary matrices (3.106) becomes clear in these solution steps. The first operation is a simple matrix-vector product which gives the condensed right hand side as in equation (3.43). Afterwards, two solutions of linear systems are carried out, where

the left hand side matrices V and S are already factorized. Finally, another matrix-vector product gives the solution of q. In fact, the LU-factorization is carried out with pivoting and, because of this, some steps require permutation operations, which are not shown here for simplicity.

In the dynamic solution algorithm, the same methodology is performed with the only difference that at each time step the new right hand sides have to be computed and then the steps (3.107) are repeated.

Remark 3.7. The procedures introduced for the solution of the final systems of equations have in general a cubic complexity. This means that the factorization of an $N \times N$-matrix hat the complexity $\mathcal{O}(N^3)$. In case of the finite element stiffness matrix (3.17), the sparsity pattern can reduce the number of required operations down to $\mathcal{O}(Nb^2)$ for the optimal case of a symmetric positive definite matrix with bandwidth b [36]. Note $b \ll N$ and b is independent of N. For large N, an iterative solution procedure would prevail, for instance, a preconditioned conjugate gradient method [95]. The block system of the boundary element discretization (3.42), on the other hand, is indefinite and the iterative solution has to be adapted to this situation [104]. In any case, a classical iteration procedure solves the system without generating a factorization such that in a dynamic analysis the solution process has to be repeated at every time step. $\diamondsuit$

4 COUPLED SOLUTION ALGORITHMS

In this chapter, the partitioned analysis of the (initial) boundary value problems presented in chapter 2 is outlined using the numerical approximation methods introduced in the previous chapter 3. The partitioning considered in this work is purely spatial in the sense that the computational domain Ω is subdivided as explained in section 4.1 but the time discretization is the same for each subdomain.

The aims of such a strategy are multiple. On the one hand, Ω might already consist of several physically different subregions. In these multiphysics situations, the partitioning could be mandatory in order to tackle the problem. The case of fluid-structure interaction contains (at least) two entirely different physical models sharing an interface. See for instance the book of Ohayon and Soize [76] for the problem of acoustic-structure vibration problems. Here, only the cases with equal mathematical models but possibly different material properties are treated. Nevertheless, the extension of this work to the combination of different models is possible.

A similar situation occurs on the other hand, when the underlying geometry of the problem motivates the subdivision. This is for instance the case in soil-structure interaction, where the soil is often represented by an unbounded medium connected to the finite-sized structure. Although both parts can be governed by the same set of partial differential equations, the treatment of the unbounded soil might require a different numerical approximation method. A typical approach to such a problem is the combination of boundary and finite element discretizations in form of a *hybrid* method. The idea of combining finite and boundary element discretizations goes back to Zienkiewicz et al. [121] and a profound mathematical analysis can be found for instance in the monograph of Steinbach [106].

Finally, computational efficiency can be gained by using the partitioning for a divide-and-conquer strategy. This approach is commonly called *domain decomposition method* and allows for a significant speedup with solution algorithms especially designed for a suitable subdivision of Ω. Commonly, these algorithms perform in parallel when executed on multiprocessor computers. The book of Toselli and Widlund [114] and the survey articles of Le Tallec [65] and of Farhat and Roux [28] exhaustively describe the topic of domain decomposition methods for finite element discretizations.

Whereas in the case of multiphysics, the interfaces between the subregions are predefined by the physical structure, in domain decomposition approaches it prevails to sub-divide the given problem such that the workload for each subregion is balanced. Automatized subdivision algorithms are often employed in the latter situation. Nevertheless, the above concepts are not mutually exclusive because a multiphysics situation can still be handled

by domain decomposition algorithms where each physical subregion can be treated by different numerical approximation schemes.

In this chapter, at first the partitioning of the problem is described in section 4.1 mainly for the introduction of the employed notation and variational principles. Section 4.2 outlines so-called Dirichlet-to-Neumann maps, essential for the FETI-like methods used in this work which are presented in section 4.3. The special topic of conforming and nonconforming interface discretizations is then treated in section 4.4.

4.1 Partitioning of the Problem

The process of subdividing a given (initial) boundary value problem begins with the geometric partitioning of the domain Ω in which the problem is stated. Let Ω be decomposed into N_s subdomains $\Omega^{(r)}$,

$$\overline{\Omega} = \bigcup_{r=1}^{N_s} \overline{\Omega}^{(r)}. \tag{4.1}$$

The subdomains are non-overlapping, i.e., their mutual intersections vanish

$$\Omega^{(r)} \cap \Omega^{(p)} = \emptyset, \quad r \neq p.$$

The internal boundaries or *interfaces* due to this subdivision are defined by

$$\Gamma^{(rp)} := \overline{\Omega}^{(r)} \cap \overline{\Omega}^{(p)} \quad r, p = 1, \dots, N_s, \quad r \neq p. \tag{4.2}$$

Consequently, the boundary of each subdomain $\Omega^{(r)}$ is composed of its interfaces, a Dirichlet, and a Neumann part, i.e.,

$$\Gamma^{(r)} := \partial\Omega^{(r)} = \left(\bigcup_{p \in J^{(r)}} \overline{\Gamma}^{(rp)} \right) \cup \overline{\Gamma}_D^{(r)} \cup \Gamma_N^{(r)}, \tag{4.3}$$

where $\Gamma_D^{(r)} := \overline{\Omega}^{(r)} \cap \Gamma_D$ and $\Gamma_N^{(r)} := \overline{\Omega}^{(r)} \cap \Gamma_N$. Recall, $\Gamma = \partial\Omega = \overline{\Gamma}_D \cup \Gamma_N$ is the boundary of the original undecomposed domain consisting of Dirichlet and Neumann parts. Moreover, the set $J^{(r)}$ collects the indices of subdomains sharing an interface with $\Omega^{(r)}$,

$$J^{(r)} = \left\{ p, 1 \leq p \leq N_s, p \neq r \colon \overline{\Omega}^{(r)} \cap \overline{\Omega}^{(p)} \neq \emptyset \right\}. \tag{4.4}$$

In the union (4.3), the Dirichlet and Neumann parts $\Gamma_D^{(r)}$ and $\Gamma_N^{(r)}$ can be empty sets, whereas the union of interfaces does not vanish because otherwise the subdomain would be disconnected from the rest. The skeleton of the partition (4.1) is denoted by

$$\Gamma_s := \left(\bigcup_{r=1}^{N_s} \Gamma^{(r)} \right) \setminus \Gamma, \tag{4.5}$$
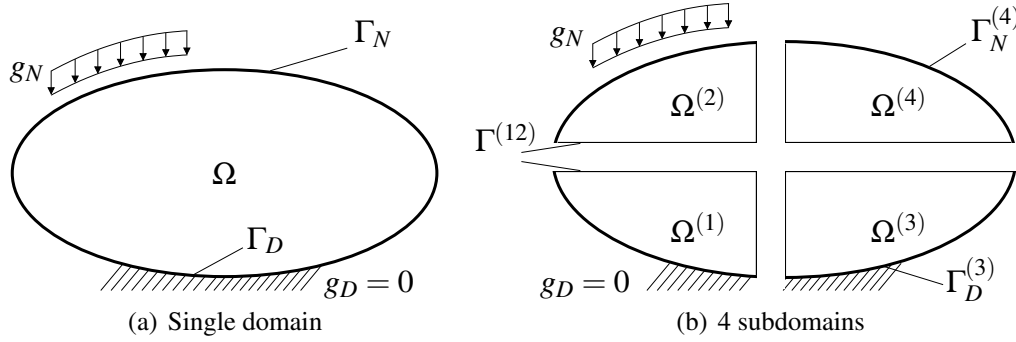
Figure 4.1: Problem statement for a single domain (a) and 4 subdomains (b) with some exemplary labeling.

i.e., the collection of all interfaces. Figure 4.1 displays the situation for a single domain 4.1(a) and its subdivision into 4 subdomains 4.1(b) with some examples of the introduced notation. The boundary $\Gamma^{(1)}$, for instance, is composed of $\Gamma^{(12)}, \Gamma^{(13)}, \Gamma_N^{(1)}$ and $\Gamma_D^{(1)}$, and its connectivity index set is $J^{(1)} = \{2, 3\}$. The skeleton of this subdivision is of course $\Gamma_s = \Gamma^{(12)} \cup \Gamma^{(13)} \cup \Gamma^{(23)} \cup \Gamma^{(24)}$.

At first, elliptic mixed boundary value problems are regarded only. Let $u^{(r)}$ denote the restriction of the unknown u to the subdomain $\Omega^{(r)}$, i.e.,

$$u^{(r)}(\mathbf{x}) := u(\mathbf{x}) \quad \mathbf{x} \in \Omega^{(r)}. \tag{4.6}$$

Thus, in every subdomain $\Omega^{(r)}$ the following problem is stated

$$\mathcal{L}^{(r)} u^{(r)}(\mathbf{x}) = f(\mathbf{x}) \qquad \mathbf{x} \in \Omega^{(r)}$$
$$u_\Gamma^{(r)}(\mathbf{y}) := (\mathrm{Tr}^{(r)} u^{(r)})(\mathbf{y}) = g_D(\mathbf{y}) \quad \mathbf{y} \in \Gamma_D^{(r)} \tag{4.7}$$
$$q_\Gamma^{(r)}(\mathbf{y}) := (\mathcal{T}^{(r)} u^{(r)})(\mathbf{y}) = g_N(\mathbf{y}) \quad \mathbf{y} \in \Gamma_N^{(r)},$$

which corresponds to the mixed elliptic boundary value problem (2.34) presented in subsection 2.3.1. If $\Gamma_D^{(r)}$ or $\Gamma_N^{(r)}$ is an empty set, the corresponding condition vanishes. Note that the operators $\mathcal{L}$, Tr, and $\mathcal{T}$ are all assigned with the subdomain superscript (r). This emphasizes the fact that the coefficients involved in $\mathcal{L}$ and $\mathcal{T}$ (for instance the material stiffness) can be different in each subdomain. In fact, it is assumed that these coefficients are constant within each subdomain but can have jumps at the interfaces. Moreover, the traces refer to the subdomain boundary $\Gamma^{(r)}$ and the outward normal vector incorporated in the definition of $\mathcal{T}$ is defined with respect to $\Omega^{(r)}$.

Considering the decomposition of the subdomain boundaries (4.3), it becomes obvious that the problem statement (4.7) is not completely formulated because conditions for $\mathrm{Tr}^{(r)} u^{(r)}$ and $\mathcal{T}^{(r)} u^{(r)}$ on the interfaces are lacking. Therefore, the so-called *interface conditions* are formulated

$$u_\Gamma^{(r)}(\mathbf{y}) - u_\Gamma^{(p)}(\mathbf{y}) = 0 \tag{4.8a}$$
$$q_\Gamma^{(r)}(\mathbf{y}) + q_\Gamma^{(p)}(\mathbf{y}) = 0 \tag{4.8b}$$

for $\mathbf{y} \in \Gamma^{(rp)}$. The first of these conditions describes the continuity of the unknown u across the interfaces, often referred to as continuity or compatibility condition. The latter condition can be interpreted as an equilibrium condition at the interfaces (recall the method of sections in basic structural mechanics). Actually, the equilibrium condition (4.8b) is a consequence of the continuity condition (4.8a) because it can be obtained by applying the respective traction operators $\mathcal{T}^{(r)}$ and $\mathcal{T}^{(p)}$ to the continuous solution u of the global problem. Now, the fulfillment of problem (4.7) for every subdomain $\Omega^{(r)}$, $1 < r < N_s$, and of the interface conditions (4.8) on the whole skeleton Γ_s is fully equivalent to the original, unpartitioned formulation of the mixed elliptic boundary value problem (2.34).

A variational formulation similar to (2.52) is obtained by regarding the first interface condition (4.8a) as a Dirichlet condition for the local subproblems:

Find $u^{(r)}$ with $u_\Gamma^{(r)} = g_D$ on $\Gamma_D^{(r)}$ and $u_\Gamma^{(r)} = u_\Gamma^{(p)}$ on all $\Gamma^{(rp)}$ such that

$$a^{(r)}(u^{(r)}, v^{(r)}) = \ell^{(r)}(v^{(r)}) \quad \text{in} \quad \Omega^{(r)} \tag{4.9}$$

for all $v^{(r)}$ with $v_\Gamma^{(r)} = 0$ on $\Gamma_D^{(r)}$ and $v_\Gamma^{(r)} = 0$ on $\Gamma^{(rp)}$, $p \in J^{(r)}$.

Here, $a^{(r)}$ and $\ell^{(r)}$ are the restrictions of the bilinear form a and the linear form ℓ of the corresponding global problem to the subdomain $\Omega^{(r)}$. Moreover, $v^{(r)}$ is the test function defined on the subdomain $\Omega^{(r)}$ and obeys the same regularity requirements as $u^{(r)}$.

Boundary integral equations for the partitioned problem are obtained via the representation formula for the r-th subdomain

$$u^{(r)}(\mathbf{x}) = \int_{\Gamma^{(r)}} u^*(\mathbf{x}, \mathbf{y}) \, q_\Gamma^{(r)}(\mathbf{y}) \, ds_\mathbf{y} - \int_{\Gamma^{(r)}} (\mathcal{T}_\mathbf{y}^{(r)} u^*)(\mathbf{x}, \mathbf{y}) u_\Gamma^{(r)}(\mathbf{y}) \, ds_\mathbf{y} + \int_{\Omega^{(r)}} u^*(\mathbf{x}, \mathbf{y}) f(\mathbf{y}) \, d\mathbf{y},$$

$$\tag{4.10}$$

which is derived in the same manner as the representation formula (2.56) by considering only $\Omega^{(r)}$. Taking the trace $\mathrm{Tr}^{(r)}$ of the above formula gives the boundary integral equation with side condition

$$\left[\left(\mathcal{C}^{(r)} + \mathcal{K}^{(r)}\right) u_\Gamma^{(r)}\right](\mathbf{x}) = \left(\mathcal{V}^{(r)} q_\Gamma^{(r)}\right)(\mathbf{x}) + \left(\mathcal{N}_0^{(r)} f\right)(\mathbf{x}) \qquad \mathbf{x} \in \Omega^{(r)} \tag{4.11}$$

$$u_\Gamma^{(r)}(\mathbf{x}) = u_\Gamma^{(p)}(\mathbf{x}) \qquad\qquad\qquad\qquad \mathbf{x} \in \Gamma^{(rp)}, \quad p \in J^{(r)}.$$

The integral operators of this equation are defined as in subsection 2.5.2 but carry now the subdomain superscript (r) in order to emphasize that the integrations are performed on $\Gamma^{(r)}$ and $\Omega^{(r)}$, respectively.

In the dynamic case, the situation is similar due to the assumption that the subdivision (4.1)

does not depend on time. Then the local problems have the form

$$
\left(\rho_o^{(r)} \frac{\partial^2}{\partial t^2} + \mathcal{L}^{(r)} \right) u^{(r)}(\mathbf{x},t) = f(\mathbf{x},t) \qquad (\mathbf{x},t) \in \Omega^{(r)} \times (0,\infty)
$$

$$
\begin{aligned}
u_\Gamma^{(r)}(\mathbf{y},t) &= g_D(\mathbf{y},t) & (\mathbf{y},t) &\in \Gamma_D^{(r)} \times (0,\infty) \\
q_\Gamma^{(r)}(\mathbf{y},t) &= g_N(\mathbf{y},t) & (\mathbf{y},t) &\in \Gamma_N^{(r)} \times (0,\infty) \\
u^{(r)}(\mathbf{x},0^+) &= u_0(\mathbf{x}) & \mathbf{x} &\in \Omega^{(r)} \\
\frac{\partial}{\partial t} u^{(r)}(\mathbf{x},0^+) &= u_1(\mathbf{x}) & \mathbf{x} &\in \Omega^{(r)}
\end{aligned}
\tag{4.12}
$$

and the interface conditions (4.8) have to hold for all $t \in (0,\infty)$. The formulation of the corresponding variational principle and boundary integral equations is straightforward and unnecessary to be shown.

Recall that the variational principle (2.52) can also be obtained by minimization of the potential $\Pi(u)$ as defined, for instance, in equation (2.44) for elasticity. In general, one can express this potential in terms of the bilinear form (2.48) and the external energy (2.50)

$$
\Pi(u) = \frac{1}{2} a(u,u) - \ell(u). \tag{4.13}
$$

By means of the interface condition (4.8), this potential can be decomposed and equipped with a side condition

$$
\Pi(u) = \sum_{r=1}^{N_s} \left(\frac{1}{2} a^{(r)}(u^{(r)},u^{(r)}) - \ell^{(r)}(u^{(r)}) \right) = \sum_{r=1}^{N_s} \Pi^{(r)}(u)
$$

$$
G(u) := \sum_{r=1}^{N_s} \sum_{p \in J^{(r)}} \left(u_\Gamma^{(r)} - u_\Gamma^{(p)} \right) = \sum_{r=1}^{N_s} \sum_{p \in J^{(r)}} G^{(rp)}(u) = 0. \tag{4.14}
$$

The variational principle (4.9) is obtained by minimizing $\Pi(u)$ among all admissible functions u which directly fulfill $G(u) = 0$. Minimization problems under side conditions are commonly tackled by Lagrange multiplier techniques [65]. Therefore, the augmented potential or Lagrangian (not to be confused with $\mathscr{L} = \mathscr{K} - \mathscr{U}$ in Hamilton's principle (2.42)) is introduced

$$
\mathscr{L}(u,\lambda) := \sum_{r=1}^{N_s} \left(\Pi^{(r)}(u) + \sum_{p \in J^{(r)}} \int_{\Gamma^{(rp)}} \lambda^{(rp)} G^{(rp)}(u) \, ds \right) \tag{4.15}
$$

with the *Lagrange multiplier* λ defined on the skeleton Γ_s. Obviously, $\lambda^{(rp)}$ is the restriction of λ to the interface $\Gamma^{(rp)}$.

Minimization of this Lagrangian functional yields the variational principle:

Find $(u^{(r)}, \lambda)$ with $u_\Gamma^{(r)} = g_D$ on $\Gamma_D^{(r)}$ such that

$$\sum_{r=1}^{N_s} \left(a^{(r)}(u^{(r)}, v^{(r)}) - \ell^{(r)}(v^{(r)}) + \sum_{p \in J^{(r)}} \int_{\Gamma^{(rp)}} \lambda^{(rp)} \left(v_\Gamma^{(r)} - v_\Gamma^{(r)} \right) \mathrm{d}s \right) = 0 \qquad (4.16a)$$

$$\sum_{r=1}^{N_s} \left(\sum_{p \in J^{(r)}} \int_{\Gamma^{(rp)}} \mu^{(rp)} \left(u_\Gamma^{(r)} - u_\Gamma^{(r)} \right) \mathrm{d}s \right) = 0 \qquad (4.16b)$$

for all admissible $(v^{(r)}, \mu)$ *with* $v_\Gamma^{(r)} = 0$ *on* $\Gamma_D^{(r)}$.

Another test function μ corresponding to λ has been introduced in this formulation. Again the extension to dynamic problems is omitted because the basic characteristics are identical and have to be valid through the course of time. A boundary integral formulation for this approach is not so straightforward. It is here preferred, to employ the notion of Dirichlet-to-Neumann maps for a method-independent formulation as introduced in the next section.

The main difference between formulations (4.9) and (4.16) is the incorporation of the interface conditions. Whereas in the first principle (4.9) the solution is sought in the space of functions fulfilling the interface condition, the second principle (4.16) only requires a weak fulfillment of the interface conditions, weighted by the Lagrange multiplier λ.

This difference becomes evident, when considering a finite element discretization of the respective variational principles. For simplicity, the number of subdomains shall be two, i.e., $N_s = 2$, and a pure Dirichlet problem is considered by setting $\Gamma_N = \emptyset$. The finite element discretization procedure explained in section 3.1.2 applied to equation (4.9) results in the system

$$\mathsf{A}^{(r)}\mathsf{u}^{(r)} = \mathsf{f}^{(r)} - \mathsf{r}^{(r)}, \quad r = 1, 2,$$

with some force residual $\mathsf{r}^{(r)}$ acting at the interfaces due to isolation of the r-th subdomain. Reordering the system according to degrees of freedom belonging to the interior of the subdomain and the interface between the domains, the set of equations is obtained

$$\begin{pmatrix} \mathsf{A}_{\mathrm{II}}^{(r)} & \mathsf{A}_{\mathrm{I\Gamma}}^{(r)} \\ \mathsf{A}_{\Gamma\mathrm{I}}^{(r)} & \mathsf{A}_{\Gamma\Gamma}^{(r)} \end{pmatrix} \begin{pmatrix} \mathsf{u}_{\mathrm{I}}^{(r)} \\ \mathsf{u}_{\Gamma}^{(r)} \end{pmatrix} = \begin{pmatrix} \mathsf{f}_{\mathrm{I}}^{(r)} \\ \mathsf{f}_{\Gamma}^{(r)} - \mathsf{r}_{\Gamma}^{(r)} \end{pmatrix}, \quad r = 1, 2 \qquad (4.17)$$

with the subscripts I and Γ referring to the interior and the interface of the domains, respectively. Obviously, $\mathsf{r} = (0, \mathsf{r}_\Gamma)^\top$ which has already been used in this expression. Note the symmetry of this expression due to the symmetric blocks $\mathsf{A}_{\mathrm{II}}^{(r)}$ and $\mathsf{A}_{\Gamma\Gamma}^{(r)}$ and $\mathsf{A}_{\Gamma\mathrm{I}}^{(r)}$ being the transposed of $\mathsf{A}_{\mathrm{I\Gamma}}^{(r)}$. The discrete interface conditions are then [114]

$$\left. \begin{aligned} u_\Gamma^{(1)} - u_\Gamma^{(2)} &= 0 \\ q_\Gamma^{(1)} + q_\Gamma^{(2)} &= 0 \end{aligned} \right\} \quad \rightarrow \quad \begin{cases} u_\Gamma^{(1)} = u_\Gamma^{(2)} =: u_\Gamma \\ \mathsf{r}^{(1)} + \mathsf{r}^{(2)} = \mathsf{f}_\Gamma - \mathsf{A}_{\Gamma\mathrm{I}}^{(1)}\mathsf{u}_\mathrm{I}^{(1)} + \mathsf{A}_{\Gamma\mathrm{I}}^{(2)}\mathsf{u}_\mathrm{I}^{(2)} + \mathsf{A}_{\Gamma\Gamma}u_\Gamma = 0. \end{cases}$$

In the last equation, the abbreviations $A_{\Gamma\Gamma} := A_{\Gamma\Gamma}^{(1)} + A_{\Gamma\Gamma}^{(2)}$ and $f_\Gamma := f_\Gamma^{(1)} + f_\Gamma^{(2)}$ have been used. Altogether, one gets the global system of equations

$$
\begin{pmatrix}
A_{II}^{(1)} & 0 & A_{I\Gamma}^{(1)} \\
0 & A_{II}^{(2)} & A_{I\Gamma}^{(2)} \\
A_{\Gamma I}^{(1)} & A_{\Gamma I}^{(2)} & A_{\Gamma\Gamma}
\end{pmatrix}
\begin{pmatrix}
u_I^{(1)} \\
u_I^{(2)} \\
u_\Gamma
\end{pmatrix}
=
\begin{pmatrix}
f_I^{(1)} \\
f_I^{(2)} \\
f_\Gamma
\end{pmatrix}.
\tag{4.18}
$$

Furthermore, the discretization process of equations (4.16) requires an approximation of the Lagrange multiplier field on the skeleton

$$
\lambda_h(\mathbf{y}) = \sum_{j=1}^{N_\lambda} \lambda_j \psi_j(\mathbf{y}) \quad \mathbf{y} \in \Gamma_s.
\tag{4.19}
$$

As usual, the test function μ is taken from the space spanned by the trial functions of λ_h, i.e., $\mu \in \mathrm{span}\{\psi_j\}$. Then the final system of equations has the form

$$
\begin{pmatrix}
A^{(1)} & 0 & C^{(1)^\top} \\
0 & A^{(2)} & C^{(2)^\top} \\
C^{(1)} & C^{(2)} & 0
\end{pmatrix}
\begin{pmatrix}
u^{(1)} \\
u^{(2)} \\
\lambda
\end{pmatrix}
=
\begin{pmatrix}
f^{(1)} \\
f^{(2)} \\
0
\end{pmatrix}.
\tag{4.20}
$$

In this equation, λ denotes the collection of the degrees of freedom due to the approximation (4.19), $\lambda[j] = \lambda_j$, and the matrices $C^{(r)}$ have components

$$
C^{(r)}[j,i] = \pm \int_{\Gamma_s} (\mathrm{Tr}^{(r)} \varphi_i^{(r)}) \psi_j \, ds.
\tag{4.21}
$$

The sign in this expression depends on a predefined numbering of the subdomains. For instance, at the interface $\Gamma^{(rp)}$ the signs are such that for $r < p$ the entries $C^{(r)}[j,i]$ are negative and the entries $C^{(p)}[j,i]$ are positive and vice versa if $r > p$. These matrices $C^{(r)}$ are henceforth referred to as *connectivity matrices* and considered in more detail in section 4.4.

4.2 Dirichlet-to-Neumann Maps

The variational framework of the previous section is well-suited for finite element discretizations but is not sufficiently abstract to formulate a partitioned problem without specification of the discretization method. Therefore, *Dirichlet-to-Neumann* maps are introduced in this section. These map the Dirichlet data onto the Neumann data which obey the regarded boundary value problem. At first, these maps are presented in a continuous setting for elliptic boundary value problems and then their finite and boundary element discretizations are given. Finally, discrete Dirichlet-to-Neumann maps are proposed for the partitioned solution of hyperbolic boundary value problems.

4.2.1 Elliptic boundary value problems

Considering the boundary integral operators from section 2.5.2, i.e.,

$$\mathcal{V}q_\Gamma = (\mathcal{C} + \mathcal{K})u_\Gamma - \mathcal{N}_0 f,$$

the Dirichlet-to-Neumann map is easily established by

$$q_\Gamma = \underbrace{\mathcal{V}^{-1}(\mathcal{C} + \mathcal{K})}_{\mathcal{S}} u_\Gamma - \underbrace{\mathcal{V}^{-1}\mathcal{N}_0 f}_{\mathcal{N}f}. \tag{4.22}$$

$\mathcal{S}$ is the so-called Steklov-Poincaré operator and $\mathcal{N}f$ another Newton potential [106]. By means of these operators, the elliptic boundary value problem (2.34) is replaced by the statement

$$\begin{aligned}
(\mathcal{S}u_\Gamma)(\mathbf{y}) &= q_\Gamma(\mathbf{y}) + (\mathcal{N}f)(\mathbf{y}) &\quad \mathbf{y} \in \Gamma \\
u_\Gamma(\mathbf{y}) &= g_D(\mathbf{y}) &\quad \mathbf{y} \in \Gamma_D \\
q_\Gamma(\mathbf{y}) &= g_N(\mathbf{y}) &\quad \mathbf{y} \in \Gamma_N.
\end{aligned} \tag{4.23}$$

This is a totally equivalent formulation which is expressed only in terms of boundary variables. In other words, the function u, which fulfills the mixed boundary value problem (2.34), also fulfills the problem statement (4.23) and vice versa. A variational principle is easily established by means of integration by parts [65]

$$\begin{aligned}
0 &= a(u, v) - \ell(v) \\
&= \int_\Omega (\mathcal{L}u - f)v \, d\mathbf{x} + \int_\Gamma q_\Gamma v_\Gamma \, ds - \int_{\Gamma_N} g_N v_\Gamma \, ds \\
&= \int_\Gamma q_\Gamma v_\Gamma \, ds - \int_{\Gamma_N} g_N v_\Gamma \, ds.
\end{aligned} \tag{4.24}$$

The replacement of q_Γ in this expression by the Dirichlet-to-Neumann map (4.22) then directly gives the variational principle [106]:

Find u_Γ with $u_\Gamma = g_D$ on Γ_D such that

$$\int_\Gamma (\mathcal{S}u_\Gamma)v \, ds = \int_{\Gamma_N} g_N v \, ds + \int_\Gamma (\mathcal{N}f)v \, ds \tag{4.25}$$

for all v with $v = 0$ on Γ_D.

Here, the test function v is only defined on the boundary Γ such that the subscript for the trace can be omitted.

In view of the partitioned problem (4.7) with the interface conditions (4.8), the first variational problem is to find the solution among those functions which directly fulfill the continuity condition across the interfaces:

Find $u_\Gamma^{(r)}$ with $u_\Gamma^{(r)} = g_D$ on $\Gamma_D^{(r)}$ and $u_\Gamma^{(r)} = u_\Gamma^{(p)}$ on $\Gamma^{(rp)}$ such that

$$\int\limits_{\Gamma^{(r)}} (\mathcal{S}^{(r)} u_\Gamma^{(r)}) v^{(r)} \, \mathrm{d}s = \int\limits_{\Gamma_N^{(r)}} g_N v^{(r)} \, \mathrm{d}s + \int\limits_{\Gamma^{(r)}} (\mathcal{N}^{(r)} f) v^{(r)} \, \mathrm{d}s \tag{4.26}$$

for all $v^{(r)}$ with $v^{(r)} = 0$ on $\Gamma_D^{(r)}$ and $\Gamma^{(rp)}$, $p \in J^{(r)}$.

As before, the introduction of Lagrange multipliers facilitates the incorporation of the interface conditions in a weak sense and allows for the variational principle:

Find $(u_\Gamma^{(r)}, \lambda)$ with $u_\Gamma^{(r)} = g_D$ on $\Gamma_D^{(r)}$ such that

$$\int\limits_{\Gamma^{(r)}} (\mathcal{S}^{(r)} u_\Gamma^{(r)}) v^{(r)} \, \mathrm{d}s$$

$$+ \sum_{p \in J^{(r)}} \int\limits_{\Gamma^{(rp)}} \lambda^{(rp)} \left(v^{(r)} - v^{(p)} \right) \mathrm{d}s \quad = \int\limits_{\Gamma_N^{(r)}} g_N v^{(r)} \, \mathrm{d}s + \int\limits_{\Gamma^{(r)}} (\mathcal{N}^{(r)} f) v^{(r)} \, \mathrm{d}s \tag{4.27a}$$

$$\sum_{p \in J^{(r)}} \int\limits_{\Gamma^{(rp)}} \mu^{(rp)} \left(u^{(r)} - u^{(p)} \right) \mathrm{d}s \quad = 0 \tag{4.27b}$$

for all $(v^{(r)}, \mu)$ with $v^{(r)} = 0$ on $\Gamma_D^{(r)}$.

Physically speaking, the first equation (4.27a) describes the equilibrium of the r-th subdomain. Hence, the boundary tractions (or fluxes) due to internal strains and the contributions from the neighboring domains have to be equal to the given Neumann datum g_N and body forces f. The second equation (4.27b) expresses the continuity of the unknown u across the interfaces in a weighted form.

It remains now to show discrete representations of the operator $\mathcal{S}$ in order to formulate a numerical approximation scheme for the partitioned problem. Such discretizations are given in the next subsection.

4.2.2 Finite and boundary element realizations for static problems

The Steklov-Poincaré operator $\mathcal{S}$ as defined in equation (4.22) itself does not allow for a discretization. But its action can be mimicked on the discrete level by considering the finite or boundary element systems of equations.

At first, the finite element discretization of a full domain is regarded where the degrees of freedom are ordered with respect to its location in the interior (subscript I) of the domain or on the boundary (subscript Γ)

$$\begin{pmatrix} A_{II} & A_{I\Gamma} \\ A_{\Gamma I} & A_{\Gamma\Gamma} \end{pmatrix} \begin{pmatrix} u_I \\ u_\Gamma \end{pmatrix} = \begin{pmatrix} f_I \\ f_\Gamma \end{pmatrix}. \tag{4.28}$$

Note that, despite the identical notation, there is a difference between this expression and equation (4.17) in the sense that here the subscript Γ refers to $\Gamma \setminus \Gamma_D$ and not only to the interface to the neighboring domain. Condensation of the internal unknowns of this system yields the equation

$$\underbrace{\left(A_{\Gamma\Gamma} - A_{\Gamma I} A_{II}^{-1} A_{I\Gamma}\right)}_{S_{FE}} u_\Gamma = \underbrace{f_\Gamma - A_{\Gamma I} A_{II}^{-1} f_I}_{g_{FE}} . \tag{4.29}$$

The matrix S_{FE} is a finite element realization of the operator $\mathcal{S}$. Since A_{II} and $A_{\Gamma\Gamma}$ are symmetric matrices and $A_{\Gamma I}$ is the transposed of $A_{I\Gamma}$, this expression is symmetric. Moreover, $\mathcal{S}$ is a positive operator [107] and this finite element representation thus results in a positive definite matrix S_{FE} [106]. If u_Γ is known, the interior degrees of freedom are computable by means of the system

$$A_{II} u_I = f_I - A_{I\Gamma} u_\Gamma . \tag{4.30}$$

In case of a direct computation of S_{FE} a factorization of A_{II} has already been performed so that the solution of system (4.30) only requires substitution steps and a matrix-vector product.

Using the boundary element discretization introduced in subsection 3.1.3, the system of equations for mixed boundary value problems is obtained,

$$\begin{pmatrix} V & -\tilde{K} \\ B & \end{pmatrix} \begin{pmatrix} q \\ u_\Gamma \end{pmatrix} = \begin{pmatrix} f_D \\ f_N \end{pmatrix} . \tag{4.31}$$

Applying the solution procedure for this system, which has been described in section 3.4, gives as an intermediate result the system

$$\underbrace{B V^{-1} \tilde{K}}_{S_{BE}} u_\Gamma = \underbrace{f_N - B V^{-1} f_D}_{g_{BE}} . \tag{4.32}$$

This representation of the Steklov-Poincaré operator $\mathcal{S}$ is nonsymmetric although the operator itself is self-adjoint [106]. The loss of symmetry is introduced by the employed representation (4.22) instead of (2.77) and due to the collocation method. By means of a Galerkin projection, a symmetric representation of $\mathcal{S}$ is possible even when only the first integral equation is used as shown by Steinbach [105]. Once the unknowns u_Γ are computed, the equation

$$V q = \tilde{K} u_\Gamma + f_D \tag{4.33}$$

delivers the solution of the unknown coefficients q. Again, in a direct solution procedure the factorization of V has been already carried out in the computation of S_{BE}.

Comparing equations (4.29) and (4.32), it becomes obvious that the framework of discrete Dirichlet-to-Neumann maps provides a setting in which the approximate solution of elliptic boundary value problems can be represented without specifying the underlying discretization scheme.

The two-domain Dirichlet problem at the end of section 4.1 is now considered again. The different variational methods (4.26) and (4.27) are represented by means of the discretized Steklov-Poincaré operators introduced above. The computation of the matrices $S^{(r)}$ is thus carried out individually for each subdomain $r = 1, 2$. Explicit requirement of continuity across the interfaces as in the variational principle (4.26) gives the system

$$S u_\Gamma = g \tag{4.34}$$

with the abbreviations $S = S^{(1)} + S^{(2)}$, $u_\Gamma = u_\Gamma^{(1)} = u_\Gamma^{(2)}$ and $g = g^{(1)} + g^{(2)}$. The Lagrange multiplier method (4.27), on the other hand, leads to the system

$$\begin{pmatrix} S^{(1)} & 0 & C^{(1)\top} \\ 0 & S^{(2)} & C^{(2)\top} \\ C^{(1)} & C^{(2)} & 0 \end{pmatrix} \begin{pmatrix} u^{(1)} \\ u^{(2)} \\ \lambda \end{pmatrix} = \begin{pmatrix} g^{(1)} \\ g^{(2)} \\ 0 \end{pmatrix}. \tag{4.35}$$

Here, the matrices $C^{(r)}$ have the coefficients as defined in equation (4.21) for the finite element discretization. In general, these matrices have the form

$$C^{(r)}[j, i] = \pm \int_{\Gamma_s} \varphi_i^{(r)} \psi_j \, ds. \tag{4.36}$$

Depending on the chosen discretization scheme, $\varphi^{(r)}$ refers to the boundary trace of the finite element trial functions for the approximation of u in Ω or to the boundary element trial functions in the approximation of u_Γ on the boundary Γ.

The remarkable feature of the systems (4.34) and (4.35) is that the matrix $S^{(r)}$ represents either a finite element discretization $S_{\mathrm{FE}}^{(r)}$ or a boundary element discretization $S_{\mathrm{BE}}^{(r)}$ of the Steklov-Poincaré operator $\mathcal{S}$. Therefore, the solution of the partitioned problem can be formulated without specification of the employed discretization scheme.

4.2.3 Dynamic problems

So far, in this section only static boundary value problems have been considered. For such problems, the underlying theory is significantly more developed (cf., e.g., Steinbach [106] and Toselli and Widlund [114]) than in the dynamic case. To the author's best knowledge, the Steklov-Poincaré operators involved in Dirichlet-to-Neumann maps have not yet been mathematically analyzed for the time-domain solution of hyperbolic initial boundary value problems. Hence, in the context of these problems, only the discrete setting is studied. Recall the system of equations resulting from the Newmark method applied to the semi-discrete system of equations of the finite element discretization (3.23). For a single domain Ω at time step n it has the form

$$\begin{pmatrix} \tilde{A}_{\mathrm{II}} & \tilde{A}_{\mathrm{I\Gamma}} \\ \tilde{A}_{\mathrm{\Gamma I}} & \tilde{A}_{\mathrm{\Gamma\Gamma}} \end{pmatrix} \begin{pmatrix} u_{\mathrm{I},n} \\ u_{\Gamma,n} \end{pmatrix} = \begin{pmatrix} \tilde{f}_{\mathrm{I},n} \\ \tilde{f}_{\Gamma,n} \end{pmatrix}, \tag{4.37}$$

where the ordering according to interior and boundary degrees of freedom has already been carried out. Due to the similarity of the structure of the static case (4.28) and this equation (4.37), the formulation of a discrete Dirichlet-to-Neumann map is easily established by computing the Schur complement of the system matrix. Therefore,

$$\tilde{S}_{FE}u_{\Gamma,n} = \tilde{g}_{FE,n} \tag{4.38}$$

is the resulting equation with the abbreviations

$$\tilde{S}_{FE} := \tilde{A}_{\Gamma\Gamma} - \tilde{A}_{\Gamma I}\tilde{A}_{II}^{-1}\tilde{A}_{I\Gamma} \quad \text{and} \quad \tilde{g}_{FE,n} := \tilde{f}_{\Gamma,n} - \tilde{A}_{\Gamma I}\tilde{A}_{II}^{-1}\tilde{f}_{\Gamma,n}. \tag{4.39}$$

Equation (4.38) can be regarded as a discrete Dirichlet-to-Neumann map for the dynamic problem. Since the Schur complement of a symmetric positive definite matrix is itself symmetric positive definite [114], so is $\tilde{S}_{FE}$.

The same procedure is applied to the boundary element discretization of dynamic systems. There, the system of equations for the n-th time step has the form

$$\begin{pmatrix} V_0 & -\tilde{K}_0 \\ B & \end{pmatrix} \begin{pmatrix} q_n \\ u_{\Gamma,n} \end{pmatrix} = \begin{pmatrix} f_D(n\Delta t) \\ f_N(n\Delta t) \end{pmatrix} - \sum_{j=1}^{n} \begin{pmatrix} V_j & K_j \end{pmatrix} \begin{pmatrix} q_{n-j} \\ u_{\Gamma,n-j} \end{pmatrix} =: \begin{pmatrix} h_{D,n} \\ h_{N,n} \end{pmatrix} \tag{4.40}$$

with the notation of equation (3.72). The column matrices $h_{D,n}$ and $h_{N,n}$ have been introduced for a shorter notation and to stress the fact that the above system has merely a constant left hand side matrix with changing right hand sides and thus a similar structure as in the static case. The computation of the Schur complement yields the system

$$\tilde{S}_{BE}u_{\Gamma,n} = \tilde{g}_{BE,n} \tag{4.41}$$

and the components of it are the nonsymmetric matrix and the vector

$$\tilde{S}_{BE} := BV_0^{-1}\tilde{K}_0 \quad \text{and} \quad \tilde{g}_{BE,n} := h_{N,n} - BV_0^{-1}h_{D,n}, \tag{4.42}$$

respectively. With system (4.41) the dynamic Dirichlet-to-Neumann map is established for a boundary element discretization.

The systems of equations (4.38) and (4.41) provide exactly what is needed to extend the methodology for partitioned static problems of section 4.2.2 to dynamic problems. Although a continuous formulation does not seem to be available, the similarity of discrete static and dynamic systems suggests the discrete formulation of dynamic Dirichlet-to-Neumann maps.

4.3 The FETI-framework

In the previous section, a variational framework for the method-independent formulation of a partitioned boundary value problem by means of the Steklov-Poincaré operator has

been presented. Moreover, it has been shown that on the discrete level the expressions can be easily transferred to the treatment of dynamic problems. The following part is dedicated to the discrete systems of equations and their solution procedure.

So far, two different approaches for the incorporation of the interface condition (4.8a) have been presented. The first was the direct fulfillment of this condition and led to the variational principles (4.9) or (4.25), using the original boundary value problem or the Dirichlet-to-Neumann map, respectively. This approach is usually referred to as a *substructuring method* (cf., for instance, Przemieniecki [87]) and basically consists of assembling stiffnesses as it can be seen from the systems of equations (4.18) and (4.34) for the two domain example. The alternative variational expressions (4.16) and (4.27) have become popular due to the advent of the so-called FETI (finite element tearing and interconnecting) method as introduced by Farhat and Roux [28]. This method provides a higher parallelism than the classical sub-structuring approach and come up with very robust and efficient iterative solution procedures. The literature on FETI is extensive, but the basic method is presented in the publications of Farhat and Roux [28, 29] and convergence proofs are given by Mandel and Tezaur [69]. Many other good introductions are available but shall not be listed here.

The idea of using the FETI-framework for boundary element discretizations goes back to Langer and Steinbach, who at first analyzed this methodology for a pure boundary element solver, thus coining the term BETI [61] (*boundary* element tearing and interconnecting). Later, the same authors combined both methodologies to so-called coupled BETI/FETI methods [62, 63].

One aim of this work is a relaxation of the continuity condition (4.8a) established by Lagrange multipliers. For this reason, only the methods arising from the saddle point problem (4.27) are considered and, therefore, a short introduction to the FETI algorithm is given at first. Although its original version is expressed in terms of finite element stiffness matrices [28], the starting point is here the discretized Steklov-Poincaré operator $S^{(r)}$ in either its finite element (4.29) or boundary element version (4.32). At the subdomain level, one has the equations

$$S^{(r)}u_\Gamma^{(r)} = g^{(r)} - r_\Gamma^{(r)}, \qquad (4.43)$$

for $r = 1, \ldots, N_s$, N_s being the number of subdomains, $g^{(r)}$ the boundary forces due to given force terms and boundary conditions. The vector $r_\Gamma^{(r)}$ is the residual force due to isolation of $\Omega^{(r)}$. In fact, the introduced field of Lagrange multipliers λ is physically equivalent with the interface tractions or fluxes and, therefore, by means of the connectivity matrices (4.36) the residual in the interface equilibrium is expressed as

$$r_\Gamma^{(r)} = C^{(r)^\top}\lambda. \qquad (4.44)$$

This relation has already been employed in equations (4.20) and (4.35) and stems directly from the variational principles involving the Lagrange multiplier field (see, again, equations (4.16) and (4.27)). Hence, the discrete equilibrium equation for the *r*-th subdomain

is the Neumann problem

$$S^{(r)} u_\Gamma^{(r)} = g^{(r)} - C^{(r)^\top} \lambda. \tag{4.45}$$

Assume, for the time being, that this expression is solvable for the interface unknowns, i.e.,

$$u_\Gamma^{(r)} = S^{(r)^{-1}} \left(g^{(r)} - C^{(r)^\top} \lambda \right) \tag{4.46}$$

is a valid. The continuity equation (4.8a), on the other hand, leads to the system of equations

$$\sum_{r=1}^{N_s} C^{(r)} u_\Gamma^{(r)} = 0. \tag{4.47}$$

In the FETI context, equation (4.45) is obtained after the *tearing* of the subdomains, whereas equation (4.47) represents the *interconnecting* step. Inserting the local interface unknowns (4.46) into the continuity expression (4.47), gives a system of equations for the coefficients of the approximation of the Lagrange multiplier field

$$F\lambda = d, \tag{4.48}$$

where the following abbreviations have been introduced

$$
\begin{aligned}
F &:= \sum_{r=1}^{N_s} C^{(r)} S^{(r)^{-1}} C^{(r)^\top}, &\quad F &\in \mathbb{R}^{N_\lambda \times N_\lambda} \\
d &:= \sum_{r=1}^{N_s} C^{(r)} S^{(r)^{-1}} g^{(r)}, &\quad d &\in \mathbb{R}^{N_\lambda}.
\end{aligned}
\tag{4.49}
$$

Recall that N_λ is the number of coefficients in the approximation (4.19). Note that the matrix F is an assembly of flexibility matrices, contrary to the classical substructuring where stiffnesses are added [28].

Once system (4.48) is solved for the unknown λ, the local interface degrees of freedom are computable by means of equation (4.46) and these, in turn, determine the interior degrees of freedom $u_I^{(r)}$, see equation (4.30), or the secondary unknown $q^{(r)}$, see equation (4.33), in case of finite or boundary element systems, respectively.

In order to illustrate this procedure, consider again the two-domain example. Now subdomain 1 is handled by a finite element and subdomain 2 by a boundary element discretization scheme. Then, the global system of equations is of the form

$$
\begin{pmatrix}
A_{II}^{(1)} & A_{I\Gamma}^{(1)} & & & \\
A_{\Gamma I}^{(1)} & A_{\Gamma\Gamma}^{(1)} & & & C^{(1)^\top} \\
& & V^{(2)} & -\tilde{K}^{(2)} & \\
& & B^{(2)} & & C^{(2)^\top} \\
& C^{(1)} & & C^{(2)} &
\end{pmatrix}
\begin{pmatrix}
u_I^{(1)} \\
u_\Gamma^{(1)} \\
q^{(2)} \\
u_\Gamma^{(2)} \\
\lambda
\end{pmatrix}
=
\begin{pmatrix}
f_I^{(1)} \\
f_\Gamma^{(1)} \\
f_D^{(2)} \\
f_N^{(2)} \\
0
\end{pmatrix}.
$$

The first step consists in condensation of the internal unknowns $u_I^{(1)}$ and secondary unknowns $q^{(2)}$ by computing the Schur complements of the subblocks for the first and the second subdomain as shown in equations (4.29) and (4.32), respectively. The reduced system is then

$$
\begin{pmatrix} S_{FE}^{(1)} & & C^{(1)^\top} \\ & S_{BE}^{(2)} & C^{(2)^\top} \\ C^{(1)} & C^{(2)} & \end{pmatrix} \begin{pmatrix} u_\Gamma^{(1)} \\ u_\Gamma^{(2)} \\ \lambda \end{pmatrix} = \begin{pmatrix} g_{FE}^{(1)} \\ g_{BE}^{(2)} \\ 0 \end{pmatrix}.
$$

If the reduction process is continued by elimination of the local interface unknowns $u_\Gamma^{(1)}$ and $u_\Gamma^{(2)}$, the system (4.48) is finally obtained.

In case of a dynamic problem, the situation is very similar. The final system of equations reads

$$
\tilde{F}\lambda_n = \tilde{d}_n \tag{4.50}
$$

for the *n*-th time step and now the left and right hand sides are of the type

$$
\tilde{F} := \sum_{r=1}^{N_s} C^{(r)} \tilde{S}^{-1} C^{(r)^\top}
$$

$$
\tilde{d}_n := \sum_{r=1}^{N_s} C^{(r)} \tilde{S}^{-1} \tilde{g}_n^{(r)}. \tag{4.51}
$$

Hence, at each time step the solution procedure is exactly the same as in the static case. If the coefficients λ_n are known, the local unknowns $u_{\Gamma,}^{(r)}$ can be computed and, finally, the remaining unknown degrees of freedom, $u_{I,n}^{(r)}$ or $q_n^{(r)}$.

4.3.1 Floating subdomains

In the previous outline of the FETI-framework, it has been assumed that the local problems (4.45) are uniquely solvable or, in other words, the inverse of $S^{(r)}$ exists. In general, this is not the case. Consider for instance the solution of the Laplace equation on a sub-domain which, due to the partitioning, does not have any share of the Dirichlet boundary Γ_D of the original problem. Then any $u_{\mathcal{R}}^{(r)} = c\mathbf{1}$, where $c \in \mathbb{R}$ and $\mathbf{1}$ is a vector composed of ones only, leads to

$$
S^{(r)} u_{\mathcal{R}}^{(r)} = 0. \tag{4.52}
$$

The vector $u_{\mathcal{R}}^{(r)}$ is a member of the space $\mathcal{R}$, as defined in equation (2.33a) containing the nontrivial solutions of the homogeneous Neumann problem. Because of this, the matrix $S^{(r)}$ has in the considered case a nontrivial kernel and $\mathcal{R}$ is its null space. $u_{\mathcal{R}}^{(r)}$ is the eigenvector to its zero eigenvalue and a solution to the problem (4.45) can be specified only up to a scalar times a constant vector.

In the case of elastostatic problems, the situation is more involved. Consider the spaces $\mathcal{R}$ for two- and three-dimensional problems, equations (2.33b) and (2.33c), respectively, which contain translations and rotations, i.e., rigid body modes. Any $u_{\mathcal{R}}^{(r)}$ comprising a linear combination of the basis vectors of $\mathcal{R}$ fulfills equation (4.52). Such a subdomain is referred to as a *floating* subdomain.

In summary, two problems are posed by a floating subdomain. First, the inverse of $S^{(r)}$ can not be computed and, second, the solution of equation (4.45) is not unique. Moreover, in elastostatics, it is not straightforward to see if a subdomain has such rigid body modes. The techniques presented below are mainly taken from the article of Farhat and Geradin [26] who have thoroughly analyzed the problem of floating subdomains and provide a robust scheme which is used in this work.

In order to keep notation simple, the task can be described as follows. The space of solutions to the equation

$$Ax = b \tag{4.53}$$

is sought, where A is a square matrix of size $N \times N$ and of rank $N - k$. Obviously, b has to be in the range or image space of A, which is not trivially fulfilled for a singular A. Any vector x that fulfills this equation is of the form

$$x = A^{+}b + Nc, \tag{4.54}$$

where $A^{+} \in \mathbb{R}^{N \times N}$ is a generalized inverse of A, $N \in \mathbb{R}^{N \times k}$ contains a basis of the null space of A and $c \in \mathbb{R}^{k}$ is a vector of arbitrary constants. It suffices here to request a generalized inverse A^{+}, which fulfills [28]

$$AA^{+}A = A \tag{4.55}$$

and is not unique, unless A has full rank. A concise overview of generalized inverses and their construction can be found in the book of Ben-Israel and Greville [8]. Assume now that the matrix A is already ordered in the form

$$A = \begin{pmatrix} A_{11} & A_{12} \\ A_{21} & A_{22} \end{pmatrix}, \tag{4.56}$$

where $A_{11} \in \mathbb{R}^{(N-k) \times (N-k)}$ has full rank $N - k$ and is thus invertible. Moreover, $N - k$ is the rank of A and its subblock A_{11} if it holds [8]

$$A_{22} = A_{21}A_{11}^{-1}A_{12}. \tag{4.57}$$

One possible generalized inverse is easily given by

$$A^{+} = \begin{pmatrix} A_{11}^{-1} & 0 \\ 0 & 0 \end{pmatrix}, \tag{4.58}$$

which obviously obeys the criterion (4.55) by the help of property (4.57). Furthermore, the partitioning (4.56) directly gives an expression for the sought null space of A

$$N = \begin{pmatrix} -A_{11}^{-1}A_{12} \\ I \end{pmatrix}, \tag{4.59}$$

where I is the $k \times k$-identity matrix. $\mathsf{AN} = 0$ is easily verified, again by means of the property (4.57).

It remains to determine the value k and construct an efficient method to compute the generalized inverse A^+ and the null space N. The first approach in the original FETI-publication [28] by Farhat and Roux was a truncated factorization of the local stiffness matrix. Performing a Cholesky or an LU-decomposition of the singular matrix A with total pivoting, at a certain point a zero pivot appears. In theory, this happens at the $(N-k)$-th step. If an LU-factorization by means of Gaussian elimination [36] is carried out in-place (as, for instance, in the corresponding LAPACK routine [2]) and stopped when this zero pivot is encountered, the matrix will have the form

$$\begin{pmatrix} (\mathsf{L}_{11} \backslash \mathsf{U}_{11}) & \mathsf{L}_{11}^{-1} \mathsf{A}_{12} \\ \mathsf{A}_{21} & \mathsf{A}_{22} \end{pmatrix}$$

where $\mathsf{L}_{11} \mathsf{U}_{11} = A_{11}$ is the factorization of the non-singular matrix block A_{11} and the triangular factors are stored in-place. Moreover, a backward substitution applied on the $k \times (N-k)$-block $\mathsf{L}_{11}^{-1} \mathsf{A}_{12}$ yields the component $\mathsf{A}_{11}^{-1} \mathsf{A}_{12}$ of the null space of A. Reversing the sign of this block and replacing A_{22} by the $k \times k$-identity matrix, gives finally the desired results: a factorization of the non-singular part of A and a basis for its null space.

Unfortunately, this procedure is not robust as shown by Farhat and Geradin [26]. Using a floating-point arithmetic, one cannot generally decide whether a pivot is simply small due to a bad conditioning of the problem or effectively zero. Hence, it is mandatory to determine the number k, i.e., the rank decay, a priori in a reliable fashion applicable to all possible constellations. Obviously, one has $k = 1$ for potential problems on subdomains without connection to the Dirichlet boundary and $k = 3$ (6) for elastostatic problems in two (three) spatial dimensions on such totally disconnected subdomains. The problematic cases are thus elastostatic problems on domains, which have some part of the Dirichlet boundary, because then it is not straightforward to decide, how many rigid body modes are possible. The key feature of the method of Farhat and Geradin [26] is to determine the value of k by considering the given Dirichlet conditions for a subdomain. A brief description of the method is given here, whereas it is referred to the original publication [26] for a complete outline.

The infinitesimal rigid body movement of a body with respect to the origin of the coordinate system is described by [35]

$$\mathbf{v}(\mathbf{x}) = \mathbf{v}_0 + \boldsymbol{\omega} \times \mathbf{x}. \tag{4.60}$$

Here, $\mathbf{v}_0$ is the translation of the origin and $\boldsymbol{\omega}$ the vector describing the infinitesimal rotation of the considered point $\mathbf{x}$ around the origin. On the discretized geometry, the j-th vertex $\mathbf{x}_j$ undergoes a movement expressed by

$$\mathsf{v}_j = \mathsf{R}_j \boldsymbol{\alpha}_j. \tag{4.61}$$

Denoting the number of possible rigid body modes by n_r ($n_r = 3$ in two and $n_r = 6$ in three space dimensions), the matrix R_j is of size $d \times n_r$ and α_j a vector of length n_r. It has the entries

$$R_j^{2D} = \begin{pmatrix} 1 & 0 & x_{j2} \\ 0 & 1 & -x_{j1} \end{pmatrix} \quad \text{and} \quad R_j^{3D} = \begin{pmatrix} 1 & 0 & 0 & 0 & x_{j3} & -x_{j2} \\ 0 & 1 & 0 & -x_{j3} & 0 & x_{j1} \\ 0 & 0 & 1 & x_{j2} & -x_{j1} & 0 \end{pmatrix} \quad (4.62)$$

for two and three space dimensions, respectively, with x_{ji} denoting the i-th component of the vertex $\mathbf{x}_j$. The first step of the algorithm is to collect those rows of R_j for all vertices $\mathbf{x}_j$, which correspond to a prescribed Dirichlet datum and gather them in a matrix $Z \in \mathbb{R}^{n_d \times n_r}$. The number of coefficients prescribed by a Dirichlet datum has been denoted by n_d. The key point of this method is that the rank decay of Z equals the desired rank decay k of the considered singular matrix A. The rank of Z can be easily determined by a SVD (singular value decomposition, see Golub and van Loan [36]). Note that the application of an SVD to the original matrix A would also yield the rank decay k and its generalized inverse A^+. But the problem remains to decide which singular value of A numerically represents zero. The matrix A represents in the given case the discretized Steklov-Poincaré operator of a certain subdomain and is full of error sources, whereas the entries of the matrix Z are exact to machine precision. Therefore, one can expect a significant gap between singular values larger than zero and the ones numerically representing zero. Additionally, the cost of the SVD, which is a computationally expensive operation for the $N \times N$-matrix A, is negligible for the matrix Z since it is cubic in n_r and only linear in n_d [36].

The rank of Z is $n_r - k$ and once this number k is known, the factorization process described above can be applied and truncated after $N - k$ steps, a number now known a priori. In summary, the algorithm contains the following steps:

- generate Z from the given Dirichlet data and compute its rank decay k,

- perform a LU-factorization with total pivoting (or a Cholesky factorization for a symmetric positive definite A) on the matrix $A \in \mathbb{R}^{N \times N}$ which stops after $N - k$ steps,

- the upper left $(N - k) \times (N - k)$-block now contains the factors L_{11} and U_{11} of the non-singular block A_{11},

- the upper right block contains $L_{11}^{-1} A_{12}$, which after a backward substitution with U_{11} gives the component $A_{11}^{-1} A_{12}$ of the null space,

- reversing the sign of $A_{11}^{-1} A_{12}$ and replacing the lower right block by the $k \times k$-identity matrix finally lets the right k columns of the original matrix contain the basis vectors of the null space.

Going through these steps, a factorization of A, which mimics the action of its generalized inverse A^+, and a basis of the null space are obtained such that the solution space (4.54) of equation (4.53) can be expressed.

Remark 4.1. In order to avoid the computation of the null space, a so-called *all-floating* method is proposed by Of [74], in which every subdomain is considered as totally disconnected such that always $k = 3$ (6) for two (three) space dimensions holds. Another advantage of this approach is that Dirichlet boundary conditions can be considered in a general form and, therefore, a remedy to the problem mentioned in remark 3.1 is provided. See also the work of Park and Felippa [80], who describe different variational formulations, where the possibility of disconnecting the Dirichlet boundaries is considered. ◇

Returning now to the original problem, i.e., the expression of the local interface unknowns $u_\Gamma^{(r)}$ of the *r*-th subdomain, one can state that

$$u_\Gamma^{(r)} = S^{(r)^+} \left(g^{(r)} - C^{(r)^\top} \lambda \right) + N^{(r)} \alpha^{(r)}. \qquad (4.63)$$

Now, $S^{(r)^+}$ is the generalized inverse of $S^{(r)}$ and coincides with its standard inverse if it exists. $N^{(r)}$ is the corresponding null space which vanishes if $k^{(r)} = 0$, i.e., the considered subdomain $\Omega^{(r)}$ is not floating. The $k^{(r)}$ coefficients of the vector $\alpha^{(r)}$ determine the contribution of each rigid body mode contained in $N^{(r)}$ and are referred to as rigid body mode amplitudes. Due to equation (4.63), another $N_\alpha = \sum_{r=1}^{N_s} k^{(r)}$ unknowns are introduced into the global system and thus N_α additional equations are required. The original statement (4.45) is

$$S^{(r)} u_\Gamma^{(r)} = g^{(r)} - C^{(r)^\top} \lambda$$

and this expression is only valid if the right hand side is in the range of $S^{(r)}$. Equivalently, it has to be orthogonal to the left null space $\tilde{N}^{(r)}$ of the matrix $S^{(r)}$ which implies

$$\tilde{N}^{(r)^\top} S^{(r)} = 0 \quad \Rightarrow \quad \tilde{N}^{(r)^\top} \left(g^{(r)} - C^{(r)^\top} \lambda \right) = 0. \qquad (4.64)$$

This equation is a discrete representation of the solvability condition (2.32) for the pure Neumann problem as shown in subsection 2.3.1. Obviously, the left null space $\tilde{N}^{(r)}$ of $S^{(r)}$ is the (right) null space of its transposed $S^{(r)^\top}$, $S^{(r)^\top} \tilde{N}^{(r)} = 0$. In case of a symmetric matrix, i.e., the finite element representation of $\mathcal{S}$, the two null spaces coincide. Unfortunately, the considered boundary element discretization of $\mathcal{S}$ results in a nonsymmetric matrix. Nevertheless, $\mathcal{S}$ is a symmetric operator [106] and it can be expected that its boundary element representation has the property that its left and right null spaces coincide. A mathematical basis of this assumption is lacking here, but the numerical experiments confirm this idea.

System (4.64) thus gives in total the required N_α equations for the global system. The global FETI-like system is now easily obtained by inserting the expressions (4.63) into the constraint (4.47) and assembling the local solvability conditions (4.64). The final saddle point problem is of the following form [28, 29]

$$\begin{pmatrix} F & -G \\ -G^\top & \end{pmatrix} \begin{pmatrix} \lambda \\ \alpha \end{pmatrix} = \begin{pmatrix} d \\ -e \end{pmatrix}. \qquad (4.65)$$

Now, the block matrices and vectors are defined by

$$
\begin{aligned}
\mathsf{F} &:= \sum_{r=1}^{N_s} \mathsf{C}^{(r)} \mathsf{S}^{(r)^+} \mathsf{C}^{(r)^\top}, & \mathsf{F} &\in \mathbb{R}^{N_\lambda \times N_\lambda} \\
\mathsf{d} &:= \sum_{r=1}^{N_s} \mathsf{C}^{(r)} \mathsf{S}^{(r)^+} \mathsf{g}^{(r)}, & \mathsf{d} &\in \mathbb{R}^{N_\lambda} \\
\mathsf{G} &:= \left(\mathsf{C}^{(1)} \mathsf{N}^{(1)}, \dots, \mathsf{C}^{(N_s)} \mathsf{N}^{(N_s)} \right) & \mathsf{G} &\in \mathbb{R}^{N_\lambda \times N_\alpha} \\
\mathsf{e} &:= \left(\mathsf{g}^{(1)^\top} \mathsf{N}^{(1)}, \dots, \mathsf{g}^{(N_s)^\top} \mathsf{N}^{(N_s)} \right)^\top & \mathsf{e} &\in \mathbb{R}^{N_\alpha} \\
\alpha &:= \left(\alpha^{(1)^\top}, \dots, \alpha^{(N_s)^\top} \right)^\top & \alpha &\in \mathbb{R}^{N_\alpha}
\end{aligned}
\tag{4.66}
$$

and λ contains the coefficients of the approximation (4.19), i.e., $\lambda[i] = \lambda_i$ with the index $i = 1, \dots, N_\lambda$. A straightforward and direct approach to the solution of system (4.65) is the factorization of F and the computation of the Schur complement. After solving for α, the Lagrange multiplier coefficients λ are computed and the local interface unknowns are determined by expression (4.63).

Independently of the Dirichlet conditions, the local problems (4.46) are uniquely solvable in the consideration of dynamic problems. Therefore, it suffices to consider system (4.50).

Remark 4.2. The original FETI-method [28] was developed with the aim of reaching the highest possible degree of parallelism. Therefore, a projected conjugate gradient method is proposed as solver, involving only matrix-vector products of F which are easily carried out in parallel. The local solution procedure can be carried out for each subdomain individually, independent of the choice of the solver (direct or iterative). It depends on the size of the local problems which choice is preferable. See the discussion by Farhat et al. [27] for the respective choice of local and global solvers and optimal preconditioners. In this work, the idea of FETI is not executed until this very end. Considering the boundary element discretization procedure of section 3.1.3, the development of an iterative local solver will be rather cumbersome (cf. also remark 3.7). The chosen nonsymmetric formulation finally leads to a nonsymmetric matrix F such that even on the global level, an iterative solution procedure is not easily applied. Furthermore, dynamic problems introduce another dimension of discretization such that the computable problems are often comparably small in terms of spatial degrees of freedom, especially in case of the boundary element discretizations and thus a direct solver would prevail. In case of pure finite element discretizations, the application to dynamic problems is less costly in terms of the storage of the time history and the extension of FETI to such problems has already been carried out by Farhat and Crivelli [25] (see also Farhat et al. [24] for a discussion on this extension and the development of a modified FETI algorithm especially tailored for such problems). Subsuming, the development of an iterative and fully parallel solution procedure is beyond the scope of this work but definitely an important further development of the proposed methods. $\diamond$

(a) Matching interfaces   (b) Nonmatching interfaces
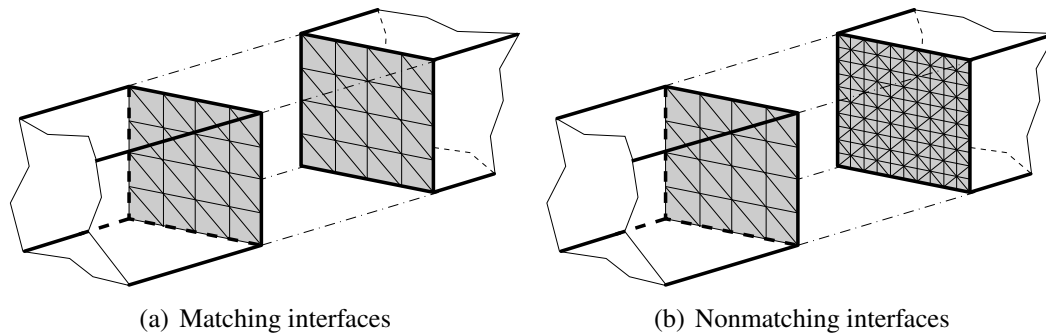
Figure 4.2: Matching and nonmatching interface discretizations.

4.4 Connectivity Matrices

Until now, the choice of trial functions for the approximation of the Lagrange multiplier field (4.19) has not been specified. This choice is directly linked to the question whether the different subdomain discretizations match at the respective interfaces. The original FETI-method [28] is applied to a domain partitioning applied to a global discretization. This means that at first the whole model is discretized by, for instance, finite elements and then divided into subdomains such that connected groups of elements are assigned to a subdomain. In this case, the discretizations match exactly at the interfaces. In many other situations, one might find it desirable to allow for nonmatching or *nonconforming* interface discretizations, where the discretizations do not necessarily match each other. In figure 4.2, such interface situations are depicted, where figure 4.2(a) shows the matching or *conforming* and figure 4.2(b) the nonmatching situation.

Nonconforming situations occur for instance, when the subdomains are discretized independently by different work groups or different preprocessing tools. Moreover, during the course of the numerical analysis mesh-refinements or simply changes in the local meshes might be required such that the matching situation cannot be maintained. Other than that, although the nodes of the respective discretizations coincide, different orders of the polynomials used for the trial functions can occur. As an example, imagine that for one side of the situation in figure 4.2(a) quadrilaterals are used instead of any two triangles. Then, the nodes still coincide but not the approximations for the interface unknown. In fact, the condition

$$u_\Gamma^{(r)}(\mathbf{y}) = u_\Gamma^{(p)}(\mathbf{y}) \qquad \mathbf{y} \in \Gamma^{(rp)}$$

will be violated on most of the interface. On the contrary, if the interface nodes coincide *and* the same trial functions are used for both subdomains, the above condition is fulfilled everywhere on the interface.

The connection of nonconforming interface discretizations has many obvious advantages and, therefore, has been analyzed thoroughly in the mathematical community. There are, for instance, the monograph of Steinbach [106], where this problem is considered within the analysis of different kinds of domain decomposition methods, and the monograph of

Wohlmuth [119] with the analysis of so-called *mortar* methods. Mortar methods commonly use special trial functions for the Lagrange multipliers such that the connectivity matrices become easily invertible and, therefore, one side of the interface unknowns can be easily expressed by the other, see also the publication of Puso [88] with applications to elasticity. From the engineering side, the work of Park et al. [81, 83] has to be considered. These authors have worked out a three-field method (also analyzed by Steinbach [106]) by introduction of another set of unknowns defined on the skeleton of the domain partitioning and using Lagrange multipliers to link the interface degrees of freedom with the skeleton degrees of freedom. In order to avoid the tedious interface integrations, they use point constraints associated with these special degrees of freedom. Unfortunately, the placement of these constraints is not trivial as discussed by the same authors [82].

One of the reasons to choose the FETI-framework presented in section 4.3 is that, being a Lagrange multiplier method, such nonconforming situations are easily incorporated. Recall the approximation of the Lagrange multiplier field (4.19),

$$\lambda_h(\mathbf{y}) = \sum_{j=1}^{N_\lambda} \lambda_j \psi_j(\mathbf{y})$$

with yet unspecified trial functions ψ_j. The standard FETI-method [28] works with nodewise constraints. This choice yields

$$\mathsf{C}[j,i] \in \{-1,0,1\} \tag{4.67}$$

and the sign is adjusted such that

$$u_{h,\Gamma}^{(r)}(\mathbf{y}_j) - u_{h,\Gamma}^{(p)}(\mathbf{y}_j) = 0 \qquad \mathbf{y}_j \in \Gamma^{(rp)}.$$

Property (4.67) is computationally advantageous since matrix operation with theses Boolean connectivity matrices do not really require floating-point arithmetic but only extraction operations. Nevertheless, the use pointwise constraints for the Lagrange multipliers requires conforming interfaces. Moreover, one has to be cautious at so-called *cross points*, i.e., points where more than two subdomains meet. Such a situation is shown in figure 4.3, where the three subdomains $\Omega^{(r)}$, $\Omega^{(p)}$, and $\Omega^{(q)}$ are connected at a vertex $\mathbf{y}_j$. In the case of figure 4.3(a), obviously only two of the three Lagrange multipliers $\lambda_j^{(rp)}$, $\lambda_j^{(pq)}$, and $\lambda_j^{(qr)}$ are linearly independent and the final matrix F is only positive semi-definite in such cases [29]. In a careful implementation, such redundancies are avoided and a constellation like in figure 4.3(b) results. Alternatively, Park et al. propose so-called *localized* Lagrange multipliers as a remedy to this problem [81]. Nevertheless, the introduction of a new set of skeleton unknowns and, especially, the problem of placing the point constraints used by these authors seems to limit their approach enormously.

A different choice, for instance, is the approximation of the Lagrange multipliers with piecewise constant trial functions associated with the elements τ_j of the interface discretization. In the following, $\tau_j^{(r)}$ refers to an element of the spatial discretization by

(a) Redundant Lagrange multipliers   (b) Non-redundant Lagrange multipliers
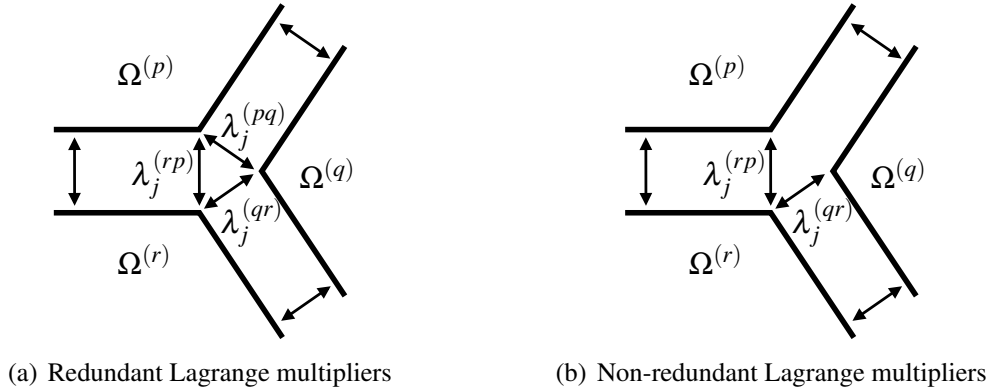
Figure 4.3: Cross point with redundant and non-redundant Lagrange multipliers.

boundary elements on an interface of the subdomain $\Omega^{(r)}$ or to the corresponding face of a volume element of a finite element discretization. In a conforming interface situation, the element $\tau_j^{(r)}$ coincides with some other element $\tau_j^{(p)}$ of the discretization of the neighboring subdomain $\Omega^{(p)}$. Note that the index j corresponds now to an element numbering on the skeleton Γ_s and not to the subdomain discretizations. Assuming $r < p$ in order to determine the sign of the connectivity matrices, the choice of constant Lagrange multipliers yields

$$\mathsf{C}^{(r)}[j,i] = -\int\limits_{\tau_j^{(r)}} \varphi_i^{(r)}\,\mathrm{d}s = -\int\limits_{\tau_j^{(p)}} \varphi_k^{(p)}\,\mathrm{d}s = -\mathsf{C}^{(p)}[j,k],\qquad(4.68)$$

where the shape functions $\varphi_i^{(r)}$ and $\varphi_k^{(p)}$ are defined with respect to the same vertex on Γ_s. Henceforth, $\psi_j(\mathbf{y}) = 1$ if $\mathbf{y}$ is located in the j-th element $\tau_j^{(r)}$ and $\psi_j(\mathbf{y}) = 0$ otherwise. Such connectivity matrices $\mathsf{C}^{(r)}$ are mathematically denoted as mass matrices as the matrix B in the boundary element discretization, recall equation (3.41), and are sparsely populated. The disadvantage of this choice is the computational effort involved in the computation of these matrix entries and the fact that the projections $\mathsf{C}^{(r)}\mathsf{S}^{(r)^+}\mathsf{C}^{(r)}$ now involve real matrix-matrix products contrary to the standard FETI method. Using Lagrange multipliers associated with interface elements instead of nodes circumvents the problem of cross points directly. No redundancies are thus possible with this approach.

Going a step further, one introduces the arbitrary notion of *slave* and *master* by defining that at the interface $\Gamma^{(rp)}$ subdomain $\Omega^{(r)}$ is the slave and $\Omega^{(p)}$ the master if $r < p$ and vice versa otherwise. The basic concept is now to let the slave domain completely determine the Lagrange multiplier approximation. In other words, the underlying spatial discretization in equation (4.19) is inherited from the slave side of the interface only without consideration of the master side. Using again piecewise constant trial functions ψ_j, the connectivity

$$\Omega^{(p)} \qquad\qquad \Omega^{(p)} \qquad\qquad \Omega^{(p)}$$

$$\Omega^{(r)} \qquad\qquad \Omega^{(r)} \qquad\qquad \Omega^{(r)}$$

(a) Nodal forces   (b) Traction field — conform   (c) Traction field — noncon-
                                                                       form
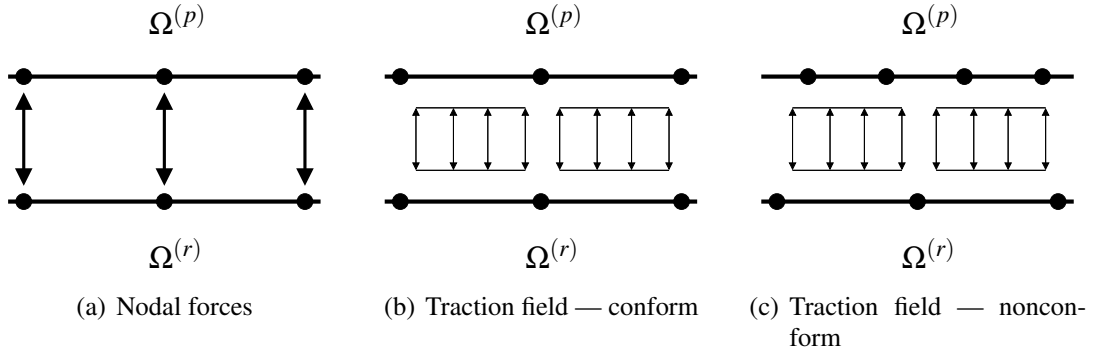
Figure 4.4: Different choices for the approximation of Lagrange multipliers.

matrices are for $r < p$

$$\mathsf{C}^{(r)}[j,i] = -\int\limits_{\tau_j^{(r)}} \varphi_i^{(r)}\, \mathrm{d}s \tag{4.69a}$$

$$\mathsf{C}^{(p)}[j,k] = \int\limits_{\tau_j^{(r)}} \varphi_k^{(p)}\, \mathrm{d}s\,. \tag{4.69b}$$

Whereas the slave side (4.69a) does not differ from the previous situation, the master side (4.69b) contains now an integration of a trial function belonging to subdomain $\Omega^{(p)}$ over the interface element taken from $\Omega^{(r)}$ and, therefore, the relation (4.68) is no longer valid for a general situation. The details of carrying out this integration is discussed below.

Figure 4.4 summarizes the above introduced choices of Lagrange multipliers at the interface $\Gamma^{(rp)}$. In figure 4.4(a), the classical FETI approach is depicted, where the Lagrange multipliers enforce nodal constraints and can be understood as nodal forces. With the same physical interpretation, the figures 4.4(b) and 4.4(c) show Lagrange multipliers as traction fields associated with the elements. The former is the conforming situation, where both interface discretizations are still matching, and the latter presents a nonmatching interface. Note that in this picture $\Omega^{(r)}$ would be the slave and $\Omega^{(p)}$ the master domain. As the pictures already indicate, the nonconforming approach contains the conforming one and, obviously, expression (4.69b) fulfills the identity (4.68) if $\tau_j^{(r)} = \tau_j^{(p)}$, i.e., the elements coincide.

Remark 4.3. In this work the approximation of the Lagrange multipliers is entirely carried out by piecewise constant functions. This choice is the simplest to be implemented and the results shown in chapter 5 seem to justify this choice. Nevertheless, it has to be noted that the instabilities occurring due to the choice of piecewise constant trial functions for q_h, as discussed in remark 3.3, are likely to occur here in the same way. Note the similarity between the matrix B of equation (3.41) and the connectivity matrices as defined in equation (4.36). At least, in the extension of the method of this work to a domain decomposition solver this problem should be avoided in order to have a robust method.   ◊

(a) Piecewise plane interfaces   (b) Curved interfaces
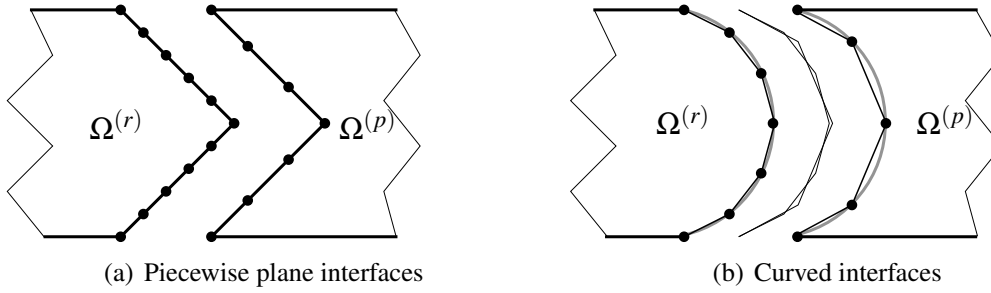
Figure 4.5: Piecewise plane (a) and curved (b) interfaces.

4.4.1 Nonconform interface integrals

The computation of the integrals of type (4.69b), i.e., the matrix entries of a nonconform interface discretization, contains some delicate details to which the remainder of this section is dedicated.

The interfaces of the computational domain shall be composed of plane regions. Therefore, curved interfaces are excluded from the following considerations. In figure 4.5, such piecewise plane and curved interfaces are depicted. Whereas in the plane case of figure 4.5(a) the geometry discretization is exactly placed on the interface lines, in figure 4.5(b) the gray line indicates the curved interface which differs from the traverse of the piecewise linear geometry approximation. In order to indicate the problem of such curved interfaces, the lines of the respective discretizations are copied and superimposed in the in the middle of figure 4.5(b) and clearly show the resulting voids and overlaps due to the nonconform meshes.

Remark 4.4. Although there are methods to handle the voids and overlaps of interfaces which are not plane, cf., e.g., Heinstein and Laursen [47], this case is excluded here for the sake of simplicity. Nevertheless, it can be expected that with decreasing mesh size the influence of the voids and overlaps is vanishing. It has to be noted that this exclusion can be a severe restriction when considering a multiphysics situation, where the manifold of material discontinuity is simply not plane. $\Diamond$

Recall now the expressions (4.69) for the computation of the matrix entries. The first of these expressions, equation (4.69a), consists of the normal integration as carried out for instance for the matrix B of the chosen boundary element method, compare equation (3.41). A lot more subtle is the problem of computing the master-slave connectivity matrix according to equation (4.69b). Now, the shape function $\varphi_k^{(p)}$ has to be integrated over the element $\tau_j^{(r)}$, which belongs to a different spatial discretization.

This situation is depicted in figure 4.6, where on the one side, in figure 4.6(a), a one-dimensional interface $\Gamma^{(rp)}$ is shown with the trial functions for the approximations $u_{\Gamma,h}^{(r)}$, $u_{\Gamma,h}^{(p)}$, and λ_h. It becomes clear that the computation of $C^{(r)}$ is rather straightforward,

(a) One-dimensional interface   (b) Two-dimensional interface
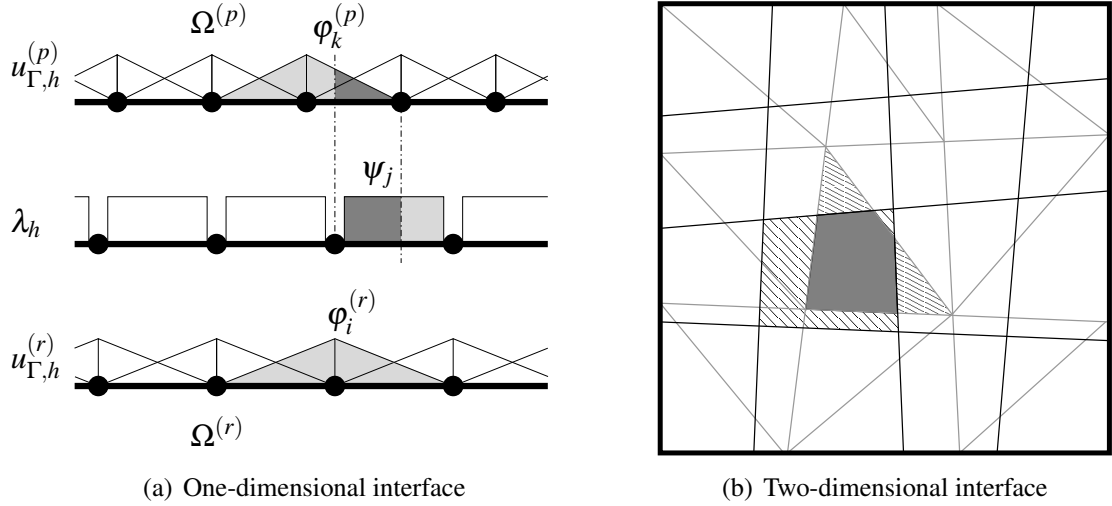
Figure 4.6: One- and two-dimensional interfaces with nonconforming discretizations.

whereas $C^{(p)}$ needs some special consideration. At first, the support of the product $\varphi_k^{(p)} \psi_j$ has to be determined, which is the overlap of the elements where the respective functions are defined. Once this overlap is known, the integration is carried out easily for this one-dimensional interface. The dark shaded regions are thus the contributions to the integral. The situation in figure 4.6(b) is worse. To determine the overlap of the considered elements in three dimensions is not a trivial task and, moreover, the resulting section polygon is of a very general type. For instance, the streaked regions in figure 4.6(b) are a slave and a master element and their intersection, the dark shaded area, is a polygon with 5 vertices, on which the integration is defined. Finally, one has to add, that the shape functions of the master side unknown have to be expressed in the reference coordinate system of the slave domain in order to apply a suitable quadrature rule. The two crucial steps, the computation of the element overlap and performing the integration, are outlined in the following

Computation of the overlap. At first, the global coordinates of the considered elements of the master and slave sides have to be expressed in the same reference coordinate system. Consequently, the slave element determines the reference coordinates. Let $\Omega^{(M)}$ and $\Omega^{(S)}$ denote the master and slave subdomains at the considered interfaces, respectively. Accordingly, $\tau^{(M)}$ and $\tau^{(S)}$ are the considered elements on each subdomain. The global coordinates $\mathbf{y}$ of a fixed element of the interface are now expressed through

$$\mathbf{y} = \mathbf{y}(\xi) = \sum_i \varphi_i^{(S)}(\xi^{(S)})\mathbf{y}_i^{(S)} \tag{4.70}$$

with the trial functions $\varphi_i^{(S)}$ and vertices $\mathbf{y}_i^{(S)}$ of the slave element $\tau^{(S)}$. In order to determine the vertices $\mathbf{y}_k^{(M)}$ of the master element $\tau^{(M)}$ in terms of the slave coordinates, the

system of equations is established

$$\mathbf{y}_k^{(M)} = \sum_i \varphi_i^{(S)}(\xi_k^{(S)}) \mathbf{y}_i^{(S)}$$

and has to be solved for the reference coordinates $\xi_k^{(S)}$. It is assumed here that it suffices to consider a purely linear coordinate mapping such that the above equations read

$$\mathsf{T}^{(S)} \xi_k^{(S)} = (\mathbf{y}_k^{(M)} - \mathbf{y}_0^{(S)}). \tag{4.71}$$

The matrix $\mathsf{T}^{(S)}$ contains the tangent vectors of the slave element and $\mathbf{y}_0^{(S)}$ is a reference point. In fact $\mathbf{y}_0^{(S)}$ is the vertex $\mathbf{y}_1^{(S)}$ in case of linear triangles and it will be the elements midpoint, i.e., $\mathbf{y}_0^{(S)} = \mathbf{y}(\mathbf{0})$, for line and quadrilateral elements. This expression (4.71) is exact in case of linear line elements and triangles. It is still exact for bilinear quadrilaterals if the shape of the element is a parallelogram because in that case the quadratic term $\xi_1 \xi_2$ vanishes. The system (4.71) contains d equations for $(d-1)$ unknowns and is thus overdetermined. By premultiplication with the transposed of $\mathsf{T}^{(S)}$ one obtains the least squares system of $(d-1) \times (d-1)$ equations

$$\left(\mathsf{T}^{(S)^\top} \mathsf{T}^{(S)} \right) \xi_k^{(S)} = \mathsf{T}^{(S)^\top} (\mathbf{y}_k^{(M)} - \mathbf{y}_0^{(S)}). \tag{4.72}$$

Solving equation (4.72) repeatedly for the vertices $\mathbf{y}_k^{(M)}$ yields the corresponding reference coordinates $\xi_k^{(S)}$. In case of a two-dimensional analysis, the reference system for the interface is one-dimensional. Therefore, one has to simply check if the interval of local coordinates $\xi_k^{(S)}$ intersects with the reference interval $(-1, 1)$. The intersection is then the desired overlap. A three-dimensional analysis has two-dimensional interfaces and, therefore, the coordinates $\xi_k^{(S)}$ form a convex polygon in two dimensions. The task is now to compute the intersection of this polygon with the polygon of the slave reference element. The intersection of polygons is a common problem in computer graphics and in this field often referred to as *polygon clipping*. Here, the General Polygon Clipper library by Alan Murta is used which is an implementation of the algorithm of Vatti [116]. Consider again the situation depicted in figure 4.6(b), where the intersection of a triangle and a quadrilateral element is shown by the dark shaded region. Finally, this overlap shall be denoted by

$$\bar{\tau} = \{ \xi^{(S)} \in \hat{\tau}^{(S)} : \mathbf{y}(\xi^{(S)}) \in \tau^{(M)} \}, \tag{4.73}$$

where $\hat{\tau}^{(S)}$ is the reference element of the slave side.

In this work, the possible overlap of every element on the master side with every element on the slave side is considered. Obviously, if the resulting intersection polygon is empty, this combination does not have to be regarded any further. In any case, this approach has a quadratic complexity in terms of the number of elements on the interface. This complexity could be reduced by a hierarchical clustering of the interface elements which would allow to discard whole groups of combinations. Nevertheless, the computation of the matrices $\mathsf{C}^{(r)}$ is currently not crucial for the speed of the computation.
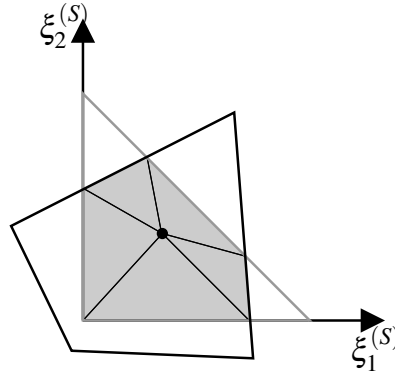
Figure 4.7: Polygon intersection in the slave reference coordinate system and subdivision into triangles.

Computation of the integral.   By means of the above, the overlap $\bar{\tau}$ is determined and it remains to carry out the integration

$$\bar{I} := \int_{\bar{\tau}} \varphi^{(M)}(\xi^{(S)}) \sqrt{G_S(\xi^{(S)})} \, d\xi^{(S)}, \qquad (4.74)$$

where the Gram determinant $G_S(\xi^{(S)})$ is due to the coordinate transformation from $\mathbf{y}$ to $\xi^{(S)}$ as defined in equation (3.79). Two difficulties are still included in this expression. The overlap $\bar{\tau}$ is in a three-dimensional analysis a convex polygon of rather arbitrary shape and the master shape function $\varphi^{(M)}$ is defined in the master reference system, not in the slave reference coordinates.

Considering first the two-dimensional analysis, the evaluation of the integral is rather easy. The overlap $\bar{\tau}$ is simply an interval contained in $(-1, 1)$. Moreover, in the computation of this overlap the vertices of the master element $\tau^{(M)}$ in reference coordinates have been computed. These are the values of $\xi_k^{(S)}$ and in case of linear $\varphi_k^{(M)}$, the Kronecker delta property (3.14) allows to uniquely determine the linear trial functions in this coordinate system. A simple mid-point rule will be sufficient because the integrand of expression (4.74) is linear.

In the three-dimensional case, the section polygon is the region of integration and has m vertices. In the considered cases of triangles and quadrilaterals, one can restrict this number by $3 \le m \le 8$. The first step is thus to divide this polygon in triangles in order to apply a quadrature rule. One could think of a subdivision into quadrilateral elements, but the use of triangles is a lot easier. This is simply done by computing the midpoint of the polygon and constructing m triangles which are formed by two adjacent vertices of the polygon and this midpoint. Figure 4.7 shows such a situation with a reference triangle $\hat{\tau}^{(S)}$ and the projection of the master quadrilateral into the slave reference system. The shaded region is the computed intersection polygon and subdivided into triangles.

The master trial function $\varphi^{(M)}$ can be bilinear such that a simple mid-point rule is not applicable. Here, a quadrature rule is used, which evaluates the integrand at the midpoints

of the edges and uses weights of $1/3$ times the area of the triangle (cf., e.g., Jung and Langer for such a rule [52]). If an edge-midpoint of the considered sub-triangle is denoted by $\xi_g^{(S)}$, the last problem to tackle is the evaluation of $\varphi^{(M)}(\xi_g^{(S)})$, i.e., the master trial function, which is defined on the reference element of the master subdomain, evaluated at this point is given in the reference coordinates of the slave subdomain. In a first step, the global coordinates corresponding to this point of evaluation are computed by

$$\mathbf{y}_g := \mathbf{y}(\xi_g^{(S)}) = \mathsf{T}^{(S)}\xi_g^{(S)} + \mathbf{y}_0^{(S)}, \tag{4.75}$$

simply using the coordinate transformation from local slave coordinates $\xi^{(S)}$ to global coordinates, which is uniquely defined anyway. This point $\mathbf{y}_g$ can now be expressed in the local master coordinates by a similar projection as used for the computation of the overlap, see equation (4.72), now expressed for the master side

$$\left(\mathsf{T}^{(M)^\top}\mathsf{T}^{(M)}\right)\xi_g^{(M)} = \mathsf{T}^{(M)^\top}(\mathbf{y}_g - \mathbf{y}_0^{(M)}). \tag{4.76}$$

The solution of this 2×2-system (remember that now only the three-dimensional case is considered) gives the representation of the evaluation point $\xi_g^{(S)}$ in the master reference coordinate system, in which the trial function $\varphi^{(M)}$ is defined. In summary, the integral under consideration (4.74) is expressed by

$$\bar{I} = \sum_{\mu=1}^m \int_{\bar{\tau}_\mu} \varphi^{(M)}(\xi^{(S)})\sqrt{G_S(\xi^{(S)})}\,\mathrm{d}\xi^{(S)} = \sum_{\mu=1}^m \sum_{g=1}^3 \varphi^{(M)}(\xi_g^{(M)})\sqrt{G(\xi_g^{(S)})}\,w_g \tag{4.77}$$

with w_g being a third of the area of the μ-th sub-triangle $\bar{\tau}_\mu$ and $\xi_g^{(M)}$ the master coordinate representation of the g-th edge midpoint of the μ-th sub-triangle obtained by expressions (4.75) and (4.76).

5 NUMERICAL RESULTS

In this chapter, the methods introduced in chapters 3 and 4 are applied to some examples. At first, some typical verifications are conducted by comparing the numerical results with analytical solutions. This is done by single domain analyses for the testing of the employed finite and boundary element discretization methods and, afterwards, by using the coupled algorithm proposed in this work. Some reference solutions are given in appendix B. But before presenting these results, some details on the approximation methods and their implementation have to be given. Moreover, the considered material data are summarized below.

The finite element discretizations are all carried out with isoparametric bilinear quadrilaterals and trilinear hexahedra for two- and three-dimensional problems, respectively (see, e.g., the book of Hughes [49] for the definition of such element types). The quadrature methods for the regular volume integrals according to section 3.3 are classical tensor-product Gauss rules [55] based on two- and three-point rules for the integrals of the stiffness and mass matrices, respectively. The solution of the finite element equation systems is done using a sparse Cholesky factorization of the CHOLMOD package, see the algorithm of Davis [18].

For the boundary element discretizations, on the other hand, surface line elements with piecewise linear continuous trial functions for the approximation of u_Γ and piecewise linear discontinuous functions for q_Γ are used in two spatial dimensions. The same approximation orders are employed for the triangular elements used for three-dimensional problems. The collocation points are placed as pointed out in remark 3.2 and the quadrature is performed according to section 3.3. The line elements are treated by a 20-point Gauss quadrature and a 42-point rule of order 14 is used for the triangles from the triangle quadrature rules of Dunavant [22]. In case of the singular integration, the logarithmic quadrature uses a four-point rule and the modified quadrature for the one-dimensional principal value integration is of second order (the former can be found in the book of Press et al. [86] and the latter in the thesis of Diethelm [19]). The employed Duffy coordinates, on the other hand, boil down to a tensor-product rule which again is based on a one-dimensional 20-point rule. As pointed out in remark 3.4, an adaptive quadrature rule would be of a great benefit for the boundary element surface integrals. The FFTW library [32] is employed for an efficient computation of the integration weights of the convolution quadrature method as presented in subsection 3.2.2. The final system of equations is solved by using LAPACK routines [2].

The connectivity matrices, which are of mass matrix type, are computed by the technique explained in subsection 4.4.1 using either a mid-point rule or a second-order triangle quadrature for two or three spatial dimensions, respectively. As already mentioned in the

same subsection, the polygon intersections are computed by means of the GPC polygon
clipping library.

Materials.   The material models used for the numerical examples consist of an acoustic
fluid, modeled by the acoustic wave equation (2.9), and solids governed by the elasto-
dynamic equations (2.21). These materials with their respective properties are listed in
table 5.1.

Material name	ρ_0 $[\text{kg}/\text{m}^3]$	κ $[\text{N}/\text{m}^2]$	c $[\text{m}/\text{s}]$
Air	1.2	$1.4153 \cdot 10^5$	343.43

(a) Material model for the acoustic fluid

Material name	ρ_0 $[\text{kg}/\text{m}^3]$	λ $[\text{N}/\text{m}^2]$	μ $[\text{N}/\text{m}^2]$	c_1 $[\text{m}/\text{s}]$	c_2 $[\text{m}/\text{s}]$
Soil	1884	$1.3627 \cdot 10^8$	$1.3627 \cdot 10^8$	465.82	268.94
Steel	7850	0	$1.055 \cdot 10^{11}$	5184.5	3666.0
Concrete	2400	$9.7222 \cdot 10^9$	$1.4583 \cdot 10^{10}$	4025.4	2465.0

(b) Material models for the elastic solid

Table 5.1: Material data for the chosen acoustic fluid and the elastic solids. For the con-
struction of a purely one-dimensional problem, the material steel has no lateral
contraction ($v = 0$).

The one-dimensional verification problems of subsections 5.1.1 and 5.1.2 are formulated
using the material steel without lateral contraction. Moreover in this specific case of $v = 0$,
the two-dimensional elasticity cases plane stress and plane strain coincide.

5.1 Single Domain Solutions

5.1.1 Cantilever beam

The first problem to be considered is the cantilever beam loaded by a vertical force as
depicted in figure 5.1. Using the Bernoulli beam theory, this problem is described by the
equation

$$\left(EI \frac{\partial^4 w}{\partial x^4} \right)(x) = 0,$$

$$w = (\partial w/\partial x) = 0 \qquad \qquad \qquad \qquad \qquad \qquad \qquad F = 1\,\text{N}$$

$$\Omega = (0, \ell)$$
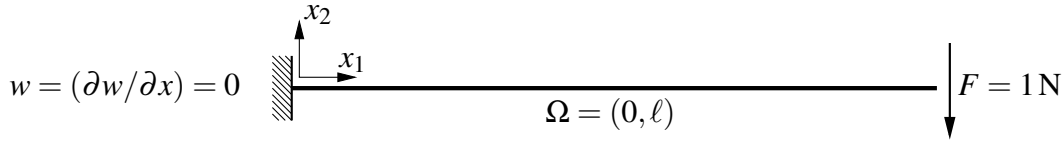
Figure 5.1: Cantilever beam loaded with a vertical force.

where $w(x)$ denotes the vertical deflection of the beam with $x \in (0, \ell)$ being the coordinate along the main axis. E is the Young's modulus and I the area moment of inertia, where both are assumed to be constant. The boundary conditions are

$$w(0) = \frac{\partial w}{\partial x}(0) = 0, \quad \left(EI\frac{\partial^2 w}{\partial x^2}\right)(\ell) = 0 \quad \text{and} \quad \left(EI\frac{\partial^3 w}{\partial x^3}\right)(\ell) = F\,.$$

The solution to this problem is easily obtained and has the form

$$w(x) = \frac{F\ell^3}{6EI}\left(3\frac{x^2}{\ell^2} - \frac{x^3}{\ell^3}\right). \tag{5.1}$$

The validity of the Bernoulli beam theory is restricted to large values of ℓ/b, where ℓ denotes the length and b the extension orthogonal to the main axis and in the plane of deflection of the beam. In this example, a beam of $10\,\text{m}$ length and $1\,\text{m}$ width and height is chosen such that $\ell/b = 10$ and, therefore, the Bernoulli theory is applicable.

A numerical solution to the above described cantilever beam problem was obtained by solving the elastostatic equations (2.25) for two and three spatial dimensions using the material steel from table 5.1 without lateral contraction and, therefore, allows for the one-dimensional beam theory as a reference. The force F acting at $x = \ell$ is modeled by a constantly distributed surface traction field over the surface in downward direction. Therefore, the boundary value problem for d dimensions, $d = 2, 3$, has the form

$$-\mu\nabla\cdot(\nabla\mathbf{u}(\mathbf{x})) - (\lambda+\mu)\nabla(\nabla\cdot\mathbf{u}(\mathbf{x})) = 0 \qquad \mathbf{x} \in \Omega = (0, 10\,\text{m}) \times (0, 1\,\text{m})^{d-1}$$
$$\mathbf{u}_\Gamma(\mathbf{y}) = 0 \qquad \mathbf{y} \in \overline{\Gamma}_D = \left\{\mathbf{x} \in \overline{\Omega}\colon x_1 = 0\right\} \tag{5.2}$$
$$\mathbf{t}(\mathbf{y}) = \mathbf{g}_N(\mathbf{y}) \quad \mathbf{y} \in \Gamma_N = \Gamma \setminus \overline{\Gamma}_D\,,$$

where $\mathbf{g}_N = -1\,\text{N/m}^2$ in the vertical component at $x_1 = 10\,\text{m}$ is the only non-zero part of the prescribed Neumann datum. At first the results of the finite element and then of the boundary element discretizations are presented.

Finite element discretization. Different spatial discretizations are compared for both dimensions. In two dimensions the coarsest mesh contains 1×10 quadrilaterals, which is then refined to 2×20, 4×40, and 8×80 elements. Similarly, the four three-dimensional meshes start with $1 \times 1 \times 10$ and end with $8 \times 8 \times 80$ hexahedra. The second finest mesh with $4 \times 4 \times 40 = 640$ elements is displayed in figure 5.2. In terms of the mesh size the used meshes correspond to $h = 1\,\text{m}$, $0.5\,\text{m}$, $0.25\,\text{m}$, and $0.125\,\text{m}$.
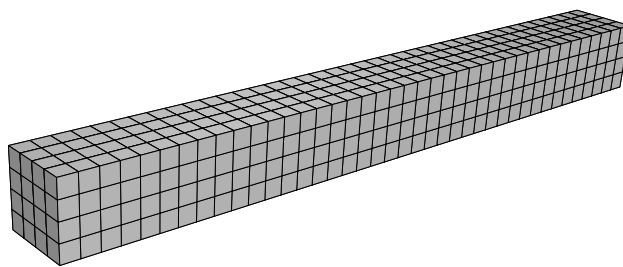
Figure 5.2: Three-dimensional finite element discretizations of the cantilever beam with 640 hexahedra trilinear elements.
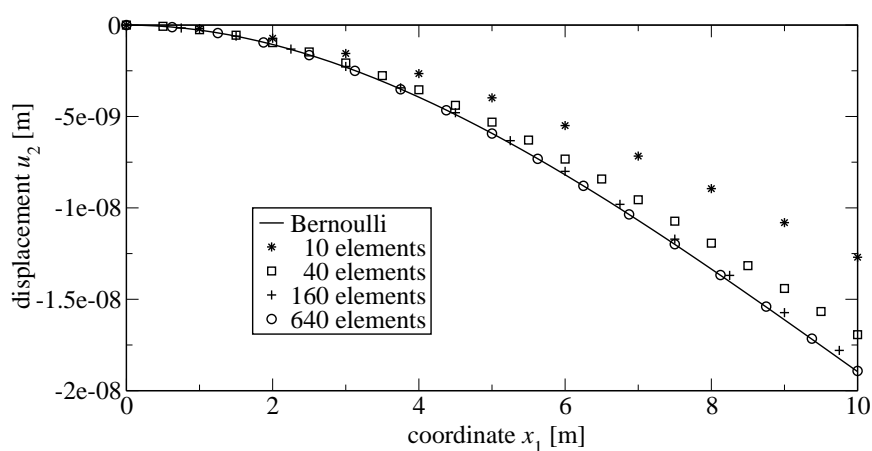
(a) Two-dimensional simulation
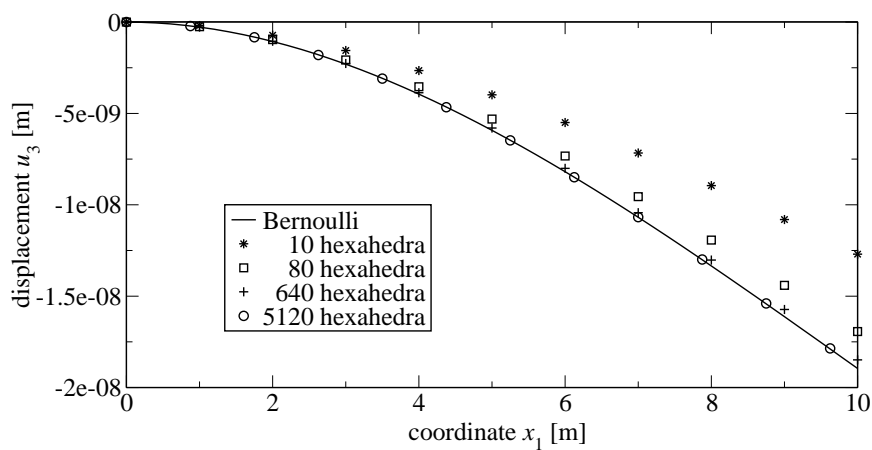
(b) Three-dimensional simulation

Figure 5.3: Finite element solutions of the deflection of the cantilever beam along the x_1-axis for different meshes.

In order to judge the numerical outcome, the values of the vertical displacements along the x_1-axis, see figure 5.1, are plotted together with the solution of the Bernoulli beam theory (5.1). In figure 5.3(a), the results for a two-dimensional simulation are displayed, whereas figure 5.3(b) shows the results of a three-dimensional analysis. Clearly, the results converge with decreasing mesh size to values close to the Bernoulli solution in both cases. Although the Bernoulli beam theory underlies severe assumptions, e.g., no shear deformation, the given length-width ratio ℓ/b is large enough such that it certainly serves as a good reference. For both dimensions, the two finer discretizations, i.e., for $h = 0.25\,\text{m}$ and $h = 0.125\,\text{m}$, give good results which mimic well the cubic shape of the deflection line.

Boundary element discretization. The same problem is now analyzed by the introduced boundary element method. Again, two- and three dimensional simulations with different meshes are carried out. In the plane strain situation, five different meshes are used which have mesh sizes from $h = 1\,\text{m}$ down to $h = 0.0625\,\text{m}$ obtained by bisection. The three-dimensional analysis uses three different meshes with surface triangles of sizes $h = 1\,\text{m}$, $h = 0.5\,\text{m}$, and $h = 0.25\,\text{m}$. Note that in this case h refers to the lengths of the catheti of isosceles right triangles. Figure 5.4 shows the finest of these three-dimensional discretizations with 1344 triangles.

The results of these simulations are displayed in figure 5.5. Clearly, in the both cases of a two- and a three-dimensional analysis, the results get closer to the reference solution (5.1) of the Bernoulli beam theory. Especially the two-dimensional simulation displayed in figure 5.5(a) converges quickly and the finest discretizations with $h = 0.125\,\text{m}$ and $h = 0.0625\,\text{m}$ mesh width, respectively, give very good results. In fact, these results are better than even the finest discretization of the three-dimensional simulation shown in figure 5.5(b). Due to the fact that the integration error in the boundary element approach is not controlled, see also remark 3.4, the numerical outcome of a simulation with an even finer mesh than depicted in figure 5.4 is useless and not shown here. The reduced approximation error due to the finer mesh was no longer dominating the result but the integration error. Moreover, the results seem to indicate that the condition of the system matrices rapidly worsens with the mesh refinement.

5.1.2 Rod with longitudinal step load

Next, the dynamic problem as depicted in figure 5.6 is considered. This problem has already been stated in the introductory example in subsection 1.2.2. It is a purely one-dimensional problem and governed by the initial boundary value problem for the domain
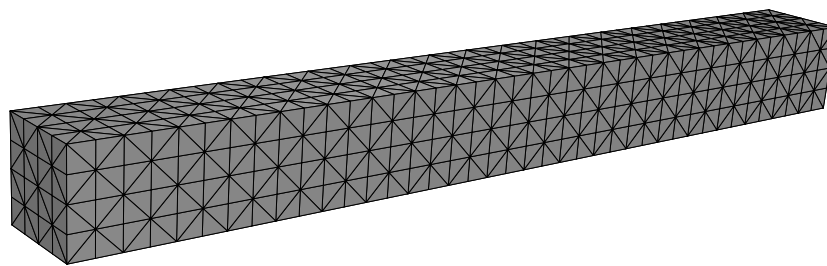
Figure 5.4: Three-dimensional boundary element discretizations of the cantilever beam with 1344 triangles.
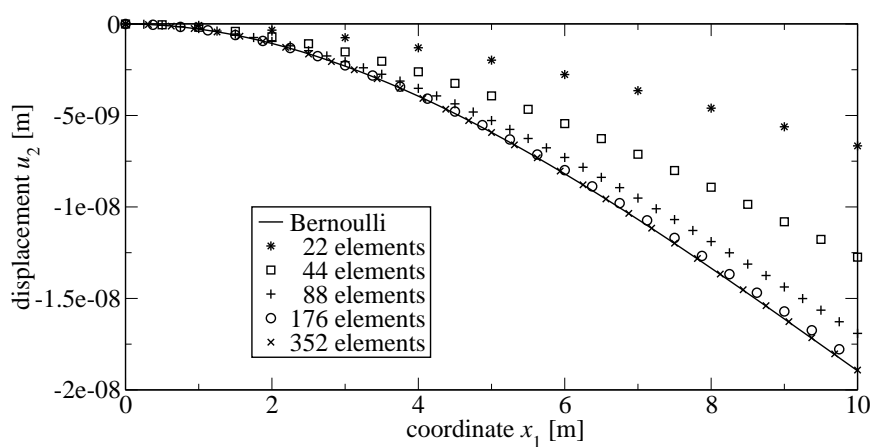
(a) Two-dimensional simulation
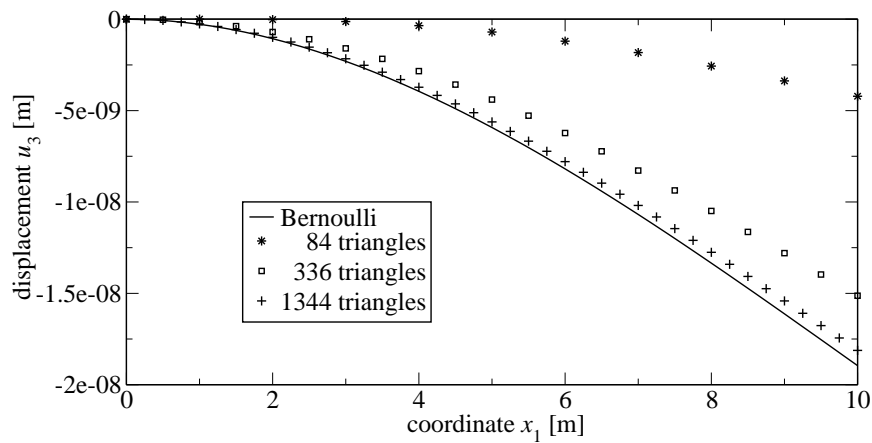
(b) Three-dimensional simulation

Figure 5.5: Boundary element solutions of the deflection of the cantilever beam along the x_1-axis for different meshes.
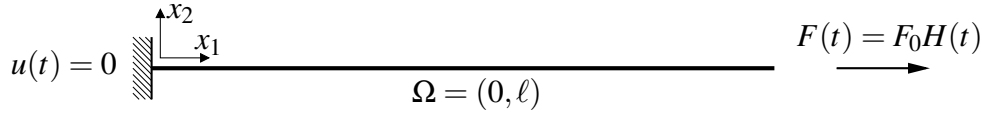
Figure 5.6: Rod with impact force.

$\Omega = (0, \ell)$ with boundary $\Gamma = \{0, \ell\}$

$$\rho_0 \left(\frac{\partial^2 u}{\partial t^2} \right)(x,t) - \kappa \left(\frac{\partial^2 u}{\partial x^2} \right)(x,t) = 0 \qquad (x,t) \in (0,\ell) \times (0,\infty)$$

$$u_\Gamma(0,t) = 0 \qquad t \in (0,\infty)$$
$$q_\Gamma(\ell,t) = F_0 H(t) \qquad t \in (0,\infty) \qquad (5.3)$$
$$u(x,0) = \left(\frac{\partial u}{\partial t} \right)(x,0) = 0 \qquad x \in (0,\ell),$$

where $q_\Gamma(x,t)$ denotes the outward axial force or acoustic flux at the boundary points. This initial boundary value problem is the one-dimensional analogue to both the acoustic wave equation (2.9) and the elastodynamic system (2.21) with the corresponding boundary and initial conditions. Here, these both cases shall be considered and thus two- and three-dimensional finite and boundary element analyses of an acoustic fluid and of an elastic solid are carried out using the respective equations. The materials considered are air on the one hand and steel on the other hand. In the abstract writing introduced in section 2.3, the d-dimensional counterpart to problem (5.3) reads

$$\rho_0 \left(\frac{\partial^2 u}{\partial t^2} \right)(\mathbf{x},t) - \kappa (\nabla \cdot \nabla u)(\mathbf{x},t) = 0 \qquad (\mathbf{x},t) \in \Omega \times (0,\infty)$$

$$u_\Gamma(\mathbf{y},t) = 0 \qquad (\mathbf{y},t) \in \Gamma_D \times (0,\infty)$$
$$q_\Gamma(\mathbf{y},t) = g_N(\mathbf{y},t) \qquad (\mathbf{y},t) \in \Gamma_N \times (0,\infty) \qquad (5.4)$$
$$u(\mathbf{x},0^+) = \left(\frac{\partial u}{\partial t} \right)(\mathbf{x},0^+) = 0 \qquad \mathbf{x} \in \Omega.$$

The domain Ω is now the cuboid $(0,\ell) \times (0,b)^2$ or the rectangle $(0,\ell) \times (0,b)$ for the three- or two-dimensional representations, respectively. The Dirichlet boundary Γ_D is the face at $x_1 = 0$ and the Neumann boundary Γ_N comprises the rest of the surface. The prescribed Neumann datum g_N is zero everywhere but on the face opposite the Dirichlet boundary, i.e., at $x_1 = \ell$. In case of the fluid model it is simply an applied surface flux q along the axis, whereas in case of elastodynamics it is a surface traction field $\mathbf{t}$ which is only non-zero in the first component. In other words, on the face $x_1 = \ell$ either $q(\cdot,t) = F_0 H(t)/b^{(d-1)}$ or $\mathbf{t}(\cdot,t) = (F_0 H(t)/b^{(d-1)}, 0, 0)^\top$ is applied, depending on the model of a fluid or a solid, respectively. Finally, the unknown u represents either the acoustic pressure p or the displacement field $\mathbf{u}$. For the elastic case, the compressibility κ is taken as the bulk modulus of the material, i.e., $\kappa = \lambda + 2\mu$.

The geometric dimensions of this problem are henceforth fixed to $\ell = 3\,\mathrm{m}$ and $b = 1\,\mathrm{m}$. Moreover, the force is of unit magnitude and, therefore, $F_0 = 1\,\mathrm{N/m^2}$. Various sizes of the

time steps will be tested and it is common in dynamic analyses to consider the factor

$$\chi := \frac{c\Delta t}{h} \tag{5.5}$$

to measure stability. This factor is usually called the *Courant-Friedrichs-Lewy* number (CFL) in honor to their publication on the stability of finite difference schemes [15]. The components of this factor are the velocity c at which information travels and the size of the temporal and spatial discretizations, Δt and h, respectively. In case of the acoustic fluid, c is simply the speed of the pressure wave, $c^2 = \kappa/\rho_0$, and for elastodynamics the *P*-wave is considered with the speed $c_1^2 = (\lambda + 2\mu)/\rho_0$, see also equation (2.23). Returning to the considered numerical example, the wave speeds c for the respective models are simply taken from table 5.1.

The analytical solution of problem (5.3) is known and given in appendix B.1. As in the case of the cantilever beam example, at first the results from a finite element discretization with the Newmark time stepping scheme are discussed before considering the outcome of the time-domain boundary element method based on the convolution quadrature method. In most cases the tip displacement or pressure, represented by u_Γ at $x_1 = \ell$, is considered which has the classical zigzag form. In the context of the boundary element method, also the value of q_Γ, i.e., the surface traction in longitudinal direction of the acoustic flux, at the Dirichlet boundary $x_1 = 0$ is taken into account.

Finite element discretization.   The spatial discretization is similar to the previous cantilever beam example. Therefore, it is sufficient to refer to figure 5.3 for an image of a three-dimensional discretization.

At first, a variation of the CFL number χ is carried out. Therefore, the mesh size is fixed to $h = 0.5$ m such that the discretizations have 12 quadrilaterals in the two-dimensional case and 24 hexahedra in three dimensions. Considering first the acoustic fluid, i.e., air from table 5.1, the wave speed is $c = 343.43$ m/s and the different time steps are chosen such that the CFL number has values of $\chi \in \{0.1, 0.5, 1.0, 2.0\}$. The results of this variation of χ are shown in figure 5.7 for a maximal time of $t = 0.11$ s. The outcome of the two-dimensional case is given in figure 5.7(a). Figure 5.7(b) contains the three-dimensional results for the elastodynamic computation of steel. The significant wave speed is then the speed of the pressure wave $c_1 = 5184.5$ m/s. The other cases of a three-dimensional analysis of the acoustic fluid and the two-dimensional analysis of the elastic solid are omitted in order to avoid redundancies because the characteristics of the solutions are identical.

In both cases the worst result is obtained for the choice $\chi = 2.0$. In fact, this is a violation of the CFL condition [15], which states that the CFL number has to bounded such that always $0 < \chi \leq 1$. Physically speaking, a number $\chi > 1$ would let information travel in the numerical approximation scheme faster than the speed c at which it travels according to the physical model. Nevertheless, this violation does not yield instabilities but simply reduces the amplitudes and causes a phase shift as it can be seen from the results in figure 5.7. A similar deviation from the analytical solution is obtained for the limit choice
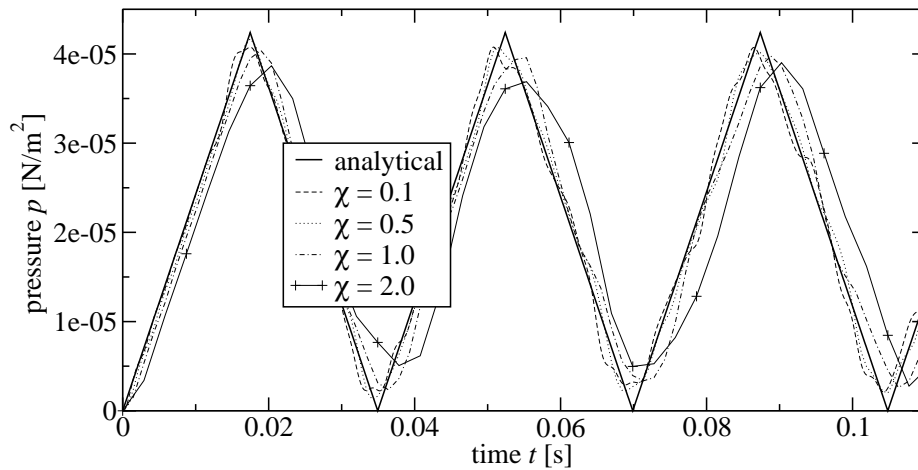
(a) Two-dimensional simulation of an acoustic fluid
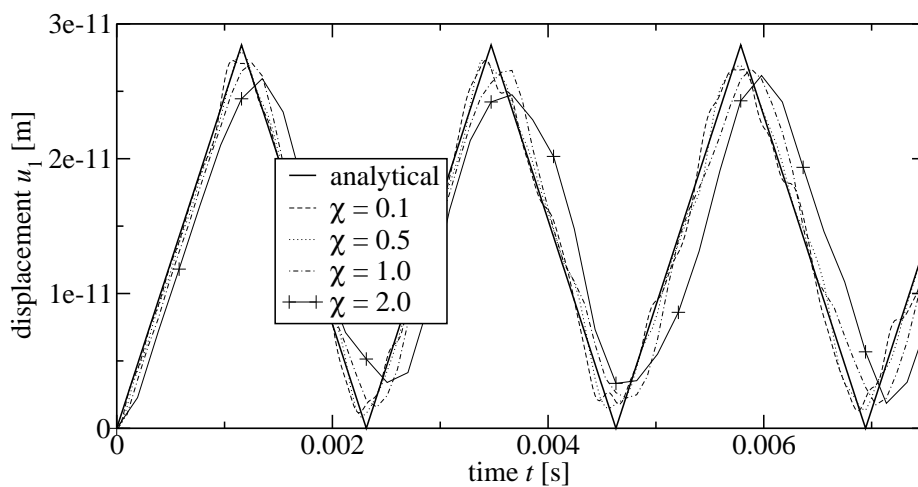
(b) Three-dimensional simulation of an elastic solid

Figure 5.7: Results of the finite element analysis of the dynamic rod — pressure of the acoustic fluid in two dimensions and displacement of the elastic solid three dimensions for the time interval $0 < t < 0.075\,\text{s}$ for different CFL numbers χ.

$\chi = 1$. On the other hand, the smallest value of $\chi = 0.1$ results in a slightly shaky curve without causing instabilities. Recall that the underlying Newmark algorithm as presented in subsection 3.2.1 is unconditionally stable for the choice of parameters $\beta = \frac{1}{4}$ and $\gamma = \frac{1}{2}$, see also Hughes [49]. The best result among these different CFL numbers is obtained for the value $\chi = 0.5$ which gives a rather smooth curve with very little damping of the amplitudes and a negligible phase shift.

The results of an analysis of the three-dimensional elastic solid are shown for a larger time $0.075\,\text{s} < t < 0.08\,\text{s}$ in figure 5.8(a). The discretization has the mesh size $h = 0.5\,\text{m}$ and now the five values of $\chi = 0.1$ to $\chi = 0.5$ are considered. Apparently, all of these values yield a phase shift to the left and the curves are not very smooth. Moreover, the deviation
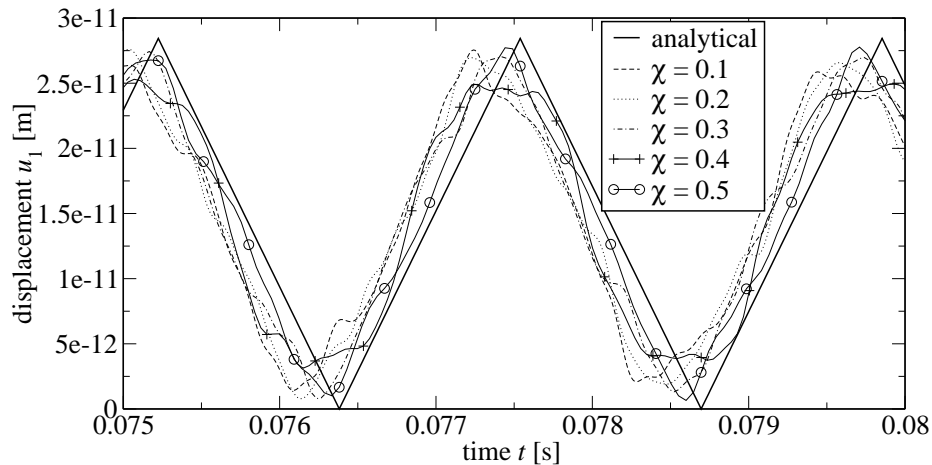
(a) Results at larger times.
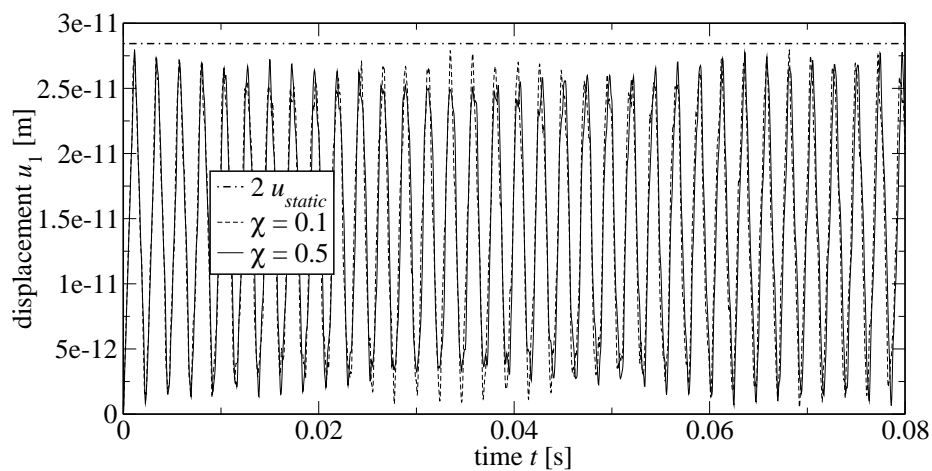
(b) The whole time range.

Figure 5.8: Three-dimensional finite element simulation of the elastodynamic solid — tip
displacements in a larger time range for various CFL numbers χ.

from the maximal value, i.e., twice the static solution u_{static}, and the minimal value of zero
is similar for all choices of χ. The whole range $0 < t < 0.08\,\mathrm{s}$ is shown in figure 5.8(b) for
the CFL numbers $\chi = 0.1$ and 0.5. In addition, the maximal displacement of the analytical
solution is plotted in order to emphasize the deviation of the numerical solution. One
cannot state that either of the two compared solution has a better behavior in this long
range consideration. The error in terms of the maximal displacement is significant in both
cases. Nevertheless, the considered discretization is rather coarse and refined meshes are
expected to yield better results as considered below.

It can be deduced from figure 5.7 that the difference between the two physical models,
acoustic fluid and elastic solid, and the difference between the two- and three-dimensional
analyses is not significant. Therefore, the following investigation deals only with three-
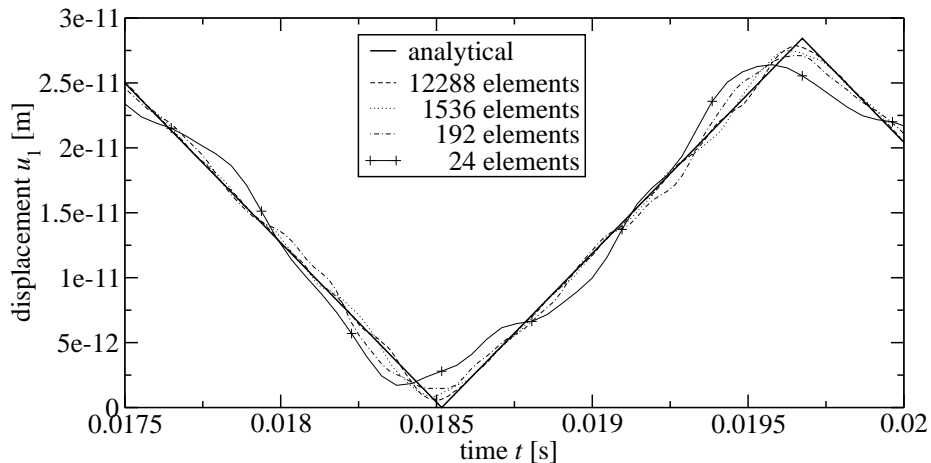
Figure 5.9: Three-dimensional finite element simulation of the elastodynamic solid — tip displacement in a specific time window with a fixed $\chi = 0.5$ and different mesh sizes.

dimensional elastodynamics, whereas the characteristics are expected to be similar for the three other situations.

Finally, four different mesh sizes are compared with $h = 0.0625\,\text{m}$ to $h = 0.5\,\text{m}$ or, in other words, with 12288, 1536, 192 and 24 elements. The results of this simulation are depicted in figure 5.9 where the CFL number is fixed to $\chi = 0.5$. In order to visualize the difference in the obtained results, only the time window $0.0175\,\text{s} < t < 0.02\,\text{s}$ is selected. The comparison of the four different spatial discretizations clearly shows that finer meshes yield better results. Whereas the coarsest discretization with only 24 elements significantly deviates from the analytical solution, the result of the finest mesh with 12 288 elements are hardly distinguishable from the reference solution. One can only observe differences at the turning points, i.e., the minimal or maximal values. Considering the cost of these simulations, one has to stress the fact that due to the fixed CFL number a refinement of the spatial discretization also requires a refinement of the time grid. The finest mesh, for instance, does not only have 512 times as many elements as the coarsest but also requires eight times as many time steps for the simulation of the same time interval.

Boundary element discretization. In the following, the solution of the initial-boundary value problem (5.4) by means of the boundary element method introduced in subsection 3.1.3 together with the convolution quadrature method of subsection 3.2.2 is analyzed. The spatial discretization is similar to the one used in the previous cantilever beam example, see figure 5.5. A lot of numerical analyses of three-dimensional elastodynamics for the same problem have been carried out by Schanz [98]. Therefore, this case will not be repeated here in detail. In summary, one can deduce from the work of Schanz that a value of $\chi = 0.2$ seems to be a good choice for different discretizations, whereas values significantly smaller than 0.2 lead to severe instabilities throughout the course of the simulation.
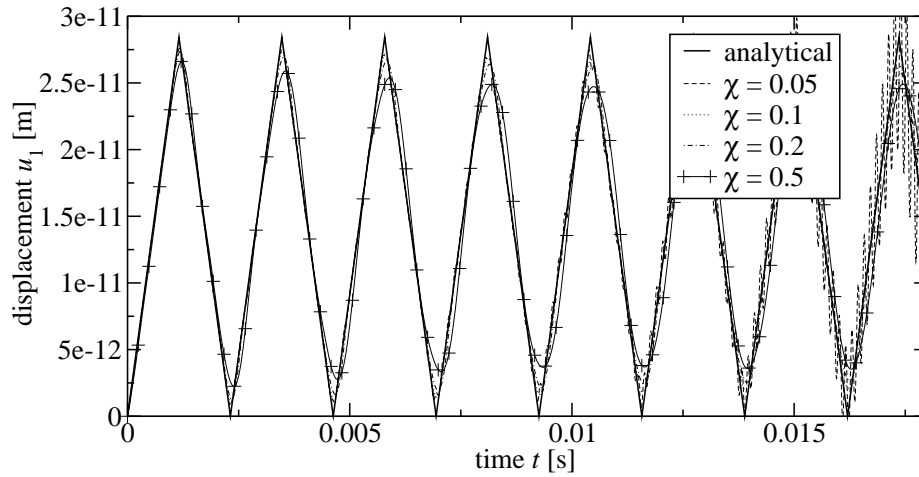
(a) The whole time range.
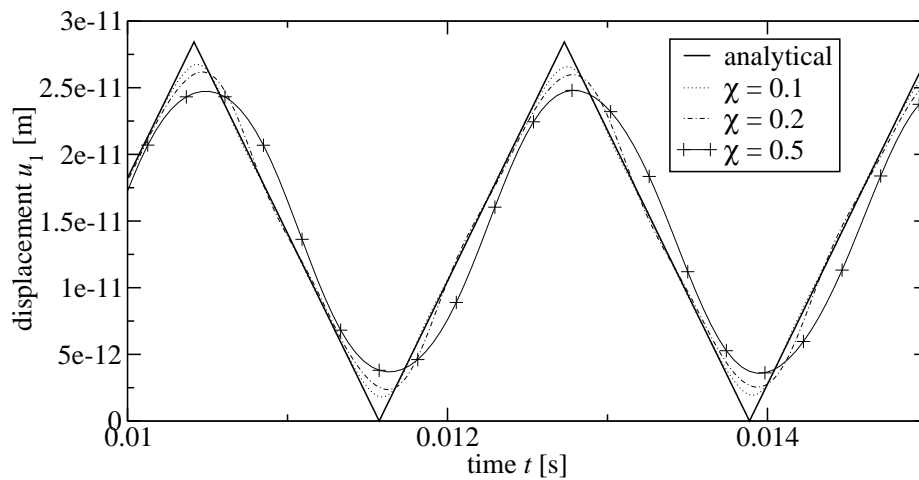
(b) Results at larger times.

Figure 5.10: Tip displacement of the two-dimensional boundary element simulation of the elastodynamic solid against time for different values of χ with fixed mesh size $h = 0.5$ m.

Since the basic characteristics of this problem are the same in the case of the acoustic fluid and the elastic solid, it follows only the consideration of the two-dimensional elastodynamic case.

Figure 5.10 shows the results for a fixed mesh size $h = 0.5$ m, i.e., 16 elements, and various time step sizes such that the CFL number varies through $\chi \in \{0.05, 0.1, 0.2, 0.5\}$. In figure 5.10(a), the tip displacement u_1 at $x_1 = \ell$ for the range $0 < t < 0.018$ s is shown and it can be seen that in case of the lowest value $\chi = 0.05$ the solution becomes instable and gets out of bound. The time window 0.01 s $< t < 0.015$ s is displayed in figure 5.10(b) with the instable solution excluded for the sake of clarity. In this picture, one can clearly see that a decreasing value of χ leads to better accuracy. This illustrates the dilemma of
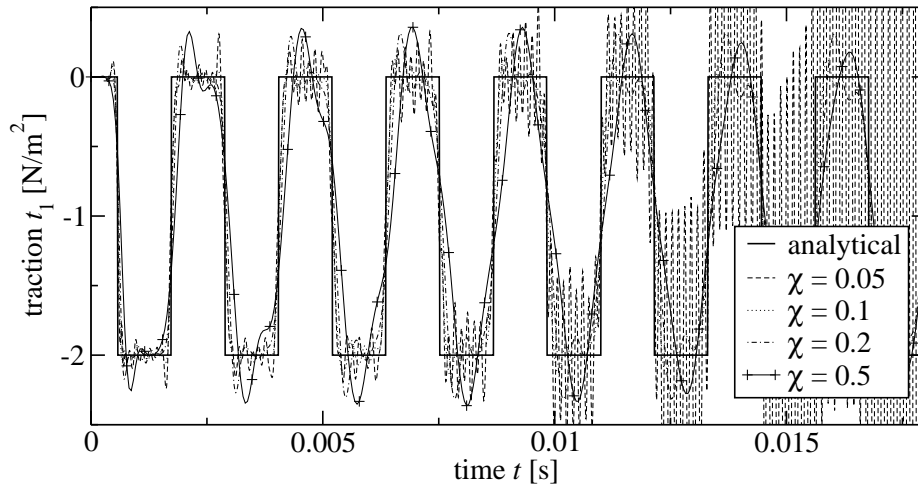
(a) The whole time range
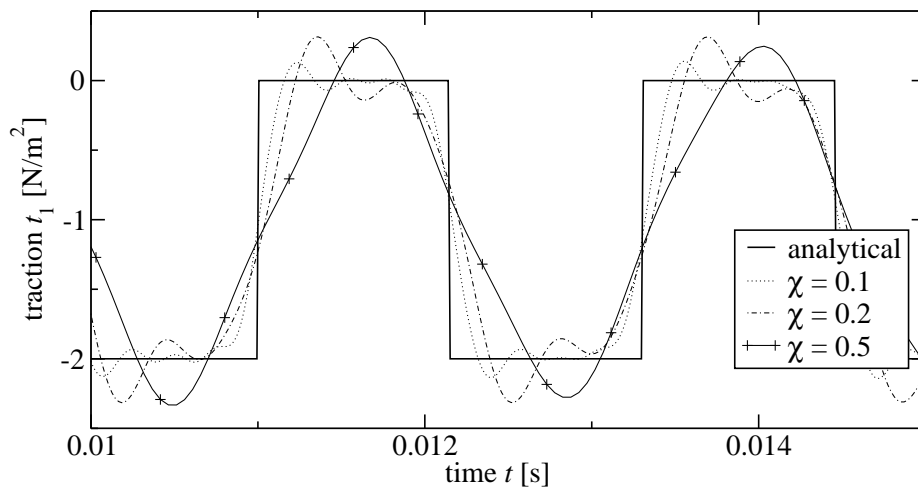
(b) Results at larger times.

Figure 5.11: Surface traction at fixed end of the two-dimensional elastodynamic solid against time for various χ and fixed mesh size $h = 0.5\,\text{m}$.

time-domain boundary element methods that, on the one hand, higher accuracy is obtained by smaller time steps (as in any other time integration method), but, on the other hand, the solutions becomes instable if the time step is below a certain threshold. It has to be noted that the situation is even worse in classical time-domain boundary elements [70] where this threshold is higher than in the considered convolution quadrature method, see also Schanz [98–100] for such comparisons.

Figure 5.11 contains the results of the surface traction at the Dirichlet boundary for the very same cases as in figure 5.10. Apparently, the instability for $\chi = 0.05$ occurs a lot earlier in the traction solution than in the displacement solution as it can be seen in figure 5.11(a). Moreover, the different solution curves shown in figure 5.11(b) for the time
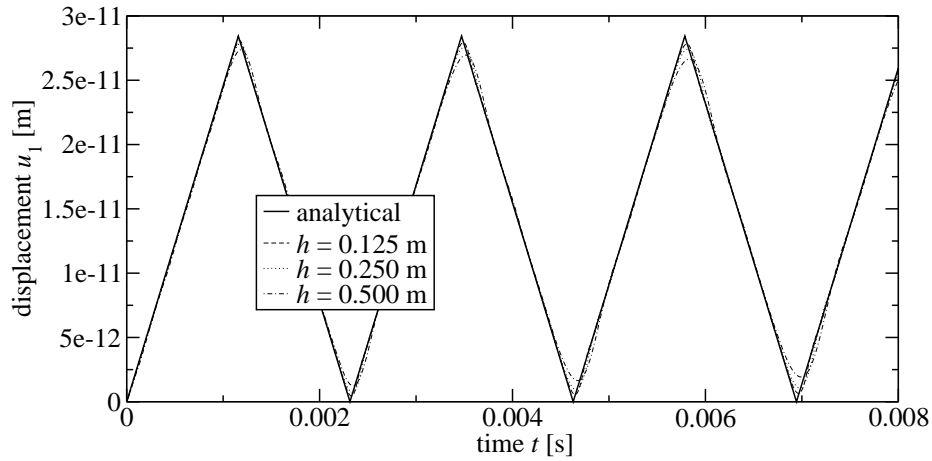
(a) Tip displacement.
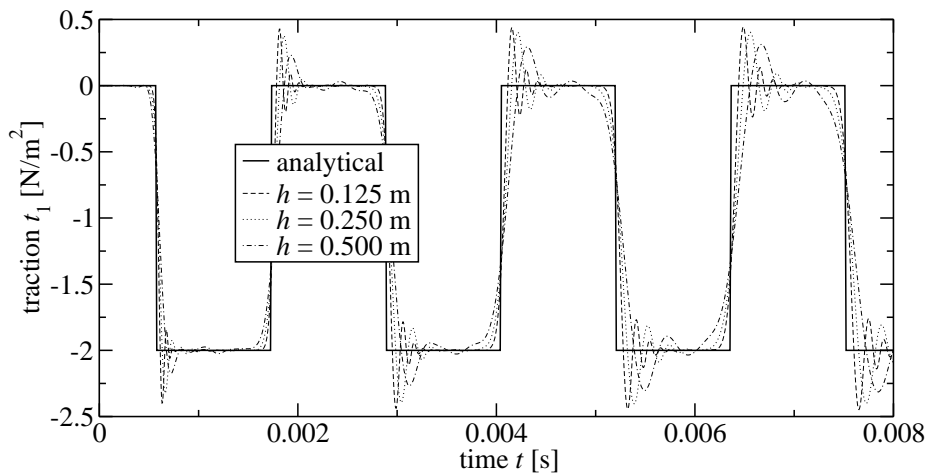
(b) Surface traction.

Figure 5.12: Tip displacement and surface traction of the two-dimensional elastodynamic solid against time for a fixed CFL number $\chi = 0.2$ and different mesh sizes.

window $0.01\,\text{s} < t < 0.015\,\text{s}$ show more clearly the respective qualities of the approximations for different CFL numbers. With decreasing χ the curves get closer to the piecewise constant traction curve of the analytical solution.

Finally, in figure 5.12 the solution curves for different mesh sizes are displayed. The tip displacement is shown in figure 5.12(a) and the corresponding surface tractions at the Dirichlet boundary in figure 5.12(b). Obviously, the results get closer to the analytical solution with decreasing mesh sizes. Whereas the displacement solutions in figure 5.12(a) are very close to the analytical solution and only deviate at the minima and maxima, the traction solutions still differ significantly from the reference curve. One can observe that with decreasing mesh size the solution gets closer to the piecewise constant graph of the analytical solution but oscillates greatly after each jump discontinuity. This behavior is
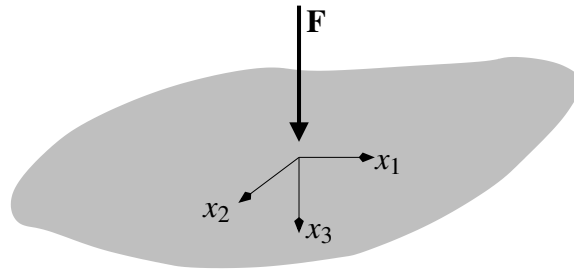
Figure 5.13: Elastic halfspace with point force.

similar to the well-known Gibbs phenomenon occurring in Fourier series of such discontinuous functions. The overshoots get more pronounced but also more concentrated to the discontinuity with decreasing mesh size.

5.1.3 Elastic halfspace with surface point force

This subsection is concerned with the elastic halfspace in three dimensions, i.e., in the following it holds

$$\Omega = \left\{ \mathbf{x} \in \mathbb{R}^3 : x_3 > 0 \right\} \quad \text{and} \quad \Gamma = \left\{ \mathbf{x} \in \mathbb{R}^3 : \mathbf{x}_3 = 0 \right\} . \tag{5.6}$$

Moreover, the problem statement is such that $\Gamma_N = \Gamma$ and, consequently, $\Gamma_D = \emptyset$, which is a pure Neumann problem. The prescribed surface tractions are zero everywhere but at the origin, where a point force in direction of the x_3-axis is acting. The prescribed Neumann datum has thus the form $\mathbf{g}_N = \mathbf{F}\delta(\mathbf{x})$ with $\mathbf{F} = (0,0,F)^\top$. Now, F is either a constant value, $F = F_0$, for the static case or a step function in time, $F = F_0 H(t)$, for the dynamic case. Note that the Dirac delta impulse $\delta(\mathbf{x})$ on a surface has the unit $1/\text{m}^2$ such that $\int_\Gamma \delta(\mathbf{x}) \, d\mathbf{x} = 1$ holds and the above Neumann datum is meaningful. The analytical solutions to both static and dynamic cases are given in the appendix B.2. Since Ω is an unbounded domain, the treatment of these problems by means of a standard finite element discretization is inapt. The necessary truncation of the spatial discretization would introduce some artificial boundary. Whereas in the static case the local effects around the point source can still be represented by a finite element method with a large mesh, in dynamics non-physical wave reflections would occur due to this artificial boundary. Therefore, these reflected waves pollute significantly the numerical solution. The boundary element method, on the other hand, does not suffer from this effect. Although the discretization of the unbounded boundary Γ has to be truncated somewhere, the introduced artificial effects are negligible. Hence, the above described problem is analyzed in the following using only boundary element discretizations. See also the book of Givoli [34] for a discussion of the applicability of numerical methods to problems with unbounded domains.
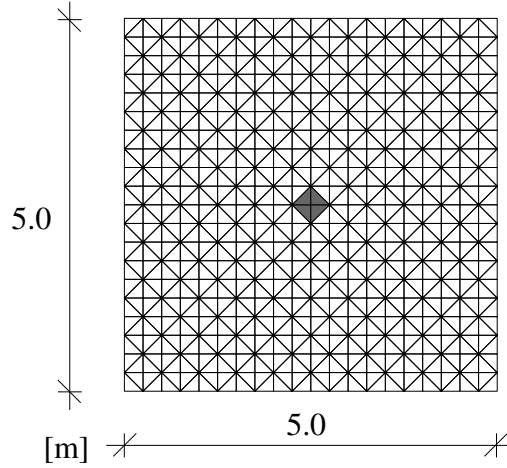
Figure 5.14: Discretization of the surface patch with 800 triangles. The shaded area is subjected to a vertical traction field.

Static case.   The numerical solution of the elastostatic system of equations (2.25) is considered in this paragraph. Let $F_0 = 1\,\mathrm{N}$, i.e., the applied static force be of unit magnitude. The surface Γ described by equation (5.6) is now represented by the surface patch

$$\Gamma_h = \left\{ \mathbf{x} \in \mathbb{R}^3 \colon x_3 = 0, (x_1, x_2) \in (-2.5\,\mathrm{m}, 2.5\,\mathrm{m})^2 \right\} \subset \Gamma. \tag{5.7}$$

This computational surface patch is discretized by surface triangles and the four triangles surrounding the origin are loaded by a constant traction field $g_{N,h}$ such that an equivalent force of $1\,\mathrm{N}$ is applied, i.e., $\int_{\Gamma_h} g_{N,h}(\mathbf{y})\,\mathrm{d}\mathbf{y} = 1\,\mathrm{N}$. Three different meshes are used for the simulation of this problem with $h = 0.5\,\mathrm{m}$, $0.25\,\mathrm{m}$, and $0.125\,\mathrm{m}$, whereas the middle one with 800 triangles is shown in figure 5.14. The chosen material is soil from table 5.1.

The outcome of the simulation with these three different meshes is displayed in figure 5.15 together with the analytical solution due to Boussinesq, see equation (B.3) in appendix B. The markers actually represent the numerical values along a coordinate line $x_2 = x_3 = 0$ through the origin such that the radial displacements in figure 5.15(a) are in fact the component u_1 and the tangential displacements are the component u_2. Approaching the origin, the analytical solution has singularities of order $\mathcal{O}(|\mathbf{x}|^{-1})$ in both the radial and the vertical displacement components and a decay behavior of the same order for large values of $|\mathbf{x}|$. The singularities around the origin cannot be reproduced by the numerical approximation, because a point force is not representable by the trial functions used for the approximation of the surface traction $\mathbf{t}$. Therefore, the deviations between Boussinesq and boundary element solution close to the origin are due to the numerical model itself. Nevertheless, the finer the mesh size the closer the approximation gets to the poles at the singularities. This fact is clearly shown in figures 5.15(a) and 5.15(c). A second modeling error is the representation of the unbounded surface Γ by the bounded set Γ_h as given in equation (5.7). It can be seen in figures 5.15(a) and 5.15(c) that the approximate solution values are very close to the Boussinesq solution at distances $2.0\,\mathrm{m} < |\mathbf{x}| < 1.0\,\mathrm{m}$ but deteriorates again beyond $|\mathbf{x}| > 2.0\,\mathrm{m}$ towards the end of the surface discretization. It can be expected that
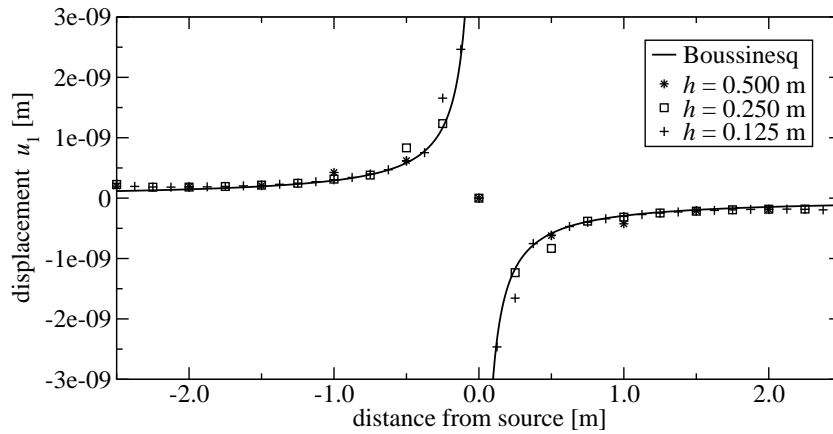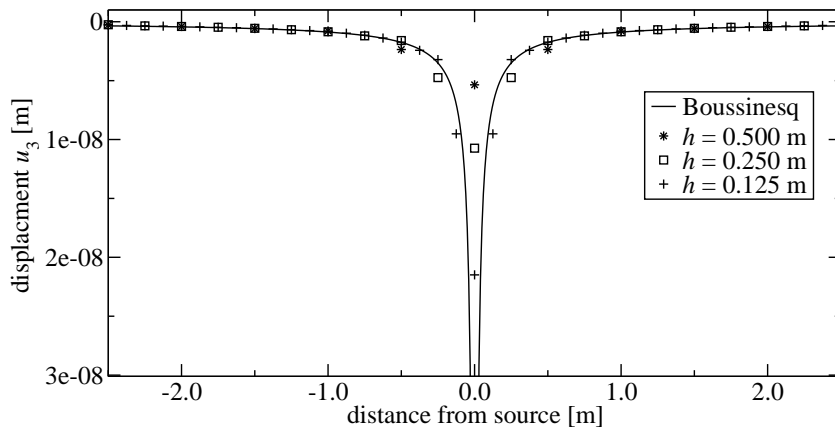
(a) Radial displacements.
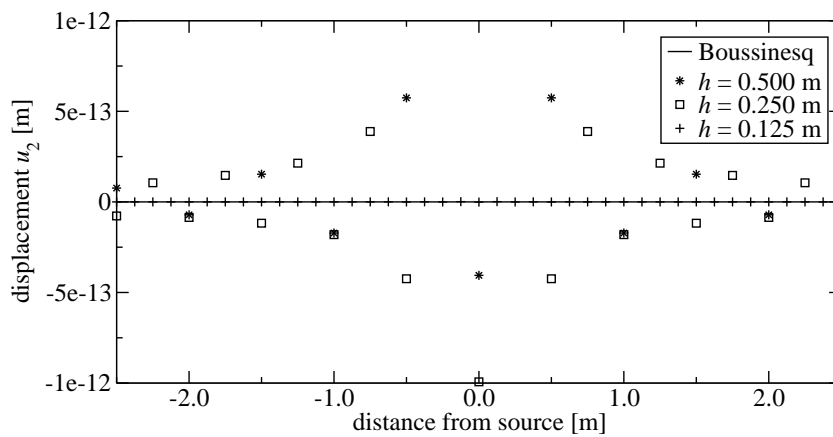
(b) Tangential displacements.

(c) Vertical displacements.

Figure 5.15: Boundary element solution of the static halfspace problem — radial, tangential and vertical displacements along the coordinate line $x_2 = x_3 = 0$ and $-2.5\,\mathrm{m} < x_1 < 2.5\,\mathrm{m}$.
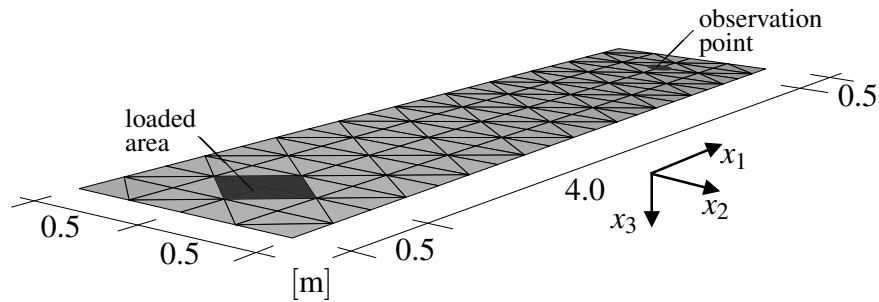
Figure 5.16: Halfspace discretization with 160 triangles, loaded area and observation
point. Note that the coordinate system is shifted from the origin.

this deviation is the truncation error, i.e., the above mentioned error in the model due to
the truncation of the discretization.

A good measure of the error in the approximate solution is the result of the tangential
displacement shown in figure 5.15(b). Since the Boussinesq solution is exactly zero for
this displacement component, the numerical outcome represents the absolute error of it.
It can be seen that the two coarser meshes with $h = 0.5\,\mathrm{m}$ and $h = 0.25\,\mathrm{m}$, respectively,
give results of around four orders of magnitude smaller than in the other components. The
maximal deviation for the finest mesh is even two orders of magnitude smaller and cannot
be distinguished from the zero line in the scale of figure 5.15(b).

In conclusion, one can state that the presented boundary element formulation is capable
of representing static problems with open surfaces. Only the results close to the necessary
mesh truncation are critical. It has to be noted that the modeling error at the point force
does not alter this statement because it is independent of the topology of Ω.

Dynamic case.   In this paragraph, the applied point force varies now as a step function in
time. For this special case analytical solutions are available due to Pekeris [85] and given
in appendix B.2.2.

A surface discretization with 160 triangles is depicted in figure 5.16 where each triangle
has catheti of length $h = 0.25\,\mathrm{m}$. A second spatial discretization is used which has 320
triangles and is obtained by bisection of the lengths in x_1-direction. These two meshes
are referred to as mesh 1 and mesh 2 in the following. In figure 5.16, also the loaded
triangles are emphasized by the shaded region. At $4.0\,\mathrm{m}$ distance from the center of this
loaded area the observation point is located at which the vertical and radial displacements
are detected.

Figure 5.17 contains the outcome of the boundary element simulation of this surface pulse
problem. The two meshes are compared with each other and each mesh has been used
with two different time steps such that $\chi = 0.2$ and $\chi = 0.3$. For the value of h in the
definition of the CFL number (5.5) the shorter side of the triangle is used, i.e., $h = 0.25\,\mathrm{m}$
for mesh 1 and $h = 0.125\,\mathrm{m}$ for mesh 2. As a comparison the numerical solution curves
are plotted together with the analytical solution of Pekeris [85]. Like in the previous case
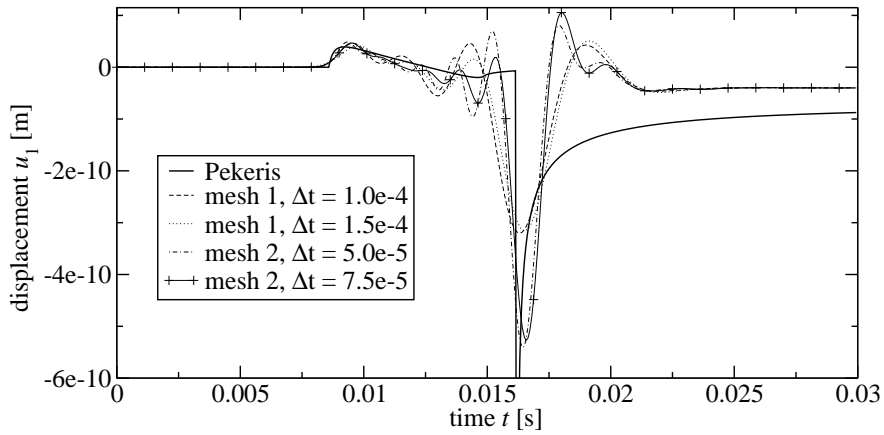
(a) Radial displacements
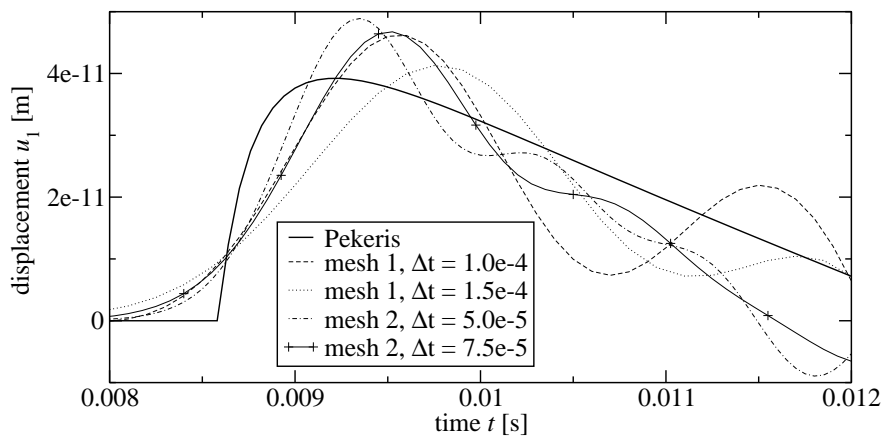
(b) Radial displacements (magnified)
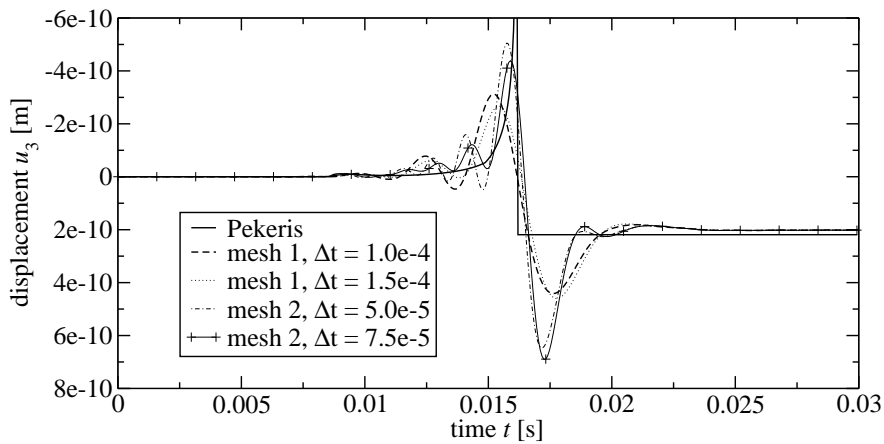
(c) Vertical displacements

Figure 5.17: Boundary element solution of the surface pulse problem — radial and vertical displacements at the observation point shown in figure 5.16.

of the elastostatic analysis of the halfspace, the point source cannot be modeled exactly and it is represented by a constant traction load over a certain small area, see figure 5.16. Therefore, one cannot expect the arrival of the pressure wave at the same time instant and with the same sharp front as in the analytical model. Nevertheless, the numerical results imitate well the arrival of the pressure wave as it can be seen in figure 5.17(a) and even better in figure 5.17(b), where the critical region is magnified. After the pressure wave the shear wave arrives at the observation point causing a slight decay in the radial and vertical displacements. This is followed by the Rayleigh surface wave which contains a singularity in the analytical limit as apparent in figures 5.17(a) and 5.17(c). Cf. the books of Achenbach [1] and Graff [37] for the theoretical background of these three different wave types. Although this large displacement phenomenon is reproduced well by the numerical approximations, it causes a severe overshoot after the surface wave has passed. The analytical solution coincides with the Boussinesq solution of the previous paragraph for the vertical displacements right after the Rayleigh wave has passed and for the radial displacements if time gets large, see also figure B.3. This static limit is reproduced by the approximations only in the vertical components, whereas the radial component deviates significantly from the static solution. Compare the right sides of figures 5.17(a) and 5.17(c) for this effect.

Comparing the different discretizations, one can see that the difference between different time steps for the same mesh size is only apparent in the magnification of figure 5.17(b). But in the total view the curves for different time steps are very close to each other. The difference between mesh 1 and mesh 2 is most significant in the way the singularity of the Rayleigh wave is captured. The finer discretization of mesh 2 reproduces a lot better the peak of this surface wave but also significant overshoots occur after the wave has passed.

In summary, the presented boundary element solution of the surface pulse problem reproduces well some basic characteristics of the physical phenomenon. The arrival and magnitude of the pressure wave front are approximated in a good manner. Moreover, the peak of the surface wave is clearly visible, especially with the finer discretization. Nevertheless, oscillations and overshoots occur after the different wave types arrive and significantly pollute the solution.

5.2 Coupled Solutions

Finally, in this section the coupling algorithm presented in chapter 4 is applied to some test cases. These are mainly verification examples as the cantilever beam and the rod with longitudinal step load. A possible application of the proposed methodology are the static and dynamic analyses of a foundation on an elastic halfspace which are presented in the end of this section.
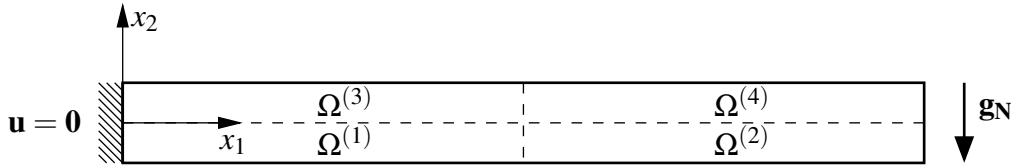
Figure 5.18: Model of cantilever beam with 4 subdomains.

5.2.1 Cantilever beam

The first considered test case for the coupling algorithm of this work is the cantilever beam. Again, the geometry has the length $\ell = 10\,\text{m}$ and width and height $b = 1\,\text{m}$. The considered material is steel from table 5.1. This beam is now represented by a d-dimensional domain $\Omega = (0, \ell) \times (0, b)^{d-1}$ which is subdivided into four equally sized subdomains $\Omega^{(r)}$, $r = 1, \ldots, 4$. This constellation is shown in figure 5.18 together with boundary conditions of the model for the two-dimensional model. At the right end at $x_1 = \ell$ a downward traction field of constant value $\mathbf{g}_N = -1\,\text{N/m}^2$ is applied. Obviously, subdomains $\Omega^{(2)}$ and $\Omega^{(4)}$ are *floating* and, therefore, undergo the solution procedure described in subsection 4.3.1.

At first, a two-dimensional analysis of this problem is considered. In any of the tested cases, the subdomains $\Omega^{(1)}$ and $\Omega^{(4)}$ are treated by the same approximation method with the same mesh width $h_1 := h^{(1)} = h^{(4)}$. Similarly, subdomains $\Omega^{(2)}$ and $\Omega^{(3)}$ are treated equally and have $h_2 := h^{(2)} = h^{(3)}$ as the mesh size. Table 5.2 shows the mesh sizes and total number of elements for boundary and finite element discretizations that are used in this example. A *fine* and a *coarse* mesh are used for better comparison of the different

mesh	h_1 [m]	$N_{1,\text{BEM}}$	$N_{1,\text{FEM}}$	h_2 [m]	$N_{2,\text{BEM}}$	$N_{2,\text{FEM}}$
fine	$1/10$	110	250	$1/8$	88	160
coarse	$1/6$	66	90	$1/8$	88	160

Table 5.2: Parameters of fine and coarse meshes for the two-dimensional model.

cases. These two meshes are used for the three cases of a BEM-BEM coupling, i.e., using a boundary element discretization for all subdomains $\Omega^{(1)}$ to $\Omega^{(4)}$, a FEM-FEM coupling with a pure finite element approach for all subdomains, and the hybrid situation BEM-FEM, where subdomains $\Omega^{(1)}$ and $\Omega^{(4)}$ are treated by a boundary element discretization whereas for subdomains $\Omega^{(2)}$ and $\Omega^{(3)}$ the finite element method is used. One can easily deduce from the mesh sizes given in table 5.2 that in every possible combination the interfaces are nonconforming. This is obviously done in order to point out that the methodology works for such situations rather than really needing nonconforming interfaces for such a simple test case.

Figure 5.19 shows the outcome for this two-dimensional analysis of the cantilever beam. In order to make the differences between the solution curves more visible, only the coordinate range $4\,\text{m} < x_1 < 6\,\text{m}$ is displayed. The curves represent the line of deflection for $x_2 = 0$,
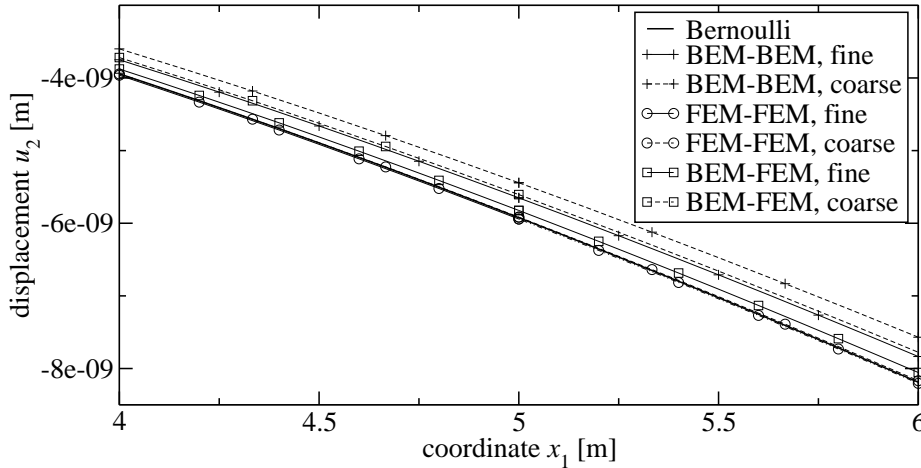
Figure 5.19: Two-dimensional coupled analysis of the cantilever beam — deflection in the interval $4\,\mathrm{m} < x_1 < 6\,\mathrm{m}$.

i.e., the centerline of the domain, cf. figure 5.18. Considering each of the three coupling strategies (BEM-BEM, FEM-FEM, or BEM-FEM), the finer mesh always yields better results than the coarser mesh similar to the results shown in subsection 5.1.1. Obviously, the results for a FEM-FEM coupling are closest to the reference solution of the Bernoulli beam theory as in equation (5.1). The outcome of the hybrid approach, i.e., BEM-FEM, are still better than in the pure BEM-BEM analysis. This fact is confirmed by the observations made in subsection 5.1.1 which showed a better convergence of the finite element method than the boundary element method for the given example.

The same analysis is now carried out for a three-dimensional model of the cantilever beam. Again the three coupling cases (BEM-BEM, FEM-FEM, and BEM-FEM) are considered each with a fine and a coarse discretization according to table 5.3. The combination BEM-BEM with the fine discretization is not considered because it requires to much computer memory.

mesh	h_1 [m]	$N_{1,\mathrm{BEM}}$	$N_{1,\mathrm{FEM}}$	h_2 [m]	$N_{2,\mathrm{BEM}}$	$N_{2,\mathrm{FEM}}$
fine	$1/10$	3200	2500	$1/8$	2048	1280
coarse	$1/6$	1152	540	$1/8$	2048	1280

Table 5.3: Parameters of fine and coarse meshes for the three-dimensional model.

In figure 5.20, the discretization for the BEM-FEM coupling with the coarse meshes due to table 5.3 is depicted. The front side of the model is the side of prescribed homogeneous Dirichlet data whereas on the (not visible) back side the downward traction field is applied, compare figure 5.18. Clearly, the employed discretizations of each subdomain are nonconforming. The nodes at the interfaces do not match and, moreover, the approximation orders
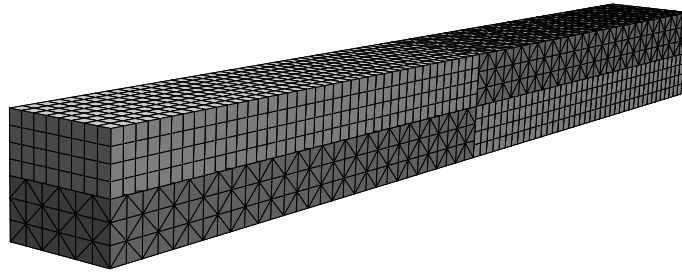
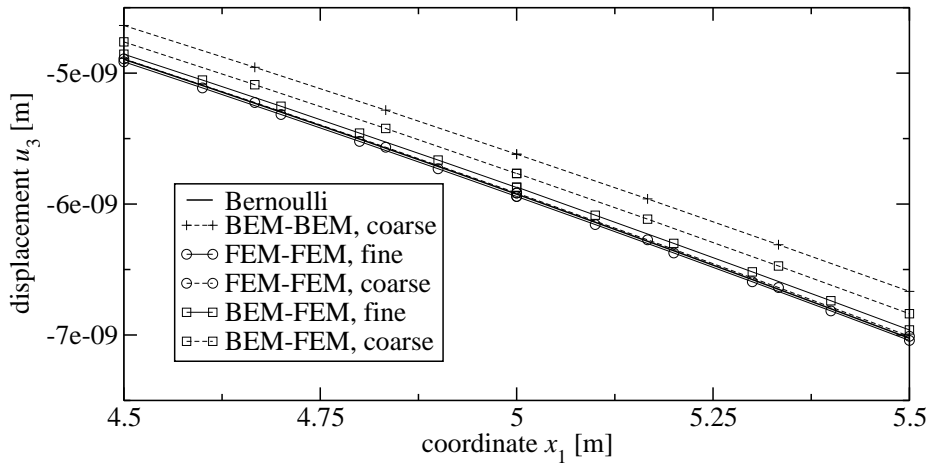Figure 5.20: Discretization of the three-dimensional model with boundary and finite elements.

Figure 5.21: Three-dimensional coupled analysis of the cantilever beam — deflection in the interval $4.5\,\text{m} < x_1 < 5.5\,\text{m}$.

are different. The boundary elements are linear surface triangles and the restrictions of the finite element shape functions to the surface are bilinear.

The outcome of the computations for this three-dimensional case is given in figure 5.21. As before, the deflection curves are plotted together with the solution due to the Bernoulli beam theory. Here, only the range $4.5\,\text{m} < x_1 < 5.5\,\text{m}$ is shown such that the curves are distinguishable. The same observations as in the two-dimensional case can be made. The FEM-FEM coupling yields better results than the BEM-FEM coupling. The latter coupling gives in turn better results than the pure boundary element approach. Of course, in all cases the fine discretization performs better than the coarse discretization.

In summary, it can be stated that the proposed algorithm for the combination of boundary and finite element discretizations with nonconforming interfaces works well for static problems. Moreover, the treatment of floating subdomains due to Farhat and Geradin [26] as outlined in subsection 4.3.1 is successful and the generalized inverses are computed correctly. The considered case of the cantilever beam with the partitioning as shown in figure 5.18 contains two non-floating subdomains and two totally floating subdomains. Due to the fact that the subdomains $\Omega^{(2)}$ and $\Omega^{(4)}$ have no prescribed Dirichlet datum at
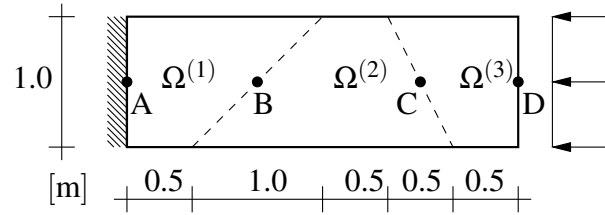
Figure 5.22: Two-dimensional model for the rod with three subdomains.

all, the computation of the rank deficiency of the corresponding system matrices is trivial. Both subdomains have the full set of three (six) rigid body modes for two (three) space dimensions. Nevertheless, the method for detecting the rigid body modes works well as it detected that the subdomains $\Omega^{(1)}$ and $\Omega^{(3)}$ are fully constrained and do not have any rigid body modes. Finally, due to the partitioning in four subdomains at $x_1 = 5\,\mathrm{m}$, $x_d = 0$, cross points occur. Whereas these points need special considerations in the original FETI method [29], the considered approach with Lagrange multiplier fields is robust with respect to such situations.

5.2.2 Rod with longitudinal step load

In this subsection, the dynamic analysis of the problem already considered in subsection 5.1.2 and depicted in figure 5.6 is now treated by means of the presented coupling strategy.
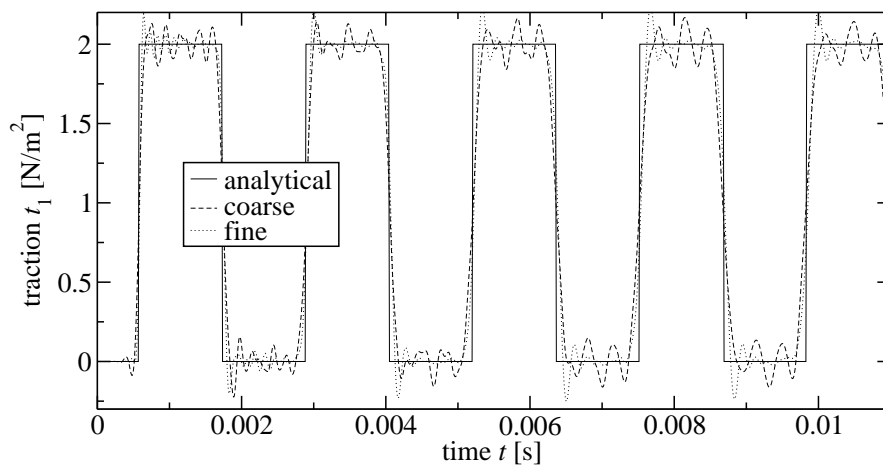
Two-dimensional elastodynamics. As a first test, the two-dimensional elastodynamic system is considered with the somewhat arbitrary partitioning of the domain as shown in figure 5.22. The material is steel from table 5.1 and the respective mesh size of subdomain $\Omega^{(r)}$ is denoted by $h^{(r)}$. Denoting by x_1 the coordinate direction of the load and by x_2 the orthogonal direction, the domain under consideration can be expressed as $\Omega = \left\{ \mathbf{x} \in \mathbb{R}^2 : 0 < x_1 < 3\,\mathrm{m}, 0 < x_1 < 1\,\mathrm{m} \right\}$ and the three subdomains are as shown in figure 5.22. A boundary element analysis is now carried out for this partitioned problem where the mesh sizes of each subdomain are chosen differently.

Two different spatial discretizations are used. The mesh sizes for the subdomains $\Omega^{(1)}$ and $\Omega^{(3)}$ are fixed as $h^{(1)} = h^{(3)} = 0.25\,\mathrm{m}$ and with five elements at the interfaces. The mesh size for the middle domain $\Omega^{(2)}$ is varied. The coarse mesh refers to $h^{(2)} = 0.5\,\mathrm{m}$ with two elements at each interface and the fine mesh has a mesh size $h^{(2)} = 0.25\,\mathrm{m}$ and four interface elements. Note that the mesh sizes $h^{(r)}$ only refer lines parallel to the coordinate axes, whereas at the interfaces it is adapted to fill the length. The time step is fixed to $\Delta t = 5.79 \cdot 10^{-6}\,\mathrm{s}$ such that the CFL number varies between $\chi = 0.12$ and 0.24 for all subdomains.
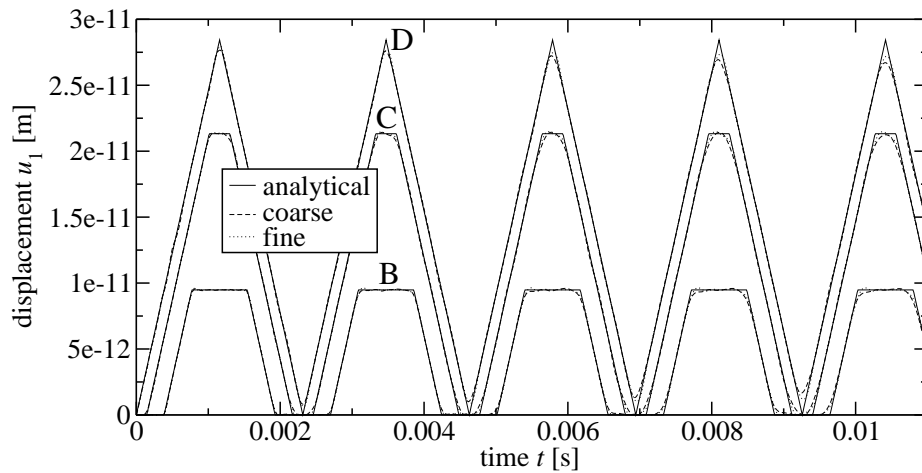
(a) displacements

(b) tractions

Figure 5.23: Coupled boundary element simulation of the rod for two-dimensional elasto-dynamics — tip displacements are given for points B, C, and D and surface tractions at point A against time.

In figure 5.23, the outcome of the coupled analysis is plotted. The displacements are given in figure 5.23(a) for the points B, C, and D, which correspond to $x_1 = 1.0$ m, 2.25 m, and 3.0 m along the middle line, see figure 5.22. The results are very close to the analytical solution due to appendix B.1 for both the coarse and the fine meshes. Moreover, the solution curves are very smooth and noticeable reflections due to the artificial interfaces do not appear. The traction plots in figure 5.23(b) show the typical oscillations as in case of the single domain solutions of subsection 5.1.2. Similarly, the finer mesh shows a better congruence with the analytical piecewise constant curve but has higher overshoots after the jumps. Any alterations of the solution due to the interfaces are not visible.

Three-dimensional acoustic fluid. Another test case is to model the rod as an acoustic fluid in three spatial dimensions where the material air from table 5.1 is used. Therefore, the domain $\Omega = (0, 3\,\mathrm{m}) \times (0, 1\,\mathrm{m})^2$ is subdivided into three cubes with side length of $1\,\mathrm{m}$ each. These subdomains $\Omega^{(1)}$, $\Omega^{(2)}$, and $\Omega^{(3)}$ are then discretized independently. The outer regions $\Omega^{(1)}$ and $\Omega^{(3)}$ are treated by a boundary element discretization with mesh size of $h^{(1)} = h^{(3)} = 0.25\,\mathrm{m}$ such that the surfaces consist of 192 triangles each. The middle domain is discretized by finite elements with $h^{(2)} = 0.5\,\mathrm{m}$ and $0.2\,\mathrm{m}$ such that two different finite element meshes with 8 and 125 hexahedra, respectively, are used. Confer figure 5.24 for a visualization of the finer discretization. These two discretizations are referred to as the coarse and the fine mesh.

The discretization shown in figure 5.24 is obviously nonconforming across the interfaces and the coarser discretization with $h^{(2)} = 0.5\,\mathrm{m}$, too. Similar to the previous example, several observation points are used. The pressure is plotted for the points B, C, and D which are located along the middle axis $x_2 = x_3 = 0.5\,\mathrm{m}$ at positions $x_1 = 1\,\mathrm{m}$, $2\,\mathrm{m}$, and $3\,\mathrm{m}$, respectively. The surface flux is considered at the point A with coordinate $x_1 = 0$ on the same axis as the other points. The time step is chosen fixed to $\Delta t = 1.46 \cdot 10^{-4}\,\mathrm{s}$ and the CFL number in the boundary element subdomains $\Omega^{(1)}$ and $\Omega^{(3)}$ has thus the value $\chi = 0.2$. In the finite element subdomain $\Omega^{(2)}$ this number is either 0.1 or 0.25 for the coarse and the fine meshes, respectively.

In figure 5.25, the numerical outcome of this analysis is shown. Again, the results for the first variable, i.e., now the pressure p, are very smooth and close to the analytical solution. Also, the use of a finer discretization for the middle domain gives a significantly better result than for the coarser one. Contrary to the results of the single domain approach of subsection 5.1.2, the coarse mesh shows slight deviations from the analytical curve along the straight parts and not only at the turning points. These shakes clearly denote spurious reflections from the artificial interfaces. Nevertheless, this effect is not noticeable for the finer finite element discretization. The surface flux q has a similar behavior as the tractions in the elastodynamic example. The coarse mesh gives a rather bad agreement with the piecewise constant analytical curve. The fine mesh yields results which are significantly better but have the tendency to overshoot at the jumps.

Concluding these two examples, it can be stated that the proposed coupling algorithm is useful for this dynamic problem. The propagation of the impulse wave is represented well in the first variable, surface displacements or pressure. The damping is small and a phase shift is not visible. Although worse, the outcome for the second variable, surface tractions or flux, is still in good agreement with the analytical solution considering the complexity of the numerical approximation of a piecewise constant function.

5.2.3 Elastic halfspace with foundation

As an example for possible applications of the proposed coupling method the static and dynamic analyses of an individual footing on an elastic halfspace are considered. The
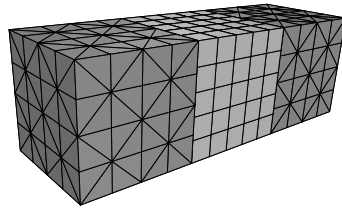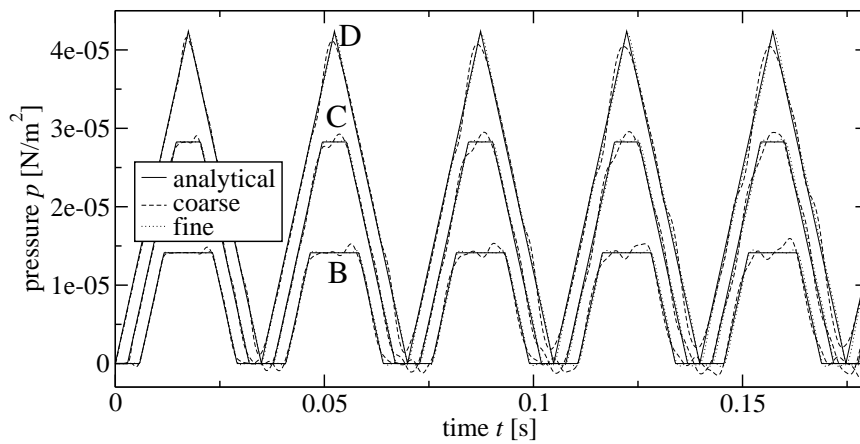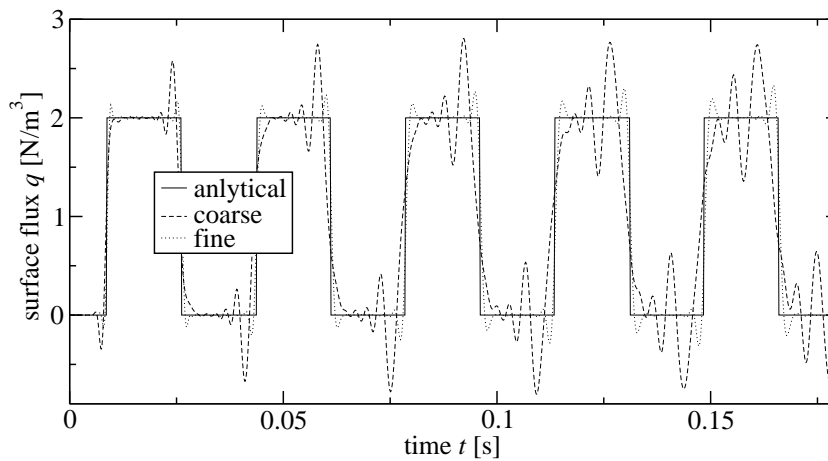
Figure 5.24: Boundary element and finite element discretization of the dynamic rod.

(a) pressure

(b) surface flux

Figure 5.25: Coupled boundary and finite element solution for the three-dimensional acoustic fluid — pressures at points B, C, and D and surface flux at point A against time.
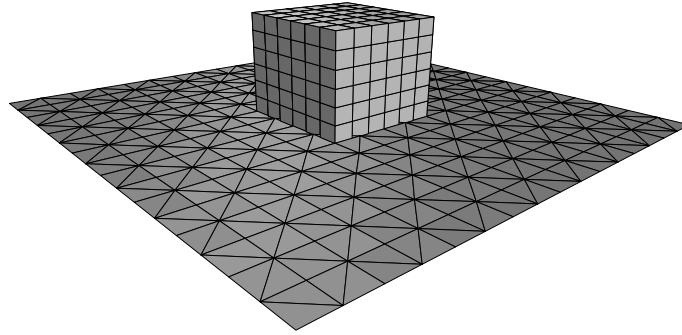
Figure 5.26: Discretization of foundation and soil for the static analysis.

foundation is made of concrete and, therefore, assumes the material parameters as shown in table 5.1. For simplicity, the foundation has a cuboid shape and is subjected to a vertical, uniformly distributed load on its top surface. The elastic halfspace is taken as the soil from table 5.1. In order to emphasize the potential of this method, the foundation is discretized by a finite element and the soil by a boundary element method. By means of this choice, the respective advantages of each method are made use of, i.e., the boundary element method for unbounded domains and the finite element method for bounded domains, possibly occupied by a nonlinear material.

Static analysis.   At first, the static case is considered. Therefore, the above described problem of the individual footing is discretized as shown in figure 5.26. The patch of triangles $\Omega^{(1)} = (0,5\,\text{m})^2 \times \{0\}$ represents the halfspace. The cubical foundation occupies the domain $\Omega^{(2)} = (0,1.25\,\text{m})^2 \times (0,1\,\text{m})$ with a shift in the origin such that it is centered on the plane. The upper surface of the foundation is subjected to a constant pressure of $0.64\,\text{N}/\text{m}^2$. The mesh sizes are $h^{(1)} = 5/16\,\text{m}$ and $h^{(2)} = 5/24\,\text{m}$ for the triangular boundary elements and the hexahedra finite elements, respectively. These sizes correspond to the discretization shown in figure 5.26. Additionally, a finer mesh is used for the halfspace with mesh size $h^{(1)} = 5/32\,\text{m}$, whereas the mesh of the finite element subdomain $\Omega^{(2)}$ stays the same. The expressions *coarse* and *fine* in figure 5.27 refer to these different values of the mesh size $h^{(1)}$.

The outcome of this static analysis is given in the figures 5.27(a) and 5.27(b) for the vertical and the horizontal displacements, respectively. The lines show the displacements of the lower surface of the foundation and of the soil along the axis $x_1 = 2.5\,\text{m}$ on the surface at $x_3 = 0$. Both results somehow resemble the displacements of the elastic halfspace under a point load for points away from the foundation, see subsection 5.1.3 and the Boussinesq solution in appendix B.2.1. Moreover, the effects due to the truncation of the mesh are visible at coordinates $|x_1| > 2.0\,\text{m}$. Whereas the results for points on the surface away from the foundation are almost identical for the coarse and the fine mesh, the subsidence right under the foundation differs. But this difference is only at about 3 % of the values for the coarser mesh and bigger deviations for even finer meshes are not expected.
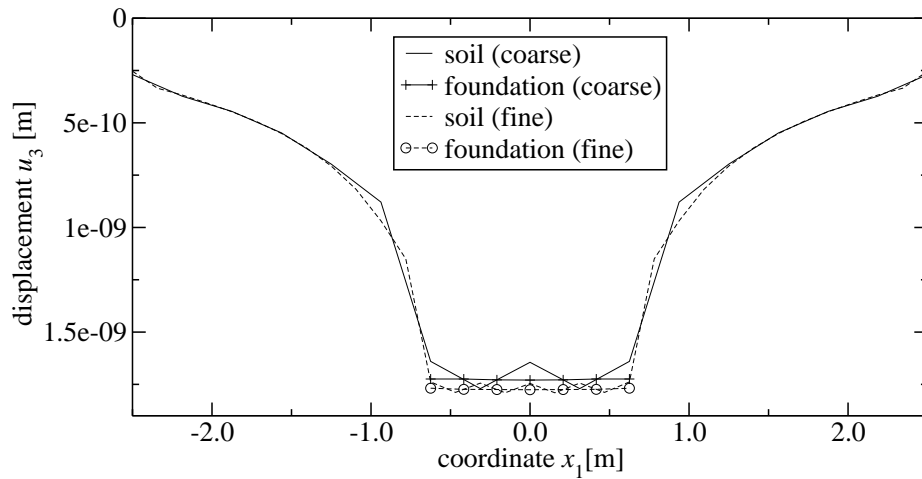
(a) Vertical displacements
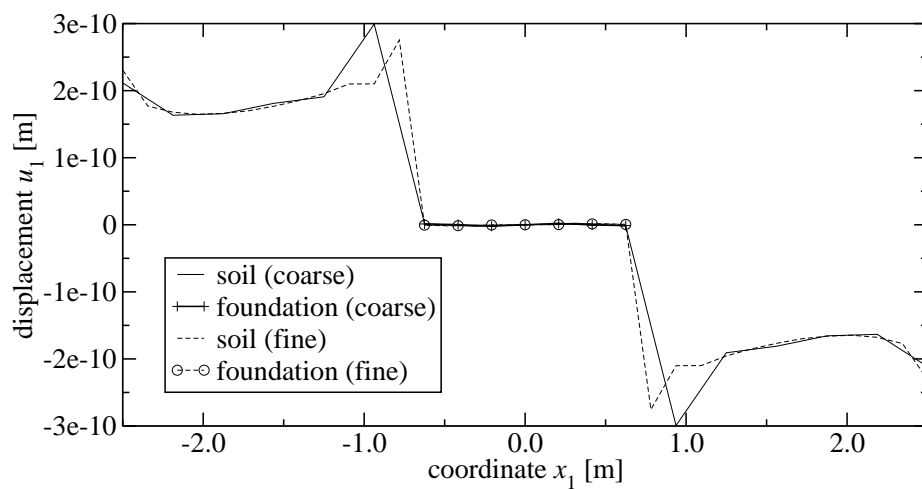
(b) Horizontal displacements

Figure 5.27: Static analysis of a foundation on an elastic halfspace — vertical and horizontal displacements along the coordinate line $2.5\,\text{m} < x_1 < 2.5\,\text{m}$, $x_2 = x_3 = 0$.

In figure 5.27(a), an interesting effect becomes visible. Due to the choice of nonconforming interfaces with piecewise constant Lagrange multipliers (cf. section 4.4 for details), voids and overlaps appear at the interface between halfspace and foundation. Nevertheless, the integral

$$\int_{\Gamma^{(12)}} \lambda\,(u_\Gamma^{(1)} - u_\Gamma^{(2)})\,\mathrm{d}s$$

vanishes and, therefore, the interface condition (4.8a), i.e., $u_\Gamma^{(1)} = u_\Gamma^{(2)}$ on $\Gamma^{(12)}$, is fulfilled in an integral sense but not pointwise. Obviously, these nodal differences at the interface diminish for finer meshes as it can be seen from comparing the outcome of the two different meshes.
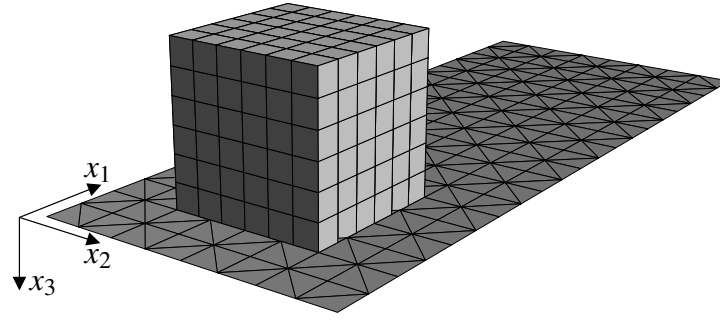
Figure 5.28: Discretization of foundation and soil for the dynamic analysis.
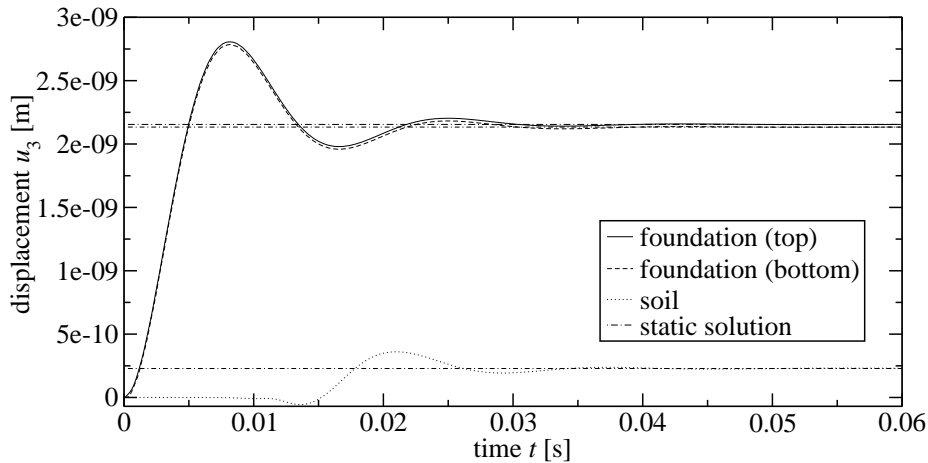

Figure 5.29: Dynamic analysis of a foundation on an elastic halfspace — vertical displacements at different positions against time.

Dynamic analysis. Here, a similar geometrical constellation is assumed. The foundation is now the cube $\Omega^{(2)} = (0, 1\,\mathrm{m})^3$ and placed on the surface patch which is given by $\Gamma^{(1)} = (0, 5\,\mathrm{m}) \times (0, 2\,\mathrm{m}) \times \{0\}$. The exact arrangement is shown in figure 5.28. The upper surface of the foundation is now subjected to a uniform load of value $1.0\,\mathrm{N/m^2}H(t)$ acting in downward direction, which is a unit step function in time. The surface patch is discretized by 320 boundary elements, the foundation by 216 finite elements and the time step of size $1.5 \cdot 10^{-4}\,\mathrm{s}$.

Using the coordinate system shown in figure 5.28, the vertical displacements at the points $(1\,\mathrm{m}, 1\,\mathrm{m}, -1\,\mathrm{m})$, $(1\,\mathrm{m}, 1\,\mathrm{m}, 0)$, and $(4.5\,\mathrm{m}, 1\,\mathrm{m}, 0)$, which correspond to the top midpoint of the foundation, the bottom midpoint, and a point on the surface of the soil at $3.5\,\mathrm{m}$ distance from the latter point in x_1-direction, respectively. The outcome of the numerical analysis for these three points is given in figure 5.29. Obviously, the result for the bottom point of the foundation is slightly shifted with respect to the results of the top point. On the one hand, the impulse arrives later since it has to travel vertically through the foundation but this horizontal shift is almost negligible due to the fast wave speed in the chosen concrete (compare the respective wave speeds c_1 of soil and concrete in table 5.1). On the other

hand the vertical displacement of the top point has to be the sum of the vertical displacement of the bottom point and the vertical compression of the foundation itself. The vertical displacement at the third point away from the foundation is zero until arrival of the compression wave similar to the analysis of the surface pulse in subsection 5.1.3. Similarly, the arrivals of the shear wave and the slightly slower Rayleigh wave are noticeable. Then, for lager times all three curves coincide with the corresponding static solution obtained by solving the same problem as a static problem. The important feature of all three curves is that no artificial wave reflection due to the interface or the mesh truncation can be detected. This demonstrates clearly the potential of the combination of finite and boundary element methods in the described manner.

6 CONCLUSION

In the previous chapters, a method has been presented which allows for the coupled solution of static and dynamic problems. The considered physical problems are the Laplace equation, elastostatics, the scalar wave equation, and elastodynamics. All of these models are treated in two and three spatial dimensions and are embedded in mixed (initial) boundary value problems. The employed numerical approximation schemes are the finite and the boundary element method. In case of dynamic problems, the system of ordinary differential equations resulting from the spatial discretizations by finite elements are treated by the Newmark method. The temporal convolution equations stemming from the boundary element discretization are integrated by means of the convolution quadrature method. Both finite and boundary element methods are used in a coupled but independent way. For this reason, the FETI-framework has been used which is a Lagrange multiplier method and allows for a method-independent formulation. Then a local Dirichlet-to-Neumann map is realized (at each time step) by the chosen discretization method of each subdomain. In principle, any discretization method which is capable of realizing such a map is suitable for this approach. Moreover, this framework is adapted such that nonconforming interface discretizations can be handled. Several test examples have been analyzed first by a single domain approach using either a finite or boundary element method. Finally, the proposed coupling strategy has been used for these test cases and the quality of the results indicates a good performance of the method.

A critical point of this work is the chosen boundary element method. The formulation is here a nonsymmetric collocation method with a totally discontinuous approximation of the Neumann data and indented collocation points. This method has been chosen, because it works with the first integral equation only. In addition, it yields a structured system of equations contrary to the common collocation approaches, where columns stemming from the discretization of the single and double layer operators are mixed according to the prescribed boundary conditions. The system of equations resulting from the chosen formulation has thus a better condition than in the classical approach. Due to the indented collocation points, the integral free term is always one half times the identity and the complicated expressions of the classical approach are thus circumvented. On the other hand, it requires a huge number of degrees of freedom because every Neumann datum is assumed to be unknown. The placement of the collocation point is rather heuristic, see remark 3.2, and the quadrature is not robust due to the quasi-singularity of the neighboring elements, see remark 3.4. In the dynamic case, the treatment of the singular integrals requires a subtraction of the singularity from the integral kernel which causes further problems as pointed out in remark 3.5. An improvement of the latter problem would be the use of a regularized double layer operator as indicated in remark 3.6. But such a representation

is only established for closed surfaces and its application to open geometries as the considered halfspace problems has not yet been established. Finally, the approximation order of the Neumann datum has to be piecewise linear in order to ensure the solvability of the final system of equations. The natural choice of piecewise constant shape functions is thus prohibited, see remark 3.3.

A remedy to most of these problems would be the use of a Galerkin method. First of all, in a Galerkin method it is needless to worry about the placement of collocation points. Moreover, in the singular integration adjacent elements are treated in a special way and, therefore, the problem of quasi-singular integrals is not so significant. In addition, the Galerkin method allows for a skew-symmetric formulation, see remark 2.1, in which the choice of constant shape functions for the Neumann datum is feasible. The final system matrix can be treated by a conjugate gradient solver after a suitable preconditioning. In remark 3.7, it has been pointed out that the use of iterative solvers would significantly speed up the solution process. This is true for both of the considered discretization methods. Nevertheless, such a Galerkin formulation with both integral equations is not directly applicable to halfspace problems because the hypersingular operator is commonly regularized by integration by parts. The same problem as with the regularized double layer operator would occur as mentioned above.

Considering the coupling strategy, the presented method is using a direct solver for the dual problem. Obviously, this is not the optimal choice for problems involving a high number of Lagrange multipliers. As explained in remark 4.2, the use of a projected conjugate gradient algorithm as in the classical FETI-methods would be the right choice. Nevertheless, a preliminary to this is a symmetric formulation which implies the use of the skew-symmetric Galerkin boundary element method as mentioned above. The choice of a direct solver has next to its inherent robustness the advantage that a factorization of the left hand side can be precomputed. In dynamic problems, where the spatial dimension is often rather small and the left hand side does not change throughout the computation, a direct solver is thus often preferred to an iterative solver.

The choice of piece-wise constant Lagrange multipliers in the coupling approach is the most direct approach. Nevertheless, stability problems can occur due to this approximation as pointed out in remark 4.3. Although in the considered test examples no such problems show up, the use of piecewise linear Lagrange multipliers is recommended for a robust algorithm. Finally, in remark 4.4 the restriction to plane interfaces is brought up. A workaround of this limitation is of course necessary for a broader range of applications.

In view of the above described troubles, the next step would be to make use of a symmetric boundary element formulation. Then both the subdomain and the skeleton solutions can be carried out by conjugate gradient methods. This would significantly speed up the solution process and additionally allow for a full parallelization of the algorithm as in the FETI-technology. Moreover, the employment of a fast boundary element method would be of great benefit. On the finite element side, one could think of considering nonlinear material behaviors or large deformations. An incorporation of nonlinear solution algorithms would not alter the coupling framework. In the same manner, contact problems could be

considered which are facilitated because nonconforming interfaces are allowed. Another extension of this work goes into the direction of fluid-structure interaction which includes acoustic problems. Especially this acoustic-structure coupling needs special consideration because in the presented method the relaxed interface condition is based on the coupling of Dirichlet data only. But acoustic-structure coupling requires the coupling of Dirichlet with Neumann data across the interfaces.

A FUNDAMENTAL SOLUTIONS

The fundamental solutions used in this work for the boundary integral equations and boundary element discretizations are listed in the following. Note that due to the use of the convolution quadrature method (see subsection 3.2.2), only Laplace transformed fundamental solutions are needed for time-dependent analyses. All of the following functions are taken from literature and adapted to the current notation. Possible references are Gaul et al. [33] and Steinbach [107] (Laplace and elastostatic equations), Love [66] (elastostatics), Kupradze [57] (three-dimensional elastostatics and -dynamics), Gaul et al. [33] (acoustics), and Cruse and Rizzo [17] and Kausel [53] (elastodynamics). A concise list of fundamental solutions for various operators is given by Ortner [77, 78].

Notation. All fundamental solutions are given for two and three spatial dimensions, denoted by $d = 2$, 3. The points $\mathbf{x}, \mathbf{y} \in \mathbb{R}^d$ are finally the collocation and the integration points in the boundary element method and have components x_i and y_i, respectively, for $i = 1, \ldots, d$. $\mathbf{n}$ is the unit outward normal vector located at the point $\mathbf{y}$ with components n_i. The complex Laplace variable is denoted by s. The considered fluid model has the compressibility κ and the wave speed c as parameters. The elastic solid is described by the Lamé parameters λ and μ and the wave speeds c_1 and c_2 of the compression and shear waves, respectively. Cf. chapter 2 for the regarded material models. Finally, the two-dimensional dynamic fundamental solutions are expressed in terms of modified Bessel functions of the second kind and j-th order, represented by the symbol K_j.

A.1 Statics

Abbreviations:

$$\gamma(\mathbf{x}, \mathbf{y}) := \begin{cases} \log \dfrac{1}{|\mathbf{y} - \mathbf{x}|} & d = 2 \\[2mm] \dfrac{1}{|\mathbf{y} - \mathbf{x}|} & d = 3 \end{cases}$$

$$\Sigma(\mathbf{x}, \mathbf{y})[i, j] := (y_j - x_j)n_i(\mathbf{y}) - (y_i - x_i)n_j(\mathbf{y}) \quad i, j = 1, \ldots, d$$

A.1.1 Laplace operator

Operators:

$$(\mathcal{L}^\Delta u)(\mathbf{x}) := -\Delta u(\mathbf{x}) = -\sum_{i=1}^{d} \frac{\partial^2 u}{\partial x_i^2}$$

$$(\mathcal{T}^\Delta u)(\mathbf{y}) := \lim_{\Omega \ni \mathbf{x} \to \mathbf{y} \in \Gamma} [\nabla u(\mathbf{x})] \cdot \mathbf{n}(\mathbf{y})$$

Fundamental solutions:

$$u^*(\mathbf{x},\mathbf{y}) = \frac{1}{2(d-1)\pi}\gamma(\mathbf{x},\mathbf{y})$$

$$(\mathcal{T}_\mathbf{y}^\Delta u^*)(\mathbf{x},\mathbf{y}) = -\frac{1}{2(d-1)\pi}\frac{(\mathbf{y}-\mathbf{x})\cdot\mathbf{n}(\mathbf{y})}{|\mathbf{y}-\mathbf{x}|^d}$$

A.1.2 Elastostatics

Operators:

$$(\mathcal{L}^E\mathbf{u})(\mathbf{x}) := -\mu\nabla\cdot(\nabla\mathbf{u}(\mathbf{x})) - (\lambda+\mu)\nabla(\nabla\cdot\mathbf{u}(\mathbf{x}))$$

$$= -(\lambda+2\mu)\nabla\cdot(\nabla\mathbf{u}) + \mu\nabla\times(\nabla\times\mathbf{u})$$

$$(\mathcal{T}^E\mathbf{u})(\mathbf{y}) := \lim_{\Omega \ni \mathbf{x} \to \mathbf{y} \in \Gamma}\left[\lambda\nabla\cdot\mathbf{u}(\mathbf{x})\,\mathbf{I} + \mu\left(\nabla\mathbf{u}(\mathbf{x}) + (\nabla\mathbf{u}(\mathbf{x}))^\top\right)\right]\cdot\mathbf{n}(\mathbf{y})$$

Fundamental solutions:

$$\mathbf{U}^*(\mathbf{x},\mathbf{y}) = \frac{1}{4(d-1)\pi}\frac{\lambda+\mu}{\mu(\lambda+2\mu)}\left[\frac{\lambda+3\mu}{\lambda+\mu}\gamma(\mathbf{x},\mathbf{y})\,\mathbf{I} + \frac{(\mathbf{y}-\mathbf{x})(\mathbf{y}-\mathbf{x})^\top}{|\mathbf{y}-\mathbf{x}|^d}\right]$$

$$(\mathcal{T}_\mathbf{y}^E\mathbf{U}^*)(\mathbf{x},\mathbf{y}) = -\frac{1}{2(d-1)\pi}\frac{\lambda+\mu}{\lambda+2\mu}\frac{1}{|\mathbf{y}-\mathbf{x}|^d}\left[\frac{\mu}{\lambda+\mu}\Sigma(\mathbf{x},\mathbf{y})\right.$$

$$\left. + \left(\frac{\mu}{\lambda+\mu}\mathbf{I} + d\frac{(\mathbf{y}-\mathbf{x})(\mathbf{y}-\mathbf{x})^\top}{|\mathbf{y}-\mathbf{x}|^2}\right)(\mathbf{y}-\mathbf{x})\cdot\mathbf{n}(\mathbf{y})\right]$$

A.2 Dynamics

A.2.1 Acoustic wave equation

Operators:

$$(\mathcal{H}^\Delta u)(\mathbf{x},t) := \left(\frac{\partial^2 u}{\partial t^2} - c^2\mathcal{L}^\Delta u\right)(\mathbf{x},t)$$

$$(\hat{\mathcal{H}}^\Delta\hat{u})(\mathbf{x},s) = (s^2\hat{u} - c^2\Delta\hat{u})(\mathbf{x},s)$$

Abbreviation:

$$z(\mathbf{x}, \mathbf{y}, s) := \frac{s|\mathbf{y} - \mathbf{x}|}{c}$$

Two-dimensional fundamental solutions:

$$\hat{u}^*(\mathbf{x}, \mathbf{y}, s) = \frac{1}{2\pi\kappa} K_0(z)$$

$$(\kappa \mathcal{T}_{\mathbf{y}}^{\Delta} \hat{u}^*)(\mathbf{x}, \mathbf{y}, s) = -\frac{1}{2\pi} \frac{(\mathbf{y} - \mathbf{x}) \cdot \mathbf{n}(\mathbf{y})}{|\mathbf{y} - \mathbf{x}|} K_1(z)$$

Three-dimensional fundamental solutions:

$$\hat{u}^*(\mathbf{x}, \mathbf{y}, s) = \frac{1}{4\pi\kappa} \frac{\exp(-z)}{|\mathbf{y} - \mathbf{x}|}$$

$$(\kappa \mathcal{T}_{\mathbf{y}}^{\Delta} \hat{u}^*)(\mathbf{x}, \mathbf{y}, s) = \frac{1}{4\pi} \frac{(\mathbf{y} - \mathbf{x}) \cdot \mathbf{n}(\mathbf{y})}{|\mathbf{y} - \mathbf{x}|^3} (1 + z) \exp(-z)$$

A.2.2 Elastodynamics

Operators:

$$(\mathcal{H}^E \mathbf{u})(\mathbf{x}, t) := \left(\frac{\partial^2 \mathbf{u}}{\partial t^2} - c_1^2 \nabla \nabla \cdot \mathbf{u} + c_2^2 \nabla \times \nabla \times \mathbf{u} \right)(\mathbf{x}, t)$$

$$(\hat{\mathcal{H}}^E \mathbf{u})(\mathbf{x}, s) = \left(s^2 \hat{\mathbf{u}} - c_1^2 \nabla \nabla \cdot \hat{\mathbf{u}} + c_2^2 \nabla \times \nabla \times \hat{\mathbf{u}} \right)(\mathbf{x}, s)$$

Abbreviations:

$$\Sigma_1(\mathbf{x}, \mathbf{y})[i, j] := \frac{n_i(y_j - x_j)}{|\mathbf{y} - \mathbf{x}|} \quad i, j = 1, \dots, d$$

$$z_k(\mathbf{x}, \mathbf{y}, s) := \frac{s|\mathbf{y} - \mathbf{x}|}{c_k} \quad k = 1, 2$$

Abbreviations (two-dimensional):

$$\chi_1(\mathbf{x}, \mathbf{y}) := K_0(z_2) + \frac{1}{z_2} \left(K_1(z_2) - \frac{c_2}{c_1} K_1(z_1) \right)$$

$$\chi_2(\mathbf{x}, \mathbf{y}) := K_2(z_2) - \frac{c_2^2}{c_1^2} K_2(z_1)$$

$$\chi_3(\mathbf{x}, \mathbf{y}) := \frac{2}{|\mathbf{y} - \mathbf{x}|} \left(\frac{c_2^2}{c_1^2} K_2(z_1) - K_2(z_2) \right) - \frac{s}{c_2} K_1(z_2)$$

$$\chi_4(\mathbf{x}, \mathbf{y}) := \frac{2s}{c_2} \left(K_3(z_2) - \frac{c_2^3}{c_1^3} K_3(z_1) \right)$$

$$\chi_5(\mathbf{x}, \mathbf{y}) := \frac{1}{|\mathbf{y} - \mathbf{x}|} \left[\frac{2c_2^2}{c_1^2} K_2(z_1) - 2K_2(z_2) - z_1 \left(1 - \frac{2c_2^2}{c_1^2} \right) K_1(z_1) \right]$$

Abbreviations (three-dimensional):

$$\zeta_k(\mathbf{x}, \mathbf{y}) := \frac{\exp(-z_k(\mathbf{x}, \mathbf{y}))}{|\mathbf{y} - \mathbf{x}|}, \quad k = 1, 2$$

$$\chi_1(\mathbf{x}, \mathbf{y}) := -\frac{c_2^2}{c_1^2}\left(\frac{1}{z_1^2} + \frac{1}{z_1}\right)\zeta_1 + \left(\frac{1}{z_2^2} + \frac{1}{z_2} + 1\right)\zeta_2$$

$$\chi_2(\mathbf{x}, \mathbf{y}) := -\frac{c_2^2}{c_1^2}\left(\frac{3}{z_1^2} + \frac{3}{z_1} + 1\right)\zeta_1 + \left(\frac{3}{z_2^2} + \frac{3}{z_2} + 1\right)\zeta_2$$

$$\chi_3(\mathbf{x}, \mathbf{y}) := \frac{c_2^2}{c_1^2}\left(2 + \frac{6}{z_1} + \frac{6}{z_1^2}\right)\zeta_1 - \left(3 + \frac{6}{z_2} + \frac{6}{z_2^2} + z_2\right)\zeta_2$$

$$\chi_4(\mathbf{x}, \mathbf{y}) := \frac{c_2^2}{c_1^2}\left(-12 - \frac{30}{z_1} - \frac{30}{z_1} - 2z_1\right)\zeta_1 + \left(12 + \frac{30}{z_2} + \frac{30}{z_2^2} + 2z_2\right)\zeta_2$$

$$\chi_5(\mathbf{x}, \mathbf{y}) := \left[-1 - z_1 + \frac{c_2^2}{c_1^2}\left(4 + \frac{6}{z_1} + \frac{6}{z_1^2} + 2z_1\right)\right]\zeta_1 - \left(2 + \frac{6}{z_2} + \frac{6}{z_2}\right)\zeta_2$$

Fundamental solutions:

$$\hat{\mathbf{U}}^*(\mathbf{x}, \mathbf{y}, s) = \frac{1}{2(d-1)\pi\mu}\left(\chi_1\mathbf{I} - \chi_2\frac{(\mathbf{y} - \mathbf{x})(\mathbf{y} - \mathbf{x})^\top}{|\mathbf{y} - \mathbf{x}|^2}\right)$$

$$(\mathcal{T}_\mathbf{y}^E\hat{\mathbf{U}}^*)(\mathbf{x}, \mathbf{y}) = \frac{1}{2(d-1)\pi}\left(\chi_3\frac{(\mathbf{y} - \mathbf{x})\cdot\mathbf{n}(\mathbf{y})}{|\mathbf{y} - \mathbf{x}|}\mathbf{I} + \chi_3\Sigma_1(\mathbf{x}, \mathbf{y}) + \chi_5\Sigma_1^\top(\mathbf{x}, \mathbf{y})\right.$$

$$\left. + \chi_4\frac{(\mathbf{y} - \mathbf{x})(\mathbf{y} - \mathbf{x})^\top}{|\mathbf{y} - \mathbf{x}|^3}(\mathbf{y} - \mathbf{x})\cdot\mathbf{n}(\mathbf{y})\right)$$

B REFERENCE SOLUTIONS

B.1 Unit Step Loading of a Rod

The solution of the homogeneous one-dimensional wave equation

$$\frac{\partial^2}{\partial t^2}u(x,t) - \frac{\kappa}{\rho_0}\frac{\partial^2}{\partial x^2}u(x,t) = 0,$$

on the interval $\Omega = (0,\ell)$ with the boundary conditions

$$u(0,t) = 0 \quad \text{and} \quad u(\ell,t) = F(t) = F_0 H(t)$$

and vanishing initial conditions, $u(x,0) = 0$ and $(\partial u/\partial t)(x,0) = 0$, has been derived by Graff [37] for a general loading $F(t)$. In the given case of a step function $F_0 H(t)$ as the load variation in time, the solution can be found in the monograph of Schanz [98]. It has the form

$$u(x,t) = \frac{cF_0}{\kappa}\sum_{k=0}^{\infty}(-1)^k\left[(ct+x-(2k+1)\ell)H(ct+x-(2k+1)\ell)\right. \tag{B.1}$$
$$\left. -(ct-x-(2k+1)\ell)H(ct-x-(2k+1)\ell)\right]$$

$$q(x,t) = F_0\sum_{k=0}^{\infty}(-1)^k\left[H(ct-(2k+1)\ell+x)+H(ct-(2k+1)\ell-x)\right] \tag{B.2}$$

for the unknown $u(x,t)$ and its derivative $q(x,t) := \kappa(\partial u/\partial x)(x,t)$ with the one-dimensional wave speed $c^2 = \kappa/\rho_0$. A plot of these functions for specific values of the coordinate x is given in figure B.1 where u_0 refers to the static response $u_0 = F_0/(\kappa\ell)$.
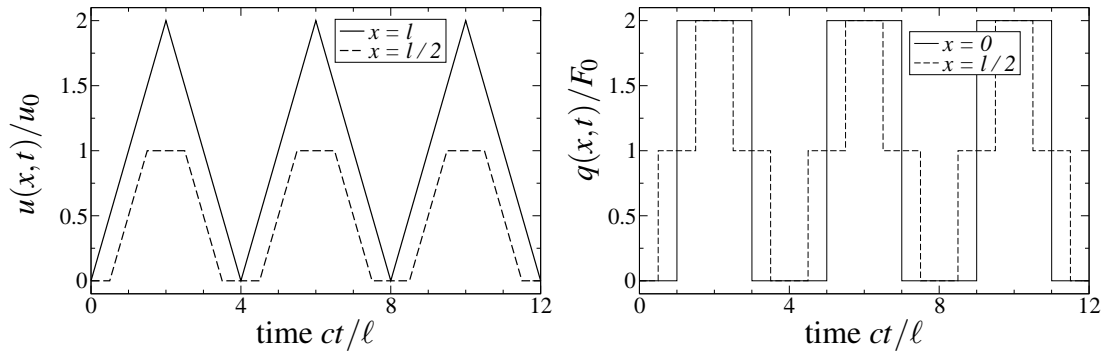

Figure B.1: Analytical solution for the dynamic rod.

B.2 Halfspace Solutions

In the following, the static and dynamic solutions for a point load on an elastic halfspace is given. The domain is thus $\Omega = \{\mathbf{x} \in \mathbb{R}^3 : x_3 > 0\}$ and $\Gamma = \{\mathbf{x} \in \mathbb{R}^3 : x_3 = 0\}$ denotes the corresponding unbounded surface. The point load acts at the origin in direction of the positive x_3-axis, i.e., $\mathbf{F} = (0, 0, F)^\top$ and F is a function of time in the dynamic case. The rest of the surface is subjected to homogeneous Neumann boundary conditions and, therefore, the prescribed surface traction is of the form $\mathbf{g}_N = \mathbf{F}\delta(\mathbf{x})$. Obviously, these problems contain a radial symmetry and the solutions are thus best described by using cylindrical coordinates. The displacement of the surface is then $\mathbf{u}_\Gamma = (u_r, 0, u_z)^\top$, because there is no displacement in tangential direction.

B.2.1 Static halfspace fundamental solution

In the static case, the problem of a halfspace subjected to a point load is the so-called halfspace fundamental solution and was first derived by Boussinesq. It is given, for instance, in the book of Love [66]. Its components are for $x_3 = 0$

$$u_r(\mathbf{x}) = -\frac{F}{4\pi}\frac{1}{\lambda + \mu}\frac{1}{|\mathbf{x}|} \tag{B.3a}$$

$$u_z(\mathbf{x}) = \frac{F}{4\pi}\frac{\lambda + 2\mu}{\mu(\lambda + \mu)}\frac{1}{|\mathbf{x}|} \tag{B.3b}$$

with the Euclidean distance $|\mathbf{x}|^2 = \sum_{i=1}^{3} x_i^2$. Obviously, the components in x_1 and x_2 direction can be obtained by multiplication of u_r with the factors $x_1/|\mathbf{x}|$ and $x_2/|\mathbf{x}|$, respectively. In figure B.2, this solution is displayed for a specific choice of material parameters along a coordinate line through the origin.

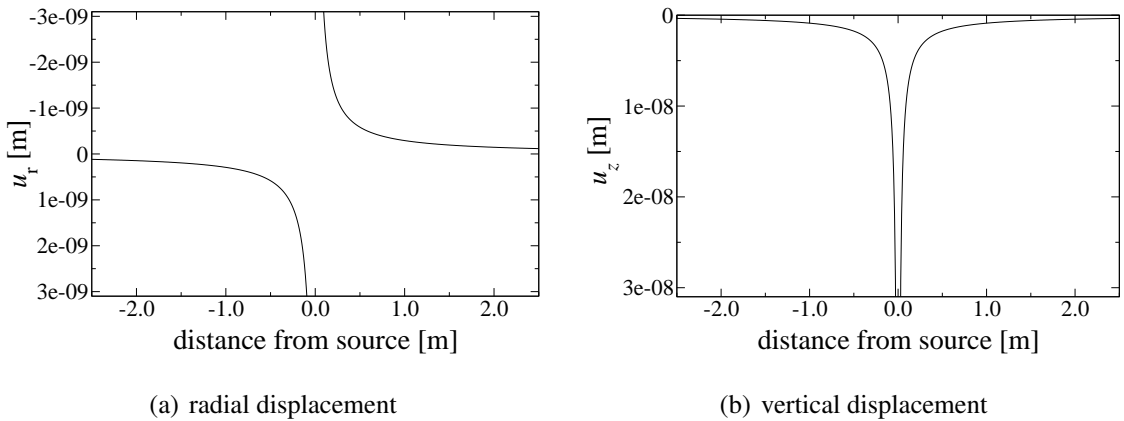(a) radial displacement   (b) vertical displacement

Figure B.2: Analytical solution for the surface displacement in radial and vertical direction for an isotropic material with $\lambda = \mu = 1.3626 \cdot 10^8 \, \text{N/m}^2$ along the coordinate line $-2.5\,\text{m} < x_1 < 2.5\,\text{m}$, $x_2 = x_3 = 0$ for a point load $F_0 = 1\,\text{N}$.

B.2.2 Impulse point load on the surface

Here, the solution to the elastodynamic equations (2.21) for a halfspace under a point load of type $F(t) = F_0 H(t)$, i.e., a unit step function in time, is given. This problem was first stated by Lamb [59]. Pekeris [85] derived a solution for the surface displacements, i.e., for $x_3 = 0$ only, under the restriction that $\lambda = \mu$ (or $\nu = 0.25$) which will be given here. For the sake of legibility, the following abbreviations are introduced, the dimensionless time $\tau := c_2 t / |\mathbf{x}|$ with the shear wave speed $c_2 = \sqrt{\mu/\rho_0}$, and the three factors $\kappa^2 := 2/(3\tau^2 - 1)$, $\gamma^2 := (3 + \sqrt{3})/4$, and $C := \sqrt{\frac{3}{2}} \tau F_0 / (16\pi^2 \mu |\mathbf{x}|)$. The vertical displacement component is then

$$
u_z(\mathbf{x},t) = \begin{cases}
0 & 0 < \tau < \dfrac{1}{\sqrt{3}} \\[2ex]
-\dfrac{F_0}{32\pi\mu|\mathbf{x}|}\left[6 - \dfrac{\sqrt{3}}{\sqrt{\tau^2 - 1/4}} - \dfrac{\sqrt{3\sqrt{3}+5}}{1/2\sqrt{\sqrt{3}+3-4\tau^2}} + \right. & \\[1ex]
\left. \hspace{4cm} \dfrac{\sqrt{3\sqrt{3}-5}}{1/2\sqrt{\sqrt{3}-3+4\tau^2}}\right] & \dfrac{1}{\sqrt{3}} < \tau < 1 \\[2ex]
-\dfrac{F_0}{16\pi\mu|\mathbf{x}|}\left[6 - \dfrac{\sqrt{3\sqrt{3}+5}}{1/2\sqrt{\sqrt{3}+3-4\tau^2}}\right] & 1 < \gamma < \gamma \\[2ex]
-\dfrac{3F_0}{8\pi\mu|\mathbf{x}|} & \tau > \gamma.
\end{cases}
\tag{B.4a}
$$

The radial displacements are expressed as

$$
u_r(\mathbf{x},t) = \begin{cases}
0 & 0 < \tau < \dfrac{1}{\sqrt{3}} \\[2ex]
C\left[6K(1/\kappa) + (6-4\sqrt{3})\Pi((20-12\sqrt{3})/\kappa^2, 1/\kappa) - \right. & \\[1ex]
\left. \quad 18\Pi(8/\kappa^2, 1/\kappa) + (6+4\sqrt{3})\Pi((20+12\sqrt{3})/\kappa^2, 1/\kappa)\right] & \dfrac{1}{\sqrt{3}} < \tau < 1 \\[2ex]
C\kappa\left[6K(1/\kappa) + (6-4\sqrt{3})\Pi((20-12\sqrt{3}), 1/\kappa) - \right. & \\[1ex]
\left. \quad 18\Pi(8, 1/\kappa) + (6+4\sqrt{3})\Pi((20+12\sqrt{3}), 1/\kappa)\right] & 1 < \tau < \gamma \\[2ex]
C\kappa\left[6K(1/\kappa) + (6-4\sqrt{3})\Pi((20-12\sqrt{3}), 1/\kappa) - \right. & \\[1ex]
\left. \quad 18\Pi(8, 1/\kappa) + (6+4\sqrt{3})\Pi((20+12\sqrt{3}), 1/\kappa)\right] + & \\[1ex]
\dfrac{F_0\tau}{8\pi\mu|\mathbf{x}|\sqrt{\tau^2 - \gamma^2}} & \tau > \gamma.
\end{cases}
\tag{B.4b}
$$

In these expressions, the complete elliptic integrals of first and third kind, $K(k)$ and $\Pi(n,k)$, respectively, appear which are defined by [85]

$$K(k) = \int_0^{\pi/2} \frac{1}{\sqrt{1 - k^2 \sin^2 \theta}} \, d\theta$$

$$\Pi(n,k) = \int_0^{\pi/2} \frac{1}{(1 + n^2 \sin^2 \theta) \sqrt{1 - k^2 \sin^2 \theta}} \, d\theta \,.$$

Note that $u_z(\mathbf{x},t)$ for the last period $t > \gamma|\mathbf{x}|/c_2$ coincides with the vertical displacement of the Boussinesq solution (B.3b) if $\mu = \lambda$. The same holds for the radial component for large times, i.e., the limit $\lim_{t \to \infty} u_z(\mathbf{x},t)$ is equal to the static solution (B.3a). The plots in figure B.3 show these radial and vertical displacement components together with the static solution due to Boussinesq.

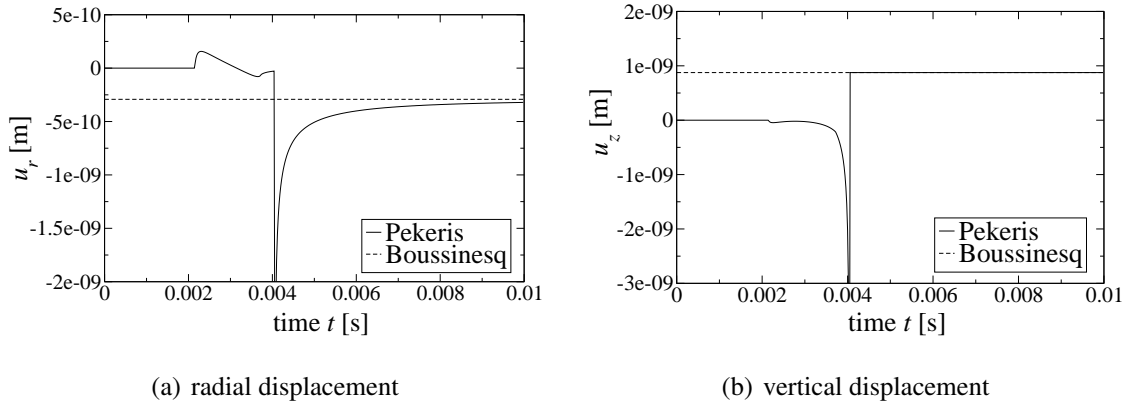(a) radial displacement

(b) vertical displacement

Figure B.3: Analytical solution for the surface displacement in radial and vertical direction for an isotropic material with $\lambda = \mu = 1.3626 \cdot 10^8 \, \text{N/m}^2$ at the distance $|\mathbf{x}| = 1 \, \text{m}$ from the point load of magnitude $F_0 = 1 \, \text{N}$.

REFERENCES

[1] J.D. Achenbach. *Wave propagation in elastic solids*. North-Holland, 2005.

[2] E. Anderson, Z. Bai, C. Bischof, S. Blackford, J. Demmel, J. Dongarra, J. Du Croz, A. Greenbaum, S. Hammarling, A. McKenney, and D. Sorensen. *LAPACK Users' Guide*. Society for Industrial and Applied Mathematics, third edition, 1999.

[3] H. Antes. Boundary element methods for wave propagation problems. Lecture Notes, Institute for Applied Mechanics, 2005.

[4] H. Antes. A short course on boundary element methods. Lecture Notes, Institute for Applied Mechanics, 2005.

[5] I. Babuška. The finite element method with Lagrangian multipliers. *Numerische Mathematik*, 20:179–92, 1973.

[6] K.-J. Bathe. *Finite element procedures*. Prentice Hall, 1996.

[7] M. Bebendorf and S. Rjasanow. Adaptive low-rank approximation of collocation matrices. *Computing*, 70:1–24, 2003.

[8] A. Ben-Isreal and T.N.E. Greville. *Generalized inverses: Theory and applications*. John Wiley & Sons, 1974.

[9] D. Braess. *Finite Elemente*. Springer, 2003.

[10] F. Brezzi and M. Fortin. *Mixed and hybrid finite element methods*. Springer, 1991.

[11] I.N. Bronštein and K.A. Semendjaev. *Handbook of mathematics*. Springer, 1997.

[12] M. Costabel. Boundary integral operators on Lipschitz domains: Elementary results. *SIAM Journal for Mathematical Analysis*, 19:613–626, 1988.

[13] M. Costabel. Time-dependent problems with the boundary integral equation method. In E. Stein, R. de Borst, and T.J.R. Hughes, editors, *Encyclopedia of Computational Mechanics*, volume 1, chapter 25, pages 703–721. John Wiley & Sons, Ltd., 2004.

[14] M. Costabel and M. Dauge. On representation formulas and radiation conditions. *Mathematical Methods in the Applied Sciences*, 20:133–150, 1997.

[15] R. Courant, K. Friedrichs, and H. Lewy. Über die partiellen Differenzengleichungen der mathematischen Physik. *Mathematische Annalen*, 100:32–74, 1928.

[16] T.A. Cruse. A direct formulation and numerical solution of the general transient elastodynamic problem. II. *Journal of Mathematical Analysis and Applications*, 22:341–355, 1968.

[17] T.A. Cruse and F.J. Rizzo. A direct formulation and numerical solution of the general transient elastodynamic problem. I. *Journal of Mathematical Analysis and Applications*, 22:244–259, 1968.

[18] T.A. Davis. Algorithm 849: a concise sparse Cholesky package. *ACM Transactions on Mathematical Software*, 31:587–591, 2005.

[19] K. Diethelm. *Numerische Approximation von Cauchy-Hauptwert-Integralen unter theoretischen und rechnerorientierten Aspekten.* PhD thesis, Universität Hildesheim, Germany, 1994.

[20] Z. Dostál, D. Horák, and R. Kučera. Total FETI — an easier implementable variant of the the FETI method for numerical solution of elleptic PDE. *Communications in Numerical Methods in Engineering*, 22:1155–1162, 2006.

[21] M.G. Duffy. Quadrature over a pyramid or cube of integrands with a singularity at a vertex. *SIAM journal on Numerical Analysis*, 19:1260–1262, 1982.

[22] D.A. Dunavant. High degree efficient symmetrical Gaussian quadrature rules for the triangle. *International Journal for Numerical Methods in Engineering*, 21:1129–1148, 1985.

[23] O. von Estorff and C. Hagen. Iterative coupling of FEM and BEM in 3D transient elastodynamics. *Engineering Analysis with Boundary Elements*, 29:775–787, 2005.

[24] C. Farhat, P.-S. Chen, and J. Mandel. A scalable Lagrange multiplier based domain decomposition method for time-dependent problems. *International Journal for Numerical Methods in Engineering*, 38:3831–3853, 1995.

[25] C. Farhat and L. Crivelli. A transient FETI methodology for large-scale parallel implicit computations in structural mechanics. *International Journal for Numerical Methods in Engineering*, 37:1945–1975, 1994.

[26] C. Farhat and M. Géradin. On the general solution by a direct method of a large-scale singular system of linear equations: application to the analysis of floating structures. *International Journal for Numerical Methods in Engineering*, 41:675–696, 1998.

[27] C. Farhat, K. Pierson, and M. Lesoinne. The second generation FETI methods and their application the parallel solution of large-scale linear and geometrically non-linear structural analysis problems. *Computer Methods in Applied Mechanics and Engineering*, 184:333–374, 2000.

[28] C. Farhat and F.-X. Roux. A method of finite element tearing and interconnecting and its parallel solution algorithm. *International Journal for Numerical Methods in Engineering*, 32:1205–1227, 1991.

[29] C. Farhat and F.-X. Roux. Implicit parallel processing in structural mechanics. *Computational Mechanics Advances*, 2:1–124, 1994.

[30] R.P. Feynman, R.B. Leighton, and M. Sands. *The Feynman lectures on physics.* Addison-Wesley, 1977.

[31] M. Fischer and L. Gaul. Fast BEM-FEM Mortar coupling for acoustic-structure interaction. *International Journal for Numerical Methods in Engineering*, 62:1677–1690, 2005.

[32] M. Frigo and S.G. Johnson. The design and implementation of FFTW3. *Proceedings of the IEEE*, 93(2):216–231, 2005.

[33] L. Gaul, M. Kögl, and M. Wagner. *Boundary Element Methods for Engineers and Scientists*. Springer, 2003.

[34] D. Givoli. *Numerical Methods for Problems in Infinite Domains*. Elsevier, 1992.

[35] H. Goldstein. *Classical Mechanics*. Addison Wesley, 1996.

[36] G.H. Golub and C.F. van Loan. *Matrix Computations*. Johns Hopkins University Press, 1996.

[37] K.F. Graff. *Wave motions in elastic solids*. Dover Publications, 1991.

[38] L. Greengard. Fast algorithms for classical physics. *Science*, 265:909–914, 1994.

[39] L. Greengard and V. Rokhlin. A fast algorithm for particle simulations. *Journal of Computational Physics*, 73:325–348, 1987.

[40] M. Guiggiani and A. Gigante. A general algorithm for multidimensional Cauchy principal value integrals in the boundary element method. *Journal of Applied Mechanics*, 57:906–915, 1990.

[41] W. Hackbusch. *Integral Equations. Theory and Numerical Treatment*. Birkhäuser, 1998.

[42] W. Hackbusch. A sparse matrix arithmetic based on $\mathcal{H}$-matrices. Part I: Introduction to $\mathcal{H}$-matrices. *Computing*, 62:89–108, 1999.

[43] W. Hackbusch and Z.P. Nowak. On the fast matrix multiplication in the boundary element method by panel clustering. *Numerische Mathematik*, 54:463–491, 1989.

[44] F. Hartmann. The discrete Babuška-Brezzi condition. *Ingenieur Archiv*, 56:221–228, 1986.

[45] F. Hartmann. *Introduction to Boundary Elements. Theory and Applications*. Springer, 1989.

[46] M.T. Heath. *Scientific Computing — An Introductory Survey*. McGraw-Hill, 2002.

[47] M.W. Heinstein and T.A. Laursen. A three dimensional surface-to-surface projection algorithm for non-coincident domains. *Communications in Numerical Methods in Engineering*, 19:421–432, 2003.

[48] G.C. Hsiao and W.L. Wendland. Boundary element methods: Foundation and error analysis. In E. Stein, R. de Borst, and T.J.R. Hughes, editors, *Encyclopedia of Computational Mechanics*, volume 1, chapter 12, pages 339–373. John Wiley & Sons, Ltd., 2004.

[49] T.J.R. Hughes. *The Finite Element Method: Linear Static and Dynamic Finite Element Analysis*. Dover Publications, New York, 2000.

[50] G.H. Hulbert. Computational structural dynamics. In E. Stein, R. de Borst, and T.J.R. Hughes, editors, *Encyclopedia of Computational Mechanics*, volume 2, chapter 5. John Wiley & Sons, Ltd., 2004.

[51] M.A. Jaswon. Integral equation methods in potential theory I. *Proceedings of the Royal Society A*, 275:23–32, 1963.

[52] M. Jung and U. Langer. *Methode der finiten Elemente für Ingenieure*. Teubner, 2001.

[53] E. Kausel. *Fundamental solutions in elastodynamics*. Cambridge University Press, 2006.

[54] R.J. Knops and L.E. Payne. *Uniqueness Theorems in Linear Elasticity*. Springer, 1971.

[55] A.R. Krommer and C.W. Ueberhuber. *Computational Integration*. SIAM, 1998.

[56] V.D. Kupradze. Dynamic problems in elasticity. In I.N. Sneddon and R. Hill, editors, *Progress in Solid Mechanics*, volume III. North-Holland, 1963.

[57] V.D. Kupradze, T.G. Gegelia, M.O. Basheleishvili, and T.V. Burchuladze. *Three-dimensional Problems of the Mathematical Theory of Elasticity and Thermoelasticity*. North-Holland, 1979.

[58] J.C. Lachat and J.O. Watson. Effective numerical treatment of boundary integral equations: a formulation for three-dimensional elastostatics. *International Journal for Numerical Methods in Engineering*, 10:991–1005, 1976.

[59] H. Lamb. On the propagation of tremors over the surface of an elastic solid. *Philosophical Transactions of the Royal Society of London, Series A*, 203:1–42, 1904.

[60] J.D. Lambert. *Numerical Methods for Ordinary Differential Systems*. John Wiley & Sons, 1990.

[61] U. Langer and O. Steinbach. Boundary element tearing and interconnecting methods. *Computing*, 71:205–228, 2003.

[62] U. Langer and O. Steinbach. Coupled boundary and finite element tearing and interconnecting methods. In R. Kornhuber, R. Hoppe, J. Periaux, O. Pironneau, O. Widlund, and J. Xu, editors, *Domain Decomposition Methods in Science and Engineering XV*, volume 40 of *Lecture Notes in Computational Science and Enginnering*, pages 83–97. Springer, 2004.

[63] U. Langer and O. Steinbach. Coupled finite and boundary element domain decomposition methods. In M. Schanz and O. Steinbach, editors, *Boundary Element Analysis — Mathematical Aspects and Applications*, volume 29 of *Lecture Notes in Applied and Computational Mechanics*, pages 61–95. Springer, 2007.

[64] D.P. Laurie. Algorithm 584, CUBTRI: Automatic cubature over a triangle. *Communications of the ACM*, 8:210–218, 1982.

[65] P. Le Tallec. Domain decomposition methods in computational mechanics. *Computational Mechanics Advances*, 1:121–220, 1994.

[66] A.E.H. Love. *Treatise on the Mathematical Theory of Elasticity*. Dover Publications, 1944.

[67] C. Lubich. Convolution quadrature and discretized operational calculus I. *Numerische Mathematik*, 52:129–145, 1988.

[68] C. Lubich. Convolution quadrature and discretized operational calculus II. *Numerische Mathematik*, 52:413–425, 1988.

[69] J. Mandel and R. Tezaur. Convergence of a substructuring method with Lagrange multipliers. *Numerische Mathematik*, 73:473–487, 1996.

[70] W.J. Mansur. *A time-stepping technique to solve wave propagation problems using the boundary element method*. PhD thesis, University of Southampton, 1983.

[71] V. Mantič. A new formula for the *c*-matrix in the Somigliana identity. *Journal of Elasticity*, 33:193–201, 1993.

[72] N.M. Newmark. A method of computation for structural dynamics. *ASCE Journal of the Engineering Mechanics Division*, 85:67–93, 1959.

[73] N. Nishimura. Fast multipole accelerated boundary integral equation methods. *Applied Mechanics Review*, 55:299–324, 2002.

[74] G. Of. *BETI-Gebietszerlegungsmethoden mit schnellen Randelementverfahren und Anwendungen*. PhD thesis, University of Stuttgart, 2006.

[75] R.W. Ogden. *Non-linear elastic deformations*. Dover publications, 1994.

[76] R. Ohayon and C. Soize. *Structural Acoustics and Vibration*. Academic Press, 1998.

[77] N. Ortner. Regularisierte Faltung von Distributionen. Teil 1: Zur Berechnung von Fundamentallösungen. *Zeitschrift für angewandte Mathematik und Physik*, 31:133–154, 1980.

[78] N. Ortner. Regularisierte Faltung von Distributionen. Teil 2: Eine Tabelle von Fundamentallösungen. *Zeitschrift für angewandte Mathematik und Physik*, 31:155–173, 1980.

[79] F. París and J. Cañas. *Boundary Element Method*. Oxford University Press, 1997.

[80] K.C. Park and C.A. Felippa. A variational principle for the formulation of partitioned structural systems. *International Journal for Numerical Methods in Engineering*, 47:395–418, 2000.

[81] K.C. Park, C.A. Felippa, and U.A. Gumaste. A localized version of the method of Lagrange multipliers and its applications. *Computational Mechanics*, 24:476–490, 2000.

[82] K.C. Park, C.A. Felippa, and G. Rebel. Interfacing non-matching finite element discretizations: the zero moment rule. In W.A. Wall, K.-U. Bletzinger, and K. Schweizerhof, editors, *Trends in Computational Mechanics*, pages 355–67. CIMNE: Barcelona, Spain, 2001.

[83] K.C. Park, C.A. Felippa, and G. Rebel. A simple algorithm for localized construction of non-matching structural interfaces. *International Journal for Numerical Methods in Engineering*, 53:2117–2142, 2002.

[84] C. Patterson and M.A. Sheikh. Interelement continuity in the boundary element method. In C.A. Brebbia, editor, *Topics in Boundary Element Research*, pages 121–141. Springer, 1984.

[85] C.L. Pekeris. The seismic surface pulse. *Proceedings of the National American Society*, 41:469–480, 1955.

[86] W.H. Press, S.A. Teukolsky, W.T. Vetterling, and B.P. Flannery. *Numerical Recipes in C++*. Cambridge University Press, 2002.

[87] J.S. Przemieniecki. *Theory of Matrix Structural Analysis*. McGraw-Hill, 1968.

[88] M.A. Puso. A 3D mortar method for solid mechanics. *International Journal for Numerical Methods in Engineering*, 59:315–336, 2004.

[89] A. Quarteroni, R. Sacco, and F. Saleri. *Numerical Mathematics*, volume 37. Springer, 2000.

[90] B.D. Reddy. *Introductory Functional Analysis*. Springer, 1998.

[91] J.N. Reddy. *Energy Principles and Variational Methods in Applied Mechanics*. John Wiley & Sons, 2002.

[92] W. Ritz. Über eine neue Methode zur Lösung gewisser Variationsprobleme der mathematischen Physik. *Journal für die reine und angewandte Mathematik*, 135:1–61, 1908.

[93] F.J. Rizzo. An integral equation approach to boundary value problems of classical elastostatics. *The Quarterly of Applied Mathematics*, 25:83–95, 1967.

[94] S. Rjasanow and O. Steinbach. *The Fast Solution of Boundary Integral Equations*. Springer, 2007.

[95] Y. Saad. *Iterative Methods for Sparse Linear Systems*. PWS Publishing Company, 1996.

[96] S. Sauter and C. Schwab. *Randelementmethoden*. Teubner, 2004.

[97] M. Schanz. Eine Randelementformulierung im Zeitbereich mit verallgemeinerten viskoelastischen Stoffgesetzen. Bericht aus dem Institut A für Mechanik Heft 1, Universität Stuttgart, 1994.

[98] M. Schanz. *Wave propagation in Viscoelastic and Poroelastic Continua - A boundary element approach*. Springer, 2001.

[99] M. Schanz and H. Antes. Application of 'Operational Quadrature Methods' in time domain boundary element analysis. *Meccanica*, 32:179–186, 1997.

[100] M. Schanz and H. Antes. A new visco- and elastodynamic time domain boundary element formulation. *Computational Mechanics*, 20:452–459, 1997.

[101] J.C. Simo and T.J.R. Hughes. *Computational Inelasticity*. Springer, 1998.

[102] D. Stefanica. Parallel FETI algorithms for mortars. *Applied Numerical Mathematics*, 54:266–279, 2005.

[103] O. Steinbach. *Gebietszerlegungsmethoden mit Randintegralgleichungen und effiziente numerische Lösungsverfahren für gemischte Randwertprobleme*. PhD thesis, Universität Stuttgart, 1996.

[104] O. Steinbach. Fast solution techniques for the symmetric boundary element method in linear elasticity. *Computer Methods in Applied Mechanics and Engineering*, 157:185–191, 1998.

[105] O. Steinbach. On a hybrid boundary element method. *Numerische Mathematik*, 84:679–695, 2000.

[106] O. Steinbach. *Stability Estimates for Hybrid Domain Decomposition Methods*. Springer, 2003.

[107] O. Steinbach. *Numerical Approximation Methods for Elliptic Boundary Value Problems*. Springer, 2008.

[108] E. Stephan. Coupling of boundary element methods and finite element methods. In E. Stein, R. de Borst, and T.J.R. Hughes, editors, *Encyclopedia of Computational Mechanics*, volume 1, chapter 13, pages 375–412. John Wiley & Sons, Ltd., 2004.

[109] C.F. Stevens. *The Six Core Theories of Modern Physics*. The MIT press, 1995.

[110] G. Strang and G.J. Fix. *An Analysis of the Finite Element Method*. Wellesley-Cambridge, 1973.

[111] G.T. Symm. Integral equation methods in potential theory II. *Proceedings of the Royal Society A*, 275:33–46, 1963.

[112] B. Szabó and I. Babuška. *Finite Element Analysis*. Wiley, 1991.

[113] E. Tonti. The reason for analogies between physical theories. *Applied Mathematical Modelling*, 1:37–50, 1976.

[114] A. Toselli and O. Widlund. *Domain Decomposition Methods — Algorithms and Theory*. Springer, 2005.

[115] E. Trefftz. Ein Gegenstück zum Ritzschen Verfahren. In *Proceedings of the Second International Congress for Applied Mechanics*, pages 131–137, 1926.

[116] B.R. Vatti. A generic solution to polygon clipping. *Communications of the ACM*, 35:56–63, 1992.

[117] J.O. Watson. Boundary elements from 1960 to the present day. *Electronic Journal of Boundary Elements*, 1:34–46, 2003.

[118] L.T. Wheeler and E. Sternberg. Some theorems in classical elastodynamics. *Archive for Rational Mechanics and Analysis*, 31:51–90, 1968.

[119] B.I. Wohlmuth. *Discretization Methods and Iterative Solvers Based on Domain Decomposition*. Springer, 2001.

[120] O.C. Ziekiewicz and R.L. Taylor. *The finite element method*. Butterworth-Heinemann, 2000.

[121] O.C. Zienkiewicz, D.W. Kelly, and P. Bettess. The coupling of the finite element method and boundary solution procedures. *International Journal for Numerical Methods in Engineering*, 11:355–375, 1977.